

Thèse de doctorat

**Atomic Force Microscopy Usage in a
Context of Multi-Mode and
Multi-Sample Correlative Measures on
Live Cells**

Bruker - CMPI

Antoine DUJARDIN

Soutenue publiquement le 18 décembre 2018

en vue de l'obtention du grade de

Docteur de l'Université de Lille

spécialité Micro-Nanosystèmes et Capteurs

M. Tuami LASRI	Université de Lille	Président
M ^{me} Touria COHEN-BOUHACINA	Université de Bordeaux	Rapporteur
M. Grégory FRANCIUS	LCPME – CNRS Nancy	Rapporteur
M ^{me} Véronique VIE	Université de Rennes	Examineur
M ^{me} Andrea SLADE	Bruker Nano Surfaces	Examineur
M. Vincent DUPRES	Université de Lille	Superviseur
M. Frank LAFONT	CMPI – CIIL (Lille)	Invité

Abstract

Soon after its development in the late 1980s, atomic force microscopy (AFM) has shown promising applications in the biomedical field. It now allows investigating biological samples from single molecules to living cells under conditions close to physiological. Despite its applicability to both eukaryotic and prokaryotic cells, it is hampered by its low throughput. While heavily automated on some well-characterized samples in air, AFM automation in fluid is very scarce, especially at the multi-sample level. During this doctoral project, an automated approach was developed in fluid, on cells. After introducing the system and the developments required, we demonstrate the approach on fixed and living bacteria as well as on epithelial cells. The usage of multi-sample automation allows gathering a greater number of samples with limited user interaction. Finally, further developments are discussed to lead the path toward higher-scale AFM automation of live samples.

Keywords Atomic Force Microscopy, PeakForce Tapping, Microbiology, Automation, Living cells, Multi-Sample.

Résumé

Assez rapidement après son apparition à la fin des années 1980, la Microscopie à Force Atomique (AFM) a démontré des perspectives prometteuses d'applications biomédicales. À l'heure actuelle, elle permet l'étude d'échantillons biologiques allant de la molécule unique à la cellule vivante proche des conditions physiologiques. Bien qu'étant applicable aux cellules eucaryotes et procaryotes, elle est entravée par son faible débit. Alors qu'elle peut être fortement automatisée sur certains échantillons bien caractérisés en air, l'automatisation de l'AFM en liquide reste rare, en particulier en multi-échantillon. Lors de ce projet doctoral, une approche automatisée a été développée pour l'étude des cellules en milieu liquide. Après une introduction du système et des développements nécessaires, nous démontrons l'approche sur des bactéries fixées et vivantes, ainsi que sur des cellules épithéliales. L'utilisation d'automatisation multi-échantillon permet d'augmenter le nombre d'échantillons analysés tout en limitant les interactions avec l'utilisateur. Enfin, les développements ultérieurs sont discutés pour aller vers un système automatisé à plus grande échelle sur échantillons vivants.

Mots-clés Microscopie à Force Atomique, PeakForce Tapping, Microbiologie, Automatisation, Cellules Vivantes, Multi-Échantillon.

Résumé

Le but principal du travail présenté consiste en le développement d'un système de microscopie à force atomique (AFM) automatisé adapté à un usage multi-échantillon sur cellules vivantes. Il a été réalisé au sein du groupe de Microbiologie Cellulaire et Physique de l'Infection (CMPI) du Centre d'Infection et d'Immunité de Lille (CIIL). Ce projet est issu d'une convention CIFRE de l'ANRT avec l'entreprise Bruker. Le présent manuscrit, clôturant ce volet du projet, est séparé en deux parties rassemblant neuf chapitres.

La première partie débute par une introduction détaillée de la microscopie à force atomique, au chapitre 2. Elle est alors suivie du chapitre 3, présentant des notions de biologie et des exemples d'applications de l'AFM dans ce domaine. Enfin, les défis actuels liés à ces applications sont présentés avec un état de l'art sur leurs solutions potentielles dans le chapitre 4. Ce dernier conclut sur l'importance d'augmenter le débit de l'AFM sur cellules. En effet, les mesures considérées n'ont de sens que sur un ensemble de cellules et la précision de celles-ci dépend du nombre de cellules prises en compte. Afin d'augmenter ce nombre, il y est montré la nécessité d'apporter de l'automatisation aux systèmes AFM, ainsi que l'avancée de la technologie dans ce domaine.

La seconde partie de ce manuscrit présente donc un système permettant l'analyse multi-échantillon automatisée par AFM d'échantillons biologiques. Le chapitre 5 présente alors les impératifs d'un tel système. Ensuite, le chapitre 6 développe les bases de ce système d'un point de vue du matériel, d'un moteur de scripts et d'un outil d'analyse des données. Ces trois éléments clés mis en œuvre, l'automatisation en tant que telle peut être

développée. Ses particularités liées au type d'échantillons utilisé sont discutés au chapitre 7. Les problématiques liées à l'apparition de bulles d'air à proximité du levier, à la détection des cellules, ainsi qu'aux contaminations y sont discutées.

Le fonctionnement du système est ensuite démontré au chapitre 8 sur le point de sa capacité à scanner de nombreuses cellules et entre plusieurs échantillons sur cellules procaryotes fixées *Yersinia pseudotuberculosis*. La démonstration est ensuite portée sur des cellules vivantes de type *Mycobacterium bovis BCG*. Finalement, le système est utilisé sur des cellules eucaryotes, issues de l'épithélium pigmentaire rétinien (RPE-1).

Ensuite, des développements futurs sont étudiés et discutés dans le chapitre 9. Y sont discutés le contrôle de position des cellules, le changement de fluide, le contrôle en température et le contrôle qualité de la pointe.

Pour terminer, le chapitre 10 rassemble la conclusion ainsi que les développements pressentis et suggérés à court, moyen et long terme.

L'automatisation permet d'augmenter le nombre d'échantillons scannés, ce qui est nécessaire pour lever l'un des problèmes majeurs de l'AFM sur cellules vivantes : la faible signification statistique parfois rencontrée, limitant ainsi sa reproductibilité. La capacité du système à travailler en multi-échantillon permet aussi de limiter les variations d'un échantillon à l'autre, améliorant la comparabilité des résultats.

Contents

1. Preface	1
1.1. Motivation	1
1.2. Stakeholders	2
1.3. Structure of the Dissertation	3
I. Introduction	5
2. Atomic Force Microscopy	6
2.1. Operation	8
2.1.1. Probe	8
2.1.2. Tip	10
2.1.3. Piezoelectric Actuators	12
2.1.4. Detection Mechanism	15
2.2. Standard AFM Modes	16
2.2.1. Imaging Modes	16
2.2.2. Contact Mode	17
2.2.3. Oscillating Modes	18
2.2.4. Force Curves	19
2.2.5. Force Volume	23
2.3. AFM in Fluid	25
2.3.1. Relevant Landmarks	25
2.3.2. Sample Preparation	26
2.4. PeakForce	28
2.4.1. Off-Resonance Tapping	28
2.4.2. Pseudo Force Curves	29
2.4.3. Operation	31
2.4.4. Hydrodynamic Effects	32
2.4.5. ScanAsyst	34
2.5. Artifacts	35
2.5.1. Hysteresis and Creep	35
2.5.2. Convolution	37

Contents

2.5.3. Double Tip	39
2.5.4. Force Deformation	40
2.5.5. Parachuting	41
2.5.6. Sawtooth	41
2.5.7. Horizontal Lines	42
2.5.8. Diagonal Stripes	43
2.5.9. Other Artifacts	43
2.6. High-Speed AFM	43
3. Biology and Relevant Applications	45
3.1. The Cell	45
3.2. Eukaryotic Cells	46
3.2.1. Membrane	48
3.2.2. Intracellular Components	49
3.2.3. Extracellular Matrix	52
3.2.4. Epithelial Cells	52
3.3. Prokaryotic Cells	52
3.3.1. Cell Envelope	53
3.3.2. Mycolata	56
3.3.3. Model Samples	57
3.4. Understanding Diseases	60
3.4.1. Pathogens	61
3.4.2. Drugs	61
3.4.3. Antibiotics	61
3.4.4. Antibiotic Resistance	62
3.4.5. Cancer	63
3.5. AFM Applications	64
3.5.1. Biological Conditions	65
3.5.2. High-Resolution	66
3.5.3. Cell Mechanics	66
3.5.4. Single Cell Analysis	69
3.5.5. Monitoring	70
4. Challenges and Current Solutions	73
4.1. Trueness	74
4.1.1. Deflection Sensitivity	75
4.1.2. Spring Constant	77
4.1.3. SNAP	79

Contents

4.2. Precision	80
4.2.1. Corresponding Problems	82
4.3. Faster Scanning	83
4.3.1. Fixed Time	84
4.3.2. Variable Time	84
4.4. Parallel Scanning	86
4.5. Unattended Scanning	90
4.5.1. Automated Steps	90
4.5.2. Automated Scan	93
4.5.3. Automated Systems	94
II. Results	98
5. Objectives and Requirements	99
5.1. Requirements	100
5.1.1. Scan	102
5.1.2. Correlation	102
5.1.3. Automation	103
5.1.4. Multi-Conditions	105
5.1.5. Cell Survival	105
5.1.6. Work Hypothesis	107
6. Methodology	109
6.1. Multi-Well	109
6.1.1. Design	109
6.1.2. Sample Preparation	112
6.1.3. Developments	112
6.2. Script Engine	114
6.2.1. Editor	115
6.2.2. Python Engine	115
6.2.3. NanoScope Package	117
6.3. Analysis Toolbox	118
6.3.1. Analysis Issue	118
6.3.2. Manufacturer Programs	119
6.3.3. Other Programs	119
6.3.4. Direct Opening	122
6.3.5. NS Python Toolbox	123

7. Live Cell Automation	125
7.1. Specialized Scripting Tools	125
7.1.1. Movement Control	125
7.1.2. Experiment	127
7.2. Issues and Solutions	132
7.2.1. Bubbles	132
7.2.2. Cell Detection	139
7.2.3. Contamination Detection	140
8. Demonstration	141
8.1. Multi-Cells	141
8.1.1. Sample Preparation	141
8.1.2. Setup	142
8.1.3. Results	142
8.2. Multi-Conditions	146
8.2.1. Sample Preparation	147
8.2.2. Analysis	147
8.2.3. Results	151
8.2.4. Conclusion	153
8.3. Living Cells	153
8.4. Eukaryotes	154
9. Further Developments	162
9.1. Controlling Cells Position	162
9.1.1. Chemical Binding on Mammalian Cells	163
9.1.2. Chemical Binding on Bacteria	163
9.1.3. Physical Confinement on Bacteria	165
9.1.4. Hybrid Systems	165
9.1.5. Interest	165
9.2. Fluid Exchange	166
9.2.1. Fluid Evaporation	166
9.2.2. Implementation	168
9.3. Heating	171
9.4. Tip Control	175
10. Conclusion and Future Outlook	181
10.1. Conclusion	181
10.2. Future Outlook	184
10.2.1. Short Term	184
10.2.2. Medium Term	186

10.2.3. Long Term 187

Appendix 191

A. Protocols 191

A.1. Consumables 191
 A.2. Coverslip Pre-Treatment 191
 A.3. *Yersinia pseudotuberculosis* 191
 A.3.1. Culture 191
 A.3.2. Treatment 192
 A.3.3. Plating 192
 A.4. Mounting 192
 A.5. Default Setup 193

B. Accuracy 195

B.1. Precision 195
 B.2. Trueness 196
 B.3. Accuracy 196

C. Models 198

C.1. Contact Models 198
 C.1.1. Elastic Models 199
 C.1.2. Hertz 200
 C.1.3. Sneddon 201
 C.1.4. Adhesive Models 201
 C.1.5. Thin Samples 202
 C.2. Tomography 202
 C.2.1. Stiffness Tomography 202
 C.3. Contact Point 203

D. Computing Science 205

D.1. Dynamic Link Libraries 205
 D.2. .NET 205
 D.3. Python 206
 D.3.1. IronPython 207
 D.4. IronPython to CPython Bridge 207

E. Developments Summary 209

E.1. Biological Medium 209

Contents

E.2. Biocompatibility	209
E.3. Limited Handling	210
E.4. Environmental Control	210
E.5. Light and Visibility	211
E.6. Immobilization	212
E.7. Fluid Exchange	212
E.8. Suitability for Cells	213

1. Preface

1.1. Motivation

Bacterial resistance to antibiotics are a major health-care issue as the pharmaceutical industry fails to keep up with the production of new drugs to compensate for the obsolescence of the current ones. Therefore, approaches other than a direct targeting of the pathogen are required, such as the study of the host-pathogen interactions in order to act on the mechanisms of the host. Shifting the targeting from the pathogen to its interactions with the host would bypass the currently existing pathogen resistances and could consequently be of great use against multi-resistant strains.

An understanding of these interactions can come from their comparison with and without gene editing or drug injection, which can be performed by screening techniques. Basic screening techniques have a single color per well depending on the viability of the cell. It yields a unidimensional “color” signal for each well, which is a very limited, almost binary, information for each drug-host-pathogen triplet. They can, however, be recorded very quickly. These very-high-throughput but low-content techniques could, therefore, only be used in the very first step of the screening process, where the throughput has to be maximized in order to keep a few hits for the subsequent, higher content but lower throughput techniques. High Content Screening with super-resolution imaging techniques can then be performed in order to gain more information of the combinations of interest while keeping a relatively high throughput.

Afterward, the new hits can be studied further with higher-content tech-

1. Preface

niques, such as Atomic Force Microscopy, Electron Microscopy, or other kinds of super-resolution microscopy. These techniques, offering the highest resolution imaging along with information on the local compositions or properties, are however much more operation intensive. They suffer, as a consequence, from a much slower throughput. It is especially the case for Atomic Force Microscopy, which is therefore still very uncommon in the study of microbiology and pathogeny. Correlative setups, merging together two or more of the techniques mentioned above, can bring the most quantitative and qualitative information on a microbiological system, at the expense of being prohibitively slow.

Therefore, we focused our work on the development of biomedically-relevant tools and applications for Atomic Force Microscopy that are centered around multi-sample analysis. During the three years leading to this thesis were developed innovative hardware, software, and methodological solutions for the sake of bringing Atomic Force Microscopy on Live Cells from a very low throughput to a medium one. Aside from pointing towards a high-content technique as mentioned above, such improvements can have a shorter-term positive impact on simply improving the statistical significance of AFM studies, which is one of its current shortcomings.

1.2. Stakeholders

This project was sponsored by France's National Association for Research and Technology (ANRT) under an Industrial Agreement of Training through Research (CIFRE) Program between a laboratory, the CMPI, and a company, Bruker. The CMPI—the Cellular Microbiology and Physics of Infection group—investigates host-pathogen interactions in the realm of infectious diseases, in particular regarding the autophagy activation as a response to infection. It uses a multidisciplinary approach based on AFM and super-resolution microscopy with a focus on the elastic properties of cells. The CMPI research group is part of the Center for Infection and Immunity

of Lille, on the campus of the Pasteur Institute of Lille, France. Bruker, on the other hand, is a high-performance scientific instruments manufacturer, operating mostly on molecular-scale technologies. It possesses, in particular, a great expertise in the manufacturing and development of Atomic Force Microscopes at its facilities in Santa Barbara, California, U.S.A, where parts of this project were carried out. As a joint venture between the two, this work benefited from both of their means and expertise.

1.3. Structure of the Dissertation

Part I of the dissertation will give an introductory overview, introducing Atomic Force Microscopy (Chapter 2) followed by biology and the corresponding applications (Chapter 3). Afterwards, we will discuss the ongoing challenges of AFM on biological matter and review existing solutions (Chapter 4). In particular, we will see the importance of sample sizes and develop on the necessity of going towards a multi-sample system.

In Part II, we will then describe a system developed to detect and scan cells autonomously. This leads us towards higher-throughput applications related to the biomedical, pharmaceutical, and other health-related fields. We will first go through the requirements of such a system in the section below before presenting our setup. This system is composed of a Multi-Well for the hardware as well as a script engine and a data analysis toolbox for the software, which are the basic methodological elements described in Chapter 6. Based on these elements, a range of domain-specific scripts have been developed for the general workflow and to solve specific issues, the topic of Chapter 7.

This system is then demonstrated in Chapter 8 on multiple cells of a sample and on multiple samples on fixed cells, then shown to be applicable to live cells and eukaryotic ones. After that, Chapter 9 introduces potential further developments for which proofs of concepts have been developed but not integrated into the main system. Chapter 10 finally closes the

1. Preface

dissertation with the conclusion and a discussion on the path towards the desired high-content medium-throughput system.

Part I.

Introduction

2. Atomic Force Microscopy

The fields of biology and medicine would still be far behind if it was not for the microscope, as microorganisms are too small for the human eye to see. Crude lenses having existed since antiquity, microscopy appeared as such in the seventeenth century, with Antonie van Leeuwenhoek, who built the first prototypes of optical microscopes, allowing him to observe the first unicellular organisms. Nowadays, this flavor of microscopy is still considered as an entry-point to the observation of microorganisms, as its functioning is close to the way our vision works, making it easier to interpret for the untrained eye.

Optical microscopy improved over time, allowing for high-resolution imaging, until reaching resolutions no longer limited by the quality of the optics but by a fundamental behavior of light: diffraction. Light, as a wave, is characterized by its wavelength (λ) and interacts in such a way that it loses its intuitive ray-like properties when the resolution approaches the scale of the wavelength. It is not possible to resolve elements smaller than about $\lambda/2$, which corresponds to a limit at 200 nm for visible light. This can be overcome by using waves of higher frequencies, such as X-rays. A higher frequency is, however, related to a higher energy, causing consequent harm to the sample.

Fluorescence microscopy overcomes some of these limitations by the use of fluorescent probes that specifically bind to elements of interest. While the resolution limit is still the same, it alleviates the need of recognizing the elements of interest in the image, the whole resolution being then used to detect their position, and sometimes structure. Furthermore, if the fluorescent probes are scarce enough to appear as separated dots in

2. Atomic Force Microscopy

the image, their location can be algorithmically recovered with a resolution an order of magnitude better, which is the base of the PALM and STORM techniques. Rather than using an algorithmic reconstruction, other methods use an extremely localized illumination scheme to push the resolution below the diffraction limit, as done initially in confocal and then STED microscopy. Still, the highest resolution is limited to several tens of nanometers, whereas many biological processes—especially in the realm of interactions between cells (prokaryotes and eukaryotes alike) or with their environment—happen at the nanometric scale.

The introduction of the scanning electron microscope (SEM) and the transmission electron microscope (TEM) allowed sub-nanometric resolution, creating therefore another breakthrough in the study of surfaces. The electron microscope, created by Ruska and Knoll in 1931, uses electrons deflected by magnetic coils acting as electromagnetic lenses, thanks to the wave properties of particles. Electron having a wavelength hundreds of thousands of times smaller than photons, they allow for such a better resolution. While allowing huge advances in our understanding of biological processes, electron microscopy requires fixing and contrasting the sample. It is, therefore, not suitable to image living samples.

Both optical and electronic microscopies mentioned above use a beam (of photons or electrons) going from a source to a detector via a sample. Because of the distance separating the sample and the detector, these are considered as “far-field” microscopes. In the eighties came the scanning tunneling microscope (Binnig, Rohrer, et al., 1982), first of the scanning probe microscopes, which act on a completely different paradigm in that a measurement is taken at the local level with a probe extremely close to the sample. This paradigm belongs to the realm of “near-field” microscopy, which removes the problem of the diffraction limit all together. In the case of the STM, a voltage difference is applied between the sample and the tip, which creates a tunneling current. While raster-scanning the sample, the tip moves up and down to keep the tunneling current constant.

The STM requires, however, to work on a conducting sample, which is

2. Atomic Force Microscopy

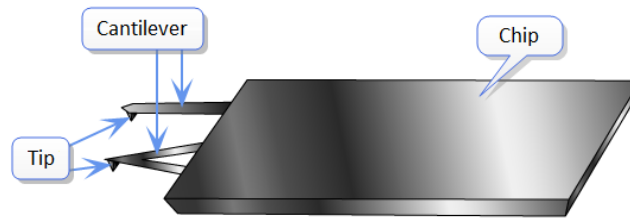


Figure 2.1.: AFM probe, composed of a tip at the end of a cantilever attached to a chip. Both a rectangular (right) and a V-shaped (left) cantilevers are represented. © Bruker, modified.

quite restrictive. This constraint led to the development of the AFM (Binnig, Quate, and Gerber, 1986), which uses the force between the sample and the probe at the atomic level, removing the need for a current and thus bringing the possibility of working on non-conducting surfaces. The probe, in this case, is composed of a tip mounted on a flexible cantilever, which act as a spring when touching the sample.

Atomic-scale AFM appeared less than a year later (Binnig, Gerber, et al., 1987). AFM is now used for R&D purposes on a lot of disciplines. These include solid-state physics, electro and polymer chemistry, as well as molecular and cell biology. It is also used for calibration purposes and quality control in the semiconductor and instrumentation industry.

2.1. Operation

The AFM is essentially composed of a probe, a sample, and a system to control and measure their relative movements. In a first time, we will assume here a hard macroscopic sample, unless otherwise specified.

2.1.1. Probe

The probe, illustrated in Figure 2.1, is made of a cantilever at the end of which lies a tip. Both are most often microfabricated from silicon nitride

2. Atomic Force Microscopy

or silicon. The cantilever is bonded to a millimeter chip, or substrate, to allow easy handling and its attachment to the system.

Cantilevers are usually long, thin rectangular beams or composed of two beams making a V shape. When a perpendicular force is applied at its end, the cantilever acts like a spring. It follows Hooke's law, which states that the vertical displacement of the end of the beam (or deflection, d) and the applied force (F) follow a constant ratio, named the spring constant (k):

$$F = k \times d. \quad (2.1)$$

In this document, we will consider the force and the deflection as positive when directed upwards.

Aside from their spring constant, cantilevers are characterized by their resonant frequency ν_0 . Both of these physical properties depend on the shape and the dimensions of the cantilever as well as the mechanical properties of the materials used for its fabrication, leading to a diversity in cantilever shapes and dimensions. In particular, for a rectangular cantilever with a constant rectangular cross-section, we have:

$$k = \frac{Ewt_c^3}{4L^3} \quad (2.2)$$

and

$$\nu_0 = 0.1615 \frac{t_c}{L^2} \sqrt{\frac{E}{\rho}}, \quad (2.3)$$

where w is width of the cantilever, t_c its thickness, L its length, with E and ρ being respectively the Young's modulus and the density of its material. Nonetheless, small variations—especially on the thickness—can have a strong effect on the resulting properties, making the use of these formula unpractical for calibration purposes. Typical dimensions of the beams are 100 μm to 200 μm for the length, 20 μm to 40 μm for the width, and 0.5 μm to 1 μm for the thickness (Butt, Cappella, and Kappl, 2005).

One may note that both the spring constant and the resonant frequency increase with E and t_c and decrease with L . These two parameters tend,

2. Atomic Force Microscopy

therefore, to correlate positively. Soft cantilevers are, however, required to avoid deforming or damaging the sample when imaging while a low resonant frequency of the cantilever limits the scanning speed. The requirement for soft cantilevers with high resonant frequencies for rapid applications led then to the design of particular cantilever geometries. For example, very small but comparatively soft cantilevers are used for high-speed applications. As we will see in Section 2.2.4, the spring constant is further constrained for nanomechanical measurement, where the stiffness of the cantilever and the sample should be similar.

There might be more than one cantilever on the substrate, although only one can be used at a time. The chip, along with the cantilever, is tilted forward with an angle usually ranging from 7° to 20° to allow the tip to be slightly below the rest of the probe. It allows for the tip to be the first element to get in contact with the sample when lowered to it, as described further below.

2.1.2. Tip

The tip, shown in Figure 2.2, is the centerpiece of the instrument, as it is directly in contact with the sample. Its shape determines the resolution of the image (Abraham, Batra, and Ciraci, 1988), which is a “convolution”* of the object surface by the shape of the tip.

As a consequence, the ideal tip shape for image resolution would be an infinitely thin and sharp tip at an angle compensating the tilt of the probe so that it touches the sample vertically. Even though carbon nanotube tips following that design have been developed in labs and used for high-resolution imaging of fixed cells (Koehne et al., 2011), it is not usable in practice as they are extremely brittle and can pierce through soft matter. A more common tip shape is a pyramid with a deltoid base, which can be microfabricated with steep angles and where the end can be further

*It is actually not equivalent to a mathematical convolution, but this will be discussed in Section 2.5.2.

2. Atomic Force Microscopy

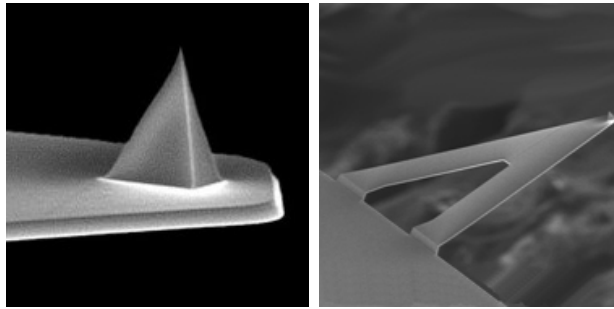


Figure 2.2.: ScanAsyst-Fluid probe. Scanning Electron Microscopy images of the tip (left) and cantilever (right), taken upside down. © Bruker.

sharpened by etching. While less brittle, the sharpness of this design is still unsuitable for scanning live cells.

When measuring the mechanical properties of locally homogeneous and flat materials, large and well-characterized shapes are needed. The resulting data can then be analyzed by fitting it to a contact model, such as described in Appendix C.1, most of which being based on the Hertz model (Hertz, 1882). Such shapes include the square pyramid, sphere, paraboloid, cone, or cylinder, usually with dimensions ranging from one to a few micrometers at their base. Spherical tips, or colloidal probes, usually have a diameter ranging from $2\ \mu\text{m}$ to $20\ \mu\text{m}$ and have particularly well-characterized models (Butt, Cappella, and Kappl, 2005).

For applications where the mechanical properties are recorded locally to form a nanomechanical “image” of the sample, a trade-off has to be found between the locality of the probe and its characterization. Some well-characterized shapes such as the square pyramid and the cone might be suitable under certain conditions while spherical and cylindrical are inadequate for imaging. More complex tip geometries can then be used, such as diamond-shaped ones with a spherical cap end to allow both a high resolution and a good characterization.

Although it is often made out of the same material as the cantilever,

2. Atomic Force Microscopy

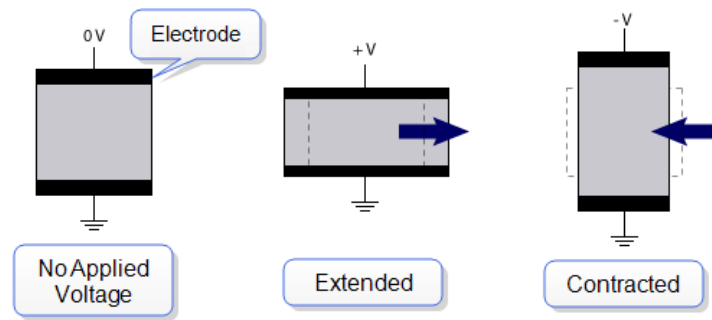


Figure 2.3.: Piezo extension and retraction, depending on the applied voltage. © Bruker.

other materials can be used for specific applications. As an example, diamond tips are often used on very hard samples.

Tips are characterized by their tip radius, which ranges from less than 1 nm in the case of atomically sharp probes to 20 μm for colloidal probes.

2.1.3. Piezoelectric Actuators

High-resolution scanning is made possible by the use of piezoelectric transducers, also called positioners, scanners, or actuators, usually named piezos. Thanks to their atomic structure, piezoelectric materials have the property of changing their shape depending on a voltage applied to their extremities. The actuators are made by placing electrodes on two opposite sides of the material and applying a voltage difference between the two. Depending on the orientation of the voltage difference, the piezo will contract or retract along the corresponding axis (here, the vertical one).

A relation can be established between the relative displacement and the voltage difference, although it is affected by hysteresis and creep, which have to be controlled, minimized, and/or taken into account by the controller and the software. The piezos have the opposite movement in the two other axes (here, the horizontal and out-of-plane axis). In the case shown in Figure 2.3, applying a positive voltage on the top electrode will

2. Atomic Force Microscopy

contract the piezo vertically and expand it horizontally whereas a negative voltage will have the opposite effect. Several piezos are used to control the movement of the probe relative to the sample in the X, Y, and Z direction. The X and Y scanners control the movements parallel the plane of the sample, whereas the Z one is perpendicular. Since only their relative positions matter, the scanners can either be placed to actuate the tip or the sample. In the Dimension FastScan AFM, used for most of the work presented further, the three scanners control the tip. Some other systems, however, have the horizontal (X-Y) or all scanners controlling the sample.

Because of the complexity of the non-linear relation between the voltage and the displacement, it is difficult to blindly control the position of the tip with a great confidence. Thankfully, the piezoelectric effect can also generate a voltage difference from a displacement and can, as such, bring us to piezoelectric sensors. A first application of these sensors is to record the actual displacement and take it into account in the analysis. With sufficiently fast electronics, however, it is possible to use the measurement as a feedback to correct the applied voltage in real-time in what is known as “closed loop”.

In this configuration, the actuators, the probe, the sample, and the optical lever are connected with a feedback circuit, represented in Figure 2.4. A controller records the deflection signal from the microscope and processes it. It then controls the (vertical) Z piezo actuator to keep the deflection at a certain setpoint. It should be noted that, while allowing a better control of the position, this technique can introduce some additional noise in the system.

When properly calibrated, piezoelectric actuators and sensors can perform or record displacements with precisions of the order of the Ångström ($1 \text{ \AA} = 0.1 \text{ nm}$).

2. Atomic Force Microscopy

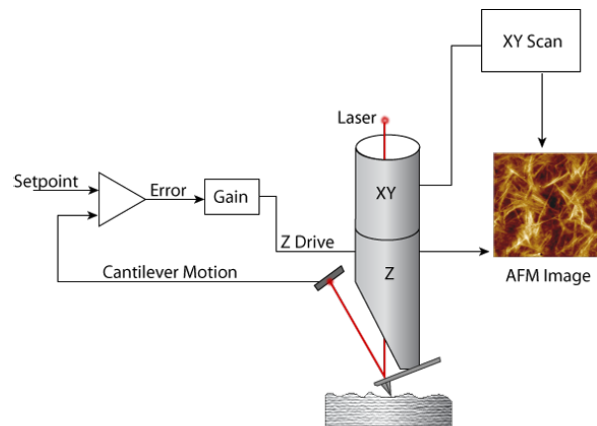


Figure 2.4.: Feedback loop. As the X and Y piezos are raster-scanned on the sample, the cantilever motion is continuously compared to a setpoint to correct the position of the vertical Z piezo, realising the data. © Bruker.

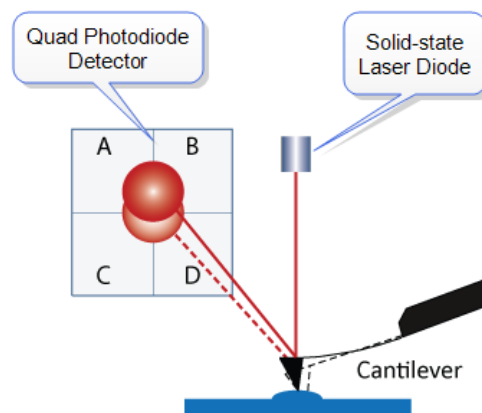


Figure 2.5.: Optical lever system. A laser is bounced on the back of the cantilever and targeted on a four-quadrants photodetector. A deflection of the cantilever, here due to the substrate, creates a displacement of the laser spot on the detector. © Bruker

2.1.4. Detection Mechanism

As described above, the tip is mounted on the end of a long thin cantilever. Interaction forces between the sample and the tip will induce a deflection of the cantilever, which, on most current AFMs, is recorded by an optical lever system by means of a laser beam. This laser beam is pointed on the back of the cantilever with a vertical incidence, close to the position of the tip. The back of the cantilever is often coated with metal, such as gold or aluminum, to improve its reflectivity.

As shown in Figure 2.5, the cantilever reflects the beam towards a photodetector composed of four photodiodes, which translate the intensity of light they receive into a voltage. The laser is originally aligned to fall in the center of the photodetector, with an equivalent coverage of all the photodiodes so that they all output similar voltages. In practice, mirrors are used to align the elements of the optical lever without moving them physically. Lenses and other optics are also used to better focus the laser spot on the cantilever.

The laser source, the cantilever, and the photodetector form an optical lever. Assuming small displacements, the deflection of the cantilever will change the bending angle proportionately. The vertical incidence of the laser makes it close to perpendicular to the cantilever so that the laser spot stays at the same position, reflecting it towards the photodetector proportionally. Therefore, the position of the laser spot on the photodetector changes linearly with the deflection.

In the pictured case, the cantilever and the beam are deflected upwards, increasing the intensity of light received by diodes A and B and decreasing the one received by C and D proportionately. The ratio

$$d_V = \frac{A + B}{A + B + C + D}, \quad (2.4)$$

is then directly proportional to the deflection and usually assimilated as such and considered as the deflection “in Volts”. This value, along with

2. Atomic Force Microscopy

the signal from the Z sensor, is recorded by the controller and sent to the computer, where it can be processed as developed below, displayed as an image or curves, and saved.

The relationship between the deflection in distance units d and this value can be expressed as:

$$d = d_s \times d_V, \quad (2.5)$$

where d_s is the deflection sensitivity, a constant that is measured during the calibration of the system.

To record the vertical deflection of the cantilever, two photodiodes would suffice, merging A-B and C-D. Splitting the photodetector into four quadrants allows, however, better centering the laser spot at its center. The difference in laser intensity between the two left segments and the two right ones allows us to record a horizontal signal, which quantifies any lateral or twisting motion of the tip that can be used for recording friction.

The first AFMs, however, used a method based on the scanning tunneling microscope. Essentially, the tip and cantilever were simply a “mobile coating” of the sample. Rather than coating the sample before scanning it with the STM, a tip and cantilever were added to the end of the STM. When being in contact with the sample, the cantilever acted like the metallic coating allowing the tunneling effect while keeping the sample intact.

2.2. Standard AFM Modes

2.2.1. Imaging Modes

During imaging modes, the feedback loop is used to adapt the tip position to the height of the sample in order to keep constant the interactions between the two. The tip is raster-scanned on the sample, usually with a fast linear movement along one axis, called the fast axis. As represented in Figure 2.6, this movement is repeated back and forth while a slow linear movement along the other, slow axis is performed. The back and forth

2. Atomic Force Microscopy

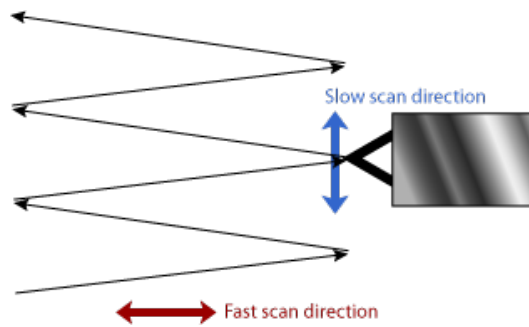


Figure 2.6.: Raster-scan motion. The probe and the sample are scanned against each other along one axis, the fast scan direction, while moving at a slower pace along the slow scan axis, or direction.
© Bruker

movements along the fast axis are called “trace” and “retrace”, respectively.

The image obtained correspond to the topography of the sample, plus a “convolution” of the tip shape, the deformation of the sample caused by the scanning, and instabilities in the feedback system, among others common artifacts described below.

2.2.2. Contact Mode

As a simple application of a feedback loop on the deflection of the cantilever, contact mode (Hansma, Elings, et al., 1988) is the earliest imaging mode of AFM. It raster-scans the tip over the sample while adjusting the height to keep the cantilever deflection (hence the force) at the user-defined setpoint. It usually generates two images: the vertical position of the piezo at each X-Y position, and the deflection error (i.e. the difference between the deflection and the setpoint). If the deflection error is small, the piezo height map gives the sample topography, considering the artifacts described below. A strong disadvantage of contact mode is that it can also deform or displace the sample by the strong lateral forces due to the friction of the tip on the surface.

If the fast axis is taken perpendicular to the cantilever, the cantilever can

2. Atomic Force Microscopy

be twisted laterally by the friction forces opposing the movement of the tip on the sample. This movement translates to a horizontal displacement of the laser reflection on the photodetector, which can be recorded as a third set of data.

Contact Mode can also be used at constant height, where the deflection is recorded but not used as feedback for the piezo extension. It can allow higher scan speeds since there is no need for feedback. It is, however, restricted to very flat samples, which strongly limits its applications in biology.

2.2.3. Oscillating Modes

As the constant contact between the tip and the sample generates strong shear constraints on the latter, intermittent contact and non-contact modes were developed shortly after.

The vertical piezo (or a dedicated extra piezo) is oscillated close to the resonant frequency of the cantilever. Thanks to the resonance effect, the oscillation of the end of the cantilever is much bigger than the oscillation applied at its base by the piezo, the ratio between the two being the Q -factor. The cantilever is bent upward and downward at that frequency, creating oscillation of the deflection as recorded by the photodetector.

The idealized case only works in vacuum, however, with Q -factors ranging from 10^4 to 10^8 although its use in air is very close and quite simple, with still decent Q -factors ranging on the order of 10 to 200. The resonance in fluid, on the other hand, is strongly affected by the fluid drag, which makes the technique much more challenging as the Q -factors can be much smaller than 1 (Butt, Cappella, and Kappl, 2005).

The effective resonance frequency of the cantilever and the Q -factor depend, however, on the forces applied to the tip. As a consequence, recording shifts in amplitude, phase, or frequency can inform about changes in these forces due to the proximity of the sample. By enabling a feedback loop on one of these channels, one can generate a topography image in a similar

2. Atomic Force Microscopy

fashion as in contact mode.

Martin, Williams, and Wickramasinghe (1987) developed the first non-contact technique, where the tip was oscillated with an amplitude of up to 5 nm close to the surface. In the presence of non-contact interactions, such as the attractive van der Waals force when working close to the atomic scale, a force gradient exists close to the surface. This gradient modifies the amplitude of the oscillation, which is used for the feedback.

Although it presents the advantage of not touching the sample, hence not damaging it at all, non-contact mode only works within a narrow range of tip-sample distances. When the tip gets too close to the sample, it sticks to it and the scanning is blocked. Zhong et al. (1993) then introduced a similar concept of intermittent contact on amplitude modulation, or tapping mode, where the amplitude is much larger, typically between 20 and 100 nm. Intermittent contact with the sample allows the tip to move while not in direct contact with the sample, thus virtually eliminating the shear stress.

2.2.4. Force Curves

Contact and oscillating modes are interesting to explore the topography of a sample. Alternatively, rather than raster-scanning the sample along the horizontal axes while updating the vertical position to track the sample surface, one might want to focus on a given horizontal position and observe the reactions of the sample as it is probed.

To do so, the probe starts at a position above the surface and is lowered by the Z piezo towards the sample. At some point, the probe gets in contact with the sample and the repulsive forces applied to the tip increase until the deflection of the cantilever reaches a threshold (or trigger). This triggers the retraction of the Z piezo to an elevated position. The downward movement is called the approach or extension, the upward one is the retraction. During both the approach and the retraction, the deflection of the cantilever and the vertical position of the piezo are recorded.

Recording the deflection as shown in Equation (2.5) and using Hooke's

2. Atomic Force Microscopy

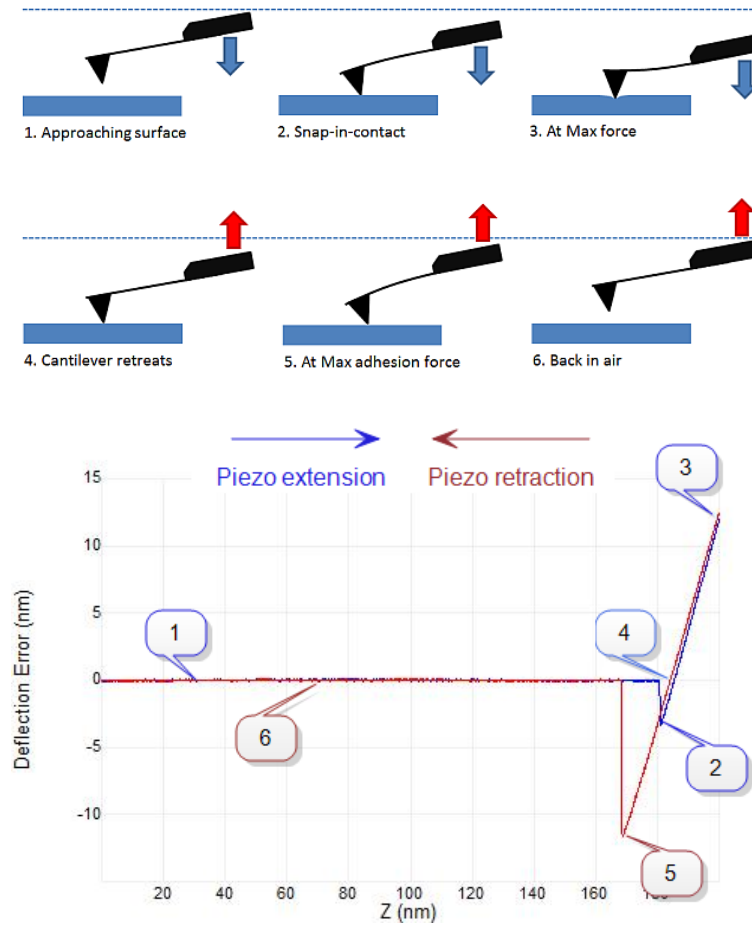


Figure 2.7.: Force curve. Left: path of the cantilever. Right: corresponding force curve. 1: non-contact approach. 2: snap-in contact. 3: trigger force. 4: zero-force contact. 5: maximum adhesion force (snap-off contact). 6: non-contact retraction. © Bruker, modified.

2. Atomic Force Microscopy

law given in Equation (2.1), one can deduce the vertical force exerted on the tip once the deflection sensitivity and the spring constant have been calibrated. Knowing the force as a function of the distance during the approach and retract phases can release Force *versus* Distance (or Force-Distance) relationships such as the one presented in Figure 2.7 that, once analyzed, can give quantitative information on mechanical properties (Butt, Cappella, and Kappl, 2005; Cappella and Dietler, 1999).

This distance is, however, the displacement of the probe as measured from the piezo and does not equate to the distance between the tip and the sample, which also depends on the deflection of the cantilever. Let this distance be

$$Z = Z_0 - d_p, \quad (2.6)$$

where Z_0 is the distance between the tip and the sample at the beginning of the approach, assuming no deflection of the cantilever nor the sample, and d_p the piezo displacement from the upper position. As d_p increase, Z decreases from Z_0 to 0 and will reach negative values when the piezo is extended past the contact point.

In this case, the tip-sample distance D can be expressed as

$$D = Z + d + \delta, \quad (2.7)$$

where δ is the indentation of the sample, as represented in Figure 2.8. When the tip and the sample are well separated, the deflection and the indentation are null and the distance equals the displacement: $d = \delta = 0$ and $D = Z$. Once the tip is in contact with the sample, at the scales used on cells (hence neglecting the variation in the interatomic distances), $D = 0$, and any further decrease in Z is balanced by an equivalent increase shared between d and δ . On an elastic sample and assuming equilibrium, δ obeys to Hooke's law as well, inducing

$$k_s \times \delta = F = k \times d \quad (2.8)$$

2. Atomic Force Microscopy

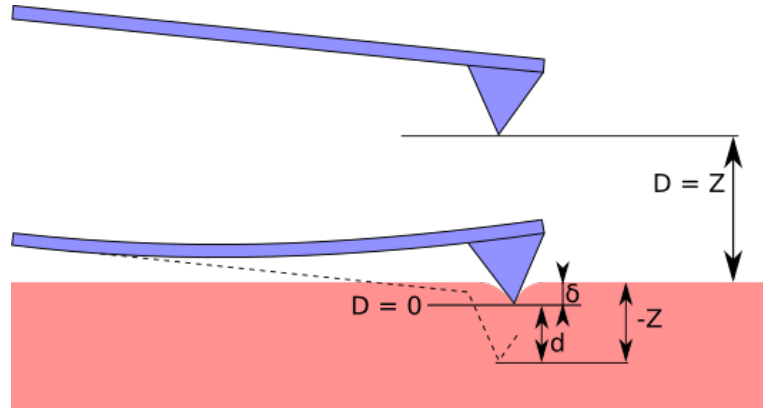


Figure 2.8.: Tip-sample distances, at a distance and in contact, as an illustration of Equation (2.7). D the actual distance between the tip and the (deformed) surface of the sample, Z the distance assuming neither sample deformation nor tip deflection, d the deflection of the tip, and δ the deformation of the sample.

where k_s is the apparent stiffness of the sample. The equality comes from the fact that the force exerted by the sample on the tip and the one by the tip on the cantilever are equivalent. It follows that, if the sample is much stiffer than the cantilever, $k_s \gg k$ causes $\delta \ll d$ and the sample is not indented in any meaningful way. This can be desired to scan the topography of the sample, although soft cantilevers cause other challenges. It is, however, not suitable for measuring mechanical properties, as they require an indentation of the sample, as shown below. Oppositely, if the cantilever is much stiffer than the sample, $k \gg k_s$ causes $d \ll \delta$ and the cantilever indents the sample without meaningful deflection, rendering the measurement—performed by recording the deflection—difficult.

The sample stiffness (k_s) can be calculated from the knowledge of the force and the indentation, which only requires the force curve data and the contact point as described in Appendix C.3. While the stiffness does not require any further assumption, it is not an intrinsic property of the material and depends on the shape of the tip as well as the indentation. In order to observe the underlying mechanical property of the sample, the

2. Atomic Force Microscopy

elasticity, it is necessary to make other assumptions and use a contact model, as is discussed in Appendix C.1.

In general, we are interested in the force as a function of the position of the tip compared to the reference position of the sample. This corresponds, when the tip and the sample are in contact, to the force as a function of the deformation of the sample. When the tip and the sample are separated, it is equivalent to the distance mentioned earlier. The separation is considered to be

$$S = Z + d, \quad (2.9)$$

which is similar to Equation (2.7), except for the fact that δ is not taken into account.

These force-separation, or -indentation curves can then be analyzed to yield information about the sample, at this position. The approach and retract curves are usually different, giving more complex information. On viscous samples, the relationship will also vary with the indentation speed, which brings extra information although no widely-accepted model exists to date. Depending on the model used, the analysis can also bring information on other properties, the relevance of which depends strongly on the application.

2.2.5. Force Volume

As represented in Figure 2.9, force volume acquires force curves over positions covering a 2D array. Compared to force curves, this significantly increases the quantity of data that can be analyzed, where force volume can be considered as a collection of force curves. Furthermore, since the points are taken along two axes, it allows seeing coherent patches on the surface, on the different channels.

This brings the interesting information from force curves, but on a 2D surface. It allows mapping properties as well as the topography. Already in the late 1990s, it allowed mechanical properties mapping with resolutions of 25 nm (Rotsch and Radmacher, 1997). The interest of measuring the

2. Atomic Force Microscopy

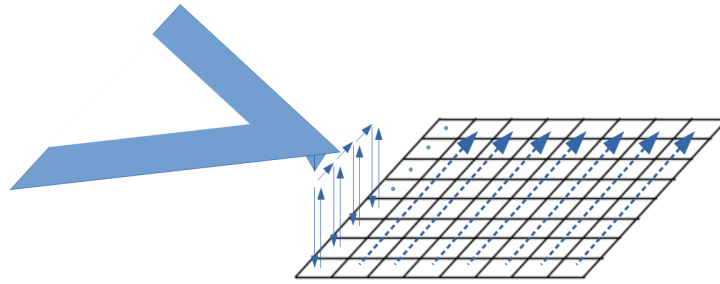


Figure 2.9.: Representation of force volume mode. The scan area is decomposed in a grid of pixels. For each line of pixels, the tip is sequentially approached and retracted in each pixel of the line, before going to the next.

mechanical properties are developed in Section 3.5. Visually, it is also possible to map the properties on the topography represented as a surface. Compared to basic imaging modes, it offers a good control of the force even for large scan size since it does not require to track the sample from one pixel to another. It does not create any shear forces and the vertical force is much better controlled than in tapping.

Nevertheless, as force volume mode requires a full approach-retraction curve for each pixel, it is much slower than imaging modes. With prior cantilever designs, a ramp frequency of 1 Hz was typical applied on cells when using ramps of 500 nm to have a proper indentation and ensuring a clean non-contact section while keeping the ramp speed under $1 \mu\text{m s}^{-1}$ to avoid overshoot, which happens when the system fails to retract sufficiently fast once the trigger threshold is met. At such a rate of one curve per second, a low-resolution, 16 by 16 pixels force volume takes already more than 4 minutes. Since the total number of pixels over the 2D image increases with the square of the resolution, a higher-resolution, 128 by 128 pixels force volume takes about 5 hours, which is too much for most applications. The speed has been increased dramatically over the last few years, thanks to improvements in the cantilever designs, the electronic components, and the

software.

2.3. AFM in Fluid

In biology, it is necessary to work in fluid for gaining relevant insight on the physiological states being studied. It also allows for weaker adhesion forces between the tip and the sample, so that smaller forces can be used for imaging, improving at the same time the resolution in force spectroscopy. On the other hand, working in fluid causes dragging forces when oscillating at medium to high frequencies. It reduces the Q factor when tracking the amplitude and adds background forces when tracking the deflection. This was illustrated by Janovjak, Struckmeier, and Müller (2005) on force spectroscopy. Cells are also very sensitive to forces and force control is critical for scanning soft elements, such as microvilli as done by Schillers, Medalsy, et al. (2016).

2.3.1. Relevant Landmarks

Scanning biologically-relevant samples brought in some more requirements to the first AFM, as designed by its creators. First, AFM had to be performed in fluid (Marti, Drake, and Hansma, 1987), which then led to AFM in aqueous solutions, made possible by the optical lever and the fluid chamber (Drake et al., 1989). These improvements allowed the scanning of living cells in the 1990s (Henderson, Haydon, and Sakaguchi, 1992; Le Grimellec et al., 1994; Radmacher et al., 1992), see the review by Ohnesorge et al. (1997).

With regard to the scanning modes, Binnig, Quate, and Gerber (1986) focuses on ramps, but contact mode was developed in the wake of its early development (Hansma, Elings, et al., 1988). Oscillating modes appeared a few years later, but these were more challenging in liquid (Zhong et al., 1993). Finally, biologically-relevant high-speed applications appeared in the early 2000s (Ando, Kodera, et al., 2001).

2.3.2. Sample Preparation

While able to work in biological conditions, one of the main drawbacks of AFM is that microscopic samples have to be immobilized on surfaces for scanning. In particular, the immobilization needs to withstand shear forces as the cantilever is scanned over the sample. Cells are presented in Section 3.1. Unless spontaneous, their immobilization can usually be achieved by chemical binding or physical confinement.

Eukaryotic Cells

Epithelial cells, such as the ones described in Section 3.2.4, simply have to be seeded and adhere easily. Their very soft nature allows them to have a good contact area with the substrate. Some other kind of cells are more difficult to immobilize but are not the focus of this project.

Yeast cells, such as *Saccharomyces cerevisiae*, do not spontaneously adhere but can be immobilized mechanically in porous membranes (Kasas and Ikai, 1995) or embedded in an agar matrix (Gad and Ikai, 1995). A hybrid chemical and physical immobilization method was also developed with microstructured, concanavalin A-functionalized PDMS stamps (Dague et al., 2011).

Prokaryotic Cells

Prokaryotic cells are difficult to immobilize, as their structure is more rigid than most eukaryotic cells, limiting the surface available for adhering with the substrate (Dufrêne, 2004). In most cases, the cells do not adhere naturally to the glass support enough to resist the forces applied by the cantilever, although very small, or stay stable during the scan.

One way to immobilize bacteria is to dry and rehydrate them, as the drying forces the interactions between the cell and the substrate. Although being one of the simplest—hence frequently used—method, it is one of the most damaging for the cell integrity. It leads to the decrease of their height

2. Atomic Force Microscopy

and width combined with the appearance of patterns at the surface, indicating a strong impact of the immobilization on their viability (Bolshakova et al., 2001). This strong impact can be useful to image topographical elements that would be otherwise invisible because too soft and motile, such as some flagella and pili, but it is necessary to keep in mind that the properties of the cell have been altered strongly (Gillis, Dupres, Delestrait, et al., 2012). Drying is therefore to be avoided and cell immobilization has to be artificially mediated, chemically or physically.

Chemical binding includes covalent binding. It can, for example, be performed by coating the substrate with 3-aminopropyltriethoxysilane (APTES). Its three ethoxy groups react with the hydroxyl groups from the glass surface to form a covalent oxygen bond between its silicon and the one of the glass. The APTES then becomes the surface of the glass, exposing its amine group. Crosslinkers, such as glutaraldehyde, can then be used to connect the amine groups of the substrate with the ones of the sample (Karrasch et al., 1993). Crosslinking should be avoided, however, as it changes the mechanical properties such as the stiffness and adhesion of the sample (Burks et al., 2003).

Non-covalent binding can be caused by poly-L-lysine (PLL) (Karrasch et al., 1993) or polyethylenimine (PEI) (Razatos et al., 1998), in which the adhesion is induced by charge differences between the cell surface and the substrate. Gelatin is another option, believed to act from a mix of hydrophobicity and the effect above (Doktycz et al., 2003). Adhesive proteins, such as Cell-Tak™ (BD Diagnostics), poly-dopamine, cyanoacrylate, and lectins such as concanavalin A, can be used as well (Louise Meyer et al., 2010; Ozkan et al., 2018).

Porous membranes, mentioned earlier for yeast cells, can also be used in bacteria, especially spherical ones (van der Mei et al., 2000). It should be noted that this technique could have been interesting to host our prokaryotic samples, rather than the glass coverslip introduced in Chapter 6. It has, however, its own limitation as it limits the accessible area to the emerging part of the cell. It also complicates the sample topography, hence the

2. Atomic Force Microscopy

detection procedure required to localize the bacteria.

No unique method works universally for all kinds of cells. Different methods perform differently depending on the cell type, the required medium (concentration of biological matter, composition, pH...), and the system requirements (such as a transparent support when using an inverted microscope) (Louise Meyer et al., 2010).

2.4. PeakForce

Given the shear forces of contact mode, the low force control of tapping mode, and the slowness of force volume, a mode avoiding their caveats was much needed. PeakForce Tapping, which performs super-fast pseudo force curves, presents the advantage of the force control of force volume, but with a speed much closer to the one of imaging modes.

Although technically an AFM mode, it is treated here separately as it is of particular importance for this work. It shares a lot of similarities with several of the other modes while being much more complex. The documentation around it is scarce or vague and its functioning tends to be poorly understood. For these reasons, it is often used with too much optimism and blind trust in its results or, oppositely, unduly criticized.

2.4.1. Off-Resonance Tapping

PeakForce is part of the off-resonance modes, which share similarities with tapping mode in that they avoid shear forces by only having an intermittent contact with the sample. Here again, the vertical position of the tip in time forms a sinusoid. Off-resonance modes are, however, different in that they operate much below the resonant frequency of the cantilever, usually by at least an order of magnitude. This strongly limits the amplification effect, so that the amplitude at the end of the cantilever is the same as the one applied by the piezo and the deflection stays constant (null) in the absence of interaction with the sample or the medium, as an opposition to

2. Atomic Force Microscopy

oscillating modes where the cantilever would actually oscillate, creating an oscillation in the deflection. As a consequence, the sinusoidal movement of the tip is due to the oscillation of the cantilever in tapping whereas it is solely due to the oscillation of the piezo in PeakForce.

2.4.2. Pseudo Force Curves

Given that the cantilever stays straight in the absence of force, the approach-retract movement of the tip is actually more similar to a force curve. The major difference with conventional force curves is that they have an approach at a constant speed, then a sudden reverting of the movement at the trigger point, and a retraction at a—possibly different—constant speed, whereas the oscillation-like movement of PeakForce gives it a smooth transition. A normal force curve and its PeakForce equivalent are shown in Figure 2.10.

Compared to their straight equivalent, one can note from Figure 2.10 that the PeakForce curve is much smoother. The smoothness in C compared to 3 in the left two images is due to the progressive deceleration and opposite acceleration of the piezo when moving from the approach to the retract sections in contact with the sample. This smoothness disappears when the time axis is changed to the piezo position one, giving back the linear end of a force curve in the corresponding graphs on the right. A second difference is the smoothness of points B and D compared to their 2 and 5 equivalents. The non-contact part, especially, is supposed to be vertical, as it can be seen in the top graphs. The reason for this smoothness is the proximity of the resonant frequency of the cantilever, which limits the speed of the tip relative to the piezo. In the case of the force curves, the movement appears vertical because of its low speed, but similar effects would be observed should the force curve be taken at the same speed. Similarly, the effect does not appear in PeakForce when stiff cantilevers are used.

Another important difference is that, whereas force curves retract when

2. Atomic Force Microscopy

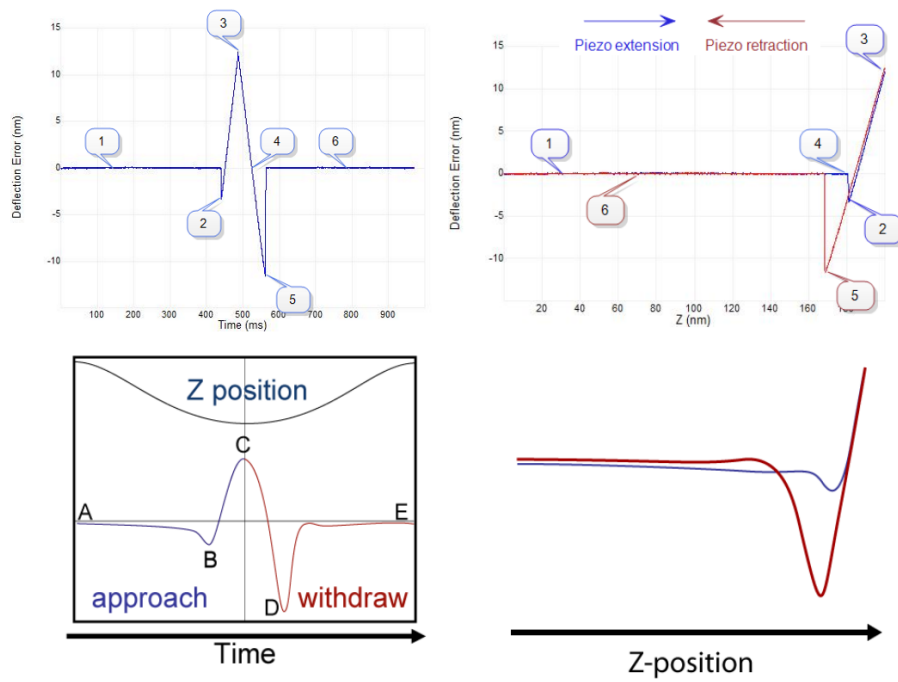


Figure 2.10.: Comparison scheme between force curves and their PeakForce equivalent. Top: force curve. Bottom: PeakForce. Left: deflection as a function of time. Right: deflection as a function of the vertical position of the piezo, for the approach (blue) and retract (red). 1/A: non-contact approach. 2/B: snap-in contact. 3/C: trigger force/peak force. 4: 0-force contact. 5/D: maximum adhesion force (snap-off contact). 6/E: non-contact retraction. © Bruker, modified.

2. Atomic Force Microscopy

triggered by the force threshold, the vertical movement of PeakForce curves is set at the beginning of the curve. Rather than retracting on a threshold, a feedback loop is applied on the detected peak force from one curve to another.

2.4.3. Operation

PeakForce can be used mainly in two circumstances: as a simple imaging mode or to extract nanomechanical information by analyzing the pseudo force curves. It operates at a set of given frequencies. Common values are 0.125 kHz, 0.25 kHz, 0.5 kHz, 1 kHz, 2 kHz, and 8 kHz and should be selected carefully.

Since the feedback is based on the previous curves, a higher frequency allows a faster feedback, hence a better tracking of the surface at high speed. It also limits the horizontal distance per cycle, therefore reducing shear stress.

On the other hand, operating at high frequency causes increased hydrodynamic effects when operating in fluid. When approaching one tenth of the resonant frequency of the cantilever, ringing effects can also be noticeable, deteriorating the quality of the force curve.

As a consequence, the technique can be used at high frequencies when focused on imaging but lower frequencies should be preferred when the quality of the curves is of importance (i.e. when probing nanomechanical properties), although the optimal values depend on the cantilever and the medium.

To work on soft samples, however, soft cantilevers have to be used. As discussed in Section 2.1.1, on most traditional cantilever designs, the resonant frequency goes in par with the spring constant. This made PeakForce initially difficult to use on soft samples, until the development of new cantilever designs, allowing a low spring constant with a comparatively high resonant frequency (Schillers, Medalsy, et al., 2016).

2.4.4. Hydrodynamic Effects

In liquid, the hydrodynamic effect applies to the cantilever a force opposite to its movement. While this effect is not specific to PeakForce since it would also apply to any movement at similar speeds, it is less common to reach these speeds with other modes. Furthermore, specific algorithms are applied in this situation.

During the sinusoidal movement, the speed of the cantilever is most important in the middle of the approach and retract curves and much lower when it touches the sample. Thus, the hydrodynamic effect mostly affects the non-contact parts of the curves, inducing what appears to be a repulsive force during the approach and an attractive one on the retraction. This background effect mostly resembles a sinusoid, although its phase is delayed by a quarter of the period.

A first method to cancel the background effect consists of recording PeakForce curves slightly above the sample, hence without close-range tip-sample interactions. This background data is then subtracted from further force curves.

Whereas this method can be sufficient on most materials, the hydrodynamic effect is especially critical on cells, where the softness and large topographical features impose a large PeakForce Amplitude (600 nm peak to peak), causing at high speed hydrodynamic forces that can reach 20 nN on most standard cantilever geometries, more than a higher of magnitude higher than the typical setpoint (Schillers, Medalsy, et al., 2016). Furthermore, the height of the cells can sometimes be close to the total height of the tip—or, at least, non-negligible. This brings the distance between the sample and the cantilever (not the tip) significantly smaller when the tip is scanning a lower part of the cell while the nucleus is under the cantilever. Oppositely, the cantilever-sample distance is significantly bigger than its normal value when the tip is scanning the top of the cell while the cantilever is over an empty area. This creates variations in the hydrodynamic background, lowering the efficacy of the method described above.

2. Atomic Force Microscopy

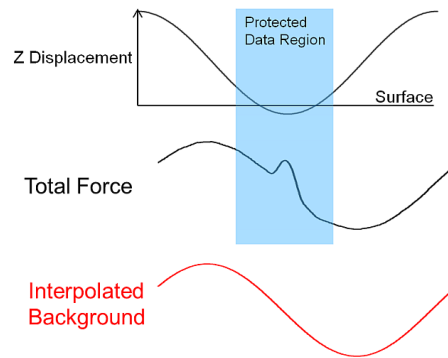


Figure 2.11.: PeakForce Live-Cell background subtraction in liquid. Line 1: the vertical axis shows the piezo displacement as a function of time, with the horizontal line corresponding to the displacement at which the tip enters in contact with the sample. Line 2 represents the corresponding total force on the cantilever. A protected data region is defined around the contact zone (in time). The interpolated background, in line 3, is obtained by taking the total force, except in the protected data region, where it is interpolated instead. © Bruker

A second, live-cell background subtraction is then performed, as illustrated in Figure 2.11. To separate the background from the tip-sample interactions, a protected data region is defined around the time at which the tip touches the sample. The total force, after the first background subtraction, is considered and the data falling out of this protected data region is assumed to be free of tip-sample interaction, hence be pure background signal. This background signal in the protected data region is interpolated from the rest of the signal, to have a complete approximation of the background signal, which can then be subtracted from the total force to recover the tip-sample interactions.

Thanks to these developments, the force control is such that it has been shown possible to image microvilli on living cells (Schillers, Medalsy, et al., 2016). PeakForce-QNM allows nanomechanical mapping at high-speed on various samples, whose stiffness vary from 700 kPa to 70 GPa (Pittenger,

2. Atomic Force Microscopy

Erina, and Su, 2010) whereas cells stiffness usually ranges from 100 Pa to 200 kPa (Kuznetsova et al., 2007). Interpreting PeakForce-QNM results on live cells may be a difficult task, but developments are being made to improve the reliability of the measurements on live cells (Pittenger and Slade, 2013) and its utilization limits are being studied.

2.4.5. ScanAsyst

PeakForce is mostly based on two parameters. First, the force setpoint is the target value for the peak force. A high setpoint will apply too high of a force on the sample while a low can lead to false detections of the peak force, leading to the tip no longer tracking the sample, and create parachuting effects detailed in Section 2.5.5. Being based on a feedback loop, a second parameter of importance is the gain. A low feedback gain can create parachuting effects as for the low force setpoint. Oppositely, a high gain will amplify noise and create sawtooth effects described in Section 2.5.6.

Although these two parameters can be set by the user, PeakForce can also be automatically parametrized, which is done with ScanAsyst. Its algorithm first tries to find a good force setpoint. Then, it places the PeakForce feedback gain on a feedback loop that tries to maximize the tracking of the sample (higher gain) and minimize the noise (lower gain) (Kaemmer, 2011). The first aims at limiting the parachuting effect mentioned Section 2.5.5 while the latter limits instabilities. Depending on its ability to keep the tracking and noise level in control, it can adjust the force setpoint.

The gain optimization is fast, making it able to change from one area of the sample to another. On cells on a glass support, the gain should be low on the glass part to avoid noise but high on the cell to be able to track the topography, while their softness allows for such higher gains. Because of this high variability in gains, the gain of the second feedback loop can be made bigger, as done in ScanAsyst-Cells, so that the system is better able

2. Atomic Force Microscopy

to adapt to the changes (Schillers, Medalsy, et al., 2016).

If desired, the user can deactivate the ScanAsyst optimization of the gain and/or the force setpoint, the latter being useful for improving reproducibility in mechanical measurements. Although ScanAsyst might not be as good as an experienced AFM user at optimizing the scanning parameters, it is able to keep them balanced over time, making it perfectly suitable in long-lasting automated experiments such as the ones of interest in this work. In this case, however, it should be set up carefully, as described in Section 7.1.2.

2.5. Artifacts

As with other techniques, the AFM image is not a perfect representation of the sample. Optical and electron microscopies have, for example, their own aberrations. Nonetheless, artifacts are very specific to the technique.

A trained user should be able to recognize these artifacts and correct them. In some cases, however, a trade-off might exist between the absence of artifacts and performance, or the correction might be impractical. In these circumstances, these artifacts have to be considered during the analysis.

When automating AFM, which will be the main focus of this work, these artifacts should to be recognized by the software. Otherwise, the parameters have to be selected carefully to avoid them. In this section, we will thus go through the main artifacts of AFM in the modes we operate, as well as their implications with regard to automation.

2.5.1. Hysteresis and Creep

The relation between the voltage applied to a piezo actuator and its displacement has three main non-ideal behaviors.

First, its non-linearity implies that its sensitivity varies with the voltage, meaning that a same variation of the voltage at two different base voltages

2. Atomic Force Microscopy

will create different variations in height. This can, however, be recorded as part of the calibration and then compensated, since there still exists a direct relationship between the voltage and the displacement (Hues et al., 1994).

Second is the hysteresis behavior, corresponding to a reaction against change. A same voltage change in absolute value will have a different effect on the displacement depending on whether that change is in the same direction as the previous one or not. It is more difficult to compensate since it depends on the previous state of the system and the direct relationship between voltage and displacement is lost (Hues et al., 1994). Although its effect is limited when working on small areas, it can have strong effects on large scans.

Finally, the creep is characterized by a change delayed in time. When the voltage changes from one value to another, the displacement moves from one equilibrium position to another in a dynamic process. Most of the displacement happens in a very short time following the voltage change but not its entirety. The resulting difference is closed by a slow deformation. This behavior depends on the history of the system as well and, as for the hysteresis, is more difficult to compensate (Hues et al., 1994).

Hysteresis and creep can affect force curves, creating a difference between the predicted Z height and its actual value. Since these effects behave differently on the approach and retract curves, they make the squeeze the first and stretch the second, under a phenomenon called “reversed path effect”. Whereas the retract curve should always be under or equal to the approach, the area between the two corresponding to the dissipated energy, this artifact can reduce this energy or have the retract curve above the approach, leading to aberrant negative values for that dissipated energy (Cappella and Dietler, 1999; Hues et al., 1994). This effect is slightly visible in Figure 2.7.

Hysteresis and creep can also happen on the horizontal axes, in imaging modes. They induce deformations of the image such as a difference between the data recorded between the trace and retrace, or apparent bowing on

2. Atomic Force Microscopy



Figure 2.12.: Illustration of the convolution artifact. A parabolic tip is represented (black and gray) as it is scanned over a sample (red). Assuming a constant deflection, the recorded height corresponds to the height of the end of the tip, which might (black) or might not (gray) be the actual point of contact between the tip and the sample. The resulting image, the path of the end of the tip, draws the yellow shape, the convolution of the tip and sample shape.

the first lines of an image.

These effects are usually easily recognized by an operator but should be avoided when working automatically. This can be done when operating in closed-loop—for both the vertical and horizontal displacements—and at speeds compatible with the feedback loop, so that the hysteresis and creep effects can be dynamically compensated. Whereas working in open loop can improve performances in some specific cases, it is required for automated systems.

2.5.2. Convolution

A common artifact in AFM imaging is the convolution of the tip shape in the resulting image, causing a characteristic broadening of the sample. It is due to the fact that the resulting image represents the height variations of the piezo which, assuming a constant deflection, corresponds to the height variations (hence the path) of the tip. As represented in Figure 2.12,

2. Atomic Force Microscopy

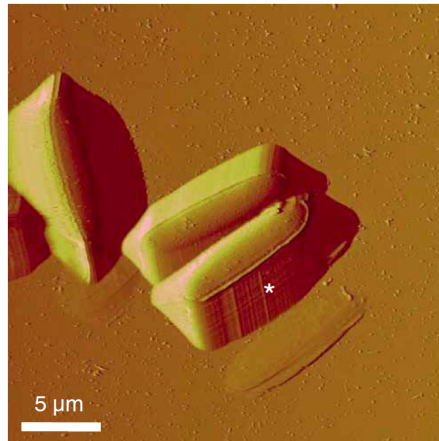


Figure 2.13.: Example of convolution artifact (*) on a deflection image of *Phaeodactylum tricorneratum* in aqueous environment. Adapted from (Dufrière, 2008).

however, the extremity of the tip might not be the point of contact between the tip and the sample, such as what happens when the sample topography is steep or has a curvature radius on the order of the one of the tip, or smaller.

This artifacts typically shows two distinct effects depending on the scale. On flat parts of the sample, it hides details at the resolution of the order of the tip radius or smaller. On cells, they can hide elements of interest such as membrane ridges, microvilli, filopodia, and lamellopodia (Koehne et al., 2011). This effect can be reduced by using sharp tips, although they can damage the sample.

The second effect happens, regardless of the sharpness of the tip, around high topographical elements that are steeper than the sides of the tip. The convolution then forms typical cliff-like borders around the sample, on the steeper edges of elements, such as represented in Figure 2.13.

The name “convolution” comes from its similarity with the identically named effect in optical microscopy, where the true image is convolved by the diffraction patterns of the light. It should be noted however that,

2. Atomic Force Microscopy

whereas the optical effect is indeed equivalent to a mathematical convolution, the AFM artifact detailed here is actually described as a mathematical dilation. As a consequence, the deconvolution technique cannot, or should not, be transferred directly.

Since this effect corresponds to the mechanical positioning of the tip relative to the sample topography, the aforementioned “cliffs” can appear along the X and Y axis, unlike the parachuting effect mentioned in Section 2.5.5. They do also not change with the scan angle, the scan speed, and the feedback parameters. They might, however, change with the setpoint force if the topography of the sample is affected.

It is worth noting that this effect can be used to reconstruct the tip shape, in particular when scanning sharp samples where the tip convolution is predominant. Two main types of reconstruction technique exist. A well-characterized surface with calibration structures can be used to compute the tip shape (Hübner et al., 2003). Alternatively, blind reconstruction techniques allow the tip characterization on a surface with sharp elements but for which the precise geometry is not known (Flater et al., 2014; Villarrubia, 1994). The first offers a more precise and better-characterized estimation of the tip shape to the expense of a precise calibration structure. The latter, on the other hand, gives a good estimation but suffering from an ill-defined lower bound. It does, however, only require a sample of high roughness. These methods can be used to control the quality of the tip, which is discussed in more detail in Section 9.4

2.5.3. Double Tip

A double tip artifact is somewhat a sub-case of the tip convolution when the AFM tip ends up with two extremities. This can be due to a breakage of the tip, caused by a failed engage, for example, or to a contamination along the tip. The presence of this double tip, in the convolution of the sample surface with the tip shape, induces a repetition of the sample with a horizontal offset corresponding to the offset between the two tips.

2. Atomic Force Microscopy

Double tips should be corrected as early as possible. In the case of contaminations, it can be possible to remove them from within the system, such as by sweeping the cantilever in contact mode on a flat clean surface. Otherwise, the probe should be changed.

2.5.4. Force Deformation

Height maps are usually recorded from the piezo height at the trigger force or other force, deflection, or amplitude setpoint. As a consequence, the measure is offset by the indentation length and the deflection. Since the deflection is part of a feedback loop aiming at keeping it at a specified setpoint, we can approximate it as a constant offset and, therefore, ignore it. The indentation length, on the other hand, would only be constant on a relatively flat sample with homogeneous mechanical properties.

In the case of soft cells such as mammalian ones on a hard substrate, the indentation of the substrate is virtually null whereas the indentation of the cell is non-negligible. This makes these cells appear smaller than they really are, unless forces are small enough to induce a negligible indentation. Similarly, stiffer parts of the cell—such as the parts of the membrane covering elements of the cytoskeleton—are less indented than the surrounding free membrane.

When the force curve data is available, its analysis can release the contact point, as described in Appendix C.3, giving a more accurate representation of the surface. This is subject to other problems, however, as the contact point can be difficult to find and, sometimes, perturbed by layers of lamellipodia or other hair-like structures. In purely imaging mode, however, the contact point—hence the true topography—can not be interpolated reliably. The indentation has then to be kept as small and constant as possible.

2.5.5. Parachuting

Not unlike the convolution effect discussed in Section 2.5.2, the parachuting effect can create cliffs shapes on the edge of elements. They are, however, not due to the tip shape but from a failure of the feedback loop to track the sample.

While imaging, when the tip moves on a higher part of the sample topography, the force on the tip increases linearly with the error in height. However, on a descending slope, the tip-sample force can only decrease to zero, at which point the tip loses contact with the sample (neglecting the adhesion). The negative errors are then bounded downwards by the setpoint force, which leads the feedback loop to approach the tip at a constant speed, creating straight descending lines on the descending edge of the sample.

Contrary to the convolution artifact that affects the two scan axes, these lines only affect the fast scan axis. Furthermore, they are only on the descending side of the sample, which is different during the trace and the retrace.

One can limit the effect by decreasing the scan speed and increasing the setpoint force. Increasing the feedback parameters can make the feedback loop more reactive, but this can also amplify noise. In PeakForce, this is automatically adjusted by ScanAsyst, although its interference with the parameters may be unwelcome in some cases. It should, therefore, be properly set up, as detailed in Section 7.1.2.

2.5.6. Sawtooth

The sawtooth artifact is specific to PeakForce. When high gains are used on a hard sample, a slight positive error in the vertical position will create a strong peak force. This strong peak force will be multiplied dramatically by the high gains, resulting in the system jumping out of contact. The tip is then slowly parachuted back on the sample, before jumping again, creating a sawtooth-shaped effects. This artifact can happen, for example,

2. Atomic Force Microscopy

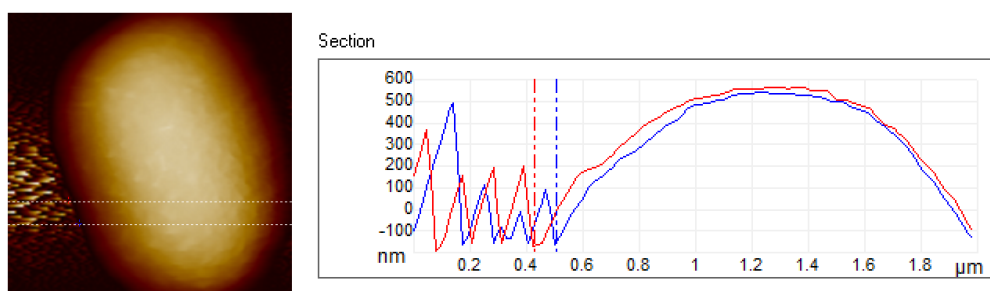


Figure 2.14.: Example of sawtooth effect. Top: height image of fixed *Y. pseudotuberculosis* in aqueous solution. Bottom: cross-sections at the lines marked on the image. Markers: cell border, separating the glass with the sawtooth artifacts (left) and the bacterium (right).

on the glass substrate when scanning cells, when the gains are optimized for the soft cell, as represented in Figure 2.14.

2.5.7. Horizontal Lines

Broad or thin lines may be present aligned with the fast scan axis, acting as steps on the slow one usually correspond to something sticking to the tip. For thin lines, it can also be due to a floating contamination or a shock and parachuting of the tip. While broad bands can be corrected by horizontal leveling, thin lines should be ignored and interpolated for the upper and lower ones.

More generally, even in the absence of contamination, slight differences exist from one line to the next. They are typically due to low-frequency noise or drifts. On relatively flat samples, they can be removed by line-by-line flattening techniques. Such techniques are, however, not available on samples with non-trivial topographies such as cells. In some circumstance, it might have to be accounted for during the analysis, such as done in Section 8.2.2.

2.5.8. Diagonal Stripes

Diagonal stripes can happen as well, corresponding most often to interferences. They can sometimes be alleviated by a re-alignment of the laser, when the latter is focused too close to the edge of the cantilever. Nevertheless, some cantilever or samples are particularly interference-prone. It is the case, in particular, when the reflectivity of the sample is close to the one of the cantilever, such as when operating with a non-coated cantilever or on a reflective sample.

These interferences are considered here as early versions of our sample holder, presented in Chapter 6, had a reflective background behind the sample.

2.5.9. Other Artifacts

Although the main artifacts have been listed above, the list could continue with artifacts whose effects are minor in our context. For example, frictions with the sample might lead the tip to bend forward, causing the cantilever to bow in a twisted fashion and leading to a smaller recorded deflection (Hoh and Engel, 1993).

2.6. High-Speed AFM

AFM scanning normally takes minutes to hours, depending on the technique, the size, the resolution, and other parameters. In the case of imaging, in particular, shortening this acquisition time would permit consecutive captures allowing the study of faster dynamical processes. This acceleration of AFM, in particular for imaging purposes, is referred to as High-Speed AFM (HS-AFM).

High-Speed AFM is most often based on tapping mode, presented in Section 2.2.3, in a setup focused on speed optimization. Thanks, notably, to the development and integration of high-speed scanners and small yet

2. Atomic Force Microscopy

soft cantilevers, it was made possible on biological samples, allowing the scanning of proteins at rates above 10 s^{-1} (Ando, Kodera, et al., 2001).

It has since then been generalized to fibrils, protein interactions, and DNA dynamics, among others (Uchihashi and Scheuring, 2017). Applications have later been realized on bacteria (Fantner et al., 2010) and on live mammalian cells (Shibata et al., 2017), although the small size of the cantilever compared to the cell is a challenge. There are contact-mode-based variants of High-Speed AFM, which have been illustrated on DNA strands and chromosomes (Picco et al., 2008).

Since it is difficult and sensitive, care and time are spent on preparing and engaging on the sample. It is then good to make movie-like scans and study the kinetics of a reaction (Uchihashi and Scheuring, 2017).

3. Biology and Relevant Applications

This work is centered around the design of applications of Atomic Force Microscopy on microbiological samples. The topic of this chapter will then be an introduction of these biological elements on which we, or the system, are going to work. It will also include general overview of the interest of their study, in particular with AFM.

3.1. The Cell

The human body is formed of systems, made of organs, acting as functional units of the body. These organs are themselves made of tissues, which are very specialized structures composed of cells and their surrounding intracellular matrix. The cell is the basic biological unit of the human body and, as a consequence, tightly connected to most of its diseases. Increasing its comprehension is thus of primary importance to understand health problems and find cures or preventions.

More generally, the cell is also the basic building block of life. It is the smallest element that can be considered “alive” on its own, and everything “alive” is either a singular cell or an organism composed of multiple ones. Although they come up in a variety of shapes, forms, structures, and functions, all but very specialized cells in multicellular organisms share the ability to replicate themselves.

Human cells, mammalian cells, and more generally the ones of verte-

3. *Biology and Relevant Applications*

brates share a common structure. The degrees of similarity progressively fades away as we consider invertebrates, then plants and fungi. All of these cells share the property of possessing a nucleus, hence qualified as eukaryotic, which will be developed in Section 3.2.

Organisms composed of one or several eukaryotic cells form the super-kingdom of the Eukaryota, in which our well-known animals, plants, and fungi constitute the kingdoms of the Animalia, Plantae, and Fungi, including therefore all of the macroscopic lifeforms. The super-kingdom also contains two kingdoms of protists, Protozoa and Chromista, which are all unicellular organisms (Ruggiero et al., 2015).

Another kind of cells exist and are called “prokaryotic” (Chatton, 1937; Stanier and van Niel, 1962). These cells differ from eukaryotic ones in that they lack their nucleus and their diversity of bounded structural elements. What they lack in complexity and their limitation to unicellular organisms is, however, compensated by their adaptability to a wide spectrum of environments and the speed of their adaptation. These prokaryotes compose the super-kingdom of the Prokaryota (Ruggiero et al., 2015; Woese, Kandler, and Wheelis, 1990), composed of two kingdoms: Bacteria and Archaea.

3.2. **Eukaryotic Cells**

Despite being considered as the basic unit of the corresponding lifeforms, eukaryotic cells are extremely complex. As represented in Figure 3.1, they are composed of several functional sub-units such as the nucleus, mitochondria, cytoskeleton, and other organelles, interacting with each other in the cytoplasm. Our bodies contain more than 10 trillion (10^{13}) of them spread across more than 200 different types (Ashrafuzzaman and Tuszynski, 2012), although these are conservative estimates and much higher numbers are sometimes put forward. They typically range from $10\ \mu\text{m}$ to $100\ \mu\text{m}$ in size (Ashrafuzzaman and Tuszynski, 2012).

3. Biology and Relevant Applications

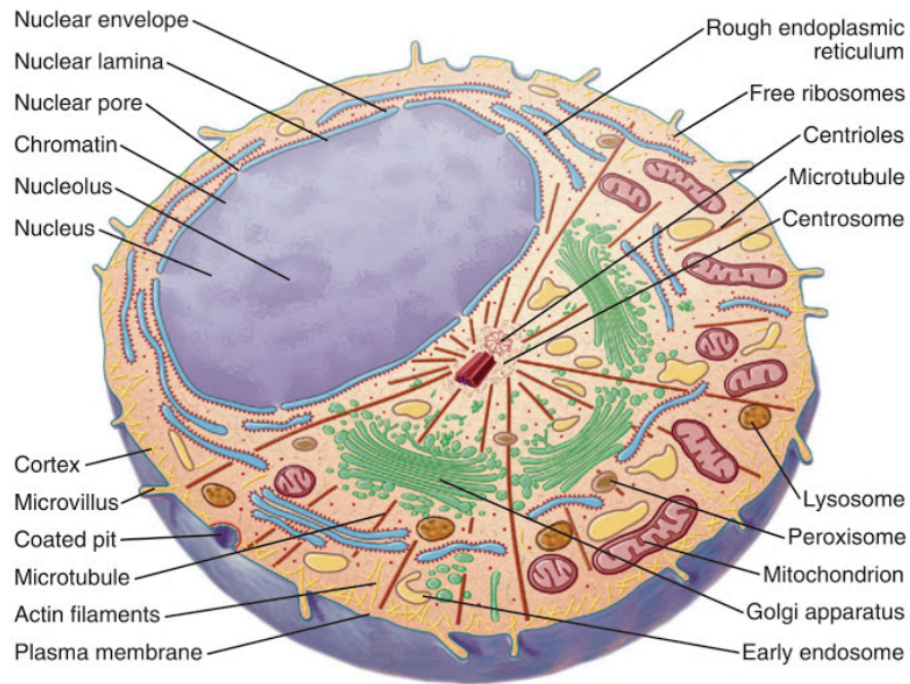


Figure 3.1.: Schematic diagram of a eukaryotic cell, with constituents.
From Pollard et al. (2016).

3. Biology and Relevant Applications

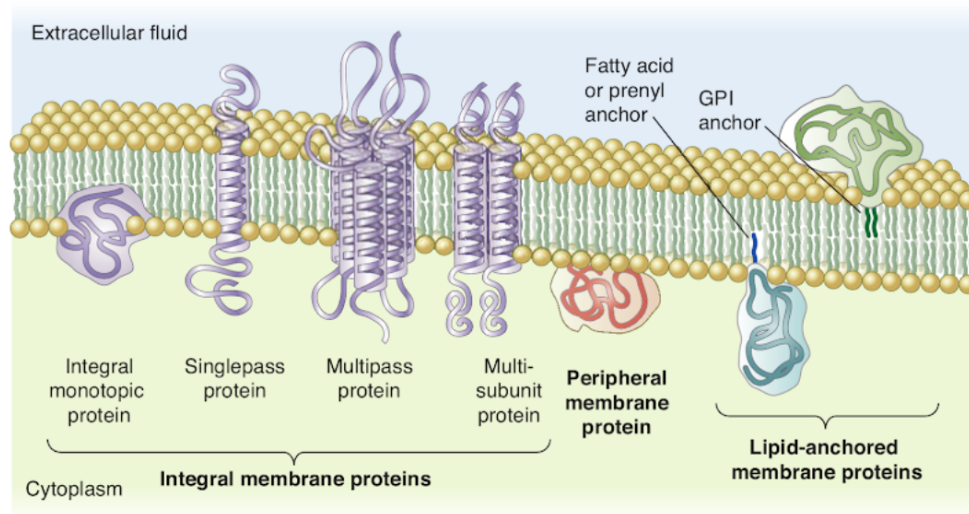


Figure 3.2.: Cell membrane and three classes of membrane proteins. From Plopper (2014).

The cell membrane, nucleus, ribosomes, mitochondria, and peroxisomes constitute the minimal set of functional parts required to have a living eukaryotic cell and are therefore considered as primary organelles (Van Lommel, 2003). Most organelles have their own membrane, which allows them to define separate areas of metabolic activity (Ashrafuzzaman and Tuszynski, 2012).

3.2.1. Membrane

Membranes compartmentalize areas of bio-activity. In the case of animal cells, for example, the whole cell is surrounded by a plasma membrane that defines their border. It makes the difference between the inside, with the cytoplasm, and the outside, extracellular matrix.

Membranes are principally composed of lipids and proteins, as represented in Figure 3.2. Among the lipids, most are phospholipids, amphiphilic molecules. They consist of a hydrophilic head being a phosphate group esterified with glycerol, and a hydrophobic tail made of two fatty

3. *Biology and Relevant Applications*

acids (esterified as well). In water-based solutions, the hydrophobic tails tend to attract each other by repulsing water, exposing their hydrophilic heads. This leads them to form from simple spherical micelles to advanced liquid crystalline structures, with bilayer somewhere in-between. These bilayers can stay open, close as lifeless vesicles, or be part of a living cell as is the case of interest (Ashrafuzzaman and Tuszynski, 2012).

The cell membrane is a thin surface of lipids and proteins behaving like a 2D fluid in which proteins are embedded. The lipid part forms a double layer composed of about 10^6 molecules per squared micrometer, its thickness approaching 5 nm (Alberts et al., 2002). The membrane holds together thanks to the hydrophobic interactions between the tails of the phospholipids. It also contains cholesterol, a small, mostly hydrophobic molecule that changes its mechanical properties. The concentration of proteins in the membrane varies among species. The cell membrane is able to selectively control intake and outtake of components. It can create and/or maintain ion gradients, which allows it to generate electric potential differences. A variety of receptors allows it to sense signals from the outside, including other cells (Alberts et al., 2002; Ashrafuzzaman and Tuszynski, 2012).

The membrane is finally of a particular interest in that, as their border, they are the only part of cells that can be probed directly by non-invasive techniques, such as AFM.

3.2.2. Intracellular Components

Nucleus The nucleus is the core of the cell, ranging from 5 μm to 10 μm . It is usually spherical or ellipsoidal depending on the elongation of the cell. Most cells have one, although erythrocytes (red blood cells) have none and some cell types can be multinuclear. It contains the genetic information of the cell. Its border is the nuclear envelope (Alberts et al., 2002; Ashrafuzzaman and Tuszynski, 2012; Van Lommel, 2003).

3. Biology and Relevant Applications

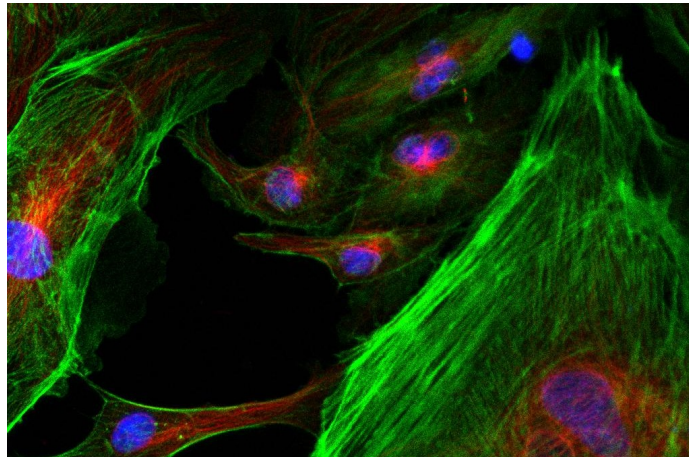


Figure 3.3.: Fluorescence microscopy image of the cytoskeleton. Nuclei, microtubules, and actin are marked blue, red, and green, respectively. Courtesy from the Bio Imaging Center Lille.

Cytoplasm The cytoplasm is the material inside the cell, to the exception of the nucleus. It contains all the organelles and the surrounding cytosol, which is the intracellular fluid in which all the organelles are floating. The cytosol is viscous and takes about half the volume of the cell and a sizable part of its water content of, which adds to 70% of the volume of the cells. Its main chemical components are potassium, sodium, and chlorium ions, and a diversity of proteins. It is a highly organized dynamic network, regulated by a mesh of filaments (Alberts et al., 2002; Ashrafuzzaman and Tuszynski, 2012).

Cytoskeleton The cytoskeleton, visible in Figure 3.3, is made of polymerized proteins, assembled in fibers. It provides the cell with its tensile strength and has an important role in membrane integrity and cell movement. It notably includes actin, known as F-actin under its polymeric form and as G-actin when monomeric (Alberts et al., 2002). Actin, represented in yellow in Figure 3.1, tends to agglomerate close to the border of the cell, to give it its structure.

3. *Biology and Relevant Applications*

Aside from the actin filaments are microtubules, with α - and β -tubulin, which are much larger and more rigid. They radiate outwards from the centrosome, as visible in Figure 3.1. They are involved in the intracellular transport of molecules as supports for kinetic motors. Finally, there are other intermediary filaments, composed of different proteins. They are less dynamic and tend to act on the positioning of organelles.

Mitochondria Most eukaryotic cells contain mitochondria. They are the power-house of the cell, a single of which can contain several hundreds of them. They are small and stiff, with a double membrane, floating in the cytoplasm. They range from small 0.5 μm -diameter spheres to 10 μm -long tubes with a diameter of 1 μm . (Alberts et al., 2002; Van Lommel, 2003)

They harvest energy from food and store it in the form of ATP, Adenosine Tri-Phosphate. ATP is the energy currency of the cell. It contains a chain of three phosphate groups, the last of which is unstably attached and whose liberation releases energy. When deprived of its last phosphate group, ATP becomes ADP, Adenosine Di-Phosphate. Mitochondria then turn ADP back into ATP, using the oxidation of carbohydrates or other energy-rich molecules. ATP is then used throughout the cell to bring the energy the metabolism requires. They have their own DNA (Alberts et al., 2002; Van Lommel, 2003).

Other Organelles Aside from the organelles cited earlier, two other main organelles are to be cited: the Golgi apparatus and the endoplasmic reticulum.

The endoplasmic reticulum is around the nucleus and is a location where proteins are synthesized (Ashrafuzzaman and Tuszynski, 2012).

The proteins from the endoplasmic reticulum are transferred to the Golgi apparatus, where they are modified and prepared for distribution. It is shaped as several connected pancake-shaped disks (Ashrafuzzaman and Tuszynski, 2012).

3.2.3. Extracellular Matrix

In vivo, eukaryotic cells are held together in an extracellular matrix (ECM) composed of proteins and polysaccharides. The ECM is made, organized, and degraded by its embedded cells. Reciprocally, cells react to changes in the ECM. Whereas most tissues contain limited quantities of ECM to hold the cells together, connective tissues are mostly composed of matrix.

A protein of particular importance in the extracellular matrix is collagen, which is the most abundant protein in mammals and especially present in connective tissues. Fibronectin is also worth mentioning, as a large protein that promotes the interactions between the cell and the ECM (Alberts et al., 2002).

Given their implication in cell adhesion, these molecules can be used to promote it. In particular, they can be coated on the substrate at specific places to control the positioning and shape of cells (Azioune et al., 2009), as discussed in Section 9.1.

3.2.4. Epithelial Cells

In Section 8.4, we discuss the applicability of the system on eukaryotic cells. Our main sample are RPE-1 cells, forming the Retinal Pigment Epithelium, which is the pigmented layer of cells in the human retina. These cells normally form a single layer.

As epithelial cells, they are particularly fit to adhere to surfaces, satisfying the immobilization issue discussed in Section 2.3.2.

3.3. Prokaryotic Cells

Aside eukaryotic cells, characterized by their nucleus, are the prokaryotic cells: bacteria and archaea, ubiquitous microorganisms. Some, such as lactic acid bacteria, are used in the food-processing industry while others have a predominant position in pharmaceuticals. However, before being a

3. *Biology and Relevant Applications*

tool in our industrial processes, many are part of our body.

On the other side, prokaryotic cells are also responsible for numerous diseases, such as tetanus, cholera, syphilis, tuberculosis, and the plague. It is then important to understand these organisms to better fight them.

Although not absent from our bodies and processes, archaea are less often encountered than bacteria and will not be discussed much further in this document. There are furthermore no known archaean pathogens.

Prokaryotic cells are typically 10 times smaller, 1000 times in volume, than their eukaryotic counterparts, as they range from 1 to 10 μm in size (Ashrafuzzaman and Tuszynski, 2012). Bacteria mainly come under two typical shapes: bacilli and cocci. Bacilli are approximately cylindrical and long of a few micrometers, whereas cocci are small spheres. Other shapes exist, mostly for archaea.

Prokaryotes do not have organelles and have their DNA directly in the cytoplasm, although mostly packed in the center. Their motility is oftentimes enhanced by flagella and pili or, oppositely, they might create a material similar to the extracellular matrix and form biofilms.

3.3.1. Cell Envelope

One of the key points in the definition of life is for an element to be localized. In the case of prokaryotes, this role is assumed by the cell envelope, which forms the boundary of the cell. It is the barrier that defines the cell from its environment by separating the interior from the exterior. The envelope protects the inside of the cell while enabling the transport of nutrients and waste and, in a broader sense, of information between the cell and its environment. In bacteria, this envelope regroups the cell wall, one or two membranes, the periplasmic space, and associated macromolecules (Seltmann and Holst, 2002; Suvorov, Fisher, and Mobashery, 2008).

The cell wall is a heteropolymer of glycan strands cross-linked by peptides, named “peptidoglycan” or “murein” (Suvorov, Fisher, and Mobashery, 2008). It is resistant enough to give the cell its shape and mechanical

3. *Biology and Relevant Applications*

resistance while allowing it to grow and divide. This wall, as a rigid layer, allows cells to resist internal pressures of up to several atmospheres generated by the osmotic effect (Ashrafuzzaman and Tuszynski, 2012). This effect is usually pretty small with eukaryotic cells, which tend to live in environments with high concentrations of ions, but is sometimes predominant for prokaryotic cells, which tend to live in harsher conditions.

Many possibilities exist to provide the cell with the functionalities they require from their envelope, giving a broad diversity of cell walls and membrane structures among bacteria, although they can be clustered (Seltmann and Holst, 2002). In particular, the Gram classification allows us to identify two main categories. This classification, developed in 1884 by Hans Christian Gram, is based on a simple method to stain the bacterial wall. First, the bacteria are gently dried and fixed with heat or methanol, before being stained with a solution of crystal violet, which enters most cells.

Besides various washes in water, the sample is then flooded with a mordant iodine solution, which solidifies the cell wall. Then, the sample is quickly decolorized with ethanol before safranin or fucsin, red counterstains, is applied to re-colorize the decolorized cells. Most bacteria appear henceforth either dark blue to violet or pink to red and are classified respectively as Gram-positive (Gram⁺) or Gram-negative (Gram⁻).

Compared in Figure 3.4, both types contain an inner membrane and cell wall. The common inner membrane is composed of phospholipids and performs the role of selective transport of the elements mentioned above. Another group of bacteria was discovered later: mycoplasma, which do not have a wall. Let us note that archaea have a different kind of rigid layer and do not fit in the Gram classification. Additionally, some bacteria might be Gram-variable or be otherwise atypical (Mohan, 2009; Seltmann and Holst, 2002; Suvorov, Fisher, and Mobashery, 2008).

Gram-Positive Bacteria As shown in the left part of Figure 3.4, Gram-positive bacteria have a thick and bare peptidoglycan layer of 20 to 80 nm. This thick layer protects the internalized crystal violet from the decoloriza-

3. Biology and Relevant Applications

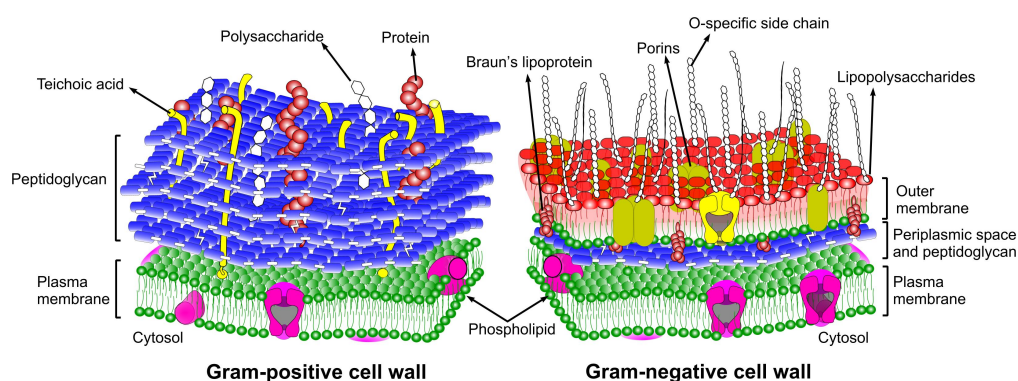


Figure 3.4.: Cell envelope of Gram-positive (left) and Gram-negative (right) bacteria. Adapted from (André, 2010).

tion, giving them a final dark blue to violet color from the Gram coloring.

Their two main components are then the inner membrane and cell wall, with an inner wall zone between the two, similar to the periplasmic space of the Gram-negative ones (Suvorov, Fisher, and Mobashery, 2008). They present a broad diversity of compositions and structures (Seltmann and Holst, 2002).

Gram-Negative Bacteria Gram-negative Bacteria, illustrated in the right part of Figure 3.4, are marked pink to red by the Gram coloring, as they do not resist to the decolorization (Suvorov, Fisher, and Mobashery, 2008). Their structures stay similar as they lack the variability of their counterparts. Their cell wall is composed of an extra outer membrane, bringing the number of layers in the cell envelope to three: an inner (cytoplasmic) membrane, a periplasmic space containing the peptidoglycan, and an outer membrane. In spite of having more layers, their envelope is usually thinner due to the fact that their peptidoglycan layer is much thinner (10-15 nm). Their outer membrane is similar to common biological membranes but much more stable as the inner side is covalently linked to the cell wall and the outer side is most often made of lipopolysaccharides, presenting their polysaccharide tail outwards (Seltmann and Holst, 2002). This mem-

3. Biology and Relevant Applications

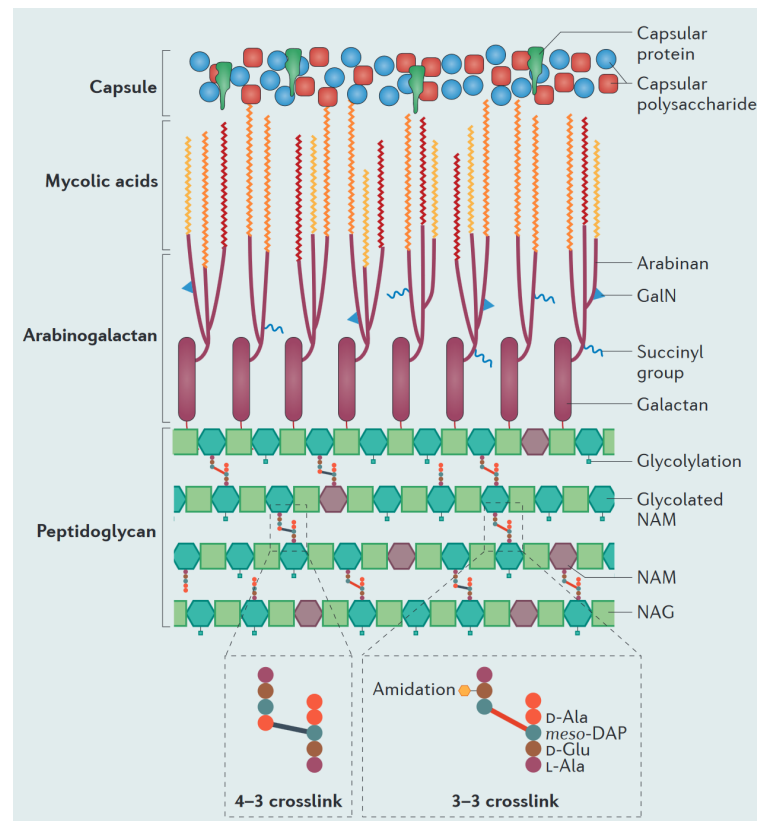


Figure 3.5.: Cell envelope of mycobacteria. From Kieser and Rubin (2014).

brane can be as stiff or stiffer than the peptidoglycan layer, sharing the mechanical constraints (Rojas et al., 2018).

3.3.2. Mycolata

Mycolata, which include Mycobacteria, are classified as Gram-positive but have a variable staining. They should not be confused with Mycoplasma, which are much smaller and do not have a cell wall nor peptidoglycan (Seltmann and Holst, 2002). Mycobacteria are slender, non-flagellar rod-shaped cells. They grow slowly, with generation times ranging 12 to 24 hours (Johnson, 2018).

3. Biology and Relevant Applications

Their peculiar Gram classification comes from their resistance to staining as they have a unique cell envelope with three layers past the peptidoglycan one, shown in Figure 3.5. First comes an arabinogalactan layer, made of arabinose and galactose sugars. Secondly, a mycolic acid layer is linked to the arabinose sugars of the previous layer. This layer is responsible for the hydrophobicity of the cell and its protection against polar molecules of the cell, causing its resistance to staining and numerous antibiotics. A final layer is made by the capsule (Daffé and Draper, 1997; Kieser and Rubin, 2014).

The thickness of these layers changes between replicative and non-replicative states. Replicative states have a thinner capsule and thicker mycolic acid layers, whereas non-replicative states have a stronger peptidoglycan layer and a thicker capsule, which can protect them under stress (Kieser and Rubin, 2014).

They are covered by Heparin-binding hemagglutinin adhesin (HBHA), an adhesin involved in their agglutination and their adherence to epithelial cells (Menozzi et al., 1996).

3.3.3. Model Samples

In this sections, we will present the main samples used in the development of the system.

Yersinia pseudotuberculosis

Yersinia pseudotuberculosis, shown in Figure 3.6, is a Gram-negative bacterium of the genus *Yersinia*, belonging to the family *Enterobacteriaceae*.

They are rod-shaped coccobacilli with dimensions of 1 μm to 3 μm in length and 0.5 μm to 0.8 μm in diameter (SMI, 2015). Their protein fibrillar capsule is synthesized at 37 $^{\circ}\text{C}$ but not under 30 $^{\circ}\text{C}$. The capsule blocks phagocytosis (Johnson, 2018).

Yersinia pseudotuberculosis is closely related to *Yersinia pestis*, which is the pathogen causing plague (Achtman et al., 1999), discovered by Alexan-

3. Biology and Relevant Applications



Figure 3.6.: Scanning Electron Microscopy image of *Yersinia pseudotuberculosis*, taken in Second Electron Imaging on a HeLa cell. Courtesy of N. Barois.

3. Biology and Relevant Applications

dre E. Yersin. *Y. pestis* has been attributed three pandemics in human history, including the Black Death. It still has mortality rates up to 90% without therapy (Mohr, 2016).

Although these two bacteria cause very different diseases, they share most of their genome (Chain et al., 2004). *Y. pseudotuberculosis*, while still pathogenic to humans, is much less dangerous, making it a good model to understand *Y. pestis* while limiting the risks of its manipulation. It is particularly frequent in animals, especially cats (Bourdin, 1979) and can be transmitted by contaminated food (Jalava et al., 2004).

***Mycobacterium bovis* BCG**

Tuberculosis (TB) was, in 2016, the ninth most important death cause worldwide and the first amongst infectious diseases (WHO, 2017). Although treatable, it is responsible for 2 million deaths each year (Luca and Mihaescu, 2013). It is caused by the bacterium *Mycobacterium tuberculosis*, which was discovered in 1882 by Robert Koch, and is sometimes called Koch's bacillus. The pathogen spreads through airborne droplets, from a cough, and goes to the lungs before spreading to the rest of the body (WHO, 2017).

Another *Mycobacterium*, *Mycobacterium bovis* can cause tuberculosis to humans and has an exceptionally wide host range, including cattle and pigs. The infection is not self-maintaining in humans, usually contaminated through unpasteurized milk from infected cows. The disease can also be airborne in the case of people working with cattle. The pathogen can survive for a few months the environment, in natural conditions (O'Reilly and Daborn, 1995).

M. bovis BCG, the Bacillus Calmette-Guérin vaccine, was created by Albert Calmette and Camille Guérin as a vaccinal strain against *Mycobacteria* after 11 years of subcultures in a custom medium (Calmette et al., 1927). It is currently the only vaccine against Tuberculosis (Luca and Mihaescu, 2013), protecting 1 patient in 4 from the infection and halving the

3. Biology and Relevant Applications

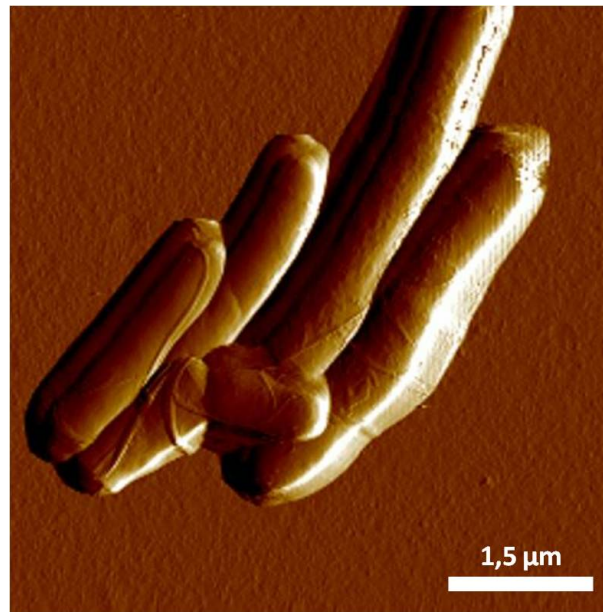


Figure 3.7.: AFM deflection error image of *Mycobacterium bovis* BCG mycobacteria. Courtesy of V. Dupres.

probability of developing the disease once an infection occurs (Roy et al., 2014). Such vaccination is key in the WHO strategy to end TB. Furthermore, *M. bovis* BCG can be used as a vaccine against leprosy and Buruli ulcer as well as for treating bladder cancer (WHO, 2018).

M. bovis bacteria, illustrated in Figure 3.7 have elongated shapes, with typical lengths of 2 to 4 μm and a section diameter of 0.2 to 0.5 μm (Davis et al., 1973; Zhang and Groves, 1988). Their surface contains a lot of mycolic acids giving them hydrophobic properties, which makes them aggregate and adhere to surfaces (Alsteens, Dague, et al., 2007).

3.4. Understanding Diseases

It is difficult to find a satisfactory biomedical definition of “disease”, as it is often defined within a social contest (Scully, 2004; WHO, 2004). In our scope, we can characterize a disease as a perturbation of homeostasis, the

3. Biology and Relevant Applications

ability of the organism to keep its internal environment stable (Casadevall and Pirofski, 1999). As emphasized by the WHO (2004), they might be caused by several of a broad variety of factors. They can, therefore, be treated or prevented by acting upon any combinations of these factors.

We will here focus on two cases: cancers and infectious diseases, which are important concerns in the society of today. Furthermore, their analysis by AFM can be routinely performed and bring useful information. In particular, their understanding and the discovery of relevant drugs would benefit from higher-content higher-throughput techniques that could be used in screening applications, to which this project is aiming.

3.4.1. Pathogens

Pathogens can be classified by their ability to cause damage to a host as a function of the immune response of the later, in the framework of host-pathogen interactions. A disease occurs when the homeostasis of the host is perturbed by the damage caused by the pathogen (Casadevall and Pirofski, 1999).

3.4.2. Drugs

Drugs are substances (natural or synthetic) that affect the structure or functioning of organisms to which they are applied, with the exception of nutrients. In particular, therapeutic drugs, or medicines, are involved in diagnosing, preventing, or treating disease (Cammack et al., 2006).

3.4.3. Antibiotics

There are several definitions for what is an antibiotic, but it can be defined as an organic chemical that inhibits or kills pathogenic bacteria, being therefore a subcategory of drugs (Mohr, 2016).

Antibiotics protect from infections that could otherwise be fatal not only by treating infections, but also preventing them on weakened individuals

3. Biology and Relevant Applications

(Medina and Pieper, 2016). They allowed relegating contagious diseases that used to be one of the leading cause of death down to negligible. They brought an end to the pandemics Humanity had suffered before, saving lives by millions (Mohr, 2016).

The first modern antibiotic, penicillin, was introduced in the early 1940s. As a β -lactam antibiotic, it inhibits the peptide cross-linking of the glycans in the bacterial cell wall (Medina and Pieper, 2016).

3.4.4. Antibiotic Resistance

Pathogenic bacterial strains have developed multiple resistances to antibiotics and are a worrying cause of increasing hospital-acquired (nosocomial) infections. Some of these bacteria are particularly difficult to target and are referred to as super-bugs (Stadler and Dersch, 2016).

The over-use of antibiotics has made resistance a big health-care issue. It is generally observed that once a new antibiotic enters the playing field and is used on a widespread fashion, resistance comes with a troubling certainty (Davies, 1996). The first penicillin-resistant strains of bacteria were discovered a year after its appearance. Cumulating resistance traits yielded multidrug-resistant (MDR) bacteria. Super-bugs include Methicillin-Resistant *Staphylococcus aureus* (MRSA), MDR *Mycobacterium tuberculosis*, and MDR *Escherichia coli*, among others. When their resistance spectrum broadens even more, the bacteria can sometimes be considered as extensively drug-resistant (XDR), or totally drug-resistant (TDR) such as it can be the case for *M. tuberculosis* (Medina and Pieper, 2016). Some bacteria can even be resistant to all known drugs (Bonomo, 2000). This is especially worrisome when considering that resistance genes can be transmitted horizontally between bacterial cells through plasmids, but also between species (Davies, 1994).

The antibiotics have been over-used. Using antibiotic permits the development of resistant bacteria and clears the floor of competitors, allowing them to thrive, in a phenomenon called antibiotic pressure, as for other

3. *Biology and Relevant Applications*

selection pressures (Carlet et al., 2011; French, 2010).

Some countries have been better at avoiding indiscriminate use of antibiotics, limiting the development of resistance on their land, but bacteria are insensitive to political borders. Rare new antibiotic classes that get discovered were initially used as last-chance to avoid disseminating their resistance but are now being increasingly used as first line treatments in some countries (Carlet et al., 2011).

New antibiotics are being developed, but the process is long and costly, especially in the 3 developmental phases of clinical trials (Medina and Pieper, 2016). With the rise in costs and the high rates of failure, pharmaceutical R&D in antibiotics has a disappointing productivity, deterring pharmaceutical companies from searching for new antibiotics (David, Tramontin, and Zimmel, 2009). On the other hand, antibiotic resistance has been spreading alarmingly fast (Walsh, 2000). There is evidence that transnational programs to strategize the use of antibiotics can help combat these issues (French, 2010). Improving the information available during the development stage, as well as its throughput, could be a key element in fighting bacterial resistance.

3.4.5. Cancer

Cancer is one of the principal causes of death in France and other developed countries. It is one of the major health issues nowadays since about 15 to 20% of currently living people might die from this group of diseases. Studying this disease further helps to understand the biology of the cell. Among the several tens trillion or more cells in the Human body, billions experience mutations every day, which can disrupt their functioning with the rest of the body. Whereas cells are normally collaborative, such disruption can cause them to escape the control of the body and acquire characteristics allowing them to proliferate indefinitely (Alberts et al., 2002).

Cancer usually starts from a single cell but is far from a lump of clones of that mother cell. It has been shown that cancer cells organize themselves

3. *Biology and Relevant Applications*

into tissues, constituting tumor organs with a variety of cell types and interacting with the rest of the body (Egeblad, Nakasone, and Werb, 2010).

Cancer comes from the accumulation of alterations in the genetic code that disrupt the functions of the cell. It appears by the acquisition of certain characteristics, the hallmarks of cancer, defined and refined by Hanahan and Weinberg (2000, 2011). These are sustaining inducing angiogenesis, proliferative signaling, evading growth suppressors, enabling replicative immortality, resisting cell death, and activating invasion and metastasis, with some added later such as reprogramming the energy metabolism and evading immune destruction. These capabilities are acquired through a development per steps and are facilitated by instabilities in the genome, creating random errors that accumulate. Aside from these primary cancer cells, the tumor as an organ tends to acquire other cells, creating a microenvironment around it.

3.5. AFM Applications

Although less intuitive than most forms of far-field microscopy, which are more commonly used in the life science community, Atomic Force Microscopy offers its own advantages and a wide range of applications. First, AFM allows a very high resolution in biological conditions. Secondly, thanks to the physical contact between the probe and the sample, it is able to record mechanical information about the sample. Lastly, as it is able to record substantial information and to do so over time on a cell without damage, it is suitable for cases where the singularity of each or some cells has to be taken care for, or for the monitoring of a few cells over time. Its applications in biology and for the biomedical field are then numerous and growing, with strong potential in biological research and pharmacology (Pillet et al., 2014).

This chapter will focus on these applications, on both a theoretical standpoint and their practical implications. While there are much more appli-

3. Biology and Relevant Applications

cations than the ones listed below, we will here focus on the usage of AFM on cells, in particular on context relevant to cancer and other diseases, with potential drugs. Stem cells are also mentioned, as they have a huge potential for biomedical applications (Shi et al., 2017).

It should be noted that, for a wide range of applications, the tip can be functionalized so as to have a specific interaction with a target molecule, which is apparent on the retract curve as adhesion events (Alsteens, Müller, and Dufrière, 2017; Lee, Kidwell, and Colton, 1994; Moy, Florin, and Gaub, 1994). Despite being an interesting technique, functionalization will not be discussed here as it does not readily apply to our setup.

3.5.1. Biological Conditions

Compared to electron microscopy techniques, which can offer a similar range of resolutions when working on cells, AFM offers the advantage of working on biological conditions. The first often requires a heavy processing and denaturing of the sample whereas AFM can be operated in liquid, on living samples.

Although it can be used to scan isolated cell elements such as DNA or proteins, or proteins embedded in a bilayer of phospholipids, our main application of interest here is the ability to work on isolated living cells with minimum processing. Eukaryotic and prokaryotic can be imaged or probed in buffer or, in some circumstance, grow medium. They require immobilization, which has been described in Section 2.3.2. This helps to ensure that the observations are not affected by the sample preparation, especially when analyzing the chemical or mechanical properties of the sample.

Regarding the sensitivity of the technique, AFM has been shown able to resolve individual microvilli on living cells and their natural behavior in liquid (Schillers, Medalsy, et al., 2016).

3.5.2. High-Resolution

As a near-field technique, AFM offers a resolution much below the diffraction limit. Despite being hampered by the convolution effect described in Section 2.5.2, the planar resolution is still at a few nanometers for small details on a surface, depending on the tip used. The vertical resolution, on the other hand, is much better defined and can be sub-nanometric.

Extremely-high resolution applications such as the imaging of protein (Scheuring, 2005), DNA (Hansma, Vesenka, et al., 1992), or the interactions between the two (Jiao et al., 2001), among others do exist but are far beyond the scope of this project and will not be discussed further.

At the cellular scale, still, some applications take advantage of the comparatively high resolution of AFM, especially for the study of topographical features of the membrane. On bacteria, it makes AFM an important tool to study pili and flagella (Gillis, Dupres, Mahillon, et al., 2012). With regard to human cells, topographical studies showed differences in the structure and proteins in human lens membrane caused by cataract (Buzhynskyy, Girmens, et al., 2007; Buzhynskyy, Hite, et al., 2007). Furthermore, studying the surface of cells can allow observing their roughness, which has been used as a marker of cancer in some studies on mammalian cells, including human ones (Kaul-Ghanekar et al., 2009).

3.5.3. Cell Mechanics

By indenting the sample, AFM can be used to evaluate the mechanical properties of the sample, as discussed in Section 2.2.4 on force curves. A measurement at the scale of the cell can be obtained by performing one or several discrete force curves with a large, well-characterized probe. Such probes, notably spherical (Mahaffy et al., 2000) and cylindrical (Koay, Shieh, and Athanasiou, 2003) ones as well as wedged cantilevers (Cattin et al., 2015) are large to average out the heterogeneities of the cell in the attempt to have one or a few meaningful measurements and their well-defined geometry allows for reproducibility. The force curves are furthermore taken

3. *Biology and Relevant Applications*

at well-defined places of the cell, such as above the nucleus or in cytoplasmic regions. Alternatively, a probe with a more localized tip can be used to perform the measurements locally across a whole grid of points to have a map of mechanical properties such as developed in Sections 2.2.5 and 2.4 for force volume and PeakForce-QNM, respectively. Despite each of these curves being more sensitive to the natural heterogeneities of the cell, the quantity of data allows for the statistical analysis of all the local values, which can be aggregated to a cell-wide measurement or assembled in a signature.

As examples of these mechanical measurements, AFM can be used to measure cell elasticity (A-Hassan et al., 1998), and viscoelasticity (Rother et al., 2014), especially in modes such as force volume and PeakForce-QNM. Evidence increases on that cell mechanics, among which the elasticity, indicate cell states (Di Carlo, 2012). These changes happen earlier than the changes in morphology (Kuznetsova et al., 2007).

Such mechanical measurement allowed, for example, AFM to estimate the thickness of the peptidoglycan layer of Gram-negative bacteria before its imaging was made possible by cryo-TEM (Goldman and Green, 2008; Yao et al., 1999).

The elasticity of the environment of stem cells also appears to be connected with their development and specialization (Engler et al., 2006; Yim et al., 2010; Yourek, Hussain, and Mao, 2007).

Cancer

For mammalian cells, cell mechanics are of particular importance in understanding cancer. Indeed, cancerous cells are usually softer, although clinical use still requires systematic studies (Lekka, 2016). AFM can then be used on cells to discriminate between normal cells and their cancerous equivalent. Examples of its application in this field include bladder (Lekka, Laidler, et al., 1999), prostate (Faria et al., 2008), breast (Li et al., 2008), ovarian (Xu et al., 2012), thyroid (Prabhune et al., 2012), kidney (Rebelo

3. *Biology and Relevant Applications*

et al., 2013), and cervix (Hayashi and Iwata, 2015) cancers from cell lines. It has also been studied on lung, breast, and pancreas cancer cells (Cross, Jin, Rao, et al., 2007) and adenocarcinoma metastasis (Cross, Jin, Tondre, et al., 2008) directly extracted from patients, and on biopsies (Plodinec et al., 2013).

Reciprocally, the substrate topography and stiffness as well as compressive and shear stresses and mechanical stretching influence cancer state (Chaudhuri, Low, and Lim, 2018; Schierbaum, Rheinlaender, and Schäfer, 2017).

Whereas measurements with colloidal probes give a physically averaged elasticity measurement, nanomechanical mapping gives a map of such values. These maps can be used to compute the average elasticity *a posteriori* from the individual local values. Alternatively, the statistical distribution of the elasticity can be used as a signature and has been shown to be significant on breast cancer tissue (Plodinec et al., 2013), where different stages of the same tumor and metastasis have different signatures.

Lastly, AFM has been used to study the structure and behavior of microvilli on live cancer cells (Iyer et al., 2009), with a colloidal probe to study their mechanical brush-like characteristics as a layer at the cell scale.

As a conclusion, AFM could have a significant impact in cancer diagnosis but would require a standardization of the operational protocols before making possible a reliable comparison of absolute measurements (Lekka, 2016).

Other Diseases

Oppositely to the softening in cancer, an increase in stiffness is generally observed in diseases, such as arthritis, asthma, malaria, sickle cell anemia, and spherocytosis (Lee and Lim, 2007). This effect has been observed by AFM for hemolytic anemia and thalassemia (Dulińska et al., 2006), for cardiomyopathies (Lanzicher et al., 2015), and diabetes (Jin et al., 2010).

Besides its applications in research, AFM could be used for the early

3. Biology and Relevant Applications

diagnosis of such diseases through the detection of elasticity alterations. Its main advantages are the ability to work with little material and to provide a high force sensitivity. It could, for example, detect osteoarthritis on live samples from biopsies (Stolz, Gottardi, et al., 2009), although it should be integrated to be conveniently used *in situ* before practical non-destructive diagnostic can be achieved. Diagnosis applications of AFM are, however, drawn back by the absence of standard protocols and of automation.

3.5.4. Single Cell Analysis

AFM has the ability to resolve and study single cells, one at a time. The resulting data can then be filtered and combined during the analysis. This can be an advantage against batch population techniques, where measurements are taken directly at the population level and cannot be decomposed further. While population-level measurements are much more robust than individual single-cell ones, they hide sample heterogeneity. This can often give misleading data, even for monoclonal populations (Elowitz et al., 2002).

Single cell techniques are then required, with multi-parameter analysis of live cells, to fully understand the dynamics of the individual cells and their population (Lidstrom and Konopka, 2010). Although these parameters still have to be averaged across a great number of samples to reach the robustness of population-level measurements, the fact that this is done during the analysis allows to filter out outliers, to have information about the distribution, or to discriminate subpopulations.

Notably, subpopulations of isogenic samples—*i.e.* *with the same genetic code*—can sometimes dominate the behavior at the macroscopic scale (Lidstrom and Konopka, 2010). An example of this is the bacterial persistence to antibiotics (Balaban et al., 2004) and latent or chronic infections (Helaine et al., 2010). Phenotypical changes can indeed happen stochastically and their importance can be significant. In AFM, wide variations in the individual reactions of a population of *E. coli* bacteria to an antimicro-

3. *Biology and Relevant Applications*

bial peptide (CM15) were recorded although the population was isogenic (Fantner et al., 2010).

In isogenic populations of stem cells, differentiation occurs at different times, such that single cells techniques are required to fully understand this behavior by identifying the changes leading to it (Wang, Liu, Shen, et al., 2018).

As another example, Mycobacteria cells split into asymmetrical daughter cells with different properties. This increases their variability to give them phenotypical diversity to better resist the environment as well as immune responses (Kieser and Rubin, 2014). The population behavior being a function of its phenotypical heterogeneity, aggregate measurements would fail to provide relevant insights.

Similarly, working with single cell analysis technique is of high interest where samples are scarce, especially when cells cannot be replicated. In particular, more than 99% of bacterial species remain uncultivated at present (Lasken and McLean, 2014).

Oppositely, AFM can also be used on grouped cells, such as polarized monolayers of epithelial cells (Cartagena-Rivera et al., 2017).

3.5.5. Monitoring

Thanks to its applicability to living cells in biological conditions, AFM can be used to monitor a cell through time. It is applicable to the observation of natural cell behaviors, such as their division, and the variations of their topography or stiffness, or the repartition of target molecules on their surface.

These phenomena can also be studied across time while a drug is added and washed off. Alternatively, the cells can be scanned in batch before and after a treatment to observe differences.

3. Biology and Relevant Applications

Prokaryotes

As examples of these applications on prokaryotes, morphological changes at the nanoscale level have been observed for various bacteria-antibiotics combinations. These include *Escherichia coli* with cefodizime (Braga and Ricci, 1998), *Streptococcus pyogenes* with rokitamycin (Braga and Ricci, 2002), *Bacillus cereus* with daptomycin (Braga, Ricci, and Sasso, 2002), *Mycobacterium bovis* with ethambutol (Verbelen et al., 2006), *Acinetobacter baumannii* with colistin (Soon et al., 2009), *Candida albicans* with allicin and amphotericin B (Kim et al., 2012), *Pseudomonas aeruginosa* with penicillin (Formosa, Grare, et al., 2012), and *Saccharomyces cerevisiae* with caspofungin (Formosa, Schiavone, et al., 2013). Antimicrobial peptide have been studied similarly, such as for *Escherichia coli* with magainin 2 and PGLa (Meincken, Holroyd, and Rautenbach, 2005), and CM15 (Fantner et al., 2010),

Regarding nanomechanical properties, changes in cell elasticity have been observed for *Staphylococcus aureus* with lysostaphin and β -lactam antibiotics (Francius et al., 2008), *Escherichia coli* and *Staphylococcus aureus* with chitosan (Eaton, Fernandes, et al., 2008), *Pseudomonas aeruginosa* with colistin and β -lactam antibiotics (Mortensen et al., 2009), and *Candida albicans* with caspofungin (Formosa, Schiavone, et al., 2013), among others (Formosa-Dague, Duval, and Dague, 2017). Although some of the effects listed above have been studied by comparing a treated sample with a control one rather than with time monitoring, the later could be performed as well and show the dynamics of the event.

Other than for the study of antibiotics, which could be potentially be used *in vivo*, methods to disinfect surfaces or samples can also be studied. For example, *Bacillus pumilus* showed nanomorphological changes under electroporation, similar to the ones appearing with drug treatments (Formosa-Dague, Duval, and Dague, 2017). Cell stiffness before and after heat treatment have been performed on *Escherichia coli*, on the same bacteria (Cerf et al., 2009).

3. Biology and Relevant Applications

Eukaryotes

Using AFM, the monitoring of eukaryotic cells in time has shown changes in elasticity with temperature variations. Both an elasticity increase (Sunyer et al., 2009) and decrease (Spedden, Kaplan, and Staii, 2013) have been reported.

Similar studies have been conducted on the impact of drugs affecting the cytoskeleton. As an example, AFM has shown a decrease of fibroblasts stiffness with treatment by f-actin-disrupting such as cytochalasins B and D, latrunculin A, and jasplakinolide (Rotsch and Radmacher, 2000). Other treatments could also be studied likewise.

Finally, time monitoring can be used to study the natural behavior of cells. AFM has notably allowed to see changes in elasticity during mitosis (Matzke, Jacobson, and Radmacher, 2001).

4. Challenges and Current Solutions

As seen in Section 3.5, one of the main advantages of AFM is its ability to work on living cells in biologically-relevant conditions, provided that the cells are immobilized on the sample substrate. This can be easy for some cells, such as epithelial ones, or a somewhat more challenging task, such as for some kinds of bacteria. It is, however, discussed in Sections 2.3.2 and 5.1.3.

AFM analysis of cells, especially mammalian ones, is further drawn back by their size being at the upper limit of what most available systems are able to work with, by their large variations in height whereas AFM tends to perform best on flat surfaces, and by their softness. Furthermore, while most bacteria evolved to thrive in favorable conditions while surviving in harsh conditions, animal cells have not evolved to withstand other conditions than the homeostasis of the body to which they belong. As a consequence, they require certain elements to be present in their medium in certain ranges of concentration, as well as a narrow-ranged pH and temperature. They may also suffer from the prolonged exposure to direct light. These problems will be discussed further on Section 5.1.

These hurdles set aside, AFM gives tremendously valuable results. These results tend, however, to vary a lot because of the differences in protocols and handling of the preparation of the sample, its measurement by the AFM, and the subsequent analysis, all of which being additionally operator-dependent. These differences add up to the ones linked to the natural heterogeneity of cells. As we will see below, these two dimensions

4. Challenges and Current Solutions

of impediments to the results act differently.

When taking a measurement, one does not always record the real underlying value. There is always some level of error, the opposite of which is accuracy. We show in Appendix B that this accuracy, the absence of errors, can be decomposed in two elements: trueness and precision.

Precision corresponds to the repeatability of a measurement. A measurement is said to be precise if identical samples give near-identical values, with little variance. The measured value, however, does not have to correspond to the underlying physical properties as a constant, systematic bias would not affect the variance, hence the precision.

The trueness, on the other hand, represents the tendency of the measurement to be around the underlying value. It corresponds to the tendency of errors to average out when the measurement is repeated.

Although a correctly calibrated AFM is very accurate as such, the same cannot be said about its applications on live cells. We would like final measurements on live cells to be accurate as well, hence precise and true. We will see that the trueness has been increased recently but the precision can only really be increased by gathering more data.

4.1. Trueness

Even with standardized procedures, such as force volume, it has been shown that comparing absolute values of the elasticity obtained in different laboratories gives very different results, even for the same cell lines (Kuznetsova et al., 2007).

As a consequence, current studies are done by comparing the elasticity of the sample of interest (treated, cancerous, sick. . . cells) with a control. The corresponding measurements have to be done with the same system, the same setup, the same kind of probe and it is not always enough so that probes from the same batch are usually preferred, even going as far as to use the exact same probe. The ideal case is to use the same probe without

4. Challenges and Current Solutions

even moving the laser spot to avoid recalibration. This is not compatible with the AFM being used as a diagnosis tool, where the measurement is compared with absolute values that are independent from the setup of the system. For screening purposes, the comparability of the data might be questioned when the probe has to be changed, which ought to happen with so many measurements.

To allow for comparing values obtained on different systems, these need to be properly calibrated. Given the complexity of the system, multiple elements need calibration and reliable methods have only been appearing in the last few years.

The most common method of calibration until recently was to measure the deflection sensitivity with a force curve and find the spring constant with the thermal tune method.

4.1.1. Deflection Sensitivity

The deflection sensitivity establishes the link between the value recorded from the photodiode and the actual deflection of the cantilever. This depends on the system, the cantilever, and the alignment of the laser. As a consequence, this calibration has to be repeated when the cantilever is changed or when the laser is re-aligned.

To find it, we can take the differential form of Equation (2.7):

$$\Delta D = \Delta Z + \Delta d + \Delta \delta, \quad (4.1)$$

where D is the tip-sample distance, d the deflection of the cantilever, δ the deformation of the sample, ΔZ the displacement of the piezoelectric actuators. In contact, we have $D = 0$ and, on a hard substrate, $\delta = 0$. We then have $\Delta d = -\Delta Z$, which, assuming that the piezos are calibrated, is known.

4. Challenges and Current Solutions

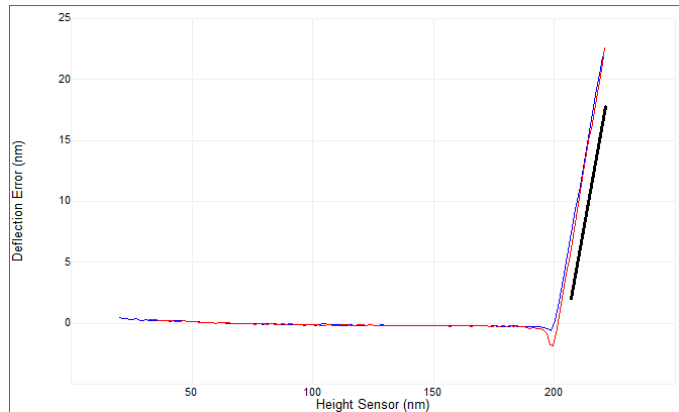


Figure 4.1.: Deflection sensitivity calibration. A force curve is taken on a hard surface and the contact region is fitted (black line, with arbitrary offset) to find the slope, giving the deflection sensitivity. © Bruker, modified.

Using this in the differential form of Equation (2.5), we have:

$$\Delta d = d_s \times \Delta d_V, \quad (4.2)$$

where d_V is the value measured in volts and d_s the deflection sensitivity, we obtain:

$$d_s = -\frac{\Delta Z}{\Delta d_V}. \quad (4.3)$$

This allows us to calibrate the deflection sensitivity by recording a force curve on a hard substrate such as glass, as represented in Figure 4.1. After ensuring that the contact region is linear, its most linear part is fitted with a straight line, whose slope gives $-\frac{\Delta Z}{\Delta d_V}$. The minus sign comes from that we took Z as the tip-sample “distance” as seen from the piezo, which goes in the opposite direction than the piezo extension.

After this calibration, the value of the deflection measured by the photodetector can be appropriately translated to the actual deflection in length units. This calibration has been shown to be very error-prone (Schillers, Rianna, et al., 2017). Furthermore, a high force threshold has to be used

4. Challenges and Current Solutions

to have a sufficiently long linear contact-zone. This can be a problem on functionalized tips since exerting too high of a force could damage the functionalization. The calibration can (and should) then be realized post-experiment, although giving less convenience and control to the user.

4.1.2. Spring Constant

The spring constant, k , is a property of the cantilever. There are ways to find its theoretical values by formulas based on the mechanical properties and shape parameters of the cantilever. These methods are, however, sensitive to the exact dimensions of the cantilever and to defaults or variations in its structure. They can vary sensibly between cantilevers, even within the same wafer, which implies that the measurements would have to be performed on each cantilever separately (Cappella and Dietler, 1999). Measurements at that scales have to be performed by Scanning Electron Microscopy, which is also difficult to calibrate for proper length measurements. Furthermore, this calibration would have to be done post-experiment.

There are, however, other methods for calibrating the spring constant. A small bead of known mass can be added at the end of the cantilever, producing a shift in the resonant frequency, which can be measured from the spectral noise of the deflection measured by the photodetector (Cleveland et al., 1993). Alternatively, the deflection caused by an added mass can be used (Senden and Ducker, 1994).

Another set of methods, mostly used because of their ease of use, focus on the response of the cantilever to thermal noise. On an idle cantilever at thermal equilibrium, the deflection stays constants except for the noise of the system, which visually broadens the baseline of the curves. Modeling the cantilever as a harmonic oscillator, one can establish a relation between the spring constant and the thermal noise of the deflection. More precisely, if the variation of the deflection* can be solely attributed to the thermal

*In practice, the relationship between the angular deflection (recorded with the

4. Challenges and Current Solutions

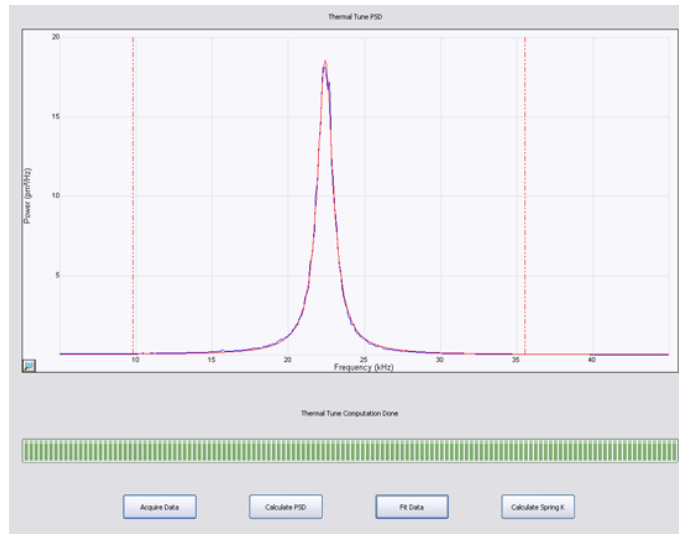


Figure 4.2.: Thermal Tune calibration of the spring constant. The power spectral density of the noise of the cantilever deflection is recorded and fitted to extract the thermal component. © Bruker, modified.

noise, we have (Hutter and Bechhoefer, 1993):

$$k = \frac{k_B T}{\text{Var}(d)} \quad (4.4)$$

where k_B is the Boltzmann constant and T the temperature of the system. For it to be reliably measurable, however, the variation of the deflection has to be within the detection range of the system. As a consequence, only relatively soft cantilevers (i.e. with a spring constant no higher than 1 N m^{-1}) can be calibrated.

As there might be other sources or noise, a further analysis can be useful. Although random, noise is not without a structure and can be decomposed in its power spectral density (PSD), the square of its Fourier transform.

optical lever effect) and the vertical deflection (the actual deflection) is slightly different on a free cantilever than when forces are applied on the tip, so a correction factor, the deflection sensitivity correction, is used.

4. Challenges and Current Solutions

Thanks to the properties of the Fourier transform, the area under the curve corresponds to the variation of the deflection used above. Modeling the cantilever as a harmonic oscillator with small damping, the corresponding PSD has the shape of a Lorentzian curve, as presented in Figure 4.2. Since the spring constant of the cantilever should be of the order of magnitude of its nominal value, giving an idea of the position of that curve in the frequency domain. Other sources of noise having widely different corresponding peak frequencies and PSD shapes, it is relatively easy to fit the data into the theoretical Lorentzian curve. Rather than using the area under the whole PSD, we can use the area P under the Lorentzian fit, which is essentially the power spectral density of the thermal noise and we have (Hutter and Bechhoefer, 1993):

$$k = \frac{k_B T}{P}. \quad (4.5)$$

A similar method, although with a different function, can be used in fluid when the damping is significant.

It should further be noted that this method is based on the analysis of the deflection, d , across time. Hence, any error in the deflection sensitivity is passed on to the spring constant.

4.1.3. SNAP

As described above, the most common cantilever calibration method in biology is to calibrate the deflection sensitivity using a force curve on a hard sample, then calibrate the spring constant using the thermal tune method. In this method, which can be named “touch calibration”, the calculation of the deflection sensitivity is made in the contact part of the curve. It was, however, acknowledged as an important source of error.

A recent method, called the Standardized Nanomechanical AFM Procedure (SNAP), aims at avoiding this error-prone measurement on the force curve (Schillers, Rianna, et al., 2017). In this non-touch calibration

4. Challenges and Current Solutions

method, the spring constant is known in advance and the deflection sensitivity is found by reverting the thermal tune method. A reliable way to calibrate the spring constant can be based on a vibrometer characterization and can be performed by the probe manufacturer. To revert the thermal tune method, the deflection sensitivity is estimated and the corresponding spring constant is calculated with that method. A correction factor λ is defined as the ratio between the calculated spring constant and the obtained value. This factor λ is then used to correct the deflection sensitivity.

The SNAP method showed a substantial increase in reproducibility across laboratories (Schillers, Rianna, et al., 2017), which is believed to be of strong help to ensure the trueness of the results, especially on eukaryotic cells.

4.2. Precision

The mechanical properties of cells depend on a lot of parameters due to the complexity of biological processes, which is what makes them interesting as they can be used in a wide range of applications. On the other hand, that also means that the properties vary from one cell to another in the same external condition as their individual internal conditions may vary. They also have a strong connection with the individual cell shape and size. With regard to the measurements, this increases the variance of the variables within a condition, considered as the within-group variance.

Furthermore, mechanical properties such as the stiffness are usually defined for bulk materials that are both homogeneous and isotropic. As it can be seen in the elasticity maps or tomography, different parts of the cells have very different local pseudo-elasticities. The “elasticity” of a cell is nothing else than an average, under some measure, of the elastic properties of the different elements, plus their interactions. Every cell has a slightly different structure, depending on its state, its neighborhood, its shape, etc. This will induce different interactions between its components,

4. Challenges and Current Solutions

hence different elastic properties. It also has to be added to the pure effect of topography which, even for a homogeneous isotropic sample, will modify the measured mechanical properties but can be corrected by shape factors. As a consequence, the measure of the elasticity of a single cell makes little sense.

In addition, differences being studied, the ones due to the actual effect are usually minutes. These differences, corresponding to between-group variances in the measurements, are usually small compared to the within-group variances representing the natural variability of cells. The overlap in the distributions of these measures is significant. Hence, one cannot compare the elasticity of two cells in two different conditions but only the distributions of these properties between the two samples.

Distributions are, however, more complex than single values. A classical way to compare distributions is to compare their mean or their median. Whereas sharing the same mean or median does not imply that the distributions are the same, having different means or medians implies that the distributions are different. Consequently, a measurement taken on two conditions that yield statistically different means or medians implies that the treatment has an effect. The actual effect, however, is subject to the interpretation of the scientist, as it might not be homogeneous on the distribution, yielding more complexity than a simple shift in the distribution.

Other parameters than the mean or the median can be used, however. For instance, one can focus on the maximum and/or minimum observed values in the distribution or, for the sake of robustness, the 5th and/or 95th percentile, or any other. The variance and the number of modes of stiffness distributions have been used to recognize signature of tumors (Plodinec et al., 2013), as well as the skewness and kurtosis (Canetta et al., 2014).

The precision of the sample distribution properties as estimators of the corresponding properties of the underlying population distribution increases with size. As a consequence, recording a precise measurement of the mean, median, or other characteristic of a distribution requires high sample sizes.

4. Challenges and Current Solutions

We mentioned above that the cell is not a homogeneous material and that their elasticity varies within each of them. Whereas large probes can be used to attempt to average out the internal variability of the cell, analysis methods can have their own interest. Indeed, one could take a mapping of the mechanical properties of the cell and consider each pixel as a sample and the cell as the micro-population. The cell elasticity can then be studied as a distribution and reduced to, for example, its mean or some percentiles. This single value can then be considered as the cell property that we can study at the sample level, as done above. The necessity of having a lot of curves per cells and many cells is well summarized by Lekka and Laidler (2009).

4.2.1. Corresponding Problems

AFM is long and operation-intensive. An operator is required to calibrate the system, load a sample, approach the probe within engaging distance from the sample, set the base parameters for the scan, find an area of interest, engage, optimize the parameters, launch the scan, save the data, wait for the scan to be completed, move to the next area of interest, and repeat. During this setup, the engaging process can take a minute or two, and scan can take up to an hour or more depending on the scan parameters such as the resolution and the speed.

This issue is well recognized in the literature. Iyer et al. (2009) say that one of the main challenges in their study concerning colloidal probe on cancer cells to study the microvilli was the lack of data for statistical significance. Taking measurement on 20 to 30 cells is common good practice when studying cell mechanical properties (Lekka, Laidler, et al., 1999; Lekka, Gil, et al., 2012; Park et al., 2005), while around 10 cells can be enough to give some insights (Sokolov, Dokukin, and Guz, 2013).

As pointed by Lekka and Laidler (2009), some studies are made on very few curves on each cell, sometimes taken at the same position (Cross, Jin, Rao, et al., 2007). While this can be enough for pointing towards

4. Challenges and Current Solutions

correlations between mechanical properties and biological state, one has to be very cautious when using it as an indicator for diagnosis.

For the publications that do not recognize the problem, many are done with too few samples to ensure proper statistical significance. This can even be misused for *p*-hacking.

The low throughput and the operational weight of AFM distinguish it badly from the current high-throughput techniques used in proteomics, genomics, lipidomics, and other omic approaches.

To benefit from the capabilities of the AFM as a single-cell technique and the specific advantage of these techniques for the study of sub-population, it is important to have a lot of data, so that the sub-data is also of a decent size.

It is, therefore, important to increase the quantity of data for the precision of AFM measurements. However, gathering AFM data is time-consuming and the time of the operator is a limiting factor. As a consequence, it is necessary to improve the quantity of data released per unit of operator time. To do so, three main possibilities should be explored:

- increasing the scanning speed;
- scanning several cells in parallel;
- loosening the dependence on the operator.

These three points are discussed in the sections below in more details, with a focus on how they would or would not solve the problem at hand. Current implementations are also listed.

4.3. Faster Scanning

The first option to accelerate the scanning process corresponds to doing what is currently done, faster. The throughput, which corresponds to the total number of scans divided by the total time spent, can be decomposed in two: fixed time and variable time.

4.3.1. Fixed Time

The fixed time is the time that does not depend on the number of scans. It is common to experiments of any scale and can be further decomposed as:

- the time to prepare the sample;
- the time to setup the system;
- the time to clean up after the experiment.

The preparation time mostly depends on the protocol being used, which often comes with time constraints guided by biological concerns. The setup time depends on the carefulness and experience of the user, as well as the design of the system. Advanced users can be faster than beginners. Oppositely, careful users might want to spend some time setting up their system properly to improve the quality of their data, often at the expense of time. Some systems might also be easier to use efficiently than others. Although there might be room for continuous improvement in the system designs and in good practices and training of the users, it is out of the scope of this project and would only account for a constant decrease in time which would not scale with the size of the experiment. Whereas fixed time operations can be the limiting factor in a short experiment where only a few scans are needed, it can usually be neglected for long ones, unless several preparations and setups are required during the session.

4.3.2. Variable Time

The variable time, on the other hand, is the part that is proportional to the number of scans. It can be expressed as the average time per scan, multiplied by the number of scans. The average time per scan can be decomposed as:

- the scanning time as such;

4. Challenges and Current Solutions

- the “dead time” between two scans.

The scanning time tends to decrease over time. Force volume images that used to take hours 10 years ago can now sometimes be achieved with a much higher resolution in minutes. This can be attributed to development in the probes, the piezos, and the electronics. Parts of these developments are pushed forward by the developments of High-Speed AFM, which is described in Section 2.6.

Physical limits exist, however, and hydrodynamic effects of the medium are exacerbated by speed. These effects are reduced on new small cantilevers, such as the ones developed for High-Speed AFM. Some small cantilever have even been used to probe the viscoelastic properties of the sample at high frequencies (Rigato, Miyagi, et al., 2017).

More importantly, the viscoelastic properties of cells themselves vary with speed (Fabry et al., 2001; Rigato, Miyagi, et al., 2017), complicating their analysis. Furthermore, in applications involving force spectroscopy, guaranteeing a minimum contact time of 250 or 500 ms can be necessary to promote interactions (Dupres et al., 2005). As a consequence, increasing scan speed is sometimes incompatible with the long-term increase of sample sizes.

Between scans, time-consuming activities include locating the area of interest on the sample, withdrawing and engaging the system in some cases, and optimizing the parameters. These activities can be shortened, with faster engage/withdraw procedures and easier optimization of the parameters. Faster localization of the areas of interest can be attained by combination with other kinds of microscopy. Still, improving the speed of these elements will not shorten the scan time *per se*, bringing only limited speed increases.

4.4. Parallel Scanning

A second possibility to be explored would be to scan several cells at the same time. Such parallelization can happen at different scales.

First, a trivial yet quite extreme solution would be to have several AFM systems that could be use in parallel by the same operator. Although this would certainly allow the user to work on one system while the other(s) are scanning, this would make the investment cost scale with the speed and require to perform the setup on each system. Furthermore, constantly moving back and forth between several systems for 8 hours a day could be mentally draining for the user.

A second solution consists of having several cantilevers on the same chip. Some work has been done on cantilever arrays since the late 1990s, with multiple developments. An iconic example is IBM “Millipede” (Vettiger et al., 2000), reporting an AFM-based data storage system. It raised hopes for ultrahigh storage density and also perspectives in increasing AFM imaging throughput but it did not appear to live up to its expectations.

The optical lever method is, however, difficult to scale with the number of cantilevers. It could be very impractical to implement because of the need to align one laser and the corresponding photodetector per cantilever, with the risk of mixing up lasers, cantilevers, and the corresponding spots on the photodetector. As a consequence, the measurement can be performed by means of microelectromechanical sensors (Minne et al., 1998), as shown in Figure 4.3, or thermal ones (Vettiger et al., 2000) associated to each cantilever, among others.

The tips are often aligned on a planar grid, with a feedback on the position and tilt of the plane as a whole, which can, for example, be based on the deflection of some dedicated cantilevers (Vettiger et al., 2000). Individual feedback loops are usually not possible, except for microelectromechanical systems (MEMS), for which cantilevers can be bent individually, although in a certain range only. Due to the electronics, these methods are difficult to apply in liquid medium, which limits their applicability to biological

4. Challenges and Current Solutions

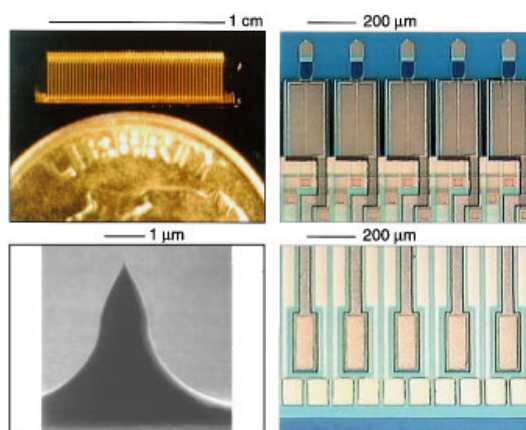


Figure 4.3.: Array of microelectromechanical cantilevers. Top left: entire array of cantilevers next to a dime. Top right: zoom on 5 of the 50 cantilevers. Bottom left: SEM image of one of the tips. Bottom right: electrical pins of the individual cantilevers. Reproduced from (Minne et al., 1998).

samples. Nevertheless, micro-array-compatible piezoresistive probes have been demonstrated on eukaryotic cells in buffer solution, although not in parallel (Polesel-Maris et al., 2007). Other kinds of electrical detection methods are suitable for use in biological conditions (Pürckhauer et al., 2018) and could possibly be used in parallel.

Still, the optical lever method has been demonstrated on tissues, with an array of 8 cantilevers operating in fluid (Weder et al., 2016). Nonetheless, the tips cannot be individually controlled, so significantly different forces can be applied by the different probes depending on the sample mechanical properties and geometry, as is described below.

Another method for measuring the deflection is to use the interferometric properties of light (Erlandsson et al., 1988). In this method, the laser beam is split in two and one beam is focused on and reflected by the cantilever before being recombined with the other. The two beams create interferences that can be recorded to measure the dephasing of the two beams, which depends on the deflection. This method is, however, sensitive to

4. Challenges and Current Solutions

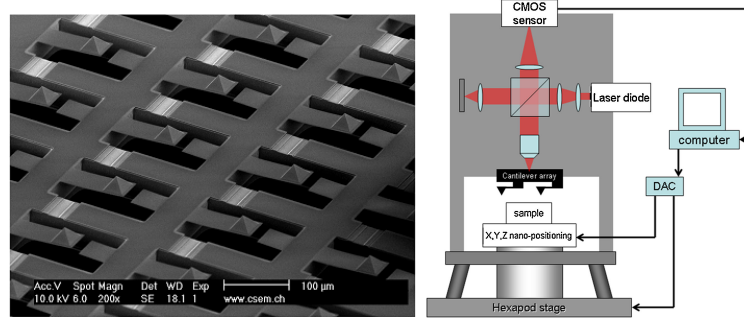


Figure 4.4.: Array of cantilever for interferometry. Left: SEM image of a section of a 4 by 7 cantilevers array used with interferometric detection. Right: representation of the corresponding interferometric detection system, based on a Linnik interferometer and a CMOS camera. Reproduced from (Favre et al., 2011).

phase wrapping since the phase causing the interference patterns is periodic. As a consequence, naive solutions use big wavelength at the expense of vertical resolution. Otherwise, unwrapping techniques are required, such as done by Favre et al. (2011).

This technique, alleviating the need of aligning the laser on the cantilever, was used in one of the extreme examples of multi-cantilever arrays. In the work of Kawakatsu et al. (2002), operating millions of cantilevers, the measurement was implemented by an interferometer going sequentially over each of them, which strongly limits the throughput. Interferometry has been, however, demonstrated on biological samples, with a global illumination covering all the cantilevers and a measurement based on image analysis of the interference patterns on the cantilevers (Favre et al., 2011), shown in Figure 4.4. Although more computationally expensive, this method allows the recording of all the cantilevers in parallel.

Without MEMS, however, the tips cannot be controlled individually. Given the lack of alignment of the cells, the tips can get in contact with the sample on different parts of cells, hence at different heights. These differences in contact height induce differences in indentation, hence in the

4. Challenges and Current Solutions

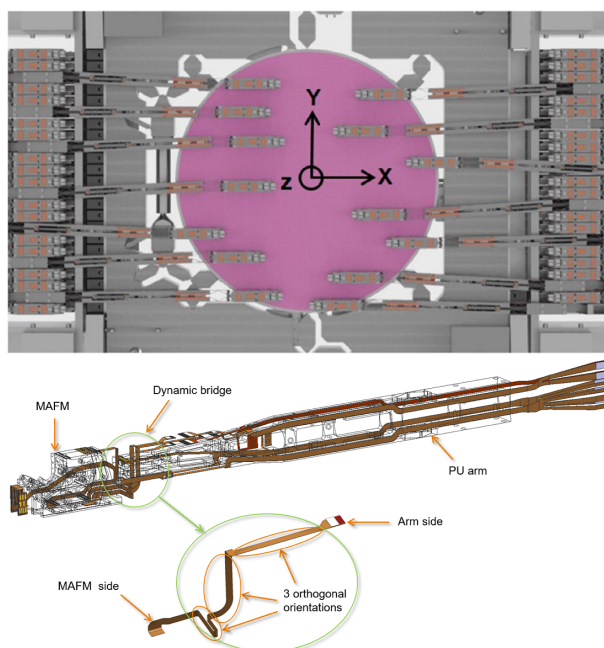


Figure 4.5.: Miniaturized AFM (MAFM) setup. Top: representation of a system with multiple MAFMs on a wafer stage. Bottom: close-up with of an MAFM and its positioning unit. Reproduced from (Sadeghian, Herfst, et al., 2015).

force. As a consequence, some tips might apply very high forces to cells while other are barely touching the sample, which can be damaging for the sample and strongly impede mechanical measurements.

Finally, a somewhat intermediate solution between having several AFMs and a cantilever array exists in having several independent probes on the same system. Groups of miniaturized AFM have been developed, shown in Figure 4.5, and have been shown to be operable in parallel (Sadeghian, Herfst, et al., 2015). Their current implementation, however, presents some challenges before working in biological conditions since they currently work in air, on large inverted samples and their electronics does not appear to be compatible with usage in water.

4.5. Unattended Scanning

A last possibility to be considered in the search for increasing the yield of scans is to remember that one of the limiting factors, in time, is the availability of the operator. As a consequence, unless the availability of full-time operators is not a concern, automating the system would improve its time of useful operation, hence increasing the overall number of measurements.

By making the operator less required, we might make the system able to work more than the standard 8 hours a day and gain time in the periods where the operator might not be present immediately, such as at the end of a long scan.

4.5.1. Automated Steps

Aligning and engaging automatically has been illustrated quite early on. Developments have followed, towards higher levels of automation.

Automated Move

Automatically moving the sample simply requires the sample and/or the AFM head to be motorized. The difficulty lies in the control of the accuracy of the positioning, which requires precise motors and sensors. Thanks to the usage of servomotors, horizontal positioning with accuracy around 2 μm are typically achieved.

While an accurate stage with sensors can allow automated moves at pre-recorded positions, it can be interesting to move to samples detected on an optical image. This requires co-registering the coordinates of the AFM and its stage with the optical image. This can be of particular interest when the field of view can be extended by combining separate images in the same registration system (Chen et al., 2015).

Automated Alignment

In an early configuration, cylindrical lenses were used to elongate the laser spot in the direction perpendicular to the cantilever (Mou, Huang, and Shao, 1995; Shao, Mou, and Huang, 1998). That way, the laser spot position only had to be controlled in one direction. Similarly, a cylindrical lens was used in front of the photodetector so that no lateral alignment was needed on the photodetector side. The mirror deflecting the laser from the cantilever to the photodetector was controlled by a stepper motor. The motorization of the alignment opened the way to computer control leading to automation. It consisted in a simple algorithm moving the laser beam from a position further than the end of the cantilever towards it until a signal is obtained. Then a rotation was applied to the mirror to maximize the total signal recorded by the photodetector, before finally tweaking the laser beam and mirror positions to optimize the detection.

When using a laser spot, a similar process is possible, although the laser has to be scanned perpendicularly to find the cantilever before doing the parallel movement to be centered at the end of the cantilever (Young et al., 1998).

Automated Engage

In the early configuration mentioned above, three stepper motors were used for engaging, simplifying the previously mostly manual procedure (Mou, Huang, and Shao, 1995; Shao, Mou, and Huang, 1998). The engagement could then be controlled by software and be performed by sequentially stepping the three motors to keep the head parallel to the sample until the tip gets in contact with the surface. Nearly all modern AFMs have automated engage, but most of them require manually realigning the laser and photodiode.

The typical engage procedure consists of probing a distance with the piezos to verify the absence of obstacle (the sample) and then do the same movement (minus a safety margin) with the step motors. To do so, the

4. Challenges and Current Solutions

vertical piezo is extended to lower the probe as for a normal ramp until a trigger force is met, which would correspond to the contact with the sample. If the end of the ramp is reached before the trigger, the probe is retracted to a safe position. The system is then lowered with step motors by a bit less than the ramp size so that the tip, still with the piezo retracted, stays within the vertical distance probed during the ramp. This ensures that the tip-sample contact does not happen during the coarse movement of the motors to avoid shocks and preserve tip sharpness. The cycle is repeated until the reaching the sample. In tapping engage, the process is similar except for that the tip is oscillated and the trigger usually falls on the amplitude.

This process being quite slow, it is still to the user to bring the tip relatively close to the sample to avoid waiting for a long period of time. If the tip-sample distance can be estimated, one can then directly lower the probe to cover most of the distance, minus a safety distance. This is the case, for example, when the tip is at a known distance from the focal point of the optics and the sample is in focus, then at a tip-focus distance from the tip. On reflective samples, it might be easier to focus on the reflection of the tip on the sample, the sample being then at half the tip-focus distance. Automatically detecting the sample optically is possible in some cases, as when the sample is feature-rich or reflective. On transparent samples, however, this procedure is more challenging.

Since it is difficult to know in advance the minimum reliably detectable trigger and for the sake of speed, the trigger used during the engage procedure might be significantly higher than the setpoint used during the scan. Indeed, the latter can be optimized by the user or an algorithm since the presence of the sample gives a direct feedback on the quality of the tracking, oppositely to the engage trigger.

Other models of automatic probe landing are still being studied. For example, a frequency modulation with amplitude imaging (FM-AI) engaging method is developed to have softer landings (Belikov et al., 2017).

Automated Cantilever Exchange

Typical automatic probe exchange is done with either vacuum or magnetism (Sadeghian, Bijmagne, et al., 2017).

Exchanging the tip without the cantilever has also been demonstrated. Long, thin tips can be placed with robotic manipulation and glued on top of a pyramidal tip or clipped at the end of specifically designed cantilevers (Rajendra Kumar et al., 2009). Pyramidal tips can also be adhered to a tipless cantilever with a fluid meniscus (Sri Muthu Mrinalini and Jayanth, 2016), although the stability of the tip positioning could be questioned and the system might not be possible in liquid.

4.5.2. Automated Scan

Automated Force Curves

Force curves can be easily repeated at a given position in an automated fashion. Force volume mode can be seen as an automated repetition of such curves, with a horizontal movement for them to be taken over a 2D array of points. In other modes, positions can be defined as a grid and then moved by the user, or each placed individually by the user before being acquired automatically.

Automated Imaging

While able to work at high speed, tapping mode requires a lot of expertise to adjust the feedback. Automating it is, therefore, difficult and has, to our knowledge, not been reported.

In contact mode, methods for semi-automatic tuning have been reported, although their purpose is more to optimize the scanning speed rather than automation *per se* (Abramovitch, Hoen, and Workman, 2009; Abramovitch and Moon, 2013) and does not appear to be available for bio-AFMs. The main problem, however, is that the vertical deflection is subject to thermal drift that can quickly become larger than the setpoint. A perceived

4. Challenges and Current Solutions

increase would force the system to retract and might stop it from tracking the sample by detaching from it. Oppositely, a decrease in the perceived deflection would make the system use a higher force, which might destroy the sample. An automated setpoint adjustment exists (Casuso and Scheuring, 2010), although it has not been shown on live cells.

In PeakForce Tapping, the ScanAsyst technology is commercially available and allows the user to define a robust setpoint on the peak force between the tip and the sample, hence offering a better force control. The algorithm is detailed in Section 2.4.5. Such a direct force feedback at each pixel is particularly suitable for nanomechanical analyses and to limit the forces—hence the degradation—of the sample and the tip.

4.5.3. Automated Systems

Implementation

Almost all existing systems implement some elements of automation cited above. Automated engage is currently widely available. Moving the stage automatically is usually possible on systems that have one, although the accuracy of the positioning might not always be sufficient for the applications. Automated alignment and imaging are, however, often lacking.

Among the systems considered, the Dimension FastScan can move and perform most of the engaging steps by itself. The BioScope Resolve can have scans defined first and performed later so that the user can give most of its input at the same time. It does, however, require regular user control to verify and correct the alignment.

Batch Scans

Once the scanning process as such has been automated, one could move to a location of interest, engage, and take a first survey image. Several positions can be selected for taking force curves, or areas chosen for taking force volume or imaging scans. If selecting at once a number of curves

4. Challenges and Current Solutions

and scans to be taken automatically, some level of automation has been achieved. These were, for example, implemented on Bruker system with “Point and Shoot” and other Microscope Image Registration and Overlay (MIRO) features.

Industrial Metrology

Fully automated AFMs exist, mostly on silicon wafers for quality-assessment purposes. This is driven by the continuous decrease in the size of electronic features, which makes them more sensitive to defects that would have been considered earlier as benign. As a consequence, the upper limit of acceptable defects decreases, and methods for defect review are pushed to required higher resolutions. Such a system can also be used for the calibration of other instruments.

A first example of automation is the systematic measurement of critical dimensions or other properties at different locations on a patterned wafer. Typically, silicon wafers in semiconductor production environments are composed of a repetition of an identical pattern over a grid covering the wafer. Each pattern can be quite complex. A typical throughput would be to define some measurements to be performed on a position of the pattern, such as a height or a width. Given the repetitive nature of the wafer, the coordinates of the patterns can be inferred from a few registration points, although image recognition techniques can be used to realign the system on each pattern. The measurements can be made on all or a subset of the grid.

When combined with a system able to check the quality and dimensions of the tip, change it if needed, and an automated sample exchange, one can have a totally automated system.

A range of more detailed applications is also possible. As an example, when combined with optical instruments allowing for detection of defects but not their characterization, the registration of the sample on the AFM and on the detection instrument can be matched. The detected areas can

4. Challenges and Current Solutions

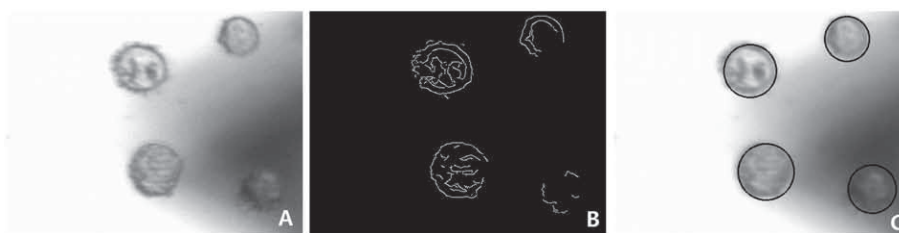


Figure 4.6.: Cell detection method on fixed Raji cells in the video image. A: original gray-scale image. B: edge detection. C: detected circles, overlaid. From Wang, Liu, Wang, et al. (2012).

then be scanned with a low-resolution scan to find the defect and a high resolution one to characterize it (Zandiatashbar et al., 2015).

Force Spectroscopy

In fluid, aside of the semi-automated systems presented above, an automated system exists for the specific field of Single-Molecule Force Spectroscopy. If in typical SMFS applications about 1 in 500 force curves show an event of interest, recording 16 such events with 95% certainty requires the capture of 11,500 curves (Struckmeier et al., 2008). The ForceRobot (JPK) was introduced as an instrument able to monitor and regulate the conditions of the experiment while taking these force curves over extended periods of time.

Cells

Wang, Liu, Wang, et al. (2012) developed an automated system on Raji cells, which were fixed with glutaraldehyde. Placed in a Petri dish, the cells were detected on the video image with a method allowing for circle detection, the Hough transform, represented on Figure 4.6. The AFM was then engaged on the center of these circles and a scan line was performed along each of the two horizontal axes, shown in Figure 4.7. On both scan lines, the limits of the cells are detected, which gives four points of the cell

4. Challenges and Current Solutions

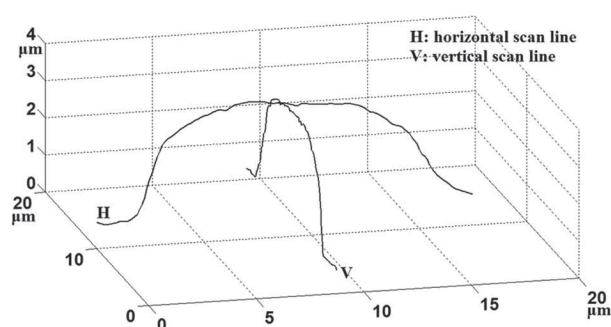


Figure 4.7.: Cell probing method on fixed Raji cells. The AFM is engaged on one of the cell detected in Figure 4.6 and a scan line is taken along each axis to better localize the cell. From Wang, Liu, Wang, et al. (2012).

border. From these four points, assuming that the cell is circular, one can then extrapolate the cell center, on which force curves could be taken.

With this system, it is possible to detect and take a few curves per cell in 3 s per cell on average. The system is, however, quite reliant in the circular shape of cells since it is used in both the optical and AFM detection. Furthermore, taking isolated force curves on cells is usually performed with colloidal probes to average out the cell heterogeneity, whereas this system requires a standard one to take the two scan lines. This system does also not address the multi-sample issue.

Others

Some automated AFM instruments are on the market. Few are able to host multiple samples, but only in air, which is incompatible with most biological applications. Efforts to associate Artificial Intelligence with AFM are also on their way, with an example where additional probings are targeted by AI image recognition with a Support Vector Machine to probe interfaces (Huang, Li, and Li, 2018).

Part II.

Results

5. Objectives and Requirements

AFM is useful in biology thanks to its high resolution and to the number of parameters to which it gives access. These parameters can, however, only be recorded in the framework of a model applied to data obtained by following protocols. As discussed in Chapter 4, such measurements can only be accurate if they are both precise, meaning that they are self-consistent when repeated on the same setup, and true, meaning that they tend to give the same results across systems, labs, measurement protocols, and technology, thus indeed corresponding to the real physical value.

While the trueness issue is being addressed by better models and better calibration methods, precision stays an issue in the biological applications of AFM. As a matter of fact, the dynamic and complex processes of life induce a lot of variability and diversity in the observed values. Considering that focusing on properties of individual cells makes no more sense than comparing two persons to generalize conclusions about their cultures, scientists focus on the distribution of these properties in populations of cells in different conditions. Distributions can be compared on some of their parameters, such as their mean or median among others, used as markers. The precision at which these markers can be measured depends on the protocol, the material, and the ability of the operator to some extent, but are fundamentally limited by the number of samples gathered. As a consequence, increasing the precision, hence the accuracy of the measurements, requires using bigger sample sizes, as discussed in Section 4.2.1.

In order to gather more data, three solutions have been considered in Chapter 4: decreasing the total time per scan, scanning several samples in parallel, or increasing the effective time. Time per scan has been and

5. Objectives and Requirements

still is decreasing over time but cannot improve by orders of magnitude without hitting on the physical limits of the sample or the operator. Several prospects exist in parallel scanning but the most promising ones seem a long way from applying to biology.

We, therefore, focused on automation, as a way to increase the effective time of scanning by removing the time inefficiencies linked to requiring almost constant input from a human operator. The objectives of this thesis are then to introduce new hardware, software, and methodological solutions going in that direction. It aims at improving AFM throughput on live cells in the perspective of going towards a correlative multi-mode and multi-sample system.

5.1. Requirements

On the long term, the desired AFM should be suitable to:

- scan cells (or other biological samples)
- in a correlative setup
- automatically
- in a multi-sample environment
- with consistent results
- over extended periods of time.

Secondarily and over subsequent improvements, the system could be evaluated on its speed and its ability to scan many cells in a row, keep the different samples in very similar conditions, and gather a maximum of data for each cell (including the number of imaging modes and the resolution). As a first constraint, since this is an early development, our initial system had to be based on a pre-existing AFM, considering the BioScope Resolve, the Dimension FastScan-Bio, and the Dimension Icon. This initial system

5. Objectives and Requirements

will allow us to gather some experience, which will be discussed across the following chapters along with potential improvements, before concluding on long-term perspectives in Section 10.2.

These microscopes are presented in the next three paragraphs. One of these microscopes then had to be chosen to develop the initial system as an early prototype. The requirements are, therefore, discussed in the sections below, along with the suitability of our three existing microscopes.

BioScope Resolve The BioScope Resolve is mounted on an inverted microscope and is specifically adapted to cells. It is able to host a single petri dish and is compatible with an adapted heater and evaporation shield, or a complete closed perfusion stage incubator (PSI), hence better able to sustain life over extended periods of time. The full vertical scan range of its piezos is at least $15\ \mu\text{m}$, with a horizontal coverage of about $100\ \mu\text{m}$ by $100\ \mu\text{m}$. It has a dedicated piezo for the PeakForce sinusoidal movement, allowing for a consistent amplitude irrespectively of the vertical piezo position. Although its developments were further transferred to the other microscopes, it was first able to scan sample as soft as mammalian cells, primarily thanks to software functionalities such as specific additions to PeakForce for living cells. During the time-frame of this project, an high-accuracy stage was released, giving it a positioning accuracy close to the one of the Dimension systems.

Dimension Icon The Dimension Icon offers similar piezo ranges as it has an $85\ \mu\text{m}$ by $85\ \mu\text{m}$ minimal horizontal scanner range, for $9.5\ \mu\text{m}$ vertically. While not compatible with inverted microscopy, the Dimension stage offers a reachable area of $180\ \text{mm}$ by $150\ \text{mm}$ with a $3\ \mu\text{m}$ bidirectional repeatability.

Dimension FastScan-Bio Lastly, the Dimension FastScan-Bio, also based on the Dimension stage, is limited to a minimal horizontal scanner range of $30\ \mu\text{m}$ by $30\ \mu\text{m}$ with $3\ \mu\text{m}$ as the minimal vertical extent, as its piezos

5. Objectives and Requirements

are optimized for rapid and precise measurements. It also offers more automation capabilities, such as an automated probe alignment.

5.1.1. Scan

The main challenges of scanning mammalian cells are their softness and their large dimensions, compared to most other samples typically encountered in AFM. Their specific requirements are, however, increasingly understood and there are specialized systems.

In our case, the Resolve was primarily more suited to scan cells for the reasons mentioned above and is most adapted to scan eukaryotic cells. The Icon can also bring good results thanks to the ranges of its piezos. In the case of the FastScan-Bio, however, it is necessary to define areas of scanning on the cells since it cannot scan them in their entirety due to the short range of its piezos.

5.1.2. Correlation

Since it can be mounted on an inverted microscope, the Resolve can natively support correlative microscopy of classical optical microscopy, but it can also be combined with fluorescence and super-resolution microscopy, which would yield interesting data about the samples and is clearly something to be developed on the long term. The Dimension stage, on the other hand, only allows top-view, bright-field optics that are ill-adapted for single cells. Super-resolution is then out of reach in the current setup for this stage. It should be noted that FastScan heads mounted an inverted microscope rather than the Dimension stage have been reported (Peric et al., 2017) but will not be discussed further as they lack the automation of that stage.

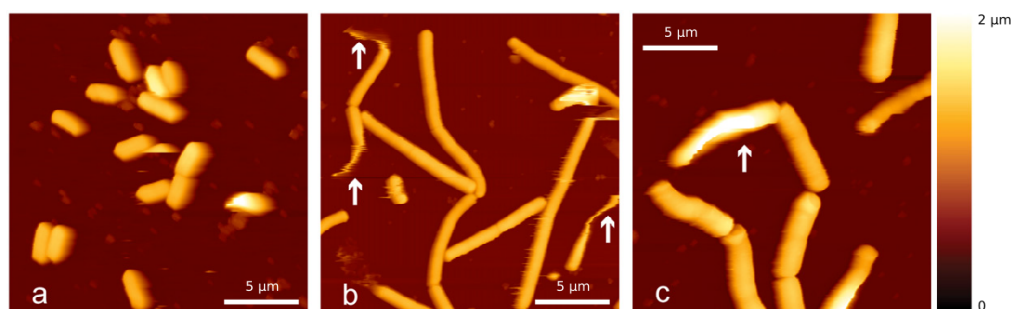


Figure 5.1.: Positioning of bacteria. AFM images of *Escherichia coli*, *Bacillus subtilis*, and *Mycobacterium sp.* bacteria. Arrows indicate distortions caused by defaults in the immobilization. From Louise Meyer et al. (2010).

5.1.3. Automation

To scan cells automatically, the system first needs to be aware of their positioning. Then, it should be able to move to the cell of interest and perform the scanning by itself.

Positioning

Most common applications of automated AFM are on quality control where, although there are some exceptions, the positions of interest are mostly known in advance. Elements have been printed and are expected to be there. The AFM is used to check if they are where they should.

For as far as live cells are concerned, on the other hand, their location is not defined. Prokaryotes and eukaryotes alike, a skilled operator can adjust the concentration of cells, leading to the part of the surface covered by cells. Similarly, the homogeneity of their repartition can be improved. Their exact positioning, however, cannot be known in advance, as illustrated by the positioning of bacteria in Figure 5.1 and of mammalian cells in Figure 5.2. Furthermore, cells might move between their detection and scanning.

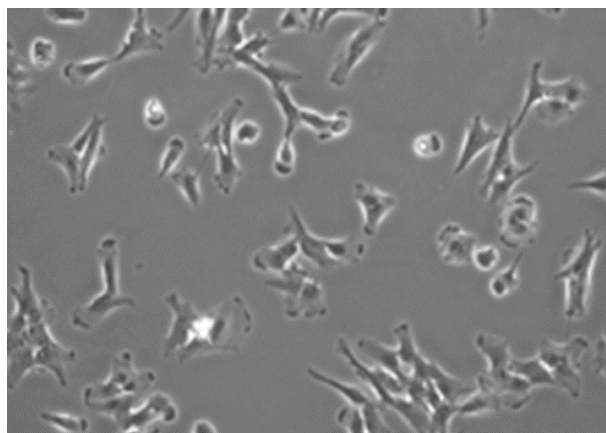


Figure 5.2.: Positioning of mammalian cells. RPE-1 in bright field inverted microscopy.

Unattended Operation

Finally, an automated scan requires a system able to behave correctly repeatedly without the presence of the operator.

Whereas all of these microscopes have the possibility to engage automatically, they require the laser to be centered on the photodetector. Over time, the laser can deviate from this position, requiring slight but frequent re-alignments by the operator. Among the three, only the FastScan has the motorization required to automate this process. Once engaged, automated scanning is available on the three systems.

Nevertheless, problems can happen while scanning. For example, particles can stick to the cantilever and perturb the measurement. While an operator would detect that something is going wrong and react accordingly, these problems need to be foreseen to allow an autonomous system. Given their diversity, these automation-related problems will be described apart, in Chapter 7.

5.1.4. Multi-Conditions

Given the variability in cell behaviors and their sensitivity to experimental conditions, it is often difficult to interpret isolated measurements. As a consequence, it would be preferable for the system to scan several samples in a row, in conditions as similar as possible. The ability to chain samples is also sought for in the perspective of a middle-throughput system that could be used in a screening setup, where several drugs, drug concentrations, or other variations could be compared.

In the current setup, the BioScope Resolve is only able to host a single petri dish. Automating it for multi-sample purposes would then require a different sample holder and a motorized system allowing it to raise the head during the automated sample exchange. With only minor developments, its automation would, however, be limited to the level of a single population.

The Dimension stage, on the other hand, is more adapted for a multi-sample setting. The FastScan, for example, offers a range of automated, multi-sample functionalities, although currently limited to air. In the case of an environment where cells could be kept alive for periods compatible with the time required to go through all the samples, such a setting would be advantageous. Multi-sample automation in fluid comes, however, with its problems, developed in Section 7.2.1.

5.1.5. Cell Survival

Scanning a multitude of cells takes time, which raises the question of their survival during the experiment. More than that, they will show alterations first in their mechanical properties, then in their topography, if their imaging conditions are not suitable, which would add variability in the resulting data. This is more of an issue for mammalian cells than for prokaryotes.

5. Objectives and Requirements

Mammalian Cells

Mammalian cells survival requires a medium with specific concentrations of certain components to keep a suitable osmotic pressure and pH level. They also require nutrients, plus heat and oxygen.

With more details, their requirements are:

- A water-based solution;
- Temperature control;
- Ions in concentration such as to keep correct osmotic pressure;
- Absence of toxic elements in solution (can be generated by the solids in contact with the medium and contaminations);
- Oxygen;
- pH (linked with carbon dioxide concentration);
- Composition of ions to match cell needs;
- Absence of contaminations;
- A controlled light environment.

Although all of these elements are important, they do not act at the same timescale. With simple heating in a pH-buffered medium, eukaryotic cells can be kept for around 3 hours. Keeping them alive for more than that usually requires a closed and controlled environment. Considering a scan of 5 minutes per cell, with a strict minimum of 10 cells per population for any level of statistical significance, up to 3 samples could be held in such an open system and used. Working on 4 samples or more would require a closed environment.

The controlled light environment is somewhat apart in that most cells are sensitive to light and suffer from constant exposure. As a consequence, the light should ideally be shut when not required.

5. Objectives and Requirements

As mentioned above, a closed environment system is available for the Resolve to keep cells alive for extended periods of time but it is not compatible with sample exchange. On the Dimension systems, such environments have yet to be developed but could offer the said multi-sample functionalities.

Prokaryotes

In the case of prokaryotes and yeasts, survival is much less of a problem as only a suitable buffer is required. Longer experiments could be designed with a partially controlled environment. They can also be scanned faster since they are smaller, allowing us to take advantage of the multi-conditions system earlier on.

5.1.6. Work Hypothesis

Neither the BioScope Resolve nor the Dimension Icon and FastScan-Bio, in their current settings, are adapted to a fully-automated setup with correlative measurement on both eukaryotes and prokaryotes. The Resolve would better be suited for cell survival, their detection, and correlative microscopy purpose than the Dimension systems. Its automation possibilities are, however, very limited. Single-population-level automation has only been made practicable by the recent apparition of the High-Accuracy stage. Multi-sample automation, on the other hand, would require consequent developments.

The Dimension stage is incompatible with correlative microscopy and makes cell detection harder. It is the only system, however, with the possibility to go over several samples. Between the Icon and the FastScan-Bio, the Icon would offer a more comfortable piezo range but lacks some important functionalities necessary its automation.

With regard to the long-term goal stated above, it is then necessary to start the development either towards correlative microscopy or towards multi-sample automation. Correlative microscopy is, however, quite well understood and addressed (Ando, Bhamidimarri, et al., 2018; Janel et al.,

5. Objectives and Requirements

2017), whereas little developments have been witnessed in AFM automation. This project then focuses on the latter and the Dimension FastScan-Bio was chosen for the early stages of development in order to better understand the challenges linked to multi-sample automation on living cells.

6. Methodology

6.1. Multi-Well

6.1.1. Design

The FastScan stage was modified to be the support of a multi-sample plate, which will be called Multi-Well in the rest of this document. This Multi-Well plate, shown in details in Figure 6.1, has 12 wells, each of which having a pedestal able to host its own sample on a coverslip. The plate is compatible with the American National Standards Institute (ANSI) specifications for potential compatibility with other systems. The wells are arranged in three rows named “A” to “C” and 4 columns numbered 1 to 4, with the wells labeled accordingly.

Its specifications are given with a margin of plus and minus $50\ \mu\text{m}$ so that, even across different plates, the height difference between one well and another does not exceed $100\ \mu\text{m}$, which is a commonly used safe distance on the FastScan. The horizontal specifications are compatible with the $2\ \mu\text{m}$ repeatability of the stage.

The coverslips (Menzel-Gläser, Braunschweig, DE) have a diameter of 8 mm and are held down by the three legs of the spring, as shown in the image. The surrounding ring of the spring is secured to the pedestal of the well with a spring clamp.

For biocompatibility purposes, the Multi-Well and the spring are realized in Titanium. The spring clamp is made of polymer ether ketone (PEEK), a polyaryletherketone (PAEK), which is a kind of semicrystalline polymer recognized for their mechanical and chemical stability. PEEK, in

6. Methodology



Figure 6.1.: Multi-Well Plate Setup. Top left: empty Multi-Well plate on the FastScan. Top right: coverslip (left), spring (middle), and spring clamp (right). Bottom: zooms on well A1 with the successive placement of the coverslip (left), spring (middle) and spring clamp (right).

6. Methodology



Figure 6.2.: Multi-Well positioning. The lateral placement of the Multi-Well is controlled by 3 adjustable ball-headed screws (A) and two retractable springs (B).

particular, has an excellent chemical resistance to organic solvents, bases, and acids. It is only degraded over time by very strong and concentrated agents. It can be sterilized by autoclave or radiation hundreds to thousands of times and is non-toxic (Sastri, 2013). It is often used in implants.

To ensure its positioning, the lower part of the Multi-Well is smooth and placed on three points on its support. The lateral positioning is defined by two points of contact on the back side and one on the left, each of which being adjustable with a screw to align the system. Opposite to these supports are two springs, one on each side, to maintain contact with these pins, as illustrated in Figure 6.2. With these 6 points of contacts and 2 retractable springs, the Multi-Well can be replaced and exchanged with the levels of precision mentioned above.

It should be noted that this version is a prototype and that plastic disposable equivalent could be used in the future, as discussed in Section 10.2.

6.1.2. Sample Preparation

To prepare the sample, the coverslips can be placed in a multi-well culture dish. In this environment, standard protocols can be used to immobilize the cells on each sample. The difficult part is then to move the coverslip on the Multi-Well while limiting dewetting as much as possible. The spring and spring clamps have to be placed fast enough so that medium can be added quickly. Once all samples have been placed, the Multi-Well can be closed and transferred to the system. Thanks to its normalized shape and dimensions, it is compatible with commercially available Corning Costar cell culture plates lid (Merck KGaA*, Darmstadt, DE).

Aside from the well-containing samples, two of the twelve wells are usually reserved, one for calibration and a second for cleaning purposes. The calibration well contains the same medium as the sample, but with a clean coverslip. The cleaning one is filled with a solution of ethanol and water.

6.1.3. Developments

This system would clearly not be suitable for an end-user in a high-throughput facility, but further iterations of the prototype can be considered, depending on the volumes required.

In a second iteration of the prototype, small trenches were added on top of the pedestals to avoid coverslip sliding.

Visibility

In the early system, it was particularly difficult to see the cells as they were mostly transparent and that the very reflective and heterogeneous metallic background was directly behind the coverslip. Being out of focus, it was not as sharp as if it were in focus, but still quite visible. First tentatives of having a homogeneous white, black, or reflective background did not show

* *ex* Sigma-Aldrich

6. Methodology

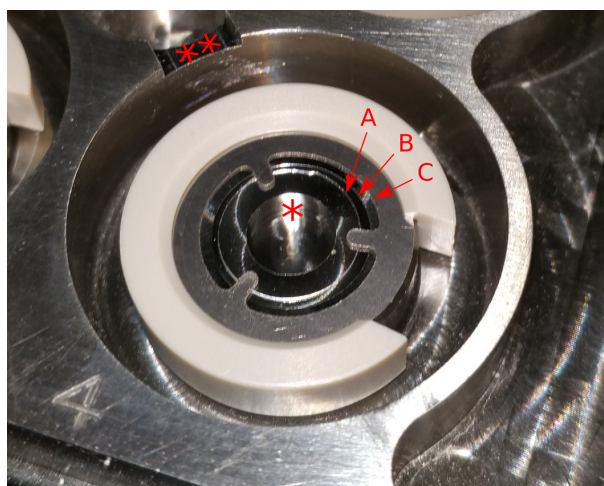


Figure 6.3.: Multi-Well plate enhancement. A hole (*) in the center allows a de-focused background lightning. A ridge (B) around the glass coverslip (A) but smaller than the inner border of the spring (C) avoids sample sliding during mounting. A spillover (**) was also implemented for testing purposes.

perspectives for development. It was observed, however, that leaving a gap of a few millimeters under the sample would help the visibility.

Therefore, holes were also positioned under the coverslips so that the reflective titanium surface would be completely out of focus when focusing on the sample, as shown in Figure 6.3. These internal wells should be filled either with liquid or air to be homogeneously transparent. In the case of air, however, the compressive medium could create drum-like effects with the oscillations of the scanner. Liquid could also leak in with time. As a consequence, these holes should be filled with liquid before placing the samples on top, to ensure a complete liquid filling and avoid the presence of bubbles or droplets under the coverslips.

6.2. Script Engine

The FastScan-Bio, as the FastScan, is controlled by the NanoScope software.

For automation purposes, NanoScope has a scripting system called NanoScript, based on the C/C++ programming language. It is a library presented as a DLL, as introduced in Appendix D.1. AFM users with a programming background can write C/C++ code importing NanoScript and using its functions to control the AFM. They can then compile their code as a DLL, which can then be loaded into NanoScope as a plug-in. NanoScope executes the code in the DLL of the user, which relies on the NanoScript DLL, using itself the internals of NanoScope. NanoScript mostly provides access at the scan level, providing stage, engagement, and scan control as well as access to some elements of the Graphical User Interface (GUI). It can grant control of the tip for nanolithography functionalities, with LithoScript.

NanoScript can be useful to develop simple routines scripts that can be launched by the user to, for example, draw a pattern, take a few scans with varying parameters, etc. The C/C++ language is, however, quite low level and large developments can quickly become difficult. Although not unable to do so, NanoScript is then not recommended for building a complete automated system. In particular, data/image analysis functions easily available in high-level languages such as Python or MATLAB would be difficult to access.

In a complete setup able not only to gather data but also analyze it and react accordingly, such a higher-level language would be preferred. Although interfaces do exist for that purpose, giving higher-level handles to NanoScope to the user, they do not allow for the same level of control than NanoScript. Combining the two would be possible, triggering NanoScripts through the interface, but adding the complexity of having two sets of codes in two different programming languages.

To provide a fine granularity of control at a higher level, a new scripting

solution was developed, using Python. Its custom Integrated Development Environment (IDE) is represented in Figure 6.4.

6.2.1. Editor

An open source code editor, Scintilla (*Scintilla and SciTE* 2018), was integrated into the software. Scintilla includes components expected for standard text editing, plus a few tools specific to code editing, such as a convenient syntax styling. Its interaction with the system, under the .NET architecture (see Appendix D.2), was made possible by ScintillaNET, (Slusser, 2017), which allows control, wrapping, and bindings for Scintilla in our environment.

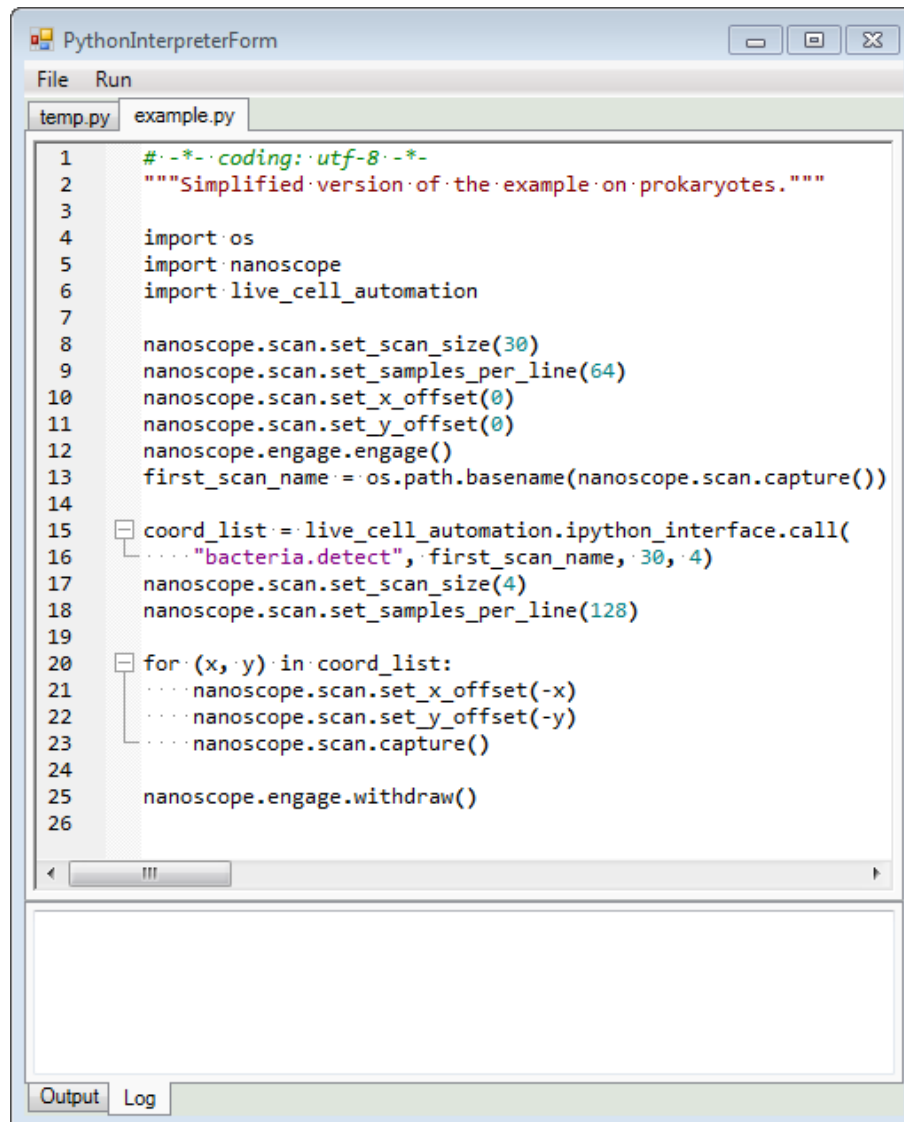
Basic file functionalities were implemented around the editor to access and manage files. An output and a log tab were also added on the lower part of the screen, to send information back to the user. The output part offers a quick “print”, whereas the logs require a few more interaction from the programmer but are timestamped and saved in log files, associated with the obtained data.

6.2.2. Python Engine

Again to fit well within the current architecture, a .NET implementation of Python was used: IronPython, described in Appendix D.3.1. IronPython is used by NanoScope to build a Python engine, which is given access to a new Python package called “nanoscope”. This “nanoscope” package is then available for the user to be imported in their scripts, as visible on line 5 in Figure 6.4, and used as a handle to the AFM. This package and its functionalities are developed in Section 6.2.3.

The script, defined by the user, can be run from the control bar of the IDE. The file is saved and fed to the Python engine of NanoScope. The engine executes the script, performing Python instructions as normal Python and controlling the AFM when “nanoscope” instructions are met. This

6. Methodology



```
1  #-*-coding:utf-8-*-
2  """Simplified version of the example on prokaryotes."""
3
4  import os
5  import nanoscope
6  import live_cell_automation
7
8  nanoscope.scan.set_scan_size(30)
9  nanoscope.scan.set_samples_per_line(64)
10 nanoscope.scan.set_x_offset(0)
11 nanoscope.scan.set_y_offset(0)
12 nanoscope.engage.engage()
13 first_scan_name = os.path.basename(nanoscope.scan.capture())
14
15 coord_list = live_cell_automation.ipython_interface.call(
16     ... "bacteria.detect", first_scan_name, 30, 4)
17     nanoscope.scan.set_scan_size(4)
18     nanoscope.scan.set_samples_per_line(128)
19
20 for (x, y) in coord_list:
21     ... nanoscope.scan.set_x_offset(-x)
22     ... nanoscope.scan.set_y_offset(-y)
23     ... nanoscope.scan.capture()
24
25 nanoscope.engage.withdraw()
26
```

Figure 6.4.: Representation of the IDE and script example. The script is a simplified example of the workflow for bacteria further described in Chapter 7.

brings the power of Python to NanoScope, or the NanoScope capabilities to Python.

In case of errors in the code, the script is aborted and NanoScope returns to its normal control. Similarly, in case of crashes, errors are raised in the script, which can be caught and acted upon by the user.

6.2.3. NanoScope Package

The “nanoscope” package allows for stage control (with speed control) in X, Y, and Z, and control of the camera focus between the tip and the sample. It can engage or withdraw the system to go on scanning mode. The scan parameters, such as its size, aspect ratio, X and Y offsets, angle, rate, resolution, and setpoint can be controlled. The values of the photodetector can be recorded and the video image can be saved. Scans can be started and captured in specific directories. The system can also switch in force volume mode and take the corresponding measurements.

The use of this package is illustrated in Figure 6.4 in lines 8 to 13, 17, 18, and from 21 onward. This simplified example sets a large scan size (line 8) and a low resolution (line 9), while re-centering the horizontal offsets (lines 10–11). The system is then engaged (line 12) and a capture is taken (line 13). In line 15, the bacteria are detected on this large, low-resolution image through the live cell automation package, which will be described in Chapter 7. The scan size is then set to small (line 17), with a high resolution (line 18) and the list of coordinates detected earlier are used as X and Y offsets (lines 21–22) for a measurement scan to be captured. Once all the elements have been captured, the system is withdrawn (line 25).

6.3. Analysis Toolbox

6.3.1. Analysis Issue

One of the key elements in this project was to be able to adapt the scripts based on the results of the scans. This functionality was not well supported by previous automation solutions as low-level tools were overly complex while higher-level options lacked refinement. This need led to the development of the script system described earlier in Section 6.2, offering a greater flexibility in the control. In order to be reactive, however, this control required to have access to the data resulting from its earlier steps. Data analysis functionalities were therefore required for the system to automatically open and analyze the files right after their capture.

It would be misleading to call this “real-time analysis” since it is not performed within NanoScope during the scan. Calling it “offline analysis” would, however, not be accurate either in that the computation is carried out during the experiment and influences it. It will then be referred to as “near real-time” for the purposes of this document.

As a consequence, the requirements were for a tool that could be called from the script and would perform relevant analyses. It would then export the resulting data in such a way as to be re-interpreted by the main script. These “relevant analyses” include bubble, cell, and contamination detection. Data analysis is, however, a recurrent problem in AFM as several tools are available, but many lack capabilities that are essential for our needs. Furthermore, there is a distinction between software centered around imaging modes and force-curve-based ones.

The first category of software corresponds to the tools required for analyzing data acquired in contact, oscillating, and non-contact modes, which generate a few images. Aside the typical height channel are maps corresponding to the deflection, amplitude, phases, among others. These maps can then be analyzed as a set of 2D grayscale images or surfaces, making their analysis a specialized subfield of image processing.

Then, force-curve-specific routines are required for the analysis of mechanical measurements. These programs are usually more specific to the needs of the laboratory as few broadly accepted algorithm exists, unlike in the previous case.

6.3.2. Manufacturer Programs

Most manufacturers come with their own software to open the files they produce. Due to their competitive nature, they are generally not inter-compatible, to the exception of WSxM. They offer a lot of functionalities, such as the implementation of most of the common algorithms in AFM, but often lack flexibility.

In our case, Bruker systems have NanoScope Analysis. In this software, it is possible to set up some automated processing by defining a macro, which will execute predetermined transformations and measurements to the analyzed file. The program can then export its resulting data as a text file. It did not, however, have the functions corresponding to the needs of this project, mostly related to bacteria detection.

It could also have been possible to call this program to transform the NanoScope files in text format to be analyzed by another tool, although this would be adding an extra layer in the processing.

6.3.3. Other Programs

Other programs than the ones of the manufacturers can work with AFM data. A first and well-known example is Gwyddion (Nečas and Klapetek, 2011), a free and open-source program used for visualizing and analyzing SPM data, developed by the Czech Metrology Institute. It has a lot of grayscale image processing, such as leveling, data correction, and statistical characterization. It has added abilities on the topographical data, where SPM-specific procedures are missing in general-purpose programs. Its abilities on force-based measurements are, on the other hand, limited.

6. Methodology

SPIP, the Scanning Probe Image Processor, is a commercial (must-buy) program used for analyzing microscopic images developed by the Danish company Image Metrology A/S. It has similar functionalities to Gwyddion but can also open files from other types of microscopes (EM, interference, confocal, optical, profilers, etc.) It has some but limited abilities in force-based measurements as well.

WSXM (Horcas et al., 2007) started as a manufacturer software created by the defunct Nanotec but could open other file formats as well.

Other systems include AtomicJ (Hermanowicz et al., 2014), ImageJ (Schneider, Rasband, and Eliceiri, 2012), OpenFovea (Roduit, Saha, et al., 2012), Pycroscopy (Eaton and West, 2010), and SFMetrics (Sánchez and Wyman, 2015), but also FemtoScan Online, PUNIAS, Image SXM, GXSM, MountainsMap SPM Image, TrueMap, and TrueSurf.

These programs, however, were either expensive or no longer maintained, would lack flexibility in analysis, or be difficult to interface with the main script engine.

Often, labs have their own custom pieces of software able to interpret text files. Some are able to open proprietary file formats, although figuring out how to recover the data from the proprietary file format can be difficult. While the first option is possible, it would require the extra step of using, in our case, NanoScope Analysis to export the file in text format.

In the case of our laboratory, a force curve analysis software, pyAF, has been developed (Popoff, 2014). This software, entirely written in Python, is represented in Figure 6.5. It has a strong focus on force curves, force volumes, and similar mechanical measurements. It possesses advanced analysis options for these files, with a strong focus on cell stiffness.

While the methods required here for the near real-time processing are centered on topography, pyAF could be of great use for the later analysis. Indeed, its open plug-in architecture and its powerful batch computing abilities could make it a great tool for going through the experiment results. It could also be streamlined with the current system to perform the analysis in parallel to the experiment.

6. Methodology

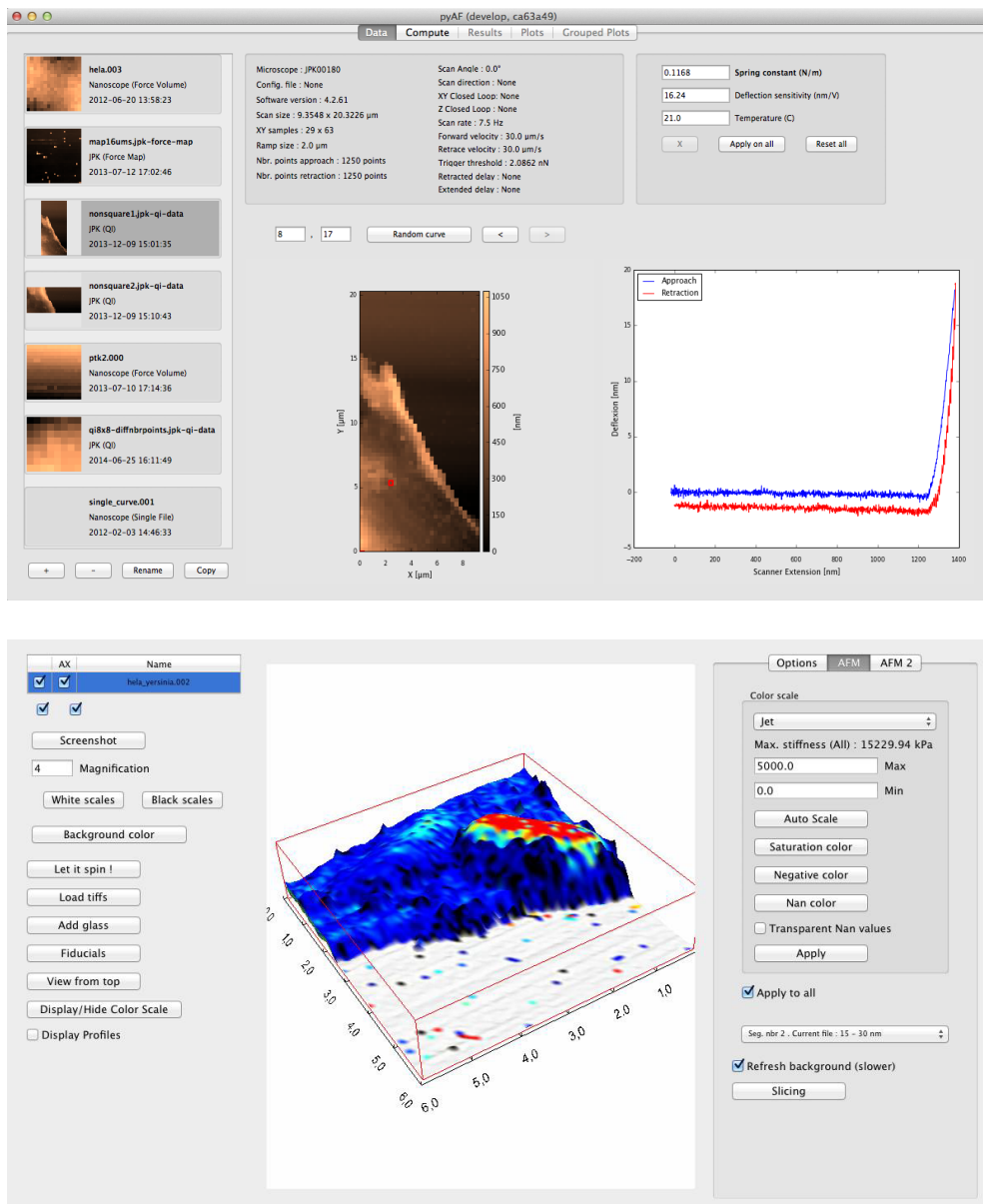


Figure 6.5.: pyAF. Top: data panel; the opened files are listed on the left while the middle screen includes the height map and selected force curves, the parameters can be changed in the header. Bottom: 3D visualization of stiffness computations as an overlay on the topography. From Popoff (2014).

As foreseen by Popoff (2014), continuous usage of pyAF through time required a substantial update to the new major versions of Python and the underlying libraries PyQt and VTK, as they had evolved substantially.

6.3.4. Direct Opening

The most convenient option would be to open directly the files in Python and work on them. Other tools include MATLAB or R. The AFM files use, however, their own format. It would be possible to use NanoScope Analysis to change the format to text first, then interpret it with these tools. Given the sparse and unclear documentation on the topic, some level of retro-engineering is required. One also needs to keep up with the format at every update.

R Package

R is an open-source programming language running in an associated software environment (R Core Team, 2018). It is widely used in statistics and data analysis. It is a very powerful tool in stats, with functions for modeling, tests, classification, etc. As an interpreted language, it can easily be used to analyze data in a command-line interpreter. It can also be used to run scripts. Originally written by Ross Ihaka and Robert Gentleman, the R Core Team then expanded (Hornik, 2017). It is vastly supported by the community.

There are two R packages relevant for AFM. The first, “AFM: Atomic Force Microscope Image Analysis”, usually called “AFM”, by Mathieu Beauvais, was first released in October 2015 (Beauvais, Liascukiene, and Landoulsi, 2018). It implements several image analysis tools for AFM images. For opening NanoScope files, it requires flattening and exporting the file in text format using NanoScope Analysis.

The second package, “afmToolkit: Functions for Atomic Force Microscope Force-Distance Curves Analysis” (or “afmToolkit”), by Rafael Benítez, was first published in April 2017 (Benítez, Bolós, and Toca-Herrera,

2017). It focuses on performing operations related to Force-Distance curves analysis. As for the previous package, it requires the text version of the file.

MATLAB Package

MATLAB is a commercial numerical computing environment. It started as a tool to do numerical computing on matrices, hence the name as an abbreviated form of “Matrix Laboratory” (Moler, 2004). It is commonly used by the scientific community, although its price can be a deterrent for some applications.

Bruker provides a MATLAB Toolbox to let users open NanoScope files on Windows. The toolbox is compatible with most NanoScope files, such as High-Speed Data Capture, force curve and force volume data (with and without Hold segment), Image files, PeakForce Capture files, among others.

This would, however, require a MATLAB license for the computer running the script, plus a MATLAB license for the analysis of the data.

6.3.5. NS Python Toolbox

As described above, existing programs and the R packages did not have the desired functionalities or required the extra step of exporting the data in text using NanoScope Analysis. The MATLAB toolbox could have been a solution but was discarded because of the necessity to keep a license just for the system, plus the ones for analyzing the data after the experiment. As a consequence, the first solution was to open the file manually and, with the help of the documentation, some guess-work, and some retro-engineering, figure out how to extract the data in its simplest form. Getting more information required guess-work, hence a higher chance of mistakes and of getting corrupted data.

Quite early in the project, the NanoScope software was updated and some assumptions made in the file opening tool were no longer true, which

6. Methodology

broke the system. In order to avoid further breaks, it seemed necessary to rely on an interface more stable than the file format.

The MATLAB Toolbox is actually mostly a MATLAB wrapper around an interface to the NanoScope Analysis software. This interface being much higher-level than the files by themselves, using it should also be more robust than the previous solution. It is also self-explanatory, hence limiting the propensity of errors.

I re-adapted the usage of the interface used by the MATLAB toolbox to Python. Since it relies on the interface, the different file formats expected to come in the future would have been managed at that level. Any further update in the format that would previously require changing the code would now only require updating that interface level and it would most likely stay compatible with further versions of the file formats without modification on the Python side.

Functionalities

Starting with only the files that were strictly needed, it quickly expanded to cover the equivalent of the previous toolbox.

The NS Python Toolbox is able to open virtually any file format created by NanoScope at the time of writing. This includes image (topography) files, force volume files, PeakForce Capture files, but also scripts and High Speed Data Capture (HSDC). The information from all the channels can be extracted in the units relevant to the user.

7. Live Cell Automation

7.1. Specialized Scripting Tools

Based on the scripting capabilities described in Section 6.2, several kinds of scripts and modules can be realized. Some can be designed to move the stage in a specific way while others describe how to control different elements of the tip quality. Finally, these elements can be put together to create the workflow of complete experiments.

7.1.1. Movement Control

Stage Movements

The basic interface allows getting the current X, Y, and Z positions of the stage and to order a movement towards a certain position along one of these axes. The movement might fail in case of shocks, which might be caused by a genuine collision but can also sometimes appear when moving at full speed a stage as heavy as a Titanium Multi-Well filled with liquid on its custom holder. As a consequence, a slightly higher-level stage move is implemented as a Python module and can be adapted by the users to fit their need. In our case, functions were implemented to retract the system to a safe height and to lower the head to a given height with a slow-down at the end of the movement.

In the horizontal movements, a function is implemented to move to a given planar position. It finishes the movement at a lower speed and with a backlash compensation to maximize the precision of the stage, moving

7. Live Cell Automation

from the announced 3 μm bidirectional repeatability to the 2 μm unidirectional one. In case of failure, it backs up and retries at a lower speed.

Multi-Well-Specific Movements

Based on the stage movements defined above, movements specific to the Multi-Well can be defined. Such a module provides functionalities to load the calibration of the Multi-Well, and calibrate it if needed. From this data, it defines the position of each well.

Finally, functions could be written for the actual movements. It was made possible to move from a well to another by retracting the system to the elevated height before moving horizontally safely and lowering back into the following well to the height of the sample plus some clearance, corresponding to the focus length of the optics. A position-based check on whether the system is in a well or not was added, as well as the possibility to move within a well to a position relative to its center.

Given the tolerances of the Multi-Well as given in Section 6.1, its 6-points connection with the stage, and the accuracy of the Dimension stage, the positions of the samples are known within a few microns once the Multi-Well has been calibrated. The movement from one place to another can thus be automated. In the current implementation, the height is only measured once and the system is assumed to be flat enough so that the same height can be kept. While it has been shown reliable enough for the sake of our experiments, it would be possible to record the height of 3 wells or more and compensate for an eventual tilt of the stage.

Movement Script

With the movement modules defined above, it becomes possible to create simple scripts of to easily go to a specific well. They allow quick shortcuts to go to the current sample of interest, to specific wells such as the calibration or cleaning ones, or a safety position.

7.1.2. Experiment

Going from there to a complete experiment requires some more complexity.

Parameter Choice

The first step in the design of the experiment is the selection of the parameters presented in Appendix A.5, such as the scan size and the PeakForce frequency. While the engage and force volume settings are more general, the scan parameters should be adapted to the sample and the application.

In particular, ScanAsyst, described in Section 2.4.5 optimizes the parameters for us in order to limit the parachuting effect (Section 2.5.5) and as well as instabilities, such as the sawtooth effect (Section 2.5.6).

When used, ScanAsyst acts on the force setpoint and the gains in order to limit these two effect. By increasing the gains, it can increase the tracking of the sample but increases instabilities. If the trade-off between the tracking and noise levels is unsatisfactory, it can increase the setpoint so that the tracking can be achieved with lower gains, thereby limiting the noise. The force setpoint can also sometimes take values potentially damaging for the sample. Therefore, for automated applications, the parameters should be chosen carefully. If the effect is too important, the algorithm might select a lower speed.

For comparability purposes, however, we want the force setpoint and the scanning speed to stay constant for the whole experiment. The ScanAsyst Auto Control is then deactivated, unless for the gain. To find suitable values for these parameters, we can use ScanAsyst on a similar sample before the actual experiment and record the parameters as follows. Since our aim is to optimize the throughput, we first try to increase the scan rate. At each step, ScanAsyst updates the force setpoint and gain to optimize the image quality. When the automated setpoint approaches the upper bound of forces acceptable by the sample, we stop increasing the scan rate. We then deactivate the ScanAsyst automated setpoint option and chose a round value close to the current one. We usually take a slightly higher

7. Live Cell Automation

value to give ScanAsyst more robustness in its management of the gains on the further samples. Using such a slightly higher value also ensures the possibility for ScanAsyst to perform with another probe, which would have slightly different characteristics.

Start-Up

Let us first define the setup upon which the experiment automated workflow can be designed. Before an experiment is run, a NanoScope “experiment” (i.e. its set of parameters) is defined as described in Appendix A.5 and saved.

When setting up the experiment, these parameters are loaded and the probe is mounted by the user. Although we have mostly been using FastScan-Fluid probes in the demonstration presented in Chapter 8, other probes can be used. The Multi-Well is prepared, as described in Section 6.1.2.

The user can then use the simple movement scripts mentioned above to get positioned in the calibration well. Once in this well containing a bare hard surface in the same medium as the sample, he or she can perform the setup. It consists of setting the parameters of the probe and aligning the laser, the photodetector, and the tip in the calibration well. Then, the calibration procedure is run, using standard thermal-tune base calibration for the prototyping phase although the SNAP method (Schillers, Rianna, et al., 2017) would be preferred for actual nanomechanical experiments, requiring pre-calibrated probes. As it depends on both the deflection sensitivity and spring constant, the trigger threshold for the force volume cannot be saved properly and is set manually, here to 1 nm. The scan size is usually set to 2 μm , although the value is changed by the script when engaging and switching between survey and measurement scans.

Basic Workflow

Once the experiment has been set up manually by the user, the rest is implemented in the code. A first, basic scheme is used as a default model and aimed at being subclassed to the more precise experiment. Represented as the green and red parts of Figure 7.1, it corresponds to the parts that are supposed to be common between experiments, while the parts in purple are subject to variations. This basic workflow defines the existence of a few sample-containing wells that are to be scanned, calibration and cleaning wells, as well as a few procedures.

This workflow also defines the file structure and timestamping system so that, when an experiment is run, its filename and timestamp are combined to form a unique folder containing the data. Different sections of the experiment are run in their own subfolder and each well within that section has its own subfolder as well. Generated files are placed in the corresponding place of the directory tree. For example, well-specific files are placed in the corresponding well directory. The logs are written in log files split across the directories, following the workflow of the experiment so that every file is closely associated with the log file that allows making sense out of it.

The basic workflow defines an initialization procedure used, among other, for the bubble detection procedure, described in Section 7.2.1. As illustrated in Figure 7.1, in each well, the cantilever is checked and a cleaning procedure can be triggered. Once this check is passed, a well scan procedure defined in the detailed experiment is carried upon. If an error happens without being dealt with by the user code, the experiment is aborted and the system is moved to a safe position. If it is aborted by the user, however, the system can be withdrawn but the current position is kept to help to debug and avoid useless travel.

7. Live Cell Automation

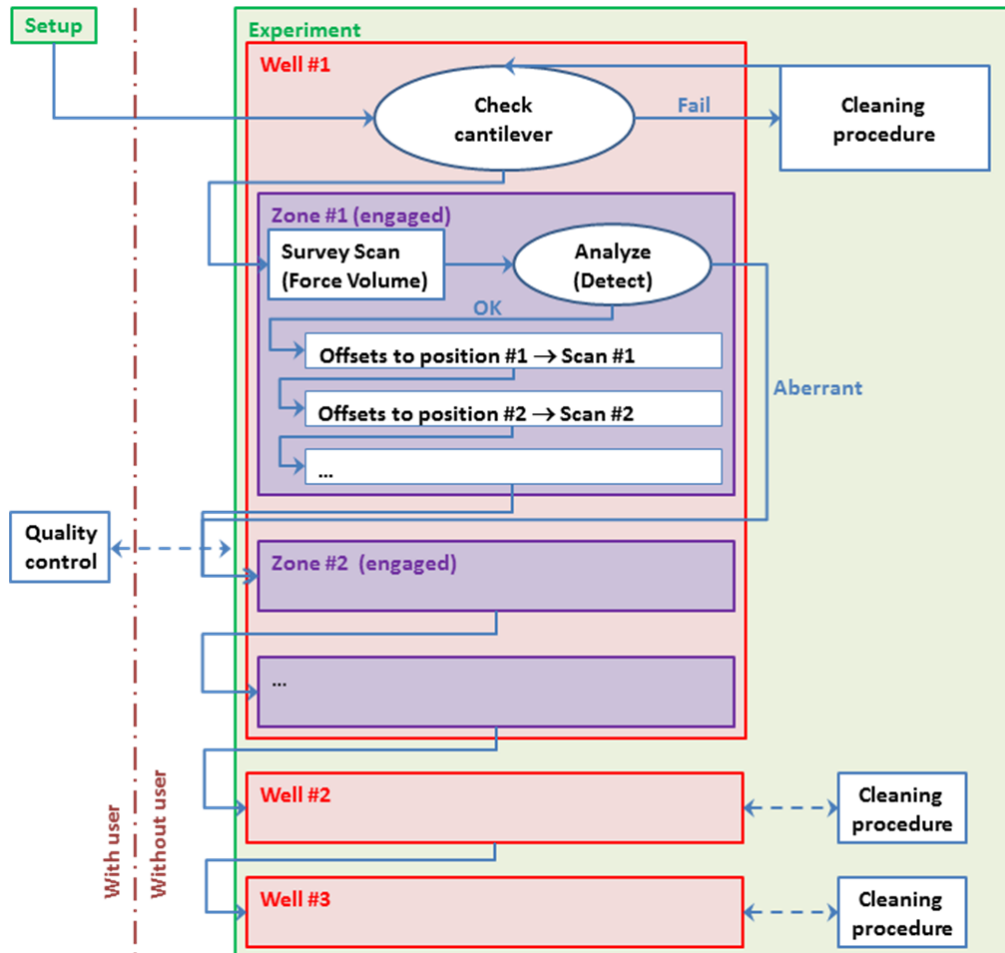


Figure 7.1.: Scheme of the experiment workflow. The green (setup, experiment) and red (wells) sections are part of the basic (common) workflow whereas the purple (zones) sections are more experiment-specific.

Detailed Workflow

The detailed workflow is programmatically inherited from the basic one. It provides the user with the possibility to set some parameters used by the basic workflow, and add some behaviors. Notably, the calibration and cleaning wells are written at this point, as well as the list of wells to visit. A complement to the initialization procedure can be added too. The most important point, however, is the description of what is to happen in each well. We will here describe a typical workflow.

Survey scans are realized to detect bacteria. Each survey scan is a square of side $30\ \mu\text{m}$, which is about the minimum guaranteed value for the piezo ranges in X and Y. To cover a large area, these survey scans are repeated over a 2D arrays of positions, every $30\ \mu\text{m}$ along the two horizontal directions. An engagement is performed at each position.

The automation of the engage is made possible by the stability of the laser on the cantilever and the automatic realignment of the photodetector. Thanks to the low tolerances of the Multi-Well and the positioning procedures defined above, the sample can be assumed to lie at the focal distance, set at the sample clearance of about $1\ \text{mm}$, plus or minus a safe distance of $100\ \mu\text{m}$. The engage is performed by NanoScope.

Once engaged, the script switches NanoScope to force volume mode to probe the $30\ \mu\text{m}$ by $30\ \mu\text{m}$ survey area. The reason why force volume was chosen is that, while it is slow by nature, its time is almost directly proportional to the number of pixels (or force curves) provided that the ramp size is bigger than the sample height. Normal imaging modes (PeakForce included), on the other hand, are tracking the sample from a pixel to the next. Thus, although they can be fast, the scan speed is relative to the scan size. For big scans such as here, PeakForce would give a resolution much higher than needed on the fast axis as required to track the sample. It would, however, be too slow for our purpose, whereas force volume scanning time does not depend on the size.

Once captured, the survey file can be analyzed to find bacteria, as de-

tailed in Section 7.2.2. Along with bacteria detection, aberrations are controlled. If the data appears to be too bad, the position is simply skipped and the system moves on to the next spot.

After detection of the positions at which bacteria are thought to be, the scan size is set to 0 and the system goes back from force volume to Peak-Force (QNM) mode, which is more adapted for high-resolution imaging. Compared to contact, tapping and other modes, it has the advantage to have automated setpoint adjustment with ScanAsyst mode, as detailed in Section 4.5.2.

The scan size is then set to at a small size, chosen here to be 2 μm , and a much higher resolution than for the force volume. The scanner is then offset to each of the detected positions, scans and capture it, logs the filename along with the corresponding offsets, and repeat. The small size value could be changed to fit the size of the bacteria or, maybe, smaller to zoom on top of it.

7.2. Issues and Solutions

In Section 5.1 were described a range of requirements we are trying to satisfy with the system studied. Among them, a challenging one is the possibility to work in an unattended fashion. Solutions, workarounds, or other perspectives regarding this problem that have been implemented in the main system are presented below. They are mostly based on software solutions with simple hardware elements.

7.2.1. Bubbles

When moving from a well to another, the probe and the z-scanner leave and re-enter the liquid medium. Crossing the air-liquid interface, can cause the appearance of bubbles from air trapped during the immersion.

Bubbles on the cantilever can be a source of problems when operating AFM in fluid. Most often, these bubbles obstruct the path of the laser,

7. Live Cell Automation

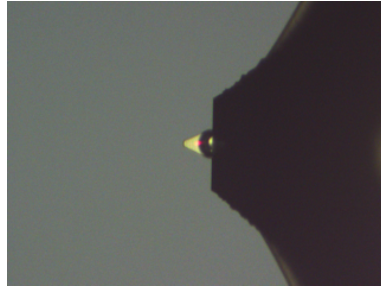


Figure 7.2.: Example of air bubble in fluid on a FastScan-C probe.

blocking the optical lever and making AFM operation impossible. In some cases, however, they can slightly perturb the laser or change the mechanical behavior of the cantilever, hence impeding the calibration.

It is thus important to detect them as they can interfere with the measurement. As described below, we based our detection method on the laser sum signal and the video image. When something is detected, the system goes to the cleaning well and then for a rinse in the well used for the calibration. The well entry is then re-attempted.

Such bubbles usually appear on top of the cantilever, when the probe enters in contact with a liquid. Some cantilever geometries are more prone to bubbles than other but its surface properties, including the presence of contaminants, can also have an impact. Their appearance can be explained by the fact that, in most systems operating in fluid, a glass is present just behind (on top of) the probe. The glass and the rest of the probe holder being flat, it is understandable that air can be easily trapped between the cantilever and the glass when the later enters vertically in the fluid, forming a bubble such as the one represented in Figure 7.2.

To avoid air bubbles, it is a good practice to add a drop of imaging medium (about 20 μ L for water or PBS on the FastScan) on the probe during the mounting phase, when the cantilever holder is upside down. Because of the different constraints, bubbles are less likely to appear in that configuration. The head is then placed in its normal position on the

7. *Live Cell Automation*

system. With a droplet of that size, the superficial tension is most often enough to keep it from falling, provided that reasonable care is given during the placement. When the head is subsequently lowered in the fluid, the liquid droplet and the imaging medium can merge and, since the probe does not have to cross any interface, bubbles are less likely to appear.

Even in that case, the non-appearance of bubbles cannot be guaranteed. Furthermore, the user might have to move the system. On the Resolve, the alignment of the laser is usually performed on a separate station with its own dish. The AFM head is then moved and placed on the inverted microscope, which hosts the dish containing the sample. This transfer moves the probe outside of the liquid medium, which can induce dewetting and the potential appearance of a bubble upon entry in the medium of the sample. A similar process happens when changing samples. The same happens on the FastScan except for the fact that the movement from one well to another is motorized.

When a bubble appears on the back of the cantilever on the Resolve, the user can usually gently tap the head close to the probe, raising it if needed, in order to induce vibrations that can cause the detachment of the bubble. If that fails, the head can be moved back to the station and the fluid around the probe absorbed by delicate tasks wipers*. The operator can then repeat the process of adding a droplet of liquid before going back to the sample.

On the FastScan, the sample can be manually less accessible to the user and raising the head is much slower since it can only be done by the motors. Tapping the side of the scanner can sometimes work, although it is difficult to know without lowering back the probe in the sample, and repeating if needed. As for the Resolve, it is possible to move the system back in probe exchange position, remove the probe, clean it, add a droplet of liquid, and go back to the sample position. . . which is a long procedure that is usually kept as a last resort. A faster yet less reliable way would be to raise the

*Touching the liquid with the border of the tissue will usually remove most of it. Care should be taken not to actually touch the probe.

7. Live Cell Automation

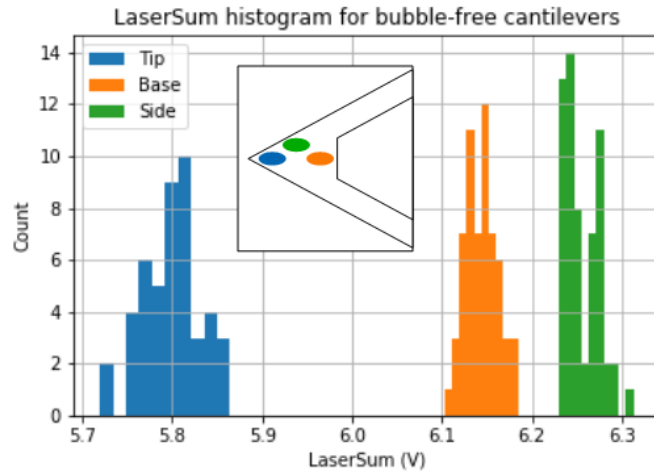


Figure 7.3.: Laser sum consistency test. Histogram of the laser sum in the three cases, agglomerated across several wells, when no bubble was present. Inset: position of the laser, centered on the tip (left), base (right), and side (top) of the cantilever.

head and use the cleaning wipe while the probe is still on the system, before going back into the sample. While removing the liquid this way can pop existing bubbles, they can reappear when going back in fluid after being dried since adding a droplet upside down is a difficult (and potentially dangerous).

Aside from being annoying for the user, bubbles make automation difficult since several well changes can happen autonomously during the experiment.

Laser Sum

The first, most trivial and robust way to detect problems is to analyze the laser sum as it varies sensibly with the position of the laser on the cantilever. This phenomenon is even used to align the laser automatically (Young et al., 1998).

In order to measure the variability, the following experiment was per-

7. Live Cell Automation

formed. Using the ScanAsyst-Fluid probe with a big spot size, the laser was centered at the tip, the base, and the side of the cantilever, as represented in the top part of Figure 7.3. For each tip centering, the head moved successively in three wells containing different samples, twenty times, taking an image and recording the laser sum every time. The first well contained a bare coverslip, the second was empty, and the last contained a metallic sample, all of which in water.

The images were then filtered manually to discard the data points where bubbles were present, which led to 14 (over 60) data points being discarded in the case of the tip centering, whereas the two other cases did not show traces of bubbles. Despite the diversity in the samples, as shown on the bottom part of the figure, the laser sum varies by less than one percent around its mean, for the base and the side case. The greater variability in the case of the tip can be explained by the stronger interferences with the sample. Further analysis showed that the different modes of the distribution correspond indeed to the different wells and that the variability is much smaller for a single well.

A three-sigma deviation would correspond to a variation from the mean of 1.7% in the case of the tip and 0.9% for both the base and the side. Since the normal centering of the laser is further in the center, limiting the interference effects, a threshold of 1.0% variation from the mean appears reasonable to be used in this configuration (ScanAsyst-Fluid probe on the Multi-Well).

Basing the threshold on a deviation from the mean requires, however, the knowledge of the mean, which is not available until the end of the experiment when all the measurements have been taken. In a real workflow, we need to apply that threshold when entering the first sample-holding well. As a consequence, the laser sum is measured during the initialization phase, but this initial value can fall within 1 percent of the mean as well, which implies that legitimate measurements should fall within 2 percents from the measured value.

Beside the natural variation mentioned above, the laser sum varies with

7. Live Cell Automation

the focus, the medium, and the elements on the path of light, or if the cantilever is strongly bent. A variation of more than 2 percent in its value is then considered significant and shows that one of these elements changed. It can then be a sign for a contamination on the back of the cantilever, a bubble, or the absence of liquid.

Regarding time-dependence, differences of less than 0.2 percent were observed from the initialization to after experiments lasting up to 16 hours, when measured in the same position in the calibration well.

Image Analysis

The laser sum method presented above fails, however, for bubbles at the base of the cantilever, among others. To detect such bubbles, it can be helpful to have a reference image of the tip. Before starting the experiment, the user sets up the system in the calibration well. He or she checks the quality of the probe. Once the system is ready, the experiment script is started and, in the initialization phase, a reference image of the checked cantilever is taken. This image can then be compared to similar ones, taken when entering a well.

This initial image is directly analyzed as illustrated in Figure 7.4 to find the border of the substrate. The border is assumed to be a straight line, which separates the clear background and the bright cantilever on the left from the dark chip on the right. This line is defined by its offset from the left side of the image, measured in pixels at the middle height of the screen, and by its slope, from the vertical.

To find the offset and the slope, we define a cost function giving to the “badness” of fit of the line defined by a given offset and slope. If the line was indeed the border, the right part should be homogeneously dark and the left part made of lighter shades. The variance of both classes should be low. If the line, however, does not correspond to the border, at least one of the two parts will contain both dark and light pixels, increasing its variance. As a consequence, we consider the badness of fit, or cost, of a

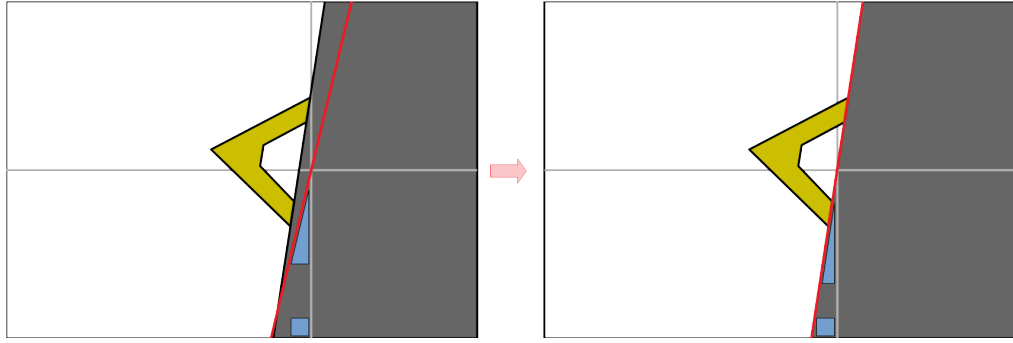


Figure 7.4.: Illustration of the bubble detection procedure. The cantilever (gold) and its chip (gray) are represented. A line (red) is defined by the offset (square) and slope (triangle) at which it intersects the horizontal line in the middle of the image. An arbitrary position is shown (left). The offset and slope are optimized so that the line falls right on the border of the chip (right).

given offset and slope as the intra-class variance of the two parts separated by the cut, on the grayscale image. The offset and slope are then optimized by minimizing this cost through a gradient descent. This is an adaptation of Otsu’s histogram thresholding method (Otsu, 1979), except for the fact that the threshold is replaced by a straight line with 2 degrees of freedom.

Several methods can then be used to detect bright spots on the right of the separation or dark spots on the left.

The image analysis part requiring functionalities not available using Iron-Python, the computation is performed using CPython using the bridge presented in Appendix D.4.

Bubble Removal

To remove the bubbles, the system goes in a solution of ethanol and water. The lower surface tension of this solution allows bubbles to disappear. The cantilever is then rinsed in the calibration well before going to the sample to avoid ethanol contaminations.

7.2.2. Cell Detection

As mentioned in Section 5.1.3, the system first has to detect the cells before they can be scanned. The FastScan was chosen for our prototype for its automation capabilities although it does not have an optical system adapted to living cells, small prokaryotes in particular. As a consequence, a cell detection method had to be designed for bacteria, without relying on the video image. Instead, the system is engaged in a position and the $30\ \mu\text{m}$ by $30\ \mu\text{m}$ area around it is probed by a large survey scan, in force volume or PeakForce. This capture is analyzed to detect the bacteria, as described below. Once detected, the bacteria can be scanned, then the system is withdrawn and repeats the process at another position.

To detect the bacteria, the survey scan file, is opened and the image channel is extracted with the NanoScope Toolbox. The image is then flattened using a 2D linear plane fit, to remove most of the tilt.

A threshold height is defined, which can be adapted to the sample. In the case of *Y. pseudotuberculosis*, we took it to be 200 nm above the minimum of the image. This value was chosen as smaller than the expected height of bacteria while high enough to avoid small contaminants. It could be re-considered for other samples. Everything higher than that threshold can be considered as part of a potential bacteria.

First, the 2D indexes of the highest point in the image are considered as a target. A mask of the small scan size is then created, centered on that point. The area higher than half the threshold falling within the mask is considered and the target is re-centered on the center of mass of this masked area. This allows the mask to be centered on the cell even in the event where the highest point would be close to an extremity. This target point is then saved as a position to be scanned and the masked area is discarded for future processing. The procedure above is repeated until the whole remaining data falls below the threshold.

As for above, the computation is performed in CPython through the system presented in Appendix D.4.

7.2.3. Contamination Detection

Contaminations are often a problem during AFM measurements. Biomolecules in the medium can attach to the cantilever and interfere with the laser measurement or to the tip and modify the tip-sample interactions (Ozkan et al., 2018). Parts of the cells can also sometimes attach after a tip-sample contact.

Contaminations on the back of the cantilever can perturb the laser and lower its intensity. Since the photodetector signal includes a normalization of the signal by dividing by the total sum, as presented in Equation (2.4), this effect should have a limited impact on the measured values. It can, however, impact negatively the signal-to-noise ratio (SNR), lowering the precision of the experiment.

Contaminations on the tip, on the other hand, have more visual effects. When on the end of the tip, they usually induce an offset, creating a step in the image. This offset is usually associated with a broadening of the image, hence a lowering of the resolution, by the convolution effect mentioned earlier, applied to the contaminant rather than the tip.

Tip contaminants have, however, been noted to be much less of a problem on oscillating modes than in contact mode (Hansma, Cleveland, et al., 1994).

During a scan, contamination can appear and disappear. As they are often characterized by steps along the slow scan axis, the average of each line is computed before the flattening in the previous step. Steps of more than a certain threshold, such as 200 nm, is considered a marker of contamination.

Similarly, if the number of bacteria detected is such that it covers more than half the plane, we assume that something might have gone wrong and the area is dropped as, in the best case, the sample is of a poor quality. These settings can, however, be adapted depending on the cell type or the expected confluence.

8. Demonstration

8.1. Multi-Cells

We have seen in Chapter 4 that one of the main challenges in AFM is the unsatisfactory number of samples customarily captured. Our first demonstration will, therefore, be regarding the possibility of scanning multiple cells in a row.

As mentioned earlier, the immobilization of the sample is currently the main issue in the system. *Yersinia pseudotuberculosis* bacteria were used as a model thanks to their ability to stick to surfaces, although they had to be fixed because of their pathogenicity. To demonstrate the approach of the system presented before, we then prepared samples of *Y. pseudotuberculosis* bacteria on coverslips and fixed them, to be scanned in fluid on the Multi-Well introduced on Section 6.1. The experiment procedure, detailed in Chapter 7, consists of paving the sample with large survey scans in force volume mode, analyzing them to find the bacteria, and scanning the detected elements of interest.

8.1.1. Sample Preparation

Our main test sample was *Yersinia pseudotuberculosis*, which was cultured and plated as specified in Appendix A.3. It was then mounted on the Multi-Well plate as described in Appendix A.4.

8.1.2. Setup

NanoScope is launched and the default setup described in Annex A.5 is loaded. The user places the probe—here a ScanAsyst-Fluid one—starts the Python interpreter, and open the relevant scripts. A script can then be used to move to the calibration well, in which the user can perform the calibration. The setup implies selecting the probe parameters, tip location, alignment of laser and then of the photodetector, with the software as for a normal use.

Calibration is performed by using standard touch calibration as implemented in the NanoScope software. It consists of doing a thermal tune to determine the relationship between the deflection sensitivity and the spring constant, then engaging on the sample to take force curves to set the deflection sensitivity. The PeakForce calibration parameters are also measured with a PeakForce equivalent of the force curve, so as to measure the Sync Distance QNM and the PeakForce Amplitude Sensitivity at the frequency of interest (here 1 kHz). In the future, the SNAP (Schillers, Rianna, et al., 2017) (non-touch) procedure could be used with calibrated levers.

Once the calibration is finished, the trigger threshold for the FV is put to 1 nm. The mask size is chosen by the operator, here 2 μm for *Y. pseudotuberculosis* bacteria. This size is used in the detection process on the survey scan and as the scan size for the measurement scan. At the end of the setup, the user starts the script and is no longer required.

8.1.3. Results

With the system as described up to this point, the experimental setup was applied to a sample of *Y. pseudotuberculosis* bacteria. In this section, we will go through the way all the elements were used together in one sample and the results that were obtained. The schematic behavior of the system is illustrated in Figure 8.1. In this image, (A) shows the Multi-Well and the sample-holding coverslips; (B) is an aggregation of the nine survey scans,

8. Demonstration

with a simple first-order flattening; (C) is one of the survey scan, with the areas of interest marked as detected during the procedure; (D) is, finally, one of the resulting measurement scans.

First, after the initial setup by the user, the system moves to the first well and starts surveying the area. It then detects the bacteria using the toolbox and a mask size of $2\ \mu\text{m}$, as described in Section 7.2.2. If a problem is detected with the area during the analysis, it is skipped. Otherwise, the system switches to PeakForce and stabilizes before setting the offsets and starting the actual scans of the detected bacteria. It sums up, for each survey area, around one minute for the engaging process, seven for the FV image, and 40 seconds to detect the bacteria and perform the switch from force volume to PeakForce.

Once the bacteria have been detected and the system has switched to the measurement setup, it takes about 50 seconds to offset to a position of interest, stabilize and capture the scan before it can go to the next one, with the current parameters (see Appendix A.5).

With the 3 by 3 array of force volume scans, a square with a side of $90\ \mu\text{m}$ is covered, discovering and scanning 501 areas of interest (prospect bacteria) in 8 hours and 35 minutes. Among the 501 scans, 16 were removed for the reason of visible contamination or for the absence of bacteria (false positive). The 485 other scans (97%) were kept for the analysis, some of which being shown in Figure 8.2. This corresponds to an average of one scan every 64 seconds. This is much faster than any human could be with the current setups because the microscope can keep in memory the position of the bacteria and move from one to the other without stopping. We can then see that the system is able to bring a lot of data in a comparatively short time, and can keep the rhythm for hours.

There is a downtime of about 8 to 9 minutes to move to the surveyed position, engage, and take the FV. The number of scans per surveyed area depends on the concentration of bacteria on the sample. Low concentrations imply fewer scans per surveyed area, hence making the survey time important. High concentrations, on the other hand, create packs of bacte-

8. Demonstration

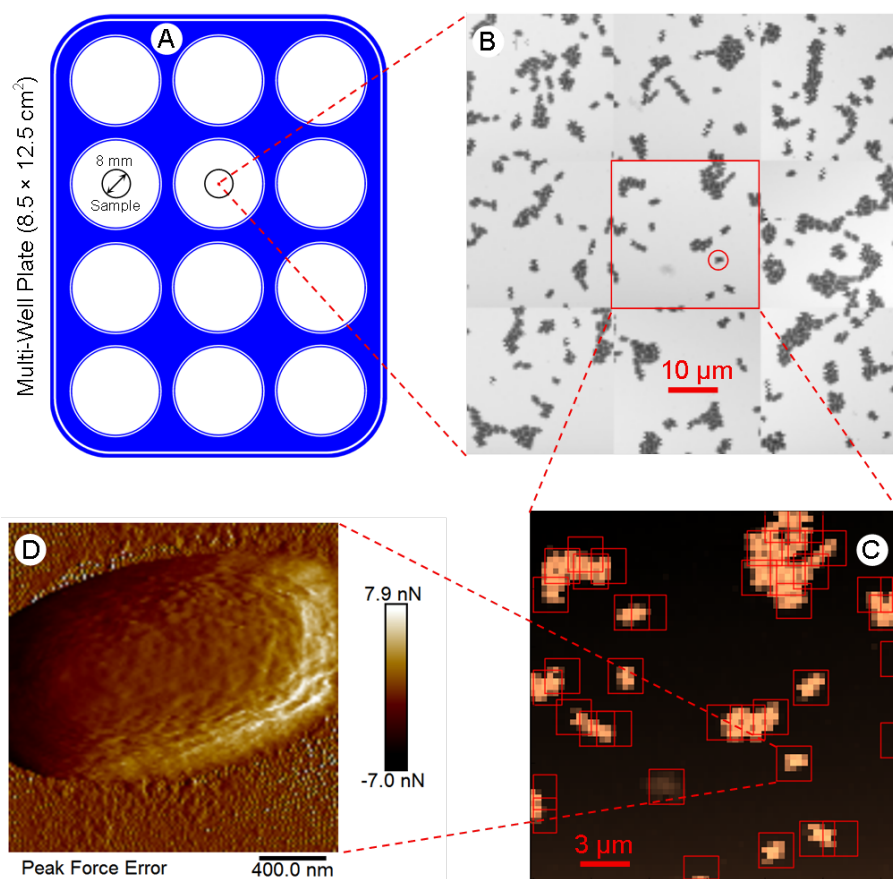


Figure 8.1.: Workflow of bacteria detection and scanning. (A) Representation of the Multi-Well. (B) Image made of the survey scans covering the area. (C) Example of survey scan. (D) Error map of a bacterium.

8. Demonstration

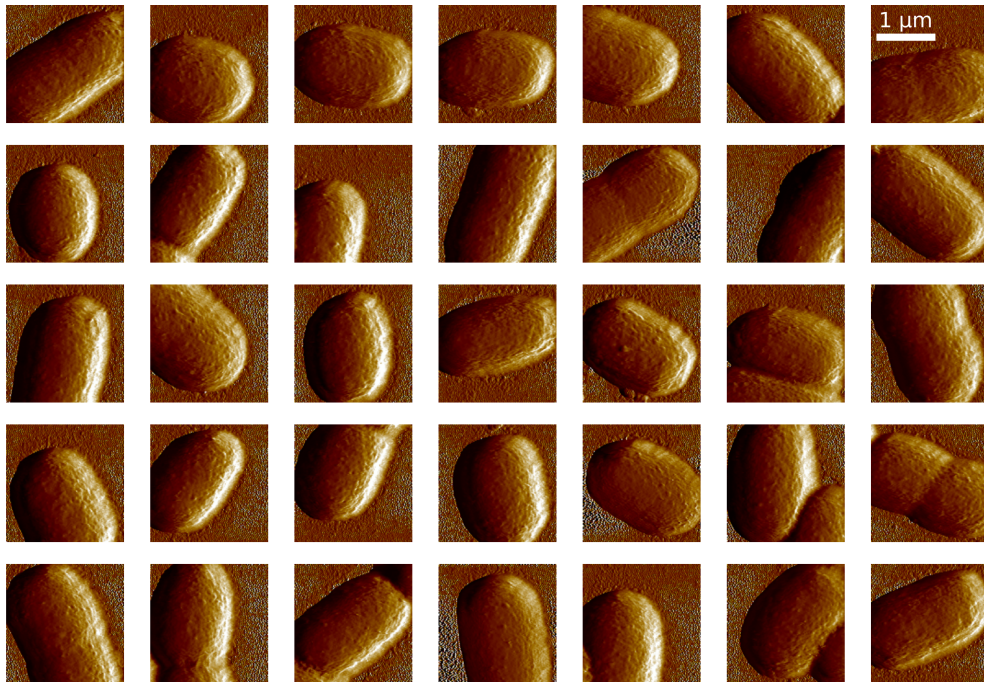


Figure 8.2.: Examples of scanned *Y. pseudotuberculosis* bacteria.

ria rather than single, individual cells. An ideal sample has a concentration such that a balance is be found. On the other hand, it could technically be much faster since the current ramp rate of 10 Hz could be sped up by an order of magnitude. This, however, makes the software a bit unstable in the current implementation, an issue that should be addressed. Once we manage to have it fast, the downtime linked to the survey should be brought to a more reasonable 2 or 3 minutes, hence allowing lower concentrations for the sample, hence more isolated bacteria.

8.2. Multi-Conditions

In the previous chapter, we showed that the system is able to scan a high number of cells. By itself, it could be sufficient when trying to obtain a nanomechanical signature (Ciasca et al., 2016; Plodinec et al., 2013) or other robust indications, which could be used for diagnostic purposes. It could also be useful when trying to analyze a sub-population. In other cases, however, such as when studying the effects of drugs, we are interested in the difference between conditions and the significance of this difference. To quantify the certitude we have on the samples being different, we consider a measurement on each side and we compare the measurements as statistics. If the two samples are similar, the underlying distributions of any statistics should be the same. By opposition, if there is a difference in the distributions (of height, roughness, stiffness...) that we observe, we can conclude that the samples are different. As a consequence, we test whether the sets of measurements that we record on both sides are likely to come from the same distribution or not. The key point, however, is that it only shows that there is a difference, which could be due to other factors, such as the operator handling. To say that the observed difference must be from the treatment, we have to ensure the treatment is the only meaningful difference between the samples. Hence, they should be prepared the same way at the same time to limit their variability.

Aside of the software tools required in the last chapter, this purpose required the sample holder to be able to keep different samples in similar conditions and to be used with the chosen AFM. This sample holder is the main custom hardware part of the system, the Multi-Well, and is described in Section 6.1.

8.2.1. Sample Preparation

As in the previous chapter, *Y. pseudotuberculosis* bacteria were used, but we applied different treatments to illustrate the ability of the system to differentiate between them. The treatments are described in Annex A.3.2 to have different conditions: a control sample (#1), a gentamicin-treated sample (#2), and a heat-treated sample (#3).

The system went smoothly among the 3 wells and took a 3 by 3 array of survey scans, then the corresponding localized measurement scans. In this case, due to changeability in the preparation, there was little data in the last sample, so we extended the scanning procedure of the last well to become 7 by 7. This gave us 357 and 69 extra samples, in the gentamicin-treated and heat-treated cases.

8.2.2. Analysis

As presented in Figure 8.3, the height maps and the PeakForce error images seem to show a difference between the two first conditions, although it is unclear. There looks like some bumps on the first sample and fine ripples on the second. The third sample, here, looks more obvious but could be a particular case. A simple visual analysis of a few images on such a subjective characterization does not allow to conclude unquestionably in any meaningful difference between the conditions. We then apply quantifiable estimators, described below, to give a more objective way to differentiate our samples. The analysis throughput is presented in Figure 8.4.

Once the experiment was finished, NanoScope Analysis, Bruker's soft-

8. Demonstration

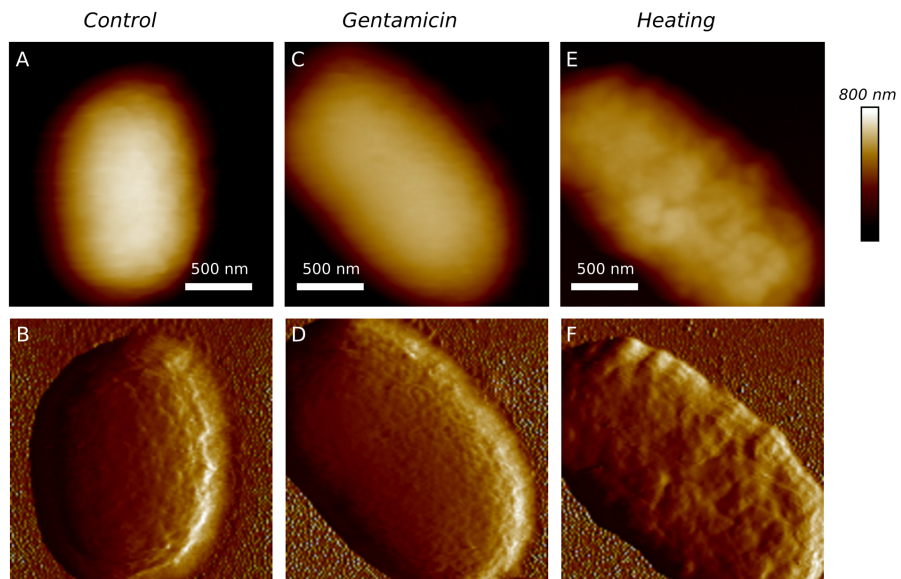


Figure 8.3.: Representative examples of the 3 conditions of *Y. pseudotuberculosis*. A, B: Control. C, D: Gentamicin-treated bacteria. E, F: Heat-treated bacteria. A, C, E: Height maps. B, D, F: PeakForce error images.

8. Demonstration

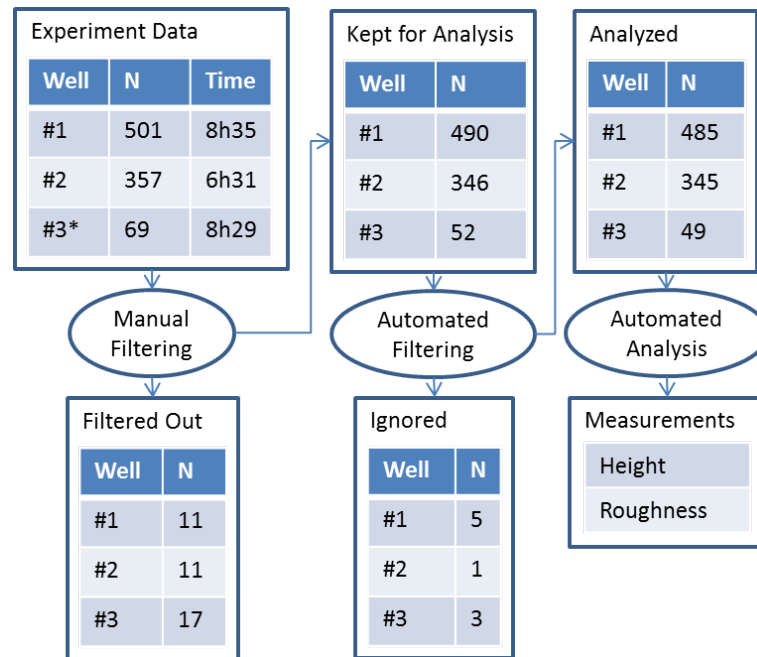


Figure 8.4.: Analysis throughput. The top left corner shows the number of scans (N) recorded for each condition and the time taken. Sample #3 required an extended scanned area. Following the arrows, a manual filtering is performed to remove clear outliers and corrupted data. Then, an automated filtering asserts some quantitative criteria for borderline cases before the analysis.

8. Demonstration

ware, was used to promptly check the quality of the data such that detected objects that were not bacteria could be removed, as well as the empty scans. Among the two samples, 345 and 49 good quality scans were kept and, as later, analyzed.

To compare the conditions, a few measurements were taken per sample, in Python with the toolbox. Thanks to the quantity of data, we can do some automated analysis. In particular, the height and roughness of the samples were measured. Such measurements are always a little bit arbitrary and subject to errors. The measured height, for example, depends on the indentation depth, hence on the probe geometry and the applied force, although the impact is neglectable on bacteria but would have to be considered on softer samples. The roughness, for its part, is ill-defined on a non-flat surface and is impacted by the probe geometry as well. In this experiment, the same probe is used with the same calibration and the same force setpoint. As a consequence, we define here our “height” and “roughness” as described below and, while different methods could be used for their definition, we are ensured that the same method is applied consistently to the three conditions.

The analysis process goes as follow. First, a smoothing was applied to the data (2D Gaussian filter, $\sigma = 3 \text{ px} = 15.625 \text{ nm}$). For the area of interest of the analysis, we took a mask corresponding in the smoothed image of anything that was higher than the minimum (post smoothing). These area of interest and mask, for the analysis purposes, are within the measurement scan and should not be confused with the areas of interest and masks of the survey scan, which where for detection purposes. We also masked on error signal being lower than -5 nm , which is the SetPoint and indicates no sample tracking. This happens a lot on the glass and shows some spikes due to the sawtooth effect described in Section 2.5.6. These spikes are filtered out as artifacts and do not matter since the height of the glass substrate is of little importance in our application.

The analysis discards anything smaller than 100 pixels and removes any scan where the usable surface of the scan was lower than 5% of the area

8. Demonstration

of the scan that could have been used otherwise (see table too, ignored). The latter area corresponds to the area eroded by 10 pixels.

Height To measure the height of a sample, we took the difference between the extreme values of the smoothed height.

Roughness To measure the roughness, which we recorded at a given “scale”, we took the arithmetical roughness R_a after subtraction of the smoothed data, but only on the area of interest (of the analysis). However, each line is slightly different so that creates streaks. To avoid this, we considered each line separately, performed the smoothing 1D instead of 2D, which would have counted that streaking effect as an undesired extra roughness. Since the measurement is done after filtration with a band of 30 nm (high-pass filter). Then that means that was left is contains information about periods smaller than 30 nm or the order thereof.

8.2.3. Results

As illustrated in the boxplots of Figure 8.5, we see a reduction in height by about 25% between the control (sample #1) and the two treatments. To differentiate between the gentamicin (sample #2) and the heat (sample #3) treatments, we can measure the roughness.

Given the complexity of the surface, measuring the roughness at different scales, hence after applying different filters, gives varying results. There is, however, a clear difference in the roughness of sample #2 and the others, which would confirm the visual observation we saw earlier. Further than changes in their mean, the histograms of Figure 8.5 shows wide differences in the distributions of these parameters.

Combining the two measurements, we can reach the conclusion that there are statistically-significant differences between the 3 samples, which can be put forward on the 2D scatterplot of Figure 8.5. This plot clearly illustrates the clustering of the 3 conditions over these parameters.

8. Demonstration

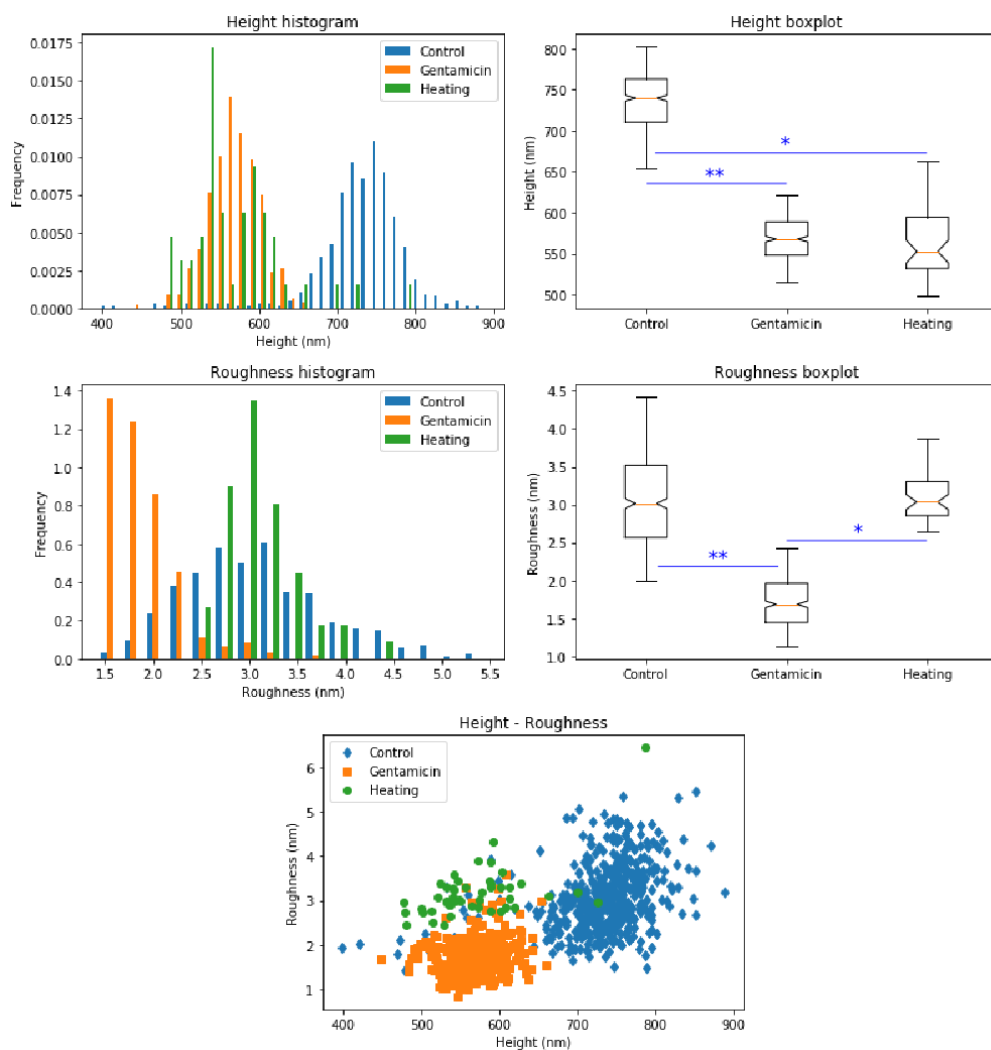


Figure 8.5.: Analysis results. First row: height histogram and boxplot. Second row: roughness histogram and boxplot. Bottom: height-roughness scatter plot. * and **: p -values smaller than 10^{-20} and 10^{-100} , respectively.

8. Demonstration

Welch's t -test (Welch, 1947) was used to check the significance as Student's t -test normally assumes that the two distributions have an equal variance. If the two distributions have the same size, Student's t -test has been shown robust against different variances (Markowski and Markowski, 1990) and is therefore widely used in biology and other fields. In our case, given the differences in sample sizes, Welch's t -test was used as it does not assume that the two distributions have equal variance.

The third sample has much fewer samples, but still more than what would usually be published. Since there are a few (but decent amount of) scans on the third, but a lot on the two others, the certitude of the underlying distributions is still important and p -values are smaller than 10^{-20} .

8.2.4. Conclusion

The analysis shown here gives very high certitudes for a fact that we can guess visually, illustrating the power of high-number of scans. Similarly, most common AFM applications are interested in differences which are much more subtle, especially in the domain of cell mechanics, where the within-group variances might be much higher than the between-group variances. For these applications, gathering a high quantity of data is crucial, and would then show normal p -values whereas the eye would not have seen anything.

8.3. Living Cells

Following the demonstration that the system was able to scan a lot of cells and that it was able to scan across different wells to compare conditions, we wanted to show that the system was also suitable for living organisms. *Y. pseudotuberculosis* bacteria were chosen as our model in that they adhere very conveniently to the surface. They are, however, not suitable for being scanned live in our system because of their pathogenicity, which is

8. Demonstration

also the reason why they are interesting to study in the first place. As a consequence, we focused on *M. bovis* BCG mycobacteria, which adhere nicely thanks to their hydrophobic surfaces (Alsteens, Dague, et al., 2007). The protocol is described in Appendix A.

As it can be seen in Figure 8.6, there are individual bacteria and aggregates. *M. bovis* BCG mycobacteria have a strong tendency to stick together but the quantity of individual bacteria can be slightly increased by a brief sonication. The observed data is consistent with prior observations (Dupres et al., 2005; Verbelen et al., 2006), showing a smooth surface. The use of PeakForce QNM gives access to mechanical properties as well, as illustrated in Figure 8.7, showing here a softer and more adhesive part close to the extremity of a mycobacterium.

M. bovis BCG mycobacteria are usually elongated and 2 to 5 μm long, whereas our previous model, *Y. pseudotuberculosis*, is much shorter and only slightly oblong. As a consequence, a bigger mask size could have been chosen. In this case, we chose to take the same scan size as in the prior experiments to show an equivalent resolution. Since the mycobacteria are bigger, this means, however, that we are taking several scans per cell. This also shows that the system does not require over-optimization of the parameters, which can be used for two unrelated kinds of bacteria.

8.4. Eukaryotes

Since we have shown applications of our system on multiple cells, on multiple samples, and living cells on prokaryotes, we would now like to illustrate its applicability to mammalian cells. These cells, using here cells of the Retinal Pigment Epithelium (RPE-1) described in Section 3.2.4, are much bigger than the previous ones. As a consequence, they cannot be detected through the method designed earlier, where a survey scan is used to find them. The cells themselves are often bigger than maximal extension allowed by the piezos of the FastScan, which are limited to 30 μm in

8. Demonstration

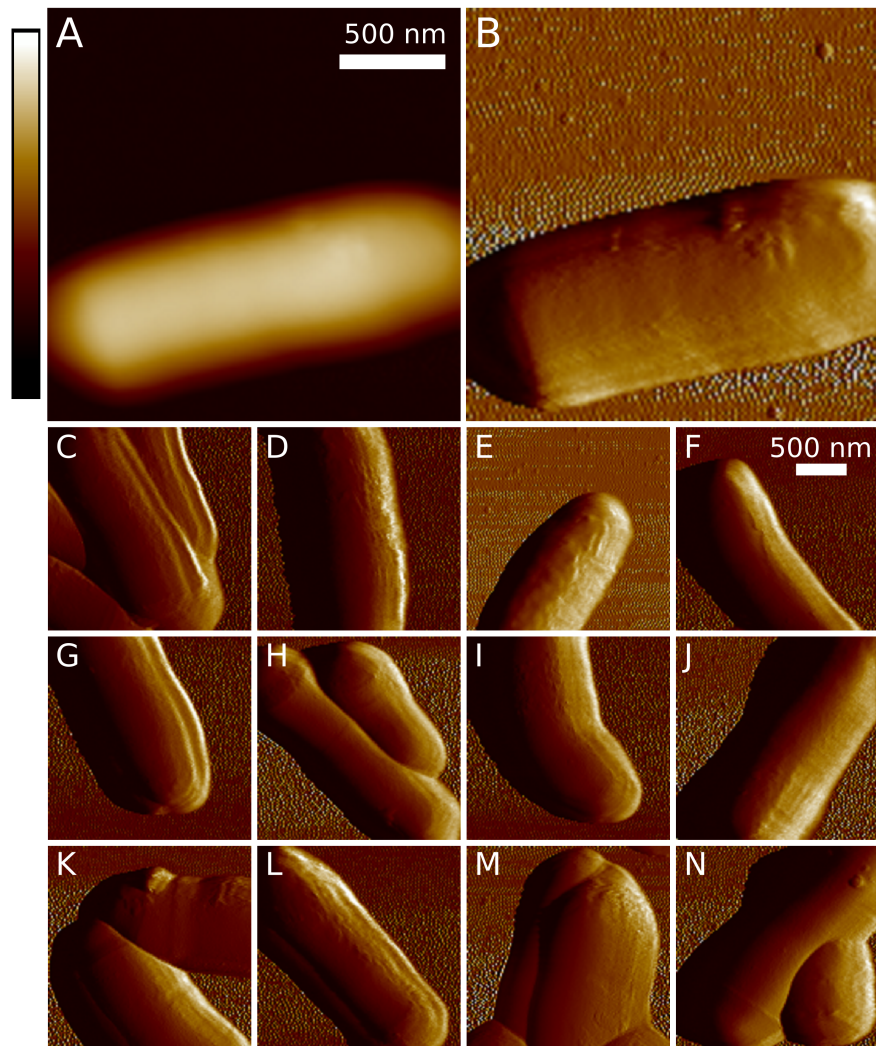


Figure 8.6.: Representative images of *M. bovis* BCG mycobacteria. (A) Height map (scale bar: 715 nm). (B) PeakForce Error of the same scan. (C-N) PeakForce Error of other scans (common scale).

8. Demonstration

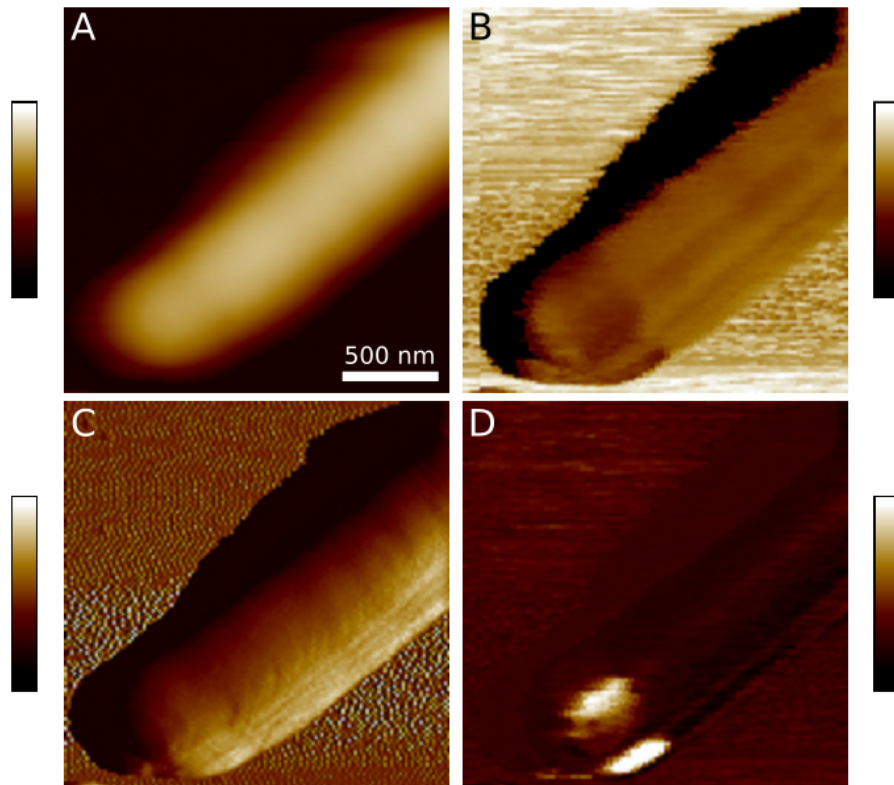


Figure 8.7.: Nanomechanical mapping of a *M. bovis* BCG mycobacterium. (A) Height map (scale bar: 0 nm to 725 nm); (B) Young's Modulus (scale bar: 10 kPa to 400 MPa, logarithmic scale); (C) PeakForce Error (scale bar: -7.7 nN to 8.7 nN); (D) adhesion (scale bar: -1.3 nN to 3.6 nN).

8. Demonstration

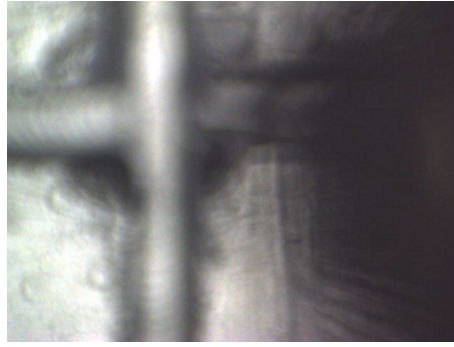


Figure 8.8.: Early visibility. RPE-1 cells on coverslip, on the Multi-Well. Focus on the sample (top of the coverslip), the heterogeneous out of focus background is predominant.

the horizontal directions and $3\ \mu\text{m}$ in the vertical one. Furthermore, given their size, we will see that not only the survey scan is impossible, but also the measurement scan can have some issues. On the other hand, these cells being of greater size, they can be detected with the optics.

On the early version of the Multi-Well, the cells could hardly be seen because of the reflective Titanium background. This background was just behind the transparent coverslip and the transparent cells, thus too close to the focal plane and almost in focus, as seen in Figure 8.8. This was solved by boring small holes under the coverslip so that the reflective background is further away. The resulting image can be seen in Figure 8.9, part A.

The image is still difficult to interpret because of the strong shadowing effect due to the probe, on the right and because of the inconsistent illumination of the cells. The cells, mostly transparent, show only a slight variation, which is also strongly dependent on the angle of the illumination. Having a different refraction index, however, they diffract the light, creating halos when slightly out of focus. As a consequence, two images are taken at $50\ \mu\text{m}$ above and below the focus correspond to parts B and C of Figure 8.9. These two images are then subtracted, in a fashion inspired from the work of Ali et al. (2008). Where there is nothing in the focal plane, the two out of focus images will be pretty much identical. Where

8. Demonstration

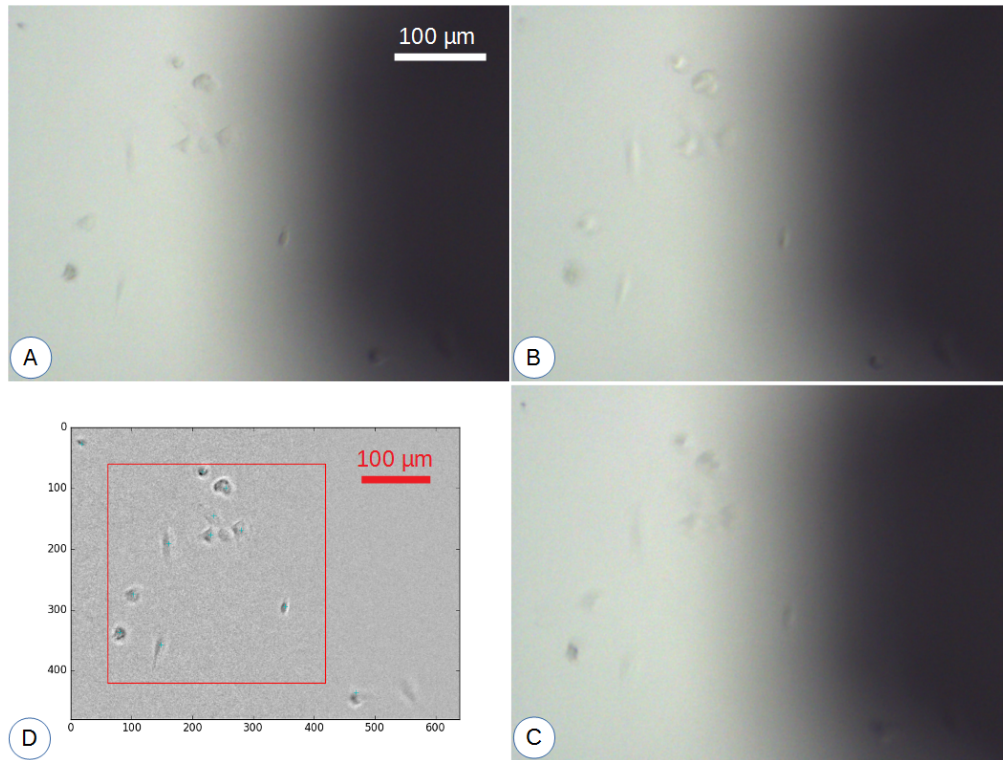


Figure 8.9.: Seeing eukaryotic cells. A-C: Optical image taken at the focus (A) as well as 50 μm above (B) and below (C), zoom . D: Difference between A and the average between B and C; the blue ticks represent the detected cells and the red square corresponds to the accurate area.

8. Demonstration

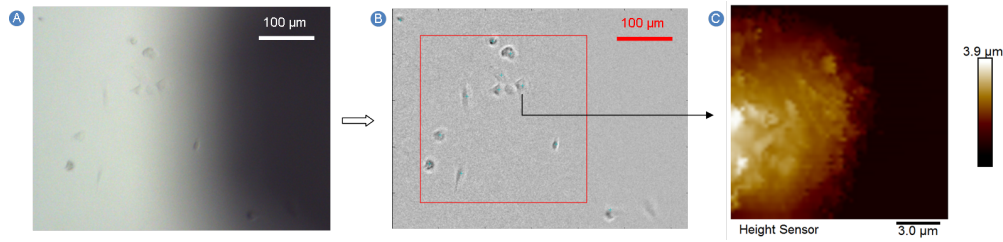


Figure 8.10.: Eukaryotic cell detection and automated scan.

there are cells, however, the signal will differ a lot. So, the result is null everywhere except for where elements located in the focal plane are. The same effect can be obtained by subtracting their average from the focal image, taking essentially:

$$D = A - \frac{B + C}{2}, \quad (8.1)$$

which will remove the background while keeping more of the sharpness of the image, giving a more visual result, shown in Figure 8.9, part D.

The cells are, on the other hand, better detected on the simple differential image. This image is smoothed and thresholded. Small elements are discarded while the others have their centroid marked in blue on the previous image.

Nevertheless, it is important to remember that since the part hidden by the probe is black in both cases, the difference image will show as if the corresponding area was empty. Similarly, there might be some effect on the border from elements outside the field of view. Thus, a safe, accurate area is defined in red, corresponding to a square having a side of 300 µm.

As seen in part B of Figure 8.10, the cells can be seen and detected, but the diversity in cell shape is such that it is difficult to reliably detect their highest point, hence where to engage.

In Figure 8.11, the cells were clicked by the user and then scanned automatically. The great similarity between the two lines shows that the

8. *Demonstration*

system was, indeed, able to come back at the same positions. The usage of force volume releases both topographical and nanomechanical information, such as the local elasticity, shown in the lower part of Figure 8.11.

However, the cells are big compared to the ranges of the piezo. Along the horizontal axes, it simply means that the full cell cannot be scanned at once. Along the vertical one, however, the impact is more difficult to manage. Engaging on the top of the cell means that the lower parts of the cells are not attainable, leaving a flat surface that is due to the piezo reaching its maximum extension rather than the actual flat substrate of the sample. This is especially visible on the right images of Figure 8.11, where the piezo did not engage at the same height between the two series, giving a different available depth. Engaging on the border of the cell, however, is worse since the tip can be in contact with the sample while fully retracted, generating high forces between the sample and the probe. This also reduces the part of the cell horizontally available since the engagement has to be performed on its side. Furthermore, the typical engage procedure consists of stabilizing the vertical piezo at the middle of its extent, further reducing the available range if the engagement is performed on the top or bottom of the sample. As a consequence, we should specifically engage on the top of the cell in a retracted configuration or engage on the border of the cell in an extended configuration. This would, however, require a detection with more detail than what is allowed by the current optics as well as a much more complex segmentation algorithm.

8. Demonstration

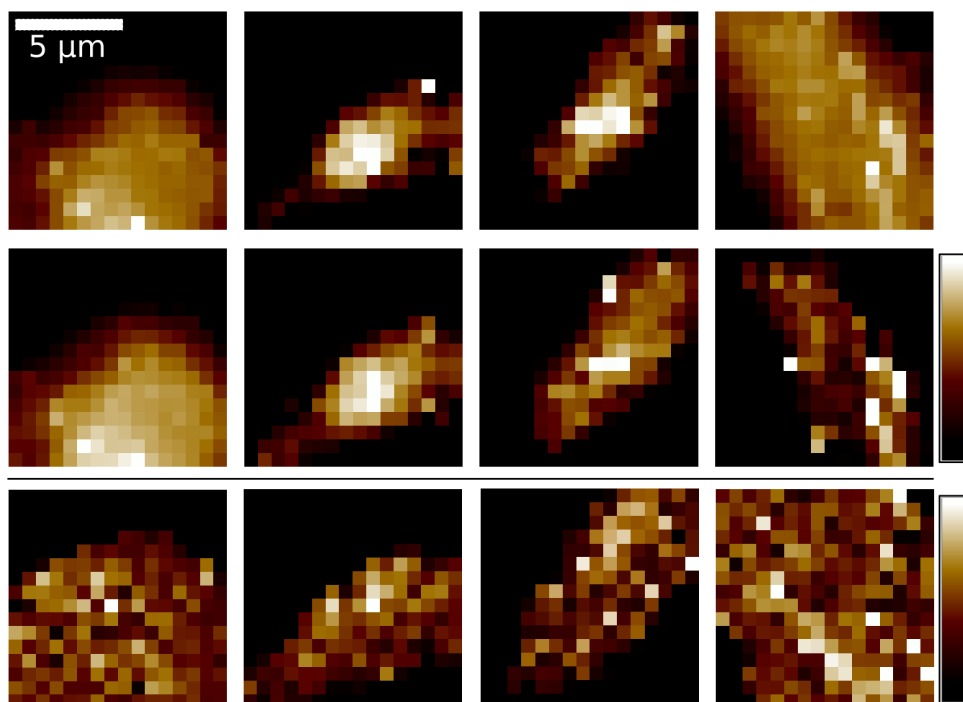


Figure 8.11.: Chained force volumes of RPE-1 cells. The cells were selected by the user in the video image, then automatically scanned twice. Corresponding height maps are shown in the top and middle rows (scale bar: $2.7 \mu\text{m}$). The bottom row shows the Young's modulus maps of the top one (scale bar: 10 kPa to 300 kPa).

9. Further Developments

Our long-term goal is to have an AFM suitable for scanning eukaryotic and prokaryotic cells automatically in a multi-sample environment over extended periods of time in a correlative setup. With the current prototype, we are able to scan prokaryotic cells automatically in a multi-sample environment. Eukaryotic applications are also possible but limited. In this chapter, we will discuss elements that have been studied with some level of details or for which proofs of concepts have been performed and that could be part of a future system.

9.1. Controlling Cells Position

As discussed in Section 5.1.3, the positioning of cells on a standard sample is not controlled. Cells tend to position themselves in an erratic way and even their surface coverage can be difficult to regulate. Ideally, we would like to control their positioning so as to be able to immobilize any kind of cell in a nice and predictable way. Furthermore, there is plenty of evidence that the behavior and mechanical properties of cells are affected by their shape (Charest, García, and King, 2007; Dalby et al., 2003; Wu et al., 2015; Yim et al., 2010). As a consequence, reducing the variability in cell shape by constraining them is likely to standardize the experiment and further reduce variability in the measurements. Finally, some cells do not naturally adhere to surfaces, so we would like such a system to be able to hold a wide range of cell types regardless of their affinities and other adhesion properties. As mentioned in Section 2.3.2, two main methods

exist for holding cells in place: physical confinement and chemical binding. These elements can be used in a structured way to immobilize the cells at specific places, usually following a pattern. Such solutions can be found in the literature, existing for both eukaryotes and prokaryotes.

9.1.1. Chemical Binding on Mammalian Cells

For eukaryotes, for instance, the glass support can be patterned with fibronectin islands, promoting cell adhesion, in a background coating of poly-L-lysine-*grafted*-polyethylene glycol (PLL-*g*-PEG), which prevents cell adhesion. To do so, a uniform PLL-*g*-PEG coating is applied and the patterning is created by exposition to a deep UV light under a patterning mask (CYTOO, Grenoble, France) to create holes in the coating with the desired shape and positioning. A fibronectin solution is then used, letting the protein adhere to the bare glass where the PLL-*g*-PEG has been removed (Azioune et al., 2009).

Alternatively, the mask can be emulated by a software-controlled UV laser (Primo, ALVEOLE, Paris, France), its effect being increased by a photoactivable reagent (PLPP). Since the mask is directly controlled by software, the patterns can be easily customized. On the other hand, the area covered by the mask being small, it takes time for the laser to cover the whole area, making it a slower system. Finally, another method consists of stamping the fibronectin first and then passivating the uncoated part with PLL-*g*-PEG (Rigato, Rico, et al., 2015).

9.1.2. Chemical Binding on Bacteria

On bacteria, immobilization is already recognized as an issue by itself, as described in Section 2.3.2. Making that immobilization regular is, then, even more difficult. As a consequence, these techniques tend to be even more specific to the cells to be immobilized. For bacteria adhering to polyethylenimine (PEI), PEI can be micro-patterned so as to have small

9. Further Developments

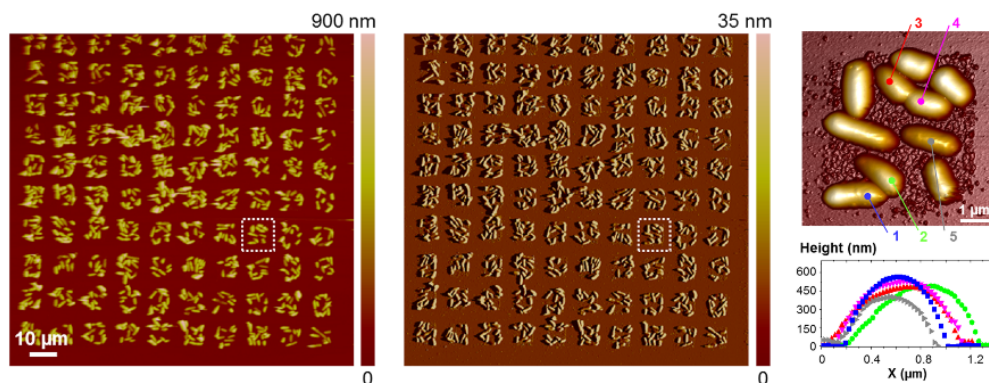


Figure 9.1.: *Pseudomonas aeruginosa* bacteria in buffer medium on a 2D array of $5\ \mu\text{m}$ square PEI Patterns. Left: height image. Middle: corresponding deflection image. Top right: relief-enhanced height image of the square previously marked. Bottom right: height profiles of the bacteria marked previously. Adapted from (Jauvert et al., 2014).

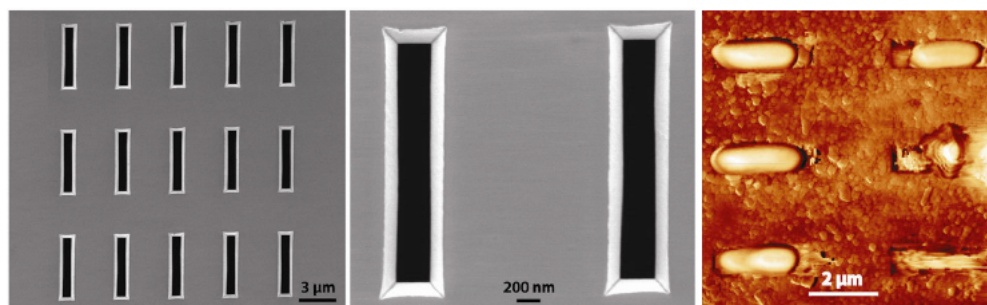


Figure 9.2.: Microfluidic bacterial traps. Left and middle: SEM images of the array. Right: Phase image of *Escherichia coli* in the microfluidic traps. Adapted from (Peric et al., 2017).

9. Further Developments

localized patches of bacteria, as represented in Figure 9.1. By adapting their size, it is possible to have on average about one bacterium per patch, although their exact number or orientation cannot be controlled (Jauvert et al., 2014).

9.1.3. Physical Confinement on Bacteria

Microfluidic wells have been designed to immobilize bacteria at defined positions using suction to attempt to give them proper locations, as represented in Figure 9.2 (Peric et al., 2017). As a physical confinement technique, it offers the advantage of not depending on the chemical affinity of cell surface proteins with a specific coating, making this technology more general-purpose. On the other hand, the size of the wells has to be only slightly smaller than the bacteria, meaning that the system has to be somewhat dimensioned for the sample.

9.1.4. Hybrid Systems

On yeast and spores, microstructured PDMS stamps functionalized with concanavalin A have been used (Dague et al., 2011), hence combining a physical confinement with a chemical binding.

9.1.5. Interest

With such a micro-patterning or microfluidics system, the positions of the cells could, in theory, be known in advance and the system would be able to find them without relying on the optics. However, this would still require to know where these locations are, hence forcing to reference the pattern positions and ensure their stability with time. It should also be noted that a one-to-one correspondence between cells and patterns appears difficult to approach in practice, especially for chemical binding.

It would then most probably still be suitable to have improved optics for working with mammalian cells. For prokaryotes, the main advantage of

9. Further Developments

micro-patterning would be to help control the concentration of bacteria so as to increase the number of isolated ones. Finally, in both cases, controlling their orientation and shape would make it possible to scan well-defined parts of the cell, increasing the repeatability of localized measurements.

In the case of our current prototype, micro-patterning would have been especially interesting on RPE-1 cells since the limitations of the AFM would have made important to be able to engage directly on a specific part of the cells. Micro-patterning would likely have made easier both the detection of the cell and the localization of their center. It was attempted to have the RPE-1 cells on micro-patterns on the coverslip, without success. Although some decent results were obtained when preparing the coverslip in a multiwell cell plate, the cells could not be observed on the AFM after being mounted on the Multi-Well. The dewetting is assumed to have been the main problem here, which would have to be solved by a redesign of the Multi-Well.

9.2. Fluid Exchange

9.2.1. Fluid Evaporation

Although the effects of evaporation can often be neglected at our scale, at room temperature, and for a few hours, they can have a major impact on the sample fluid in some of our systems. The evaporation rate depends on the area of the air-fluid interface. When considering small samples, the surface decreases with the square of the size while the volume decreases with its cube. Therefore, the volume of fluid decreases faster than the evaporation rate, which is thus much more noticeable. This effect is also exacerbated by temperature, causing problems on heated samples.

This is thus especially a problem when working on small systems with a very limited amount of fluid, such as the MultiMode, where the scanning is essentially performed on a droplet having a volume of about 200 μL . In that case, dewetting can happen as the sample dries while scanning. The

9. Further Developments

effect is unequivocal as a clear separation line is visible on the optical image between the hydrated and drying parts. Furthermore, the later being in air, it is out of focus because of the difference in refracting indexes. Finally, the laser signal is lost when the border reaches the cantilever. These clues, especially the last one, happen too late for the user to avoid sample damage. In order to avoid such problems, the user has to closely monitor the fluid level of his or her sample.

Before de-wetting the sample, fluid evaporation can also be the cause of changes in the concentrations of the elements of the buffer and its pH.

On systems similar to the Resolve, a closed environment can be achieved. This can be done by a cell with a lid having a hole in the middle, allowing for the AFM head to enter. A silicone seal around the head can then be used to seal off the sample, whose composition can be controlled by gas and liquid perfusion, while still allowing some flexibility in horizontal and vertical movements.

For the FastScan-Bio, the fluid apparatus presented in Figure 9.3 can be used to minimize the evaporation at the position of scanning, creating a localized small semi-closed environment. Liquid can be added or removed through perfusion. A system equivalent to the one presented above for the Resolve could be implemented as well. Both of these designs are, however, difficult to implement on a multi-sample configuration as this would raise the question of how to seal the samples when the AFM head is absent. Individual seals on wells that are not being scanned would save a lot of evaporation but a system would have to be designed to allow the probe and z-scanner to enter the well.

Another possibility would be to create a closed environment with all the samples. This would, however, open the question of the mobility over the whole stage extent. Although a soft seal can allow some translational freedom, it might not be realistic to do it over more than ten centimeters.

Finally, enclosing the whole system in a hood would be an option, but working at high humidity above room temperature could be dangerous for the electronic components of the machine.



Figure 9.3.: Fluid apparatus on dimension FastScan head. Fluid intake from the top right through the thin flesh-colored tube, blue fluid chamber to host the cantilever in fluid, larger transparent fluid outtake leaving on the right. © Bruker

9.2.2. Implementation

As we have seen above, fluid evaporation is an issue that is difficult to avoid. It is then necessary to have a fluid exchange system, at least to bring water in to compensate for the evaporation. Several solutions are considered, with different levels of complexity. If the evaporation can be limited, simply adding water once every few hours with a single pipe located on the head could be a minimal working option. Preferably, however, a controlled input and output should be implemented to refresh the buffer.

Fluid Exchange can allow to get rid of waste, control pH, and bring Oxygen in. The FastScan-Bio fluid apparatus, shown in Figure 9.3 could have solved part of the problem, solving at the same time the issue of the dewetting of the probe, which leads to the apparition of bubbles. By keeping the head in the fluid apparatus, it can be kept in liquid, avoiding this problem. On the other hand, this brings almost direct contact between the different wells, promoting contaminations from a well to the other.

To exchange fluids, having a micro-pipe per well for fluid entry and another one for fluid evacuation would be ideal. Nonetheless, this would raise the complexity of adding a microfluidic system and connecting all the fluid inputs and outputs which, for a 12-well plate, would make at least 24

9. Further Developments

connections.

Evaporation, in particular on a heated version of the system, causes the output to be smaller than the input, making so that one cannot simply have the input and output pipes on a same peristaltic pump to keep the volume constant. Furthermore, the evaporation itself varies from a well to another. It is then not possible to predict the evaporation rate and use a smaller output flow than the input to compensate for it. This variability implies that the fluid level needs to be controlled on a per-well basis.

This level could be monitored by an individual sensor per well, although the AFM head could be used for the recording, to the expense of creating otherwise non-necessary moves of the head from a well to another, increasing the contamination risk. If monitored, the input or the output should be controlled individually, requiring one extra pump per well. In the case of two individual pipes per well, this would mean at least 13 pumps in total.

To avoid individual monitoring of the fluid levels, a “passive” regulation system would be convenient. In this kind of system, an input of fluid is forced, but the output works on a spillway (or overflow) fashion, being effective only if a certain level of fluid is present. This would allow first the evaporation to be compensated before the threshold level is met, yielding to an actual fluid exchange in a second time. Applied regularly, this would solve the evaporation and fluid exchange problem in parallel, without needing to monitor each inflow individually. The input and output pipes could then be on the same peristaltic pump.

Such passive regulation was attempted but capillary effects are very strong at this scale, rendering simple spillways inefficient. The level of fluid would go much higher than the spillway level before the fluid starts spilling. Oppositely, a needle placed at the top of the well would start extracting the liquid at the desired height but can easily create a bridge, extracting significantly more fluid than intended. As a consequence, specific geometries and coating should be studied such as, but not limited to, sharp angles for the spillway or the needle and hydrophobic/hydrophilic

9. Further Developments



Figure 9.4.: Pictures of the fluid exchange needle, held at a fixed position from the head allowing it to be lowered in the different wells while keeping the probe holder in a safe area and vice-versa.

coating inside and outside the well.

Even in the case of passive regulation, the previous solutions would require two tubes and a potentially complex regulation system per well. Another solution could consist in having a fluid input and output attached to the head as in the fluid apparatus of Figure 9.3, although without the fluid chamber. This would be difficult to implement with the current design of the Multi-Well since the wells are barely larger than the probe holder, but the wells could be extended in a corner with a small depression acting as a chamber that could make room for these two tubes. The proximity of these tubes to the probe holder could make difficult to avoid capillary effects, but the presence of the head in the well and the fact that only one pair of fluid intake/outtake system is required would make it possible to have a finer control on the flows.

Finally, the fluid exchange system could be at a separate location. On the Dimension FastScan-Bio stage, the fluid exchange connector can be held in front of the head in a position that allows a shared use of both the probe and the fluid connector. At that position, the fluid exchange system falls in a safe empty area when the probe holder is in the well. Reciprocally, the probe holder falls in a safe empty area when the fluid exchange system

is in use in the wells. The representation in Figure 9.4 shows such a system, here with a single needle. Having the ability to control the position of the needle allows the suction to be away from the borders of the wells, hence limiting the capillary effects, although the geometry and coating of the needle should be studied to minimize them further.

9.3. Heating

Mammalian cells should usually be kept at temperatures between 36 and 37°C, hence within 0.5°C of the optimal temperature. Variation of 3°C from that point show strong effects on their growth and development (Watanabe, 1967). Although cells could support such variations for the time of the experiment, the temperature dependence of cell mechanics should be noted (Sunyer et al., 2009). As a consequence, a proper system, especially operating over several hours, should have a good temperature control, preferably with variations of less than 1°C.

Such temperature control systems are typically based on a heater composed of a heating element, a heat storage medium, and a sensor. The heat storage medium, often the heating plate, should have a very good thermal conductivity to have a homogeneous temperature and, when the objective is to keep the temperature constant, a decent thermal capacity to be able to absorb the potentially rapid temperature variations of the samples. This material is heated by the heating element, placed in a closed loop with the thermal sensor to keep the temperature at the desired setpoint.

Heat losses between the heater and the sample, however, lower the temperature of the latter. The heater should then be set at a higher temperature to compensate for these losses. From the perspective of the sample, however, the heating system is in an open loop, which offers a poor control. The offset between the heater setpoint and the sample temperature depends on the setpoint temperature, the type of sample, the room temperature, and other parameters linked to the environment or the application.

9. Further Developments

On simple heating systems such as the NanoWizard (JPK Instruments, Berlin, DE), it should be measured by the user prior to the experiment. Alternatively, a thermometer can be placed on the probe to control the actual sample temperature, as done on the BioScope Resolve. It then allows the user to modify the heater setpoint during the experiment to reach the desired temperature, hence manually closing the feedback loop. In our case, having the sensor integrated to the Multi-Well would be preferable to enforce a more stable temperature control.

Whereas the principle of using a sensor to give feedback to the user regarding the actual temperature can work thanks to the actions of the operator, unattended operations require the heating setpoint to be placed on a second closed loop with the sample-side thermometer. The problem gets more complex in the case of multiple samples. To guarantee a good control of the temperature of each sample, it would be needed to have a heating system per well, unless the homogeneity of the heating can be guaranteed. If the time variations, the intra-well variations, and the inter-well variations are to be kept within 1°C of the setpoint, an initial starting point would be to attempt keeping each of them within 0.3°C . One might argue that, in an incubator, the thermal properties of the plastic cell plates are not much of a concern. It should be noted however that a level of homogeneity similar to the one encountered in such an incubator is not attainable here, since the air cannot be kept at equilibrium with the sample medium, which would mean 100% humidity and 37°C . In these circumstances, evaporation and the lack of homogeneity in temperature would create convections around the warmer plate. These air flows would at least be perturbed by the position and proximity of the FastScan head, creating heterogeneities in the temperature of the environment that should be considered when designing the heating system. Therefore, the thermal properties of the Multi-Well have to be studied carefully if a good and homogeneous temperature control is to be met.

It should be noted that the FastScan is sometimes operated on heated systems or at high humidity. Indeed, although discouraged, operating at

9. Further Developments

high humidity at room temperature might not damage the machine* as long as the sensitive parts are sensibly warmer than the environment. This would have the effect of avoiding condensation, which concentrates on the heat sinks, namely the front glass and the external structure, closer to room temperature. Operating at high humidity and high temperature, on the other hand, could increase the risk of condensation on sensitive parts of the machine, increasing potential damages to the system.

To observe the structural ability of the Titanium body of the Multi-Well to homogenize its heat, the Multi-Well was first placed on a heater, in the FastScan hood. The heater was circular with a diameter of 38 mm, hence covering the center of the bottom side of Multi-Well plate on 11% of its surface, and centered. This created variations of up to 6 °C between the wells in the center and in the corner of the Multi-Well at equilibrium, although this was done with an open hood. Although high variations were expected since the wells in the center were fully over the heater while the ones in the corner were distant, we can see that the bare Multi-Well is not able to homogenize significantly the heating.

Afterward, two pressure-sensitive adhesive Kapton heaters were placed under the Multi-Well, represented in Figure 9.5. Their width, 2.54 cm, corresponds almost exactly to the inter-well spacing 2.60 cm, allowing a similar heating of the 12 wells, although the ones closer to the borders have more heat losses due to their higher surface area in contact with air. In this case, temperature variations between the wells of the top and middle rows were limited to 3 °C, showing an improvement. Temperatures on the bottom row were lower since the corresponding part of the Kapton heaters were actually occupied by the connectors rather than the resistor. It should be noted that for such a system to be acceptable, since the Multi-Well should be autoclavable, its components should be selected carefully and it should integrate an autoclavable connector in which to plug the wires for the heaters and the thermistor.

*at the user's risk

9. Further Developments

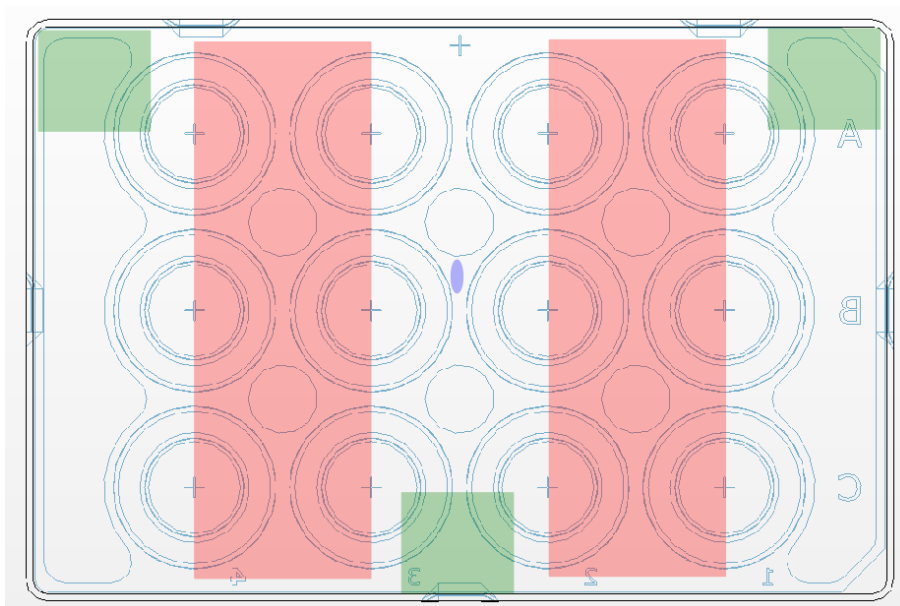


Figure 9.5.: Kapton heaters positioning. See-through drawing of the Multi-Well from below. The long red rectangles represents the Kapton heaters and the blue ellipse the main thermistor. Small green rectangles indicates areas to be secured for the contact points with the stage.

9. Further Developments

In order to reach the temperature variation goal, yet a more homogeneous integrated heater system should then be considered. A block of material with a higher thermal conductivity could be integrated under the wells, in the bulk of the Multi-Well plate. It could, however, lower precision and mixing materials with different thermal properties might create stresses during the repeated autoclaving cycles.

As a consequence, a separated heating plate could be integrated within the stage, although this would not allow the current three-point contact between the Multi-Well and its base, which would require more control to keep the desired height specifications.

An insulation border around the Multi-Well plate would also decrease the temperature gradient between the wells located at the center of the plate and the ones at the border.

It should be noted that, in such a setting, it is necessary for the fluid inflows to be pre-heated if the amount of fluid is non-insignificant compared to the amount of fluid previously in the well. Otherwise, aside of causing a potential heat-shock in the well in which they are added, they could induce the whole plate to warm up to compensate for the local heat-loss, increasing the temperature of the other wells.

9.4. Tip Control

As developed in Section 2.5.2, an AFM image is the convolution of the tip shape with the sample surface. The tip sharpness is, therefore, an element of importance as a sharp tip is necessary to limit the artifact but might not always be suitable as it can break more easily or damage the sample. Sharp tips are also usually not suitable for nanomechanical measurement as their shape is often not well characterized and they might get pierce through some layers of the cell membrane. In some cases, the shape of the tip might happen to change. In classical AFM applications, this phenomenon is generally due to a crash while engaging the sample or to tip wear due to

9. Further Developments

extended scanning or scanning at high forces. Particularly when operating in fluid on biological samples, forces are usually sufficiently low so as to limit tip wear, but biological contaminations—such as proteins, parts of membranes, or even whole bacteria—can stick to the end or the side of the tip from a tip-sample contact or from floating debris.

These contaminations modify the effective shape of the tip, most often broadening it. Should the contamination happen on the tip, it will effectively create an extra offset between the true topography and the image, appearing like a step on the scan line. If the contamination goes away in the same or following line, the step is reverted, leaving a streak in the image. Should it stay, the image would then have a step across the image, along the slow axis, hence making parts of the scan at different heights. In case of a contamination next to the tip, a double-tip artifact can also happen.

Furthermore, contaminations might be soft, hence deformable and of inconstant shape, adding some noise and lowering yet further the resolution of the image. Lastly, since they change the tip shape as well as its surface properties and stiffness, contaminations have a strong impact on nanomechanical measurements.

On a manually operated system, the clues are visible in the image hinting towards a problem. Streaks, double tips, or instabilities as described in Section 2.5 can be interpreted by the operator as a tip defect.

In an automated system, these issues should be detected by the machine and, if possible, corrected. Otherwise, the system should be paused and the operator alerted by, for example, an email.

As mentioned earlier, working in oscillating mode is already less likely to have contaminations than in contact, but they might still happen. On *M. bovis* BCG for example, most contaminations were hopping on and off the tip, which is a problem that is difficult to solve during the scan. To avoid problems, the sample preparation should be optimized to avoid cell debris and excess biological matter subject to contaminating the tip. Furthermore, the user should start by manually scanning a few cells to optimize

9. Further Developments

the force setpoint, the scanning speed, and other parameters before setting up the experiment to minimize the risk of getting such contaminations. For less frequent problems, however, a quality control should be implemented in the main workflow, one of which being the control of the tip shape.

Various methods exist to estimate the shape of the tip from samples whose geometry is known. They can include both very precise structures to measure the critical dimensions of the tip and very sharp edges—usually at distinct positions—to image the side of the tip (Itoh, Fujimoto, and Ichimura, 2006). Although required to have a real estimate rather than a guess and hence giving much more precise results, these methods are very sensitive to contaminations.

Villarrubia (1994) developed an algorithm, followed by its implementation (Villarrubia, 1997), to reconstruct the tip without prior knowledge of the sample topography. However, the reconstructed tip corresponds to the bluntest tip that could have been used to give the resulting image. The technique is, furthermore, sensitive to noise and streaks as they create inconsistent and sharp elements that can only be “explained” by a sharp tip.

This algorithm attempts at finding the truly bluntest tip compatible with the image. To reach that level of details, it analyses every possible tip position that could explain each pixel of the image, resulting in nested loops of computationally expensive mathematical morphology operations. Most of the information comes, however, from analyzing the maxima of the samples. The other pixels bringing increasingly finer refinements.

Another algorithm based on the same context is the one proposed at similar times by Williams (1996). It focuses on the local maxima of the sample topography as these points are the only ones for which one can make sure the real tip-sample point was indeed the end of the tip and not the side. Secondary local maxima can, however, happen in their vicinity due to concavities in the tip shape, such as in case of double tips. As a consequence, a distance R is chosen. Maxima within a radius R of a bigger local maximum are discarded, as well as the ones within a distance R from

9. Further Developments

the sides of the image since the data there is unknown. Finally, local maxima within a distance R from a similar point that has been removed in the steps above are flagged for removal as well since the previous point could have been removed wrongly, in which case they could be one of their secondary maxima.

The blind tip estimation method is then a poor choice to have a good characterization of the tip for applications implying critical measurements on the horizontal axes, for which the tip geometry has to be considered. In these case, precisely controlled structures and very sharp edges are required, to optimize the tip reconstruction. For our application, however, these samples would likely get contaminated quickly. As our main point is to detect relatively large contaminations on or along the tip, blind reconstruction should be sufficient, while being less sensitive to contaminations.

Still, tip characterization is usually performed in air. To test the applicability of the technique in fluid, in a multi-sample environment, a high-roughness Titanium sample (RS, Bruker) was placed in one of the wells of the Multi-Well.

First, the thickness of the RS sample has to be taken into account by the automated movement as it is about $385\ \mu\text{m}$ thicker than the coverslips. This element taken care of, the system can automatically engage on the tip check sample and scan it as for normal samples. Images are consistent when repeated after changing wells.

As illustrated in Figure 9.6, the tip can then be reconstructed. We used here the algorithm implemented in NanoScope Analysis, which is based on Williams' ((1996)) algorithm discussed above in this section. It should be noted that the resolution on the reconstructed tip is limited by the resolution of the image. On the other hand, given that we want to be robust against big double tips, we should consider sufficiently large tip size for the reconstruction. This increases, however, the distance r between acceptable peaks, hence reducing the number of peaks considered for the reconstruction. As a consequence, to have enough peaks for a $500\ \text{nm}$ squared tip reconstruction image with a lateral resolution no worse

9. Further Developments

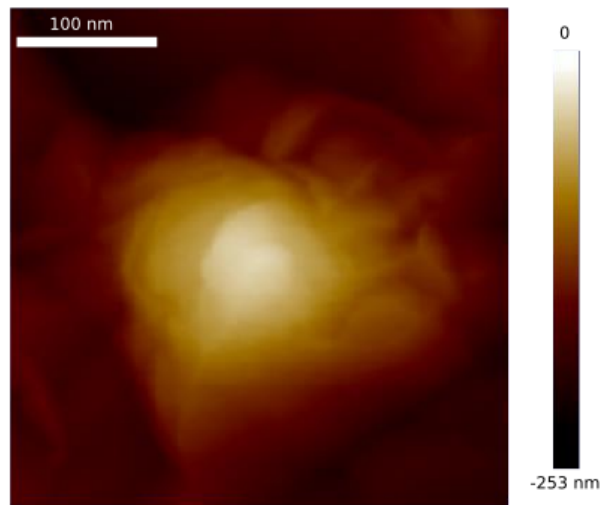


Figure 9.6.: Tip reconstruction. The tip, from a used PF-QNM Live Cell probe, was reconstructed blindly from automatically recorded images of the high roughness sample on the Multi-Well.

than 5 nm, we need a minimum of 500 scan lines over an area of $2.5\ \mu\text{m}$, oppositely to the 256 lines typically used on the samples.

We can see in Figure 9.6 that the surroundings of the tip present peculiar topographical elements. These elements come from the sample rather than from the tip as the sample does not have spikes long enough to reach these areas. The reconstructed image is, therefore, an upper bound for the tip shape and, while the distant data does not correspond to the tip geometry, it allows to conclude in the absence of a second tip or other large contamination.

Villarrubia's (1997) algorithm was implemented and tested as well. The first estimate yielded by this algorithm gave a similar tip image. The further refinements allowed for only a slightly better reconstruction while taking half an hour of computation despite a substantial optimization of the code. Such a computation-intensive process is not applicable in a near real-time system.

As it is furthermore particularly important to ensure the tracking of the

9. Further Developments

surface in this case, a specific set of scanning parameters has to be designed for the RS sample rather than keeping the parameters used for the rest of the experiment.

10. Conclusion and Future Outlook

10.1. Conclusion

Cancer and bacterial resistance to antibiotics are of great concern at the present time. The over-use of antibiotics led to the apparition of extremely resistant pathogens and new pathways need to be studied for drug discovery. Cancer, as a group of diseases characterized by the uncontrolled growth of cells caused by mutations in the genome, strikes by its prevalence.

Atomic Force Microscopy, thanks to its high-content abilities regarding notably the surface structure and mechanical properties of both prokaryotic and eukaryotic cells, can have a big impact in both of these fields. It allows a very high resolution while working on biological conditions on live samples and can access mechanical information. It has numerous biologically-relevant applications and could, in particular, be a valuable component of a correlative system. It is therefore very promising in biomedical, pharma, and other healthcare-related applications.

While its interest has been proven already for qualitative and comparative reasonings, it is still plagued with reproducibility issues in the quantitative realm for channels other than the topography. These issues correspond to the accuracy of the technique. Decomposing the accuracy between its two components: trueness and precision, we realize that both are subject to limitations in this technology.

Trueness, on the one hand, corresponds to the absence of systematic bias

10. Conclusion and Future Outlook

in the results. It was hampered by error-prone calibration methods, which are being addressed. The precision of a population-wide measurement, on the other hand, depends on the number of samples taken from that population and is limited by the sample size. For cell elasticity in particular, as elasticity is ill-defined for non-homogeneous materials, a precise measurement requires measuring a high number of curves on a high number of cells. Many publications in the field, however, currently focus on either the number of curves or the number of cells, but rarely on the two together. A high precision is of particular importance when the differences are subtle.

AFM is, however, time-costly and operation-intensive and requires a lot of operator time. Gathering the required numbers of cells is then quite demanding, sometimes pushing researchers to draw conclusions too fast, from limited data. The throughput has thus to be improved. To increase the number of samples, one can either accelerate the scanning process, parallelize it, or make it work continuously, hence without the operator.

Acceleration of the throughput happens with time as developments in the technique and components are made but no dramatic increase is to be expected as the operator is currently the limiting factor. The scanning speed is also limited by the physical properties of the cell. More than hitting its limit, going faster brings other viscosity parameters for which no broadly-accepted models exist currently. Parallelizing the scanning process does not appear to be a solution either. Cantilever arrays do not address high variability between cells as a reason of the fixed positioning of their cantilevers on the arrays, which causes significantly different forces as a function of the height of the sample. Therefore, many attempts of using parallel cantilevers lead to no applications. Groups of miniaturized AFM, while promising, still have to be demonstrated in biological setups.

Automation was then considered as a way to lower the dependency on the human factor, which is limiting the uptime of the system. While a variety of small automated steps exist and make AFM easier than in its earlier days, completely automated systems are still rare and mostly limited to quality control in the topography of micro-fabricated elements in air. There

10. Conclusion and Future Outlook

is, however, very little examples of automated systems working for biology, and none of them work on multi-samples.

The goal of the project was therefore centered towards the development of a biomedically-relevant approach enabling multi-sample measurement and analysis by Atomic Force Microscopy. We had a focus on developing the multi-sample approach both at the microscale, scanning several cells per sample, and the macro scale, scanning several samples. This system aimed at working automatically over extended periods of time. We made an automated system based on the FastScan-Bio, which was preferred for its automation capabilities, although less adapted to live cells, eukaryotes in particular.

Our system was based on a bio-compatible Multi-Well plate able to host 12 samples on small round coverslips. The usage of this hardware required some software development as well, to come up with a new interactive scripting solution with more robustness and flexibility than the previously existing ones, based on an integrated Python interpreter. On this multi-purpose script engine were then written a variety of scripts to fit our needs. A Python package was also realized to open and extract data from the file, making the scripts able to adapt their behavior to captured data.

Thanks to these hardware and software, a main script model was developed for bacteria. When setting up the experiment, the user calibrates the system in a dedicated well. Then, the system goes through the different wells, performs large survey scans to detect the cells, followed by localized measurement scans. Going from a sample to the next required a bubble-detection procedure. Working with biological matter required some level of contamination detection.

The system was then demonstrated with regard to its multi-sample abilities at two scales: the number of cells in a single sample, and the number of macroscopic samples. This lead to scanning more than 800 cells over three samples overnight on fixed *Yersinia pseudotuberculosis* bacteria in fluid. The system was then used on live *Mycobacterium bovis* BCG mycobacteria to demonstrate its applicability to live cells. Finally, the applicability

10. Conclusion and Future Outlook

of this method to eukaryotic cells was discussed, with minimal working examples.

As the last part of this document, we discussed in the previous chapter a few issues that should be a priority for further systems, for which proofs of concept were realized. These elements and their integration in potential future systems will finally be discussed in the next and last chapter of this document, where we consider key points for a next prototypical iteration and an ideal fully-fledged high-content and high-throughput system applicable complementary with existing systems for drug research.

10.2. Future Outlook

In this last chapter, we will discuss the potential developments of the system. This discussion will be decomposed between short, medium, and long term evolutions. Short-term elements would only require adjustments of the current prototype. Medium-term developments would require a new prototype as an addition for an existing system. Finally, long-term perspectives are the ones requiring substantial modifications to the AFM or a new one.

10.2.1. Short Term

First, short-term ameliorations could be brought already to the current prototype, mostly about the scripts and methods.

For comparability purposes, all scans were taken square and with the same size. This helped to ensure that all parameters were held constant. In the case of *Y. pseudotuberculosis* bacteria, square scans make perfect sense as these organisms are only slightly oblong. Other samples, such as *M. bovis* BCG mycobacteria are, however, much more elongated. In that kind of circumstances, the scan could have been made rectangular to better fit the shape of the bacteria. Indeed, if one is confident in their ability to select consistent parameters with different scan sizes and shapes, it would

10. Conclusion and Future Outlook

be possible to refine the bacteria detection to optimize the scan size, shape, and orientation to fit the bacteria. This has to be done carefully, however, as changing the scan size and shape can change the horizontal velocity, which can affect the tracking of the tip and the forces applied to the sample, hence increasing the variability between the scans.

A stronger focus could also have been put on mechanical properties of cells. They could be further analyzed on the current system, or force volume could be performed as measurement scans. With such a focus on the mechanical properties of cells, pyAF could be extended thanks to its plug-in architecture to perform batch analysis on the resulting data. It could also be streamlined with the scanning process so that the elasticity measurements can be computed in parallel to the experiment.

Several levels of measurement scans could be performed as well, with a cell-size followed by a smaller scan on the top of the bacteria. The first measurement scan could be analyzed to refine the position of the top of the cell, on which a few force curves and/or a smaller scan could be taken. Alternatively, the first of the two could be the force volume one to record the mechanical properties.

We defined here an area to scan, on which all detected cells should be scanned. It could, however, be more interesting to determine a target number of cells.

This project focused on the general issues and solutions that could be transferred across sample types. If the prototype was to be used in its current form, the development of sample-specific methods would then be required. In particular, care should be taken in having a strong immobilization of the sample. The measurement scans should also be selected for their biological relevance.

Once the system works robustly, time monitoring can be implemented as shown by the possibility to repeat scans illustrated in Chapter 8.

10.2.2. Medium Term

On the medium term, a new prototype could be designed as a more developed add-on for the FastScan-Bio. Without changes to the FastScan head, this system would likely keep a focus on prokaryotes. To allow for applications using eukaryotic cells, a custom scanner with larger piezos would be required, especially for the vertical one. Custom filters could also be required and are discussed at the end of this section.

On a recent new iteration of the prototype, the most important issue would be, there again, the focus on a reliable immobilization method. Ideally controlled to have a regular positioning of the samples it should, a least, be robust as it is more difficult for a machine than for a user to detect, avoid and/or react to anomalies in the sample. It would be preferable for this method to be applicable to a wide range of samples. Microfluidic approaches that can distribute bacteria on specific positions can be of high interest as well (Peric et al., 2017), which is also the case for micro-patterned systems for mammalian cells (Azioune et al., 2009; Rigato, Rico, et al., 2015).

While focused on prokaryotes, for which a simple new iteration of the prototype could be useful, the system should also be used as a testing ground to move towards a system able to work seemingly on eukaryotes, as introduced in Section 10.2.3 below.

The prototype should allow for limited handling of the sample. The short dewetting caused by moving the coverslip inside the Multi-Well may not have a negative impact on the bacteria, as it promotes their contact with the surface while being too short to actually cause a dehydration. The same does not hold for eukaryotic cells, for which dewetting does have a serious impact on the sample.

Consumable coverslip can be a good solution to ensure a perfectly clean surface for the cells while letting the rest of the Multi-Well re-usable. Nevertheless, it would be preferable to allow preparing the sample directly in the Multi-Well. Such a preparation is not compatible with the pedestal ar-

10. Conclusion and Future Outlook

chitecture as it makes the surrounding of the sample much deeper than the center. Since the cell concentration on the surface after adhesion depends on the depth of liquid above it, it would make substantial concentrations of cells on the borders, which could detach and perturb the measurement or produce more waste than thought for. Therefore, pedestals should be avoided or made as small as possible.

Again in the same realm, it should be possible to visualize the sample during and after the preparation steps. Having a see-through bottom would then be preferred, even if the cells are still placed on a coverslip on top of that transparent bottom. Inverted microscopes have, however, small focal lengths. The sample should, therefore, be as low as possible in the Multi-Well. Since the Z-scanner can only enter so far in a well, the wells—and therefore the Multi-Well—should be as flat as possible even should it break the ANSI standards. The Multi-Well could also be made of sterile, one-use, plastic culture dishes.

Then, a fluid exchange system should be implemented. Such a system is a necessary step to move towards eukaryotes while being useful for prokaryotes. It would, for example, allow the system to add drugs to a sample and wash it off while studying the behavior of the bacteria.

To use such a system on eukaryotic cells, a fluorescent marking could be considered, such as DAPI or cellmask. This would require specific filters and illumination at specific wavelengths but would make cells appear as easily-detectable light spots. Furthermore, it could allow specific detection of live cells against dead ones.

10.2.3. Long Term

While the BioScope Resolve is not adapted to multi-sample automation, the Dimension FastScan-Bio is limited regarding work on eukaryotes, for which the two main issues are visibility and piezo range. Having a system with the level of automation of the FastScan but with the piezo range of the Icon and Resolve would certainly be more adapted for this kind of

10. Conclusion and Future Outlook

applications.

Ideally, however, we would like this system to be integrated into a correlative approach, such as CLAFEM (Correlative Light – Atomic Force – Electron Microscopy). While Electron Microscopy can be realized later after fixation of the sample, light and atomic force microscopy can be used on live biological process and would, therefore, gain from being used synchronously. Such a system would require the motion abilities of the Dimension stage while being compatible with an inverted microscope as for the BioScope one. While the range of motion does not have to be as big as the one of the Dimension stage—95 by 70 mm would be sufficient to reach all the wells of the MultiWell—it should be able to raise the Z-scanner high enough to allow inter-well movements. Alternatively, a circular, rotating Multi-Well could lower the requirements in the horizontal translation ranges, but keep the vertical one. For a better compatibility with correlative approaches, tip scanning should be preferred.

It should be noted that, on an inverted microscope, the concept of the heater stage system would be fundamentally different from its Dimension stage equivalent discussed in Section 9.3. Whereas the latter could be made of a flat homogeneous heater plate under the sample, compatibility with inverted microscopy requires the heating to be performed from the side of the wells. In the case of a disposable Multi-Well, in particular, the heating should have to be placed in the inter-well space.

Applications of Single Molecule studies on cells on such an automated system could be manifold. The tip functionalization tends, however, to worsen with time. It would, therefore, be required to automatically evaluate the quality of the functionalization in order to know when the tip has to be changed, which could be challenging. Since functionalization is generally a multi-step process and take a few minutes, tip exchangers with pre-functionalized tips would most likely be considered.

Finally, the development of a robust interface between NanoScope and Python, applied to an autonomous system, could bring advancements from Artificial Intelligence into AFM. Machine Learning techniques, in particu-

10. Conclusion and Future Outlook

lar, could be used to detect areas of interest or to trigger specific measurements when an event is starting. These techniques require, however, a lot of data for the training phase, which causes it to be out of reach of most current AFM applications. On the other hand, an autonomous system would be able to gather the quantity of data required for the meaningful applications of these new technologies.

Appendix

A. Protocols

A.1. Consumables

Coverslips 8mm round coverslips (#1, Menzel-Gläser), purchased from Thermo Scientific;

Multidish Multidish 4 Well, purchased from NUNC;

Gentamicin Gentamicin;

PBS Phosphate Buffer Saline, purchased from gibco;

Formaline Formalin solution, 10% neutral buffered, purchased from Sigma Aldrich (ref HT5012-60ML).

Tris Tris Hydrochloride, purchased from Roche Diagnostics;

A.2. Coverslip Pre-Treatment

Prior to their use to host live cells, they were placed in each well of a Multidish 4 Well and cleaned by Oxygen Plasma at 50 W for 5 minutes.

A.3. *Yersinia pseudotuberculosis*

A.3.1. Culture

Yersinia pseudotuberculosis bacteria are prepared overnight in LB broth in an agitated incubator at 28 °C. The next morning, the culture is diluted

at 1% in 25 mL Falcon tubes and replaced in the incubator.

A.3.2. Treatment

After 4h, the cultures being turbid, they are centrifuged at $3000 \times g$ for 5 minutes. The medium is changed and the culture is kept as follow:

Control LB, then kept at ambient temperature.

Gentamicin LB with $8 \mu\text{g mL}^{-1}$ gentamicin, then kept at ambient temperature.

Heat LB, then kept at 60°C in a water bath.

All media are preheated at 28°C to avoid a thermal shock. The treatment is maintained for an hour before plating on the coverslips.

A.3.3. Plating

400 mL of the culture are put in each well of a Multidish with coverslip as detailed in Section A.2. The Multidish is then centrifuged at $3000 \times g$ for 5 minutes. Each sample is washed 3 times with PBS, then fixed during 20 minutes with formalin. Further washing with PBS is carried out again 3 times before Tris is used for 5 minutes to quench the leftover formaline. A last rinsing with PBS was proceeded before rinsing with distilled water. The samples were finally dried to improve the adherence of the sample to the coverslip and for conservation purposes.

A.4. Mounting

The placement of coverslips carrying a sample is mentioned here as “mounting”. Dried samples are first rehydrated for 20 minutes in 1 mL PBS so as to be removed from the Multidish without breaking.

Samples are placed on the Multi-Well plate. A extra clean coverslip is placed to serve as calibration sample. A spring is added on the coverslip and is secured with a spring clamp. Wells are then rinsed 3 times with PBS.

The Multi-Well plate can be brought to the FastScan and set up on the custom stage. PBS is added to fill the wells. An empty well is filled with 70% ethanol to serve for cleaning purposes.

A.5. Default Setup

The default setup is based on the default experiment for PeakForce Mapping in Fluid on the FastScan with NanoScope 9.3. The experiment is edited with the following changes:

- Height Engage (engage settings):
 - Height Engage: 500 nm
 - Engage Z delay: 2 s
- force volume:
 - Scan Size: 30 μm
 - Ramps/Line: 64
 - Ramp Size: 500 nm
 - Ramp Rate: 10 Hz
- Scan:
 - Samples/Line: 128
 - Lines: 128
 - Scan Rate: 3 Hz
 - ScanAsyst Auto Control: Individual
 - ScanAsyst Auto Setpoint: Off

A. Protocols

- Peak Force Setpoint: 5 nN
- ScanAsyst Noise Threshold: 5 nm
- Peak Force Amplitude: 300 nm
- Peak Force Frequency: 1 kHz

The experiment is then saved for further uses.

B. Accuracy

Properties often do not have a single, well-defined value. They can be represented, however, as a random variable obeying a probabilistic distribution. To study a population, we focus on parameters of this distribution. Let θ be a such parameter. While this parameter cannot be measured directly, we can take a sample and design a method to measure an estimator of that parameter: $\hat{\theta}$.

An estimator is Accurate if it estimates the quantity of interest without error. As shown below, errors can be decomposed in random errors, background, or noise on the one hand and in systematic bias on the other hand. The first corresponds to the estimator being precise while the second corresponds to it being true.

B.1. Precision

The precision corresponds to the reproducibility of a measurement. A measure will be precise if, when taken several times, the different values are in good agreement with each other, without considering its relevance to the true value. Hence, the precision corresponds to the variance of the estimator, $\text{Var}(\hat{\theta})$. Since the variance has the same units as θ^2 , one can consider its square root instead, the standard deviation, $\text{std}(\hat{\theta}) = \sqrt{\text{Var}(\hat{\theta})}$.

The precision answers the question of the error margin on any individual measure. It is relative to the difference that has to be expected when doing the same measurement twice.

In the case of the elasticity of live cells, measuring the elasticity of only

B. Accuracy

one cell as the average elasticity of the whole condition is going to give a very poor precision since doing the measurement again on a different cell will most likely give a vastly different result. Considering the average elasticity of 10 cells as our measurement will give a value closer to the actual average of the whole population corresponding to that condition since the individual effects deviating from this value average out. Measuring the average elasticity of another set of 10 cells in the same condition will most likely give a similar result. In a similar fashion, increasing the number of sample taken for a measurement will increase the precision of the obtained value.

B.2. Trueness

We will define the trueness of the estimator as the absence of bias. The bias of an estimator can be measured as the expected difference between the estimator and the real underlying value of the parameter it represents:

$$b = \mathbb{E} [\hat{\theta} - \theta] = \mathbb{E} [\hat{\theta}] - \theta.$$

The trueness essentially answers the question of whether the estimator actually represents the thing it is trying to measure. It means that, as the sample size increases, the estimator approaches the true value of the parameter it estimates.

In our case, bias can be due to the usage of poor models systematically under- or overestimating the quantity of interest or to a poor calibration of the system.

B.3. Accuracy

Finally, the Accuracy of a measurement represents the proximity of that measurement with the true value of the parameter. It is essentially the absence of the error on a measurement.

B. Accuracy

We will here consider the square root of the quadratic error (as in the least-square regression and other common tools), which can be measured as the expected value of the difference between the parameter and its estimator (Dodge, 2008). It can be represented as:

$$\sqrt{\mathbb{E} \left[(\hat{\theta} - \theta)^2 \right]},$$

which can be shown to be equal to:

$$\sqrt{\text{Var}(\hat{\theta}) + b^2},$$

which is the root sum square of the standard deviation and the bias, hence the combination of the Trueness and the Precision. The Accuracy takes then into consideration the systematic errors (biases) and the variability in the measurement. A high Accuracy, hence the absence of error, is only possible if both the Trueness and the Precision are high.

In our case as in most, both components of the Accuracy are important. A perfectly exact model on a perfectly calibrated system (giving a true estimator) would have no interest if the noise is such that the obtained values are not reproducibles (hence imprecise). Similarly, a perfectly stable system giving always the same value would not have interest if the value is off by an unknown amount. We need a system that reproducibly gives the right value, hence accurate.

It has to be noted that some will call Accuracy what we defined as Trueness, with no name for the aggregate measure that we define here as the Accuracy. The absence of error is then characterized by a high Accuracy and Precision.

C. Models

Until the 1960s, the prevailing point of view was that life was too complex to be formalized in mathematics. Nevertheless, this complexity makes it impossible for biologists to understand life without reasoning on some models. This follows that models used to be subjective and qualitative. Still, a model must be explicit and refutable, which implies some sorts of mathematics (Janin, 2013).

Cells are very complex, their behavior depends on a myriad of elements of different kinds, such as their genetic material, the components of their membrane, their proteins, signaling molecules, among others. These components interact with each other and with their environment. Cells can then be considered as complex systems.

Complex systems are difficult to model due to the sheer numbers of their components and their interactions. Like for other systems, properties emerge from the bulk of the interactions. Applying simplifying assumptions on their components is, however, much more difficult. The high number of kinds of components and the intricacy between them make it so that simplifying assumptions fail to capture the complete behavior. It is then more difficult to come up with a model that captures the essence of the behavior of the system.

C.1. Contact Models

From the Force-Separation curves described in Chapter 2, mechanical properties of the sample can be extracted. There is, however, not a unique kind

of force being applied between the cantilever and the sample. Materials have different mechanical properties. There might or might not be long-range interactions. Some force might be negligible in some cases but not in others.

One of the most basic but interesting mechanical properties a sample can have is its elasticity. Elasticity supposes a direct relationship between the indentation and the force, which is equivalent to Hooke's law. As a consequence, it is not sensitive to the speed and direction of movement of the tip during its indentation phase in the sample, which implies that the approach and retraction curves are identical in their indentation part. Plasticity might arise when a part of the deformation does not revert when the tip is retracted, inducing a permanent damage to the sample. It creates a difference between the loading and unloading curves that depends on the maximum force applied to the sample but not on the speed.

A difference between the two curves can also be induced without permanent damage to the sample, by viscous effects. The concept of viscosity is linked to a force acting as a reaction against speed, in the fashion of a damper, typical of fluids. Instead of the typical elasto-plastic behavior of hard solids, soft solids can have a behavior more similar to the viscosity of fluids, hence inheriting viscoelastic properties. As a consequence, the viscous component of the reaction might induce an apparently repulsive force during the approach, hence reinforcing the apparent elasticity, and apparently attractive during the retraction, hence weakening the apparent elasticity. At slow speed, the force curve of a viscoelastic material appears elastic but, at increasing speeds, a gap arises between the two parts of the indentation.

C.1.1. Elastic Models

Basic elastic models assume a purely elastic, homogeneous, and isotropic sample. The sample is assumed to be delimited by a flat surface and the (infinite) space below it, hence infinitely thick. It does not consider

C. Models

attractive forces. The indenter is operating orthogonally to the free surface of the sample. It neglects viscous and plastics effects, as well as surface forces and friction.

In general, the contact force is proportional to the penetration depth and the radius of contact a . In the case of a small and hard cylindrical indenter of radius a , this radius is constant. The contact force is, as a first order approximation, proportional to the penetration depth, following the equation

$$F = 2E^*\delta a, \quad (\text{C.1})$$

where E^* is the reduced Young modulus defined as

$$\frac{1}{E^*} = \frac{1 - \nu^2}{E} - \frac{1 - \nu_t^2}{E_t}, \quad (\text{C.2})$$

depending on the Young modulus E , the Poisson ratio ν of the sample and their equivalent, E_t and ν_t for the tip (Cappella and Dietler, 1999; Popov and Gray, 2010). In the case of a rigid indenter, the second term of Equation (C.2) can be neglected and we have simply

$$E^* = \frac{E}{1 - \nu^2}. \quad (\text{C.3})$$

C.1.2. Hertz

The Hertz model (Hertz, 1882) is one of these simple elastic models, using a spherical indenter of radius R (the tip). In this case, the contact radius a varies with the indentation. Furthermore, the deformation of the sample is not constant. The contact area can, however, be decomposed in finite elements on which an equation similar to Equation (C.1) can be integrated. This leads to the equation (Popov and Gray, 2010):

$$F = \frac{4}{3}E^*\sqrt{R\delta^3}. \quad (\text{C.4})$$

The sample stiffness (k_s) can be computed with Equation (2.8) simply

with the deformation and the force, but is not an intrinsic property of the material and depends on the contact radius a . This radius cannot be deduced directly from the data and requires further assumptions and modeling.

It is, however, vastly used to compute the elastic modulus of cells although they are thin, finite, viscoelastic, heterogeneous, anisotropic, etc.

C.1.3. Sneddon

Sneddon (1965) generalized Hertz model to indenters with shapes defined by a solid of revolution with an arbitrary profile indenting the sample perpendicularly. This allowed for the development of a model for conical indenters of opening angle θ , giving the formula (Popov and Gray, 2010):

$$F = \frac{2}{\pi} E^* \frac{d_s^2}{\tan \theta}. \quad (\text{C.5})$$

Since Hertz model establishes a direct relationship between the force and the indentation, only one force-indentation data point is required to extract the modulus. Finding the indentation requires, however, the knowledge of the contact point, which is a non-trivial issue. As a consequence, one can take two points on the curve, at two different force thresholds, and make the ratio of the two. Using Equation (C.4), it is then possible to deduce the contact point and, hence, find the modulus. Another, more precise but more computationally demanding technique consist of doing an actual fitting.

C.1.4. Adhesive Models

Several models exist to take adhesive contact into account. First, Bradley (1932) considers two rigid spheres on which only the Lennard-Jones potential apply, which can be useful at small scales with small forces.

After that, the DMT and the JKR theories developed respectively by Derjaguin, Muller, and Toporov (1975) and by Johnson, Kendall, and

C. Models

Roberts (1971) extends Hertz theory with forces outside the contact region. The DMT theory is more suitable for small tips and with samples that are slightly adhesive compared to their stiffness whereas the JKR theory performs better on flexible and elastic samples with large tips (Cappella and Dietler, 1999; Popov and Gray, 2010).

Maugis (1992) reconciled these two competing theories by introducing a parameter λ representing the softness, size, and adhesion of the bodies. It creates a generalization of the two preceding theories, equivalent to JKR for high values of λ and to DMT for small values.

C.1.5. Thin Samples

Hertz and Sneddon models assume an infinitely deep sample. In practice, these models are usually accepted for samples of a finite thickness supported by a hard substrate as long as the indentation depth stays below 10% of the thickness of the sample (Bueckle, 1973; Stolz, Raiteri, et al., 2004). More recent models exist for thin samples, where the contribution of an infinite, stiff substrate, such as the one derived by Gavara and Chadwick (2012).

C.2. Tomography

C.2.1. Stiffness Tomography

As described above for Hertz's model, only the contact point and one force-indentation data point, or two data points, are required to extract the Young's modulus of the material. However, heterogeneous samples present deviations from the Hertz model, yielding different Young's modulus depending on the indentations considered.

Under some approximations, the value of the Young's modulus taken between the contact point and a given indentation relates to the aggregate properties of the material between the contact point and that indentation

level. When taken between different indentations, the computed modulus correlates with the modulus at that depth, although the obtained information is lost by diffusion at higher and higher indentations. It is also much more sensitive to artifacts. These two techniques of Stiffness Tomography (Roudit, Sekatski, et al., 2009) allow to have qualitative information about the mechanical properties within the sample.

C.3. Contact Point

The mechanical properties are deduced from the force-distance curve by studying the relationship between the force and the indentation of the tip in the sample. To compute the indentation, however, it is necessary to know the contact point, as it acts as the origin of the indentation (Crick and Yin, 2007).

There are several methods to find the contact point, the accurate detection of which is required to have meaningful results. This is made difficult by the fact that, on elastic samples, the force increases following a power-law with an exponent higher than 1. As examples, we have $F \propto \delta^{3/2}$ for the Hertz model and $F \propto \delta^2$ for the Sneddon one, giving $F' = 0$ for $\delta = 0$, the contact point. As a consequence, for soft samples, the transition from the non-contact to the contact part is smooth, making it difficult to localize, especially on noisy data.

While numerous contact point methods exist, a first class of methods consist of finding the point at which the behavior of the baseline changes. As an example, one can compute the second order derivative of the curve, which gives its curvature. A smoothing is usually added to lower the noise level. This curvature is approximatively null on the non-contact part of the curve and becomes quickly positive at the contact point. When a threshold is triggered, the corresponding point can be taken as the contact point. Alternatively, the algorithm can go back to the last point that was close enough to the baseline and mark it as the contact point (Benítez, Moreno-

C. Models

flores, et al., 2013). A different approach consists of fitting a function with a running contact point, therefore allowing to find the contact point (Chang et al., 2014). However, numerous other methods exist and no real single method seem widely accepted at the moment.

D. Computing Science

D.1. Dynamic Link Libraries

Whereas user-facing programs and other independent services are usually unique and presented as executables (.exe), some elements are re-used at different places. As the interactions with basic components require a lot of code, their logic is shared between different softwares to avoid code redundancy. Microsoft Windows implements this as dynamic link libraries (DLLs), as equivalent of the shared objects (SO) on UNIX and similar systems. The first use of DLLs is thus to access Windows elements, such as dialog boxes, windows, keyboard input, etc.

Programmers can also build their own DLLs to modularize their programs in separate components. DLLs being loaded when they are needed, they allow for a faster start-up and can be used to separate plug-ins or modules from the core software.

D.2. .NET

The .NET (pronounced “dot net”) framework is a software framework for applications on Microsoft Windows, based on the Common Language Infrastructure (CLI). Languages based on this infrastructure include C# (“C sharp”), Visual Basic .NET, and IronPython, among others. Source code written in such a language is compiled into bytecode, the Common Intermediate Language (CIL), which is run under the Common Language Runtime (CLR) and transformed on native code on the target system.

D.3. Python

Python is an interpreted programming language developed by Guido van Rossum in the late 1980s. It is now one of the most popular languages in high-tech domains and among researchers. It is recognized for its strong focus on readability and its capabilities for integrating systems and for fast development.

It is a high-level language that shares characteristics with scripting and transitional programming languages. It was designed as a language for scripts targeted at an audience of computer users with a certain intelligence but no background in programming (Venners, 2003)

As for MATLAB, a major software for numerical analysis, Python is interpreted. Born as a simple, general-purpose programming language, it gained momentum in a wide range of area, including numerical computing and scientific applications. It tends to be comparatively slow with regards to compiled languages, but specialized libraries (packages) have been developed to strongly improve speed issues.

As a language, Python has different implementations, mostly open source. The reference one is CPython, based on C/C++. It is the one mostly used in the research community, with packages such as numpy, scipy, and matplotlib for numerical analysis, scientific computing, and data visualization, respectively. These packages were developed by scientific users to answer to their needs and were made possible by the open source nature of the language and its implementation. The more tools available, the more users joined, developing yet other tools. This led to IPython, allowing for yet a more interactive Python giving researchers the possibility to experiment with their data. IPython led to IPython Notebook, allowing to keep notes, code, and the result of this code together (Leloup, 2018).

D.3.1. IronPython

Another implementation of Python has been used within this project, IronPython, based on the .NET framework (*IronPython.Net* 2018). This implementation can use both the .NET and Python libraries. It can be used to provide the Python advantages of scripting language to .NET applications and libraries. The current IronPython version is 2.7.8, released on February 2018 (*IronPython.Net* 2018).

D.4. IronPython to CPython Bridge

The scripting option added to NanoScope is based on IronPython. Most data processing libraries are, however, mostly targeted at the Python reference implementation, CPython. As a consequence, these packages are extremely difficult to install in IronPython.

Therefore, the image analysis part of the workflow were implemented for IPython. To connect the two, two temporary files are created to host the arguments and the return values of a function to be called. The arguments are serialized (translated from its representation in the current environment to a format that can be stored) and saved in the first file. A normal CPython process is then started with, as arguments, the name of the function to be called and the path to the two files.

On the CPython side, the script recovers the name of the function as well as the two files. It then loads and deserializes the function arguments from the file and calls the function. The actual function behaves here as it would in any normal Python setup, allowing us to use the packages we were lacking on the other side. When the function returns, its return values are serialized and saved in the second file.

In case of error, the files are moved to the current working directory and are referred to in the logs, along with generated code that can be copy-pasted to rerun the code on these arguments for debugging purposes. Otherwise, back in IronPython, the return values are recovered from the

D. Computing Science

corresponding file, the two temporary files are deleted, and the script continues.

E. Developments Summary

As a summary, the requirements for the system can be decomposed as follows.

E.1. Biological Medium

As stated in Section 3.5.1, one of the main advantages of AFM is its ability to scan live samples in biological conditions. These samples thus need to be in a fluid that is compatible with their viability. In particular, they should be in a water-based solution with ionic compositions and concentration fitting the osmotic requirements of the cells. For longer-term experiments, the medium composition should be studied more carefully to keep them in a biologically-relevant state.

Some elements of the medium are, however, used by the cells. Similarly, they produce waste, which can accumulate if not eliminated properly. This brings the question of fluid exchange, discussed in Appendix E.7 below.

E.2. Biocompatibility

The materials in contact with the fluid should not release ions or otherwise toxic elements in the medium. The current hardware has been selected accordingly, as discussed in Section 6.1.1, and future prototypes should keep these requirements.

E.3. Limited Handling

Direct manipulations damage the sample, especially the ones implying getting it out of the medium, which can cause dewetting. Such manipulations are currently necessary for sample mounting, as referred to in Section 6.1.2.

Notches were added to prevent the coverslip from sliding during the mounting, ensuring a faster handling. In the short term, similar notches could be added to hold the springs, or the springs could be integrated in the spring clamps. Ideally, and in the long run, the sample should be put directly on the Multi-Well, not on a coverslip in a separate dish, then transferred. To host the samples directly, however, the Multi-Well would have to be transparent so that the samples can be observed on the light microscope to check for their adherence. Such a transparency is also necessary for other purposes, discussed in Appendix E.5 below.

E.4. Environmental Control

Cell survival requires some level of environmental control, as discussed in Section 5.1.5. These controls can be decomposed as follows.

Temperature Control Temperature should be managed but defining the measurement to compare to the setpoint is a difficult problem on a multi-sample system. Several samples could be at different temperatures. A tentative implementation is discussed in Section 9.3.

Heating, however, raises the problem of evaporation. This phenomenon is quite limited at room temperature, especially when the hood is closed and its humidity increased with damp tissues. In that case, it might only be needed to add water every 6 or 8 hours. Heated at 40 °C, however, the evaporation rate was measured to be between 0.17 and 0.52 mL in an hour, although the hood had been closed and humidified as described above. As a consequence, temperature control requires the implementation of a fluid exchange system, being at least a controlled inflow or a passively regulated

E. Developments Summary

inflow/outflow.

pH Control The pH should be kept constant. This is traditionally done via carbon dioxide (CO₂) control of the atmosphere, as it dissolves in the medium, lowering the pH. In our case, it could also be performed by a pH-buffered medium, renewed by the fluid-exchange system.

Oxygen Control Oxygen intake might be required in certain conditions.

Contamination Control Contaminations should be avoided from the outside to the inside, and between wells. The system must be closed so that it can be transferred from a sterile place to another. If the machine in itself is not in a sterile environment, the same applies to limit contaminations to a minimum, keeping the inside of the Multi-Well and its lid sterile, until it is open in the clean but not sterile hood of the AFM.

In the AFM, contaminations should be limited as well. The system should be cleanable with disinfectant, at least for the part close to the Multi-Well (stage), and for the parts above it (head, hood).

Contaminations of the tip should also be managed to ensure the quality of the scans. It is the topic of Section 9.4.

E.5. Light and Visibility

Transparency The bottom of the Multi-Well should be transparent for compatibility with an inverted microscope. This is necessary for the seeding, as mentioned above, as well as for the compatibility with confocal microscopy. Alternatively, it could be made of able to host small individual petri dishes, although the size of the smallest of them appears to be 40 mm, compared to the 26 mm inter-well distance of the current plate, which would require 2.5 times more space.

Correlative Microscopy Compatibility with an inverted microscope would also be required for correlative studies, introduced in Section 5.1.2.

Light sensitivity As mentioned in Section 5.1.5, some samples are light-sensitive. Illumination should be therefore be manageable by the software to be used sparingly.

E.6. Immobilization

Cells need to be immobilized to allow for the scanning process. Sample preparation is a recurrent difficulty in AFM and is discussed for cells in Sections 2.3.2 and 5.1.3. In particular for unattended scanning, the immobilization should be robust. Floating samples should be avoided as they can perturb the experiment.

While badly attached samples would not impact other measurements, scanning them is a loss of time which should be avoided if possible. An operator would, for example, discard such a sample while scanning. Translating this to software would, however, require a true real-time analysis whereas the current system can only analyze the data after capture (near real-time).

Further than being robust, the immobilization should preferably be controlled position-wise. Micro-patterning and microfluidic options are discussed in Section 9.1.

E.7. Fluid Exchange

Provided that cells can be kept alive, time monitoring is of particular interest to observe the behavior of cells through time, as discussed in Section 3.5.5. Fluid exchange, detailed in Section 9.2.2, is necessary to compensate for fluid evaporation in order to maintain buffer concentrations and composition and evacuate toxic elements, which are introduced

in Section 5.1.5. It can help maintaining some elements of environmental control detailed in Appendix E.4 above. It could also be used to add drugs or wash them off with clean medium.

E.8. Suitability for Cells

The ranges of the piezos should be compatible with cell sizes. The system should also be adapted to scan samples as soft as cells in liquid, with functionalities such as live cell background subtraction for PeakForce. This topic is discussed in Section 5.1.1.

List of Figures

2.1. AFM Probe	8
2.2. ScanAsyst-Fluid Probe	11
2.3. Piezo Extension and Retraction	12
2.4. Feedback Loop	14
2.5. Optical Lever System	14
2.6. Raster-Scan Motion	17
2.7. Force Curve	20
2.8. Tip-Sample Distances	22
2.9. Representation of Force Volume Mode	24
2.10. Comparison Scheme Between Force Curves and PeakForce	30
2.11. PeakForce Live-Cell Background Subtraction in Liquid . .	33
2.12. Illustration of the Convolution Artifact	37
2.13. Example of Convolution Artifact	38
2.14. Example of Sawtooth Effect	42
3.1. Schematic Diagram of a Eukaryotic Cell	47
3.2. Cell Membrane and Membrane Proteins	48
3.3. Fluorescence Microscopy Image of the Cytoskeleton	50
3.4. Cell Envelope of Gram-Positive and Gram-Negative Bacteria	55
3.5. Cell Envelope of Mycobacteria	56
3.6. SEM Image of <i>Y. pseudotuberculosis</i>	58
3.7. AFM Deflection Error Image of <i>M. bovis</i> BCG Mycobacteria	60
4.1. Deflection Sensitivity Calibration	76
4.2. Thermal Tune Calibration of the Spring Constant	78
4.3. Array of MEMS Cantilevers	87
4.4. Array of Cantilever For Interferometry	88
4.5. MAFM Setup	89
4.6. Cell Detection Method	96
4.7. Cell Probing Method	97
5.1. Positioning of Bacteria	103
5.2. Positioning of Mammalian Cells	104

List of Figures

6.1. Multi-Well Plate Setup	110
6.2. Multi-Well Positioning	111
6.3. Multi-Well Plate Enhancement	113
6.4. Representation of the IDE and Script Example	116
6.5. pyAF	121
7.1. Scheme of the Experiment Workflow	130
7.2. Bubble Example	133
7.3. Laser Sum Consistency Test	135
7.4. Illustration of the Bubble Detection Procedure	138
8.1. Workflow of Bacteria Detection and Scanning	144
8.2. Examples of Scanned <i>Y. pseudotuberculosis</i> Bacteria	145
8.3. Representative Examples of the 3 Conditions of <i>Y. pseudo-</i> <i>tuberculosis</i>	148
8.4. Analysis Throughput	149
8.5. Analysis Results	152
8.6. Representative Images of <i>M. bovis</i> BCG Mycobacteria	155
8.7. Nanomechanical Mapping of a <i>M. bovis</i> BCG Mycobacterium	156
8.8. Early Visibility	157
8.9. Seeing Eukaryotic Cells	158
8.10. Eukaryotic Cell Workflow	159
8.11. Chained FV of RPE-1 Cells	161
9.1. PEI Micro-Patterns	164
9.2. Microfluidic Bacterial Traps	164
9.3. Dimension FastScan Fluid Apparatus	168
9.4. Fluid Exchange Needle	170
9.5. Kapton Heaters Positioning	174
9.6. Tip Reconstruction	179

Bibliography

- A-Hassan, E., W. F. Heinz, M. D. Antonik, N. P. D'Costa, S. Nageswaran, C.-A. Schoenenberger, and J. H. Hoh (1998). "Relative Microelastic Mapping of Living Cells by Atomic Force Microscopy." In: *Biophysical Journal* 74.3, pp. 1564–1578. ISSN: 00063495. DOI: 10.1016/S0006-3495(98)77868-3 (cit. on p. 67).
- Abraham, F. F., I. P. Batra, and S. Ciraci (1988). "Effect of Tip Profile on Atomic-Force Microscope Images: A Model Study." In: *Physical review letters* 60.13, p. 1314 (cit. on p. 10).
- Abramovitch, D. Y., S. Hoen, and R. Workman (2009). "Semi-Automatic Tuning of PID Gains for Atomic Force Microscopes." In: *Asian Journal of Control* 11.2, pp. 188–195 (cit. on p. 93).
- Abramovitch, D. Y. and C. R. Moon (2013). "Automatic Tuning of Atomic Force Microscope." U.S. pat. 2013/0110262 A1. Agilent Technologies, Inc., Loveland, CO (US) (cit. on p. 93).
- Achtman, M., K. Zurth, G. Morelli, G. Torrea, A. Guiyoule, and E. Carniel (1999). "Yersinia Pestis, the Cause of Plague, Is a Recently Emerged Clone of Yersinia Pseudotuberculosis." In: *Proceedings of the National Academy of Sciences* 96.24, pp. 14043–14048. ISSN: 0027-8424, 1091-6490. DOI: 10.1073/pnas.96.24.14043. pmid: 10570195 (cit. on p. 57).
- Alberts, B., A. Johnson, J. Lewis, M. Raff, K. Roberts, and P. Walter (2002). *Molecular Biology of the Cell*. 5th ed. New York, NY: Garland Science (cit. on pp. 49–52, 63).
- Ali, R., M. Gooding, M. Christlieb, and M. Brady (2008). "Advanced Phase-Based Segmentation of Multiple Cells from Brightfield Microscopy Images." In: *Biomedical Imaging: From Nano to Macro, 2008. ISBI 2008. 5th IEEE International Symposium On*. IEEE, pp. 181–184 (cit. on p. 157).
- Alsteens, D., E. Dague, P. G. Rouxhet, A. R. Baulard, and Y. F. Dufrêne (2007). "Direct Measurement of Hydrophobic Forces on Cell Surfaces Using AFM." In: *Langmuir* 23.24, pp. 11977–11979. ISSN: 0743-7463. DOI: 10.1021/1a702765c (cit. on pp. 60, 154).

Bibliography

- Alsteens, D., D. J. Müller, and Y. F. Dufrêne (2017). “Multiparametric Atomic Force Microscopy Imaging of Biomolecular and Cellular Systems.” In: *Accounts of Chemical Research* 50.4, pp. 924–931. ISSN: 0001-4842. DOI: 10.1021/acs.accounts.6b00638 (cit. on p. 65).
- Ando, T., S. P. Bhamidimarri, N. Brending, H. Colin-York, L. Collinson, N. De Jonge, P. J. de Pablo, E. Debroye, C. Eggeling, C. Franck, M. Fritzsche, H. Gerritsen, B. N. G. Giepmans, K. Grunewald, J. Hofkens, J. P. Hoogenboom, K. P. F. Janssen, R. Kaufman, J. Klumpermann, N. Kurniawan, J. Kusch, N. Liv, V. Parekh, D. B. Peckys, F. Rehfeldt, D. C. Reutens, M. B. J. Roeffaers, T. Salditt, I. A. T. Schaap, U. S. Schwarz, P. Verkade, M. W. Vogel, R. Wagner, M. Winterhalter, H. Yuan, and G. Zifarelli (2018). “The 2018 Correlative Microscopy Techniques Roadmap.” In: *Journal of Physics D: Applied Physics* 51.44, p. 443001. ISSN: 0022-3727, 1361-6463. DOI: 10.1088/1361-6463/aad055 (cit. on p. 107).
- Ando, T., N. Kodera, E. Takai, D. Maruyama, K. Saito, and A. Toda (2001). “A High-Speed Atomic Force Microscope for Studying Biological Macromolecules.” In: *Proceedings of the National Academy of Sciences* 98.22, pp. 12468–12472. DOI: 10.1073/pnas.211400898 (cit. on pp. 25, 44).
- André, G. (2010). “The Cell Wall of Lactic Bacteria : A Nanoscale View.” Université Catholique de Louvain (cit. on p. 55).
- Ashrafuzzaman, M. and J. A. Tuszynski (2012). *Membrane Biophysics*. Biological and medical physics, biomedical engineering. OCLC: 823887764. Berlin: Springer. 179 pp. ISBN: 978-3-642-16104-9 978-3-642-16105-6 (cit. on pp. 46, 48–51, 53, 54).
- Azioune, A., M. Storch, M. Bornens, M. Théry, and M. Piel (2009). “Simple and Rapid Process for Single Cell Micro-Patterning.” In: *Lab on a Chip* 9.11, pp. 1640–1642. ISSN: 1473-0189. DOI: 10.1039/B821581M (cit. on pp. 52, 163, 186).
- Balaban, N. Q., J. Merrin, R. Chait, L. Kowalik, and S. Leibler (2004). “Bacterial Persistence as a Phenotypic Switch.” In: *Science* 305.5690, pp. 1622–1625. ISSN: 0036-8075, 1095-9203. DOI: 10.1126/science.1099390 (cit. on p. 69).
- Beauvais, M., I. Liascukiene, and J. Landoulsi (2018). *AFM: Atomic Force Microscope Image Analysis*. Version 1.2.4 (cit. on p. 122).
- Belikov, S., J. Alexander, M. Surtchev, I. Malovichko, and S. Magonov (2017). “Automatic Probe Landing in Atomic Force Microscopy Resonance Modes.” In: 2017 American Control Conference. Sheraton Seattle Hotel (cit. on p. 92).

Bibliography

- Benítez, R., V. J. Bolós, and J.-L. Toca-Herrera (2017). “afmToolkit: An R Package for Automated AFM Force-Distance Curves Analysis.” In: 9, p. 18 (cit. on p. 122).
- Benítez, R., S. Moreno-flores, V. J. Bolós, and J. L. Toca-Herrera (2013). “A New Automatic Contact Point Detection Algorithm for AFM Force Curves: Automatic Contact Point Detection for AFM Curves.” In: *Microscopy Research and Technique* 76.8, pp. 870–876. ISSN: 1059910X. DOI: 10.1002/jemt.22241 (cit. on p. 203).
- Binnig, G., H. Rohrer, C. Gerber, and E. Weibel (1982). “Tunneling through a Controllable Vacuum Gap.” In: *Applied Physics Letters* 40.2, pp. 178–180. ISSN: 0003-6951, 1077-3118. DOI: 10.1063/1.92999 (cit. on p. 7).
- Binnig, G., C. Gerber, E. Stoll, T. Albrecht, and C. Quate (1987). “Atomic Resolution with Atomic Force Microscope.” In: *EPL (Europhysics Letters)* 3.12, p. 1281 (cit. on p. 8).
- Binnig, G., C. F. Quate, and C. Gerber (1986). “Atomic Force Microscope.” In: *Physical review letters* 56.9, p. 930. DOI: 10.1103/PhysRevLett.56.930 (cit. on pp. 8, 25).
- Bolshakova, A. V., O. I. Kiselyova, A. S. Filonov, O. Y. Frolova, Y. L. Lyubchenko, and I. V. Yaminsky (2001). “Comparative Studies of Bacteria with an Atomic Force Microscopy Operating in Different Modes.” In: *Ultramicroscopy* 86.1, pp. 121–128 (cit. on p. 27).
- Bonomo, R. A. (2000). “Multiple Antibiotic-Resistant Bacteria in Long-Term-Care Facilities: An Emerging Problem in the Practice of Infectious Diseases.” In: *Clinical Infectious Diseases* 31.6, pp. 1414–1422 (cit. on p. 62).
- Bourdin, M. (1979). “Pseudotuberculosis in Man: Possible Epidemiological Role of the Cats.” In: *Comparative Immunology, Microbiology and Infectious Diseases* 1.4, pp. 243–251. ISSN: 0147-9571. DOI: 10.1016/0147-9571(79)90025-0 (cit. on p. 59).
- Bradley, R. S. (1932). “LXXIX. The Cohesive Force between Solid Surfaces and the Surface Energy of Solids.” In: *The London, Edinburgh, and Dublin Philosophical Magazine and Journal of Science* 13.86, pp. 853–862. DOI: 10.1080/14786449209461990 (cit. on p. 201).
- Braga, P. C., D. Ricci, and M. D. Sasso (2002). “Daptomycin Morphostructural Damage in *Bacillus Cereus* Visualized by Atomic Force Microscopy.” In: *Journal of Chemotherapy* 14.4, pp. 336–341. ISSN: 1120-009X. DOI: 10.1179/joc.2002.14.4.336. pmid: 12420849 (cit. on p. 71).
- Braga, P. C. and D. Ricci (1998). “Atomic Force Microscopy: Application to Investigation of *Escherichia Coli* Morphology before and after Exposure

Bibliography

- to Cefodizime.” In: *Antimicrobial agents and chemotherapy* 42.1, pp. 18–22 (cit. on p. 71).
- Braga, P. C. and D. Ricci (2002). “Differences in the Susceptibility of *Streptococcus Pyogenes* to Rokitamycin and Erythromycin A Revealed by Morphostructural Atomic Force Microscopy.” In: *Journal of Antimicrobial Chemotherapy* 50.4, pp. 457–460. ISSN: 0305-7453. DOI: 10.1093/jac/dkf180 (cit. on p. 71).
- Bueckle, H. (1973). *The Science of Hardness Testing and Its Research Applications*. Ed. by J. Westbrook and H. Conrad. Materials Park, Ohio: American Society for Metals (cit. on p. 202).
- Burks, G. A., S. B. Velegol, E. Paramonova, B. E. Lindenmuth, J. D. Feick, and B. E. Logan (2003). “Macroscopic and Nanoscale Measurements of the Adhesion of Bacteria with Varying Outer Layer Surface Composition.” In: *Langmuir* 19.6, pp. 2366–2371. ISSN: 0743-7463, 1520-5827. DOI: 10.1021/la026375a (cit. on p. 27).
- Butt, H.-J., B. Cappella, and M. Kappl (2005). “Force Measurements with the Atomic Force Microscope: Technique, Interpretation and Applications.” In: *Surface Science Reports* 59.1-6, pp. 1–152. ISSN: 01675729. DOI: 10.1016/j.surfrep.2005.08.003 (cit. on pp. 9, 11, 18, 21).
- Buzhynskyy, N., J.-F. Girmens, W. Faigle, and S. Scheuring (2007). “Human Cataract Lens Membrane at Subnanometer Resolution.” In: *Journal of Molecular Biology* 374.1, pp. 162–169. ISSN: 00222836. DOI: 10.1016/j.jmb.2007.09.022 (cit. on p. 66).
- Buzhynskyy, N., R. K. Hite, T. Walz, and S. Scheuring (2007). “The Supramolecular Architecture of Junctional Microdomains in Native Lens Membranes.” In: *EMBO reports* 8.1, pp. 51–55. ISSN: 1469-221X, 1469-3178. DOI: 10.1038/sj.embor.7400858 (cit. on p. 66).
- Calmette, A., C. Guérin, A. Boquet, and L. Nègre (1927). *La Vaccination Préventive Contre La Tuberculose Par Le "BCG"*. Masson et cie (cit. on p. 59).
- Cammack, R., T. Atwood, P. Campbell, H. Parish, A. Smith, F. Vella, and J. Stirling (2006). *Oxford Dictionary of Biochemistry and Molecular Biology*. Oxford University Press. ISBN: 978-0-19-852917-0 (cit. on p. 61).
- Canetta, E., A. Riches, E. Borger, S. Herrington, K. Dholakia, and A. K. Adya (2014). “Discrimination of Bladder Cancer Cells from Normal Urothelial Cells with High Specificity and Sensitivity: Combined Application of Atomic Force Microscopy and Modulated Raman Spectroscopy.” In: *Acta Biomaterialia* 10.5, pp. 2043–2055. ISSN: 17427061. DOI: 10.1016/j.actbio.2013.12.057 (cit. on p. 81).

Bibliography

- Cappella, B. and G. Dietler (1999). “Force-Distance Curves by Atomic Force Microscopy.” In: *Surface Science Reports* 34.1-3, pp. 1–104 (cit. on pp. 21, 36, 77, 200, 202).
- Carlet, J., P. Collignon, D. Goldmann, H. Goossens, I. C. Gyssens, S. Harbarth, V. Jarlier, S. B. Levy, B. N’Doye, D. Pittet, R. Richtmann, W. H. Seto, J. W. van der Meer, and A. Voss (2011). “Society’s Failure to Protect a Precious Resource: Antibiotics.” In: *The Lancet* 378.9788, pp. 369–371. ISSN: 01406736. DOI: 10.1016/S0140-6736(11)60401-7 (cit. on p. 63).
- Cartagena-Rivera, A. X., C. M. Van Itallie, J. M. Anderson, and R. S. Chadwick (2017). “Apical Surface Supracellular Mechanical Properties in Polarized Epithelium Using Noninvasive Acoustic Force Spectroscopy.” In: *Nature Communications* 8.1. ISSN: 2041-1723. DOI: 10.1038/s41467-017-01145-8 (cit. on p. 70).
- Casadevall, A. and L.-a. Pirofski (1999). “Host-Pathogen Interactions: Redefining the Basic Concepts of Virulence and Pathogenicity.” In: *Infection and Immunity* 67.8, pp. 3703–3713. ISSN: 0019-9567, 1098-5522. pmid: 10417127 (cit. on p. 61).
- Casuso, I. and S. Scheuring (2010). “Automated Setpoint Adjustment for Biological Contact Mode Atomic Force Microscopy Imaging.” In: *Nanotechnology* 21.3, p. 035104. ISSN: 0957-4484, 1361-6528. DOI: 10.1088/0957-4484/21/3/035104 (cit. on p. 94).
- Cattin, C. J., M. Düggelin, D. Martinez-Martin, C. Gerber, D. J. Müller, and M. P. Stewart (2015). “Mechanical Control of Mitotic Progression in Single Animal Cells.” In: *Proceedings of the National Academy of Sciences* 112.36, pp. 11258–11263. ISSN: 0027-8424, 1091-6490. DOI: 10.1073/pnas.1502029112. pmid: 26305930 (cit. on p. 66).
- Cerf, A., J.-C. Cau, C. Vieu, and E. Dague (2009). “Nanomechanical Properties of Dead or Alive Single-Patterned Bacteria.” In: *Langmuir* 25.10, pp. 5731–5736. ISSN: 0743-7463. DOI: 10.1021/1a9004642 (cit. on p. 71).
- Chain, P. S. G., E. Carniel, F. W. Larimer, J. Lamerdin, P. O. Stoutland, W. M. Regala, A. M. Georgescu, L. M. Vergez, M. L. Land, V. L. Motin, R. R. Brubaker, J. Fowler, J. Hinnebusch, M. Marceau, C. Medigue, M. Simonet, V. Chenal-Francisque, B. Souza, D. Dacheux, J. M. Elliott, A. Derbise, L. J. Hauser, and E. Garcia (2004). “Insights into the Evolution of *Yersinia Pestis* through Whole-Genome Comparison with *Yersinia Pseudotuberculosis*.” In: *Proceedings of the National Academy of Sciences of the United States of America* 101.38, pp. 13826–13831. ISSN:

Bibliography

- 0027-8424. DOI: 10.1073/pnas.0404012101. pmid: 15358858 (cit. on p. 59).
- Chang, Y.-R., V. K. Raghunathan, S. P. Garland, J. T. Morgan, P. Russell, and C. J. Murphy (2014). “Automated AFM Force Curve Analysis for Determining Elastic Modulus of Biomaterials and Biological Samples.” In: *Journal of the Mechanical Behavior of Biomedical Materials* 37, pp. 209–218. ISSN: 17516161. DOI: 10.1016/j.jmbbm.2014.05.027 (cit. on p. 204).
- Charest, J. L., A. J. García, and W. P. King (2007). “Myoblast Alignment and Differentiation on Cell Culture Substrates with Microscale Topography and Model Chemistries.” In: *Biomaterials* 28.13, pp. 2202–2210. ISSN: 01429612. DOI: 10.1016/j.biomaterials.2007.01.020 (cit. on p. 162).
- Chatton, E. (1937). *Titres et Travaux Scientifiques (1906-1937) de Edouard Chatton,...* Impr. E. Sottano (cit. on p. 46).
- Chaudhuri, P. K., B. C. Low, and C. T. Lim (2018). “Mechanobiology of Tumor Growth.” In: *Chemical Reviews*. ISSN: 0009-2665, 1520-6890. DOI: 10.1021/acs.chemrev.8b00042 (cit. on p. 68).
- Chen, W., Z. Brandes, R. Roy, M. Chekmareva, H. J. Pandya, J. P. Desai, and D. J. Foran (2015). “Robot-Guided Atomic Force Microscopy for Mechano-Visual Phenotyping of Cancer Specimens.” In: *Microscopy and Microanalysis* 21.5, pp. 1224–1235. ISSN: 1431-9276, 1435-8115. DOI: 10.1017/S1431927615015007 (cit. on p. 90).
- Ciasca, G., T. E. Sassun, E. Minelli, M. Antonelli, M. Papi, A. Santoro, F. Giangaspero, R. Delfini, and M. De Spirito (2016). “Nano-Mechanical Signature of Brain Tumours.” In: *Nanoscale*. ISSN: 2040-3364, 2040-3372. DOI: 10.1039/C6NR06840E (cit. on p. 146).
- Cleveland, J. P., S. Manne, D. Bocek, and P. K. Hansma (1993). “A Nondestructive Method for Determining the Spring Constant of Cantilevers for Scanning Force Microscopy.” In: *Review of Scientific Instruments* 64.2, pp. 403–405. ISSN: 0034-6748. DOI: 10.1063/1.1144209 (cit. on p. 77).
- Crick, S. L. and F. C.-P. Yin (2007). “Assessing Micromechanical Properties of Cells with Atomic Force Microscopy: Importance of the Contact Point.” In: *Biomechanics and Modeling in Mechanobiology* 6.3, pp. 199–210. ISSN: 1617-7959, 1617-7940. DOI: 10.1007/s10237-006-0046-x (cit. on p. 203).
- Cross, S. E., Y.-S. Jin, J. Rao, and J. K. Gimzewski (2007). “Nanomechanical Analysis of Cells from Cancer Patients.” In: *Nature Nanotechnology*

Bibliography

- 2.12, pp. 780–783. ISSN: 1748-3387, 1748-3395. DOI: 10.1038/nano.2007.388 (cit. on pp. 68, 82).
- Cross, S. E., Y.-S. Jin, J. Tondre, R. Wong, J. Rao, and J. K. Gimzewski (2008). “AFM-Based Analysis of Human Metastatic Cancer Cells.” In: *Nanotechnology* 19.38, p. 384003. ISSN: 0957-4484, 1361-6528. DOI: 10.1088/0957-4484/19/38/384003 (cit. on p. 68).
- Daffé, M. and P. Draper (1997). “The Envelope Layers of Mycobacteria with Reference to Their Pathogenicity.” In: *Advances in Microbial Physiology*. Vol. 39. Elsevier, pp. 131–203. ISBN: 978-0-12-027739-1. DOI: 10.1016/S0065-2911(08)60016-8 (cit. on p. 57).
- Dague, E., E. Jauvert, L. Laplatine, B. Viallet, C. Thibault, and L. Rossier (2011). “Assembly of Live Micro-Organisms on Microstructured PDMS Stamps by Convective/Capillary Deposition for AFM Bio-Experiments.” In: *Nanotechnology* 22.39, p. 395102. ISSN: 0957-4484, 1361-6528. DOI: 10.1088/0957-4484/22/39/395102 (cit. on pp. 26, 165).
- Dalby, M. J., M. O. Riehle, S. J. Yarwood, C. D. Wilkinson, and A. S. Curtis (2003). “Nucleus Alignment and Cell Signaling in Fibroblasts: Response to a Micro-Grooved Topography.” In: *Experimental Cell Research* 284.2, pp. 272–280. ISSN: 00144827. DOI: 10.1016/S0014-4827(02)00053-8 (cit. on p. 162).
- David, E., T. Tramontin, and R. Zimmel (2009). “Pharmaceutical R&D: The Road to Positive Returns.” In: *Nature Reviews Drug Discovery*. Drug Discovery 8.8, pp. 609–610 (cit. on p. 63).
- Davies, J. (1994). “Inactivation of Antibiotics and the Dissemination of Resistance Genes.” In: *Science-AAAS-Weekly Paper Edition-including Guide to Scientific Information* 264.5157, pp. 375–381 (cit. on p. 62).
- (1996). “Bacteria on the Rampage.” In: *Nature* 383, pp. 219–220 (cit. on p. 62).
- Davis, B. D., R. Dulbecco, H. N. Eisen, and H. S. Ginsberg (1973). *Microbiology*. 2nd ed. Harper and Row, Evanston, Il. (cit. on p. 60).
- Derjaguin, B. V., V. M. Muller, and Y. P. Toporov (1975). “Effect of Contact Deformations on the Adhesion of Particles.” In: *Journal of Colloid and Interface Science* 53.2, pp. 314–326. ISSN: 0021-9797. DOI: [https://doi.org/10.1016/0021-9797\(75\)90018-1](https://doi.org/10.1016/0021-9797(75)90018-1) (cit. on p. 201).
- Di Carlo, D. (2012). “A Mechanical Biomarker of Cell State in Medicine.” In: *Journal of Laboratory Automation* 17.1, pp. 32–42 (cit. on p. 67).
- Dodge, Y. (2008). *The Concise Encyclopedia of Statistics*. Springer Science & Business Media. 612 pp. ISBN: 978-0-387-31742-7 (cit. on p. 197).

Bibliography

- Doktycz, M., C. Sullivan, P. Hoyt, D. Pelletier, S. Wu, and D. Allison (2003). "AFM Imaging of Bacteria in Liquid Media Immobilized on Gelatin Coated Mica Surfaces." In: *Ultramicroscopy* 97.1-4, pp. 209–216. ISSN: 03043991. DOI: 10.1016/S0304-3991(03)00045-7 (cit. on p. 27).
- Drake, B., C. B. Prater, A. L. Weisenhorn, S. A. C. Gould, T. R. Albrecht, C. F. Quate, D. S. Cannell, H. G. Hansma, and P. K. Hansma (1989). "Imaging Crystals, Polymers, and Processes in Water with the Atomic Force Microscope." In: *Science* 243.4898, pp. 1586–1589. ISSN: 0036-8075. JSTOR: 1703636 (cit. on p. 25).
- Dufrêne, Y. F. (2008). "Atomic Force Microscopy and Chemical Force Microscopy of Microbial Cells." In: *Nature Protocols* 3.7, pp. 1132–1138. ISSN: 1754-2189, 1750-2799. DOI: 10.1038/nprot.2008.101 (cit. on p. 38).
- (2004). "Using Nanotechniques to Explore Microbial Surfaces." In: *Nature Reviews Microbiology* 2.6, pp. 451–460. ISSN: 1740-1526, 1740-1534. DOI: 10.1038/nrmicro905 (cit. on p. 26).
- Dulińska, I., M. Targosz, W. Strojny, M. Lekka, P. Czuba, W. Balwierz, and M. Szymoński (2006). "Stiffness of Normal and Pathological Erythrocytes Studied by Means of Atomic Force Microscopy." In: *Journal of Biochemical and Biophysical Methods* 66.1-3, pp. 1–11. ISSN: 0165022X. DOI: 10.1016/j.jbbm.2005.11.003 (cit. on p. 68).
- Dupres, V., F. D. Menozzi, C. Locht, B. H. Clare, N. L. Abbott, S. Cuenot, C. Bompard, D. Raze, and Y. F. Dufrêne (2005). "Nanoscale Mapping and Functional Analysis of Individual Adhesins on Living Bacteria." In: *Nature Methods* 2.7, pp. 515–520. ISSN: 1548-7091, 1548-7105. DOI: 10.1038/nmeth769 (cit. on pp. 85, 154).
- Eaton, P., J. C. Fernandes, E. Pereira, M. E. Pintado, and F. Xavier Malcata (2008). "Atomic Force Microscopy Study of the Antibacterial Effects of Chitosans on Escherichia Coli and Staphylococcus Aureus." In: *Ultramicroscopy* 108.10, pp. 1128–1134. ISSN: 03043991. DOI: 10.1016/j.ultramicro.2008.04.015 (cit. on p. 71).
- Eaton, P. and P. West (2010). *Atomic Force Microscopy*. Oxford University Press. 256 pp. ISBN: 978-0-19-957045-4 (cit. on p. 120).
- Egeblad, M., E. S. Nakasone, and Z. Werb (2010). "Tumors as Organs: Complex Tissues That Interface with the Entire Organism." In: *Developmental Cell* 18.6, pp. 884–901. ISSN: 15345807. DOI: 10.1016/j.devcel.2010.05.012 (cit. on p. 64).

Bibliography

- Elowitz, M. B., A. J. Levine, E. D. Siggia, and P. S. Swain (2002). “Stochastic Gene Expression in a Single Cell.” In: *Science*. ISSN: 00368075, 10959203. DOI: 10.1126/science.1073263 (cit. on p. 69).
- Engler, A. J., S. Sen, H. L. Sweeney, and D. E. Discher (2006). “Matrix Elasticity Directs Stem Cell Lineage Specification.” In: *Cell* 126.4, pp. 677–689. ISSN: 00928674. DOI: 10.1016/j.cell.2006.06.044 (cit. on p. 67).
- Erlandsson, R., G. M. McClelland, C. M. Mate, and S. Chiang (1988). “Atomic Force Microscopy Using Optical Interferometry.” In: *Journal of Vacuum Science & Technology A* 6.2, pp. 266–270. ISSN: 0734-2101. DOI: 10.1116/1.575440 (cit. on p. 87).
- Fabry, B., G. N. Maksym, J. P. Butler, M. Glogauer, D. Navajas, and J. J. Fredberg (2001). “Scaling the Microrheology of Living Cells.” In: *Physical Review Letters* 87.14, p. 148102. DOI: 10.1103/PhysRevLett.87.148102 (cit. on p. 85).
- Fantner, G. E., R. J. Barbero, D. S. Gray, and A. M. Belcher (2010). “Kinetics of Antimicrobial Peptide Activity Measured on Individual Bacterial Cells Using High-Speed Atomic Force Microscopy.” In: *Nature Nanotechnology* 5.4, pp. 280–285. ISSN: 1748-3387, 1748-3395. DOI: 10.1038/nnano.2010.29 (cit. on pp. 44, 70, 71).
- Faria, E. C., N. Ma, E. Gazi, P. Gardner, M. Brown, N. W. Clarke, and R. D. Snook (2008). “Measurement of Elastic Properties of Prostate Cancer Cells Using AFM.” In: *The Analyst* 133.11, p. 1498. ISSN: 0003-2654, 1364-5528. DOI: 10.1039/b803355b (cit. on p. 67).
- Favre, M., J. Polesel-Maris, T. Overstolz, P. Niedermann, S. Dasen, G. Gruener, R. Ischer, P. Vettiger, M. Liley, H. Heinzelmann, and A. Meister (2011). “Parallel AFM Imaging and Force Spectroscopy Using Two-Dimensional Probe Arrays for Applications in Cell Biology.” In: *Journal of Molecular Recognition* 24.3, pp. 446–452. ISSN: 09523499. DOI: 10.1002/jmr.1119 (cit. on p. 88).
- Flater, E. E., G. E. Zacharakis-Jutz, B. G. Dumba, I. A. White, and C. A. Clifford (2014). “Towards Easy and Reliable AFM Tip Shape Determination Using Blind Tip Reconstruction.” In: *Ultramicroscopy* 146, pp. 130–143. ISSN: 03043991. DOI: 10.1016/j.ultramic.2013.06.022 (cit. on p. 39).
- Formosa-Dague, C., R. E. Duval, and E. Dague (2017). “Cell Biology of Microbes and Pharmacology of Antimicrobial Drugs Explored by Atomic Force Microscopy.” In: *Seminars in Cell & Developmental Biology*. ISSN: 10849521. DOI: 10.1016/j.semcdb.2017.06.022 (cit. on p. 71).

Bibliography

- Formosa, C., M. Schiavone, H. Martin-Yken, J. M. François, R. E. Duval, and E. Dague (2013). “Nanoscale Effects of Caspofungin against Two Yeast Species, *Saccharomyces Cerevisiae* and *Candida Albicans*.” In: *Antimicrobial Agents and Chemotherapy* 57.8, pp. 3498–3506. ISSN: 0066-4804, 1098-6596. DOI: 10.1128/AAC.00105-13. pmid: 23669379 (cit. on p. 71).
- Formosa, C., M. Grare, R. E. Duval, and E. Dague (2012). “Nanoscale Effects of Antibiotics on *P. Aeruginosa*.” In: *Nanomedicine: Nanotechnology, Biology and Medicine* 8.1, pp. 12–16. ISSN: 1549-9634. DOI: 10.1016/j.nano.2011.09.009 (cit. on p. 71).
- Francius, G., O. Domenech, M. P. Mingeot-Leclercq, and Y. F. Dufrêne (2008). “Direct Observation of *Staphylococcus Aureus* Cell Wall Digestion by Lysostaphin.” In: *Journal of Bacteriology* 190.24, pp. 7904–7909. ISSN: 0021-9193, 1098-5530. DOI: 10.1128/JB.01116-08. pmid: 18835985 (cit. on p. 71).
- French, G. L. (2010). “The Continuing Crisis in Antibiotic Resistance.” In: *International journal of antimicrobial agents* 36, S3–S7 (cit. on p. 63).
- Gad, M. and A. Ikai (1995). “Method for Immobilizing Microbial Cells on Gel Surface for Dynamic AFM Studies.” In: *Biophysical Journal* 69.6, pp. 2226–2233. ISSN: 00063495. DOI: 10.1016/S0006-3495(95)80147-5 (cit. on p. 26).
- Gavara, N. and R. S. Chadwick (2012). “Determination of the Elastic Moduli of Thin Samples and Adherent Cells Using Conical Atomic Force Microscope Tips.” In: *Nature Nanotechnology* 7.11, pp. 733–736. ISSN: 1748-3387, 1748-3395. DOI: 10.1038/nnano.2012.163 (cit. on p. 202).
- Gillis, A., V. Dupres, G. Delestrait, J. Mahillon, and Y. F. Dufrêne (2012). “Nanoscale Imaging of *Bacillus Thuringiensis* Flagella Using Atomic Force Microscopy.” In: *Nanoscale* 4.5, pp. 1585–1591. ISSN: 2040-3372. DOI: 10.1039/C1NR11161B (cit. on p. 27).
- Gillis, A., V. Dupres, J. Mahillon, and Y. F. Dufrêne (2012). “Atomic Force Microscopy: A Powerful Tool for Studying Bacterial Swarming Motility.” In: *Micron*. Special issue on AFM in Biology & Bionanomedicine 43.12, pp. 1304–1311. ISSN: 0968-4328. DOI: 10.1016/j.micron.2012.01.014 (cit. on p. 66).
- Goldman, E. and L. Green (2008). *Practical Handbook of Microbiology*. 2nd ed. CRC Press. ISBN: 978-1-4200-0933-0 (cit. on p. 67).
- Hanahan, D. and R. A. Weinberg (2000). “The Hallmarks of Cancer.” In: *Cell* 100, pp. 57–70 (cit. on p. 64).

Bibliography

- Hanahan, D. and R. A. Weinberg (2011). “Hallmarks of Cancer: The Next Generation.” In: *Cell* 144.5, pp. 646–674. ISSN: 00928674. DOI: 10.1016/j.cell.2011.02.013 (cit. on p. 64).
- Hansma, H. G., J. Vesenka, C. Siegerist, G. Kelderman, H. Morret, R. L. Sinsheimer, V. Elings, C. Bustamante, and P. K. Hansma (1992). “Reproducible Imaging and Dissection of Plasmid DNA Under Liquid with the Atomic Force Microscope.” In: *Science* 256, pp. 1180–1184 (cit. on p. 66).
- Hansma, P. K., J. P. Cleveland, M. Radmacher, D. A. Walters, P. E. Hillner, M. Bezanilla, M. Fritz, D. Vie, H. G. Hansma, C. B. Prater, J. Massie, L. Fukunaga, J. Gurley, and V. Elings (1994). “Tapping Mode Atomic Force Microscopy in Liquids.” In: *Applied Physics Letters* 64.13, pp. 1738–1740. ISSN: 0003-6951, 1077-3118. DOI: 10.1063/1.111795 (cit. on p. 140).
- Hansma, P. K., V. B. Elings, O. Marti, and C. E. Bracker (1988). “Scanning Tunneling Microscopy and Atomic Force Microscopy: Application to Biology and Technology.” In: *Science* 242, pp. 209–216. DOI: 10.1117/12.944502 (cit. on pp. 17, 25).
- Hayashi, K. and M. Iwata (2015). “Stiffness of Cancer Cells Measured with an AFM Indentation Method.” In: *Journal of the Mechanical Behavior of Biomedical Materials* 49, pp. 105–111. ISSN: 17516161. DOI: 10.1016/j.jmbbm.2015.04.030 (cit. on p. 68).
- Helaine, S., J. A. Thompson, K. G. Watson, M. Liu, C. Boyle, and D. W. Holden (2010). “Dynamics of Intracellular Bacterial Replication at the Single Cell Level.” In: *Proceedings of the National Academy of Sciences of the United States of America* 107.8, pp. 3746–3751. ISSN: 1091-6490. DOI: 10.1073/pnas.1000041107. pmid: 20133586 (cit. on p. 69).
- Henderson, E., P. Haydon, and D. Sakaguchi (1992). “Actin Filament Dynamics in Living Glial Cells Imaged by Atomic Force Microscopy.” In: *Science* 257.5078, pp. 1944–1946. ISSN: 0036-8075, 1095-9203. DOI: 10.1126/science.1411511 (cit. on p. 25).
- Hermanowicz, P., M. Sarna, K. Burda, and H. Gabryś (2014). “AtomicJ: An Open Source Software for Analysis of Force Curves.” In: *Review of Scientific Instruments* 85.6, p. 063703. ISSN: 0034-6748, 1089-7623. DOI: 10.1063/1.4881683 (cit. on p. 120).
- Hertz, H. (1882). “Über Die Berührung Fester Elastischer Körper.” In: *J. Reine Angew. Mathematik* 92, pp. 156–171 (cit. on pp. 11, 200).

Bibliography

- Hoh, J. H. and A. Engel (1993). “Friction Effects on Force Measurements with an Atomic Force Microscope.” In: *Langmuir* 9.11, pp. 3310–3312. ISSN: 0743-7463. DOI: 10.1021/la00035a089 (cit. on p. 43).
- Horcas, I., R. Fernández, J. M. Gómez-Rodríguez, J. Colchero, J. Gómez-Herrero, and A. M. Baro (2007). “WSXM: A Software for Scanning Probe Microscopy and a Tool for Nanotechnology.” In: *Review of Scientific Instruments* 78.1, p. 013705. ISSN: 0034-6748, 1089-7623. DOI: 10.1063/1.2432410 (cit. on p. 120).
- Hornik, K. (2017). *R FAQ* (cit. on p. 122).
- Huang, B., Z. Li, and J. Li (2018). “Artificial Intelligent Atomic Force Microscope Enabled by Machine Learning.” In: arXiv: 1807.09985 [cond-mat, physics:physics] (cit. on p. 97).
- Hübner, U., W. Morgenroth, H. Meyer, T. Sulzbach, B. Brendel, and W. Mirandé (2003). “Downwards to Metrology in Nanoscale: Determination of the AFM Tip Shape with Well-Known Sharp-Edged Calibration Structures.” In: *Applied Physics A: Materials Science & Processing* 76.6, pp. 913–917. ISSN: 0947-8396, 1432-0630. DOI: 10.1007/s00339-002-1975-6 (cit. on p. 39).
- Hues, S. M., C. F. Draper, K. P. Lee, and R. J. Colton (1994). “Effect of PZT and PMN Actuator Hysteresis and Creep on Nanoindentation Measurements Using Force Microscopy.” In: *Review of Scientific Instruments* 65.5, pp. 1561–1565. ISSN: 0034-6748, 1089-7623. DOI: 10.1063/1.1144892 (cit. on p. 36).
- Hutter, J. L. and J. Bechhoefer (1993). “Calibration of Atomic-force Microscope Tips.” In: *Review of Scientific Instruments* 64.7, pp. 1868–1873. ISSN: 0034-6748, 1089-7623. DOI: 10.1063/1.1143970 (cit. on pp. 78, 79).
- IronPython.Net* (2018). URL: <http://ironpython.net/> (visited on 2018) (cit. on p. 207).
- Itoh, H., T. Fujimoto, and S. Ichimura (2006). “Tip Characterizer for Atomic Force Microscopy.” In: *Review of Scientific Instruments* 77.10, p. 103704. ISSN: 0034-6748, 1089-7623. DOI: 10.1063/1.2356855 (cit. on p. 177).
- Iyer, S., R. M. Gaikwad, V. Subba-Rao, C. D. Woodworth, and I. Sokolov (2009). “Atomic Force Microscopy Detects Differences in the Surface Brush of Normal and Cancerous Cells.” In: *Nature Nanotechnology* 4.6, pp. 389–393. ISSN: 1748-3387, 1748-3395. DOI: 10.1038/nnano.2009.77 (cit. on pp. 68, 82).

Bibliography

- Jalava, K., S. Hallanvuoto, U.-M. Nakari, P. Ruutu, E. Kela, T. Heinäsmäki, A. Siitonen, and J. P. Nuorti (2004). “Multiple Outbreaks of *Yersinia Pseudotuberculosis* Infections in Finland.” In: *Journal of Clinical Microbiology* 42.6, pp. 2789–2791. ISSN: 0095-1137. DOI: 10.1128/JCM.42.6.2789-2791.2004. pmid: 15184472 (cit. on p. 59).
- Janel, S., E. Werkmeister, A. Bongiovanni, F. Lafont, and N. Barois (2017). “CLAFEM.” In: *Methods in Cell Biology*. Vol. 140. Elsevier, pp. 165–185. ISBN: 978-0-12-809975-9. DOI: 10.1016/bs.mcb.2017.03.010 (cit. on p. 107).
- Janin, J. (2013). “Foreword.” In: *Modeling in Computational Biology and Biomedicine: A Multidisciplinary Endeavor*. Ed. by F. Cazals and P. Kronprobst. OCLC: 826287939. Berlin: Springer. ISBN: 978-3-642-31207-6 978-3-642-31208-3 (cit. on p. 198).
- Janovjak, H., J. Struckmeier, and D. J. Müller (2005). “Hydrodynamic Effects in Fast AFM Single-Molecule Force Measurements.” In: *European Biophysics Journal* 34.1, pp. 91–96. ISSN: 01757571. DOI: 10.1007/s00249-004-0430-3 (cit. on p. 25).
- Jauvert, E., E. Palleau, E. Dague, and L. Rossier (2014). “Directed Assembly of Living *Pseudomonas Aeruginosa* Bacteria on PEI Patterns Generated by Nanoxerography for Statistical AFM Bioexperiments.” In: *ACS Applied Materials & Interfaces* 6.23, pp. 21230–21236. ISSN: 1944-8244, 1944-8252. DOI: 10.1021/am506241n (cit. on pp. 164, 165).
- Jiao, Y., D. I. Cherny, G. Heim, T. M. Jovin, and T. E. Schäffer (2001). “Dynamic Interactions of P53 with DNA in Solution by Time-Lapse Atomic Force Microscopy.” In: *Journal of Molecular Biology* 314.2, pp. 233–243. ISSN: 00222836. DOI: 10.1006/jmbi.2001.5129 (cit. on p. 66).
- Jin, H., X. Xing, H. Zhao, Y. Chen, X. Huang, S. Ma, H. Ye, and J. Cai (2010). “Detection of Erythrocytes Influenced by Aging and Type 2 Diabetes Using Atomic Force Microscope.” In: *Biochemical and Biophysical Research Communications* 391.4, pp. 1698–1702. ISSN: 0006291X. DOI: 10.1016/j.bbrc.2009.12.133 (cit. on p. 68).
- Johnson, D. I. (2018). *Bacterial Pathogens and Their Virulence Factors*. Cham: Springer International Publishing. ISBN: 978-3-319-67650-0 978-3-319-67651-7. DOI: 10.1007/978-3-319-67651-7 (cit. on pp. 56, 57).
- Johnson, K. L., K. Kendall, and A. D. Roberts (1971). “Surface Energy and the Contact of Elastic Solids.” In: *Proc. R. Soc. Lond. A* 324.1558, pp. 301–313. ISSN: 0080-4630, 2053-9169. DOI: 10.1098/rspa.1971.0141 (cit. on p. 201).

Bibliography

- Kaemmer, S. (2011). "Introduction to Bruker's ScanAsyst and PeakForce Tapping." In: *Bruker Application Note* 133, pp. 1–12 (cit. on p. 34).
- Karrasch, S., M. Dolder, F. Schabert, J. Ramsden, and A. Engel (1993). "Covalent Binding of Biological Samples to Solid Supports for Scanning Probe Microscopy in Buffer Solution." In: *Biophysical Journal* 65.6, pp. 2437–2446. ISSN: 00063495. DOI: 10.1016/S0006-3495(93)81327-4 (cit. on p. 27).
- Kasas, S. and A. Ikai (1995). "A Method for Anchoring Round Shaped Cells for Atomic Force Microscope Imaging." In: *Biophysical Journal* 68.5, pp. 1678–1680. ISSN: 00063495. DOI: 10.1016/S0006-3495(95)80344-9 (cit. on p. 26).
- Kaul-Ghanekar, R., S. Singh, H. Mamgain, A. Jalota-Badhwar, K. M. Paknikar, and S. Chattopadhyay (2009). "Tumor Suppressor Protein SMAR1 Modulates the Roughness of Cell Surface: Combined AFM and SEM Study." In: *BMC Cancer* 9.1. ISSN: 1471-2407. DOI: 10.1186/1471-2407-9-350 (cit. on p. 66).
- Kawakatsu, H., D. Saya, A. Kato, K. Fukushima, H. Toshiyoshi, and H. Fujita (2002). "Millions of Cantilevers for Atomic Force Microscopy." In: *Review of Scientific Instruments* 73.3, pp. 1188–1192. ISSN: 0034-6748, 1089-7623. DOI: 10.1063/1.1448137 (cit. on p. 88).
- Kieser, K. J. and E. J. Rubin (2014). "How Sisters Grow Apart: Mycobacterial Growth and Division." In: *Nature Reviews Microbiology* 12.8, pp. 550–562. ISSN: 1740-1526, 1740-1534. DOI: 10.1038/nrmicro3299 (cit. on pp. 56, 57, 70).
- Kim, Y.-S., K. S. Kim, I. Han, M.-H. Kim, M. H. Jung, and H.-K. Park (2012). "Quantitative and Qualitative Analysis of the Antifungal Activity of Allicin Alone and in Combination with Antifungal Drugs." In: *PLOS ONE* 7.6, e38242. ISSN: 1932-6203. DOI: 10.1371/journal.pone.0038242 (cit. on p. 71).
- Koay, E. J., A. C. Shieh, and K. A. Athanasiou (2003). "Creep Indentation of Single Cells." In: *Journal of Biomechanical Engineering* 125.3, pp. 334–341. ISSN: 0148-0731. DOI: 10.1115/1.1572517 (cit. on p. 66).
- Koehne, J., R. Stevens, T. Zink, Z. Deng, H. Chen, I. Weng, F. Liu, and G. Liu (2011). "Using Carbon Nanotube Probes for High-Resolution Three-Dimensional Imaging of Cells." In: *Ultramicroscopy* 111.8, pp. 1155–1162. ISSN: 03043991. DOI: 10.1016/j.ultramicro.2011.01.030 (cit. on pp. 10, 38).
- Kuznetsova, T. G., M. N. Starodubtseva, N. I. Yegorenkov, S. A. Chizhik, and R. I. Zhdanov (2007). "Atomic Force Microscopy Probing of Cell

Bibliography

- Elasticity.” In: *Micron* 38.8, pp. 824–833. ISSN: 09684328. DOI: 10.1016/j.micron.2007.06.011 (cit. on pp. 34, 67, 74).
- Lanzicher, T., V. Martinelli, L. Puzzi, G. Del Favero, B. Codan, C. S. Long, L. Mestroni, M. R. G. Taylor, and O. Sbaizero (2015). “The Cardiomyopathy Lamin A/C D192G Mutation Disrupts Whole-Cell Biomechanics in Cardiomyocytes as Measured by Atomic Force Microscopy Loading-Unloading Curve Analysis.” In: *Scientific Reports* 5.1. ISSN: 2045-2322. DOI: 10.1038/srep13388 (cit. on p. 68).
- Lasken, R. S. and J. S. McLean (2014). “Recent Advances in Genomic DNA Sequencing of Microbial Species from Single Cells.” In: *Nature Reviews Genetics* 15.9, pp. 577–584 (cit. on p. 70).
- Le Grimellec, C., E. Lesniewska, C. Cachia, J. Schreiber, F. de Fornel, and J. Goudonnet (1994). “Imaging of the membrane surface of MDCK cells by atomic force microscopy.” In: *Biophysical Journal* 67.1, pp. 36–41. ISSN: 00063495. DOI: 10.1016/S0006-3495(94)80490-4 (cit. on p. 25).
- Lee, G. Y. and C. T. Lim (2007). “Biomechanics Approaches to Studying Human Diseases.” In: *Trends in Biotechnology* 25.3, pp. 111–118. ISSN: 01677799. DOI: 10.1016/j.tibtech.2007.01.005 (cit. on p. 68).
- Lee, G. U., D. A. Kidwell, and R. J. Colton (1994). “Sensing Discrete Streptavidin-Biotin Interactions with Atomic Force Microscopy.” In: *Langmuir* 10.2, pp. 354–357 (cit. on p. 65).
- Lekka, M. and P. Laidler (2009). “Applicability of AFM in Cancer Detection.” In: *Nature Nanotechnology* 4, p. 72 (cit. on p. 82).
- Lekka, M., P. Laidler, D. Gil, J. Lekki, Z. Stachura, and A. Z. Hryniewicz (1999). “Elasticity of Normal and Cancerous Human Bladder Cells Studied by Scanning Force Microscopy.” In: *European Biophysics Journal* 28.4, pp. 312–316 (cit. on pp. 67, 82).
- Lekka, M. (2016). “Discrimination Between Normal and Cancerous Cells Using AFM.” In: *BioNanoScience* 6.1, pp. 65–80. ISSN: 2191-1630, 2191-1649. DOI: 10.1007/s12668-016-0191-3 (cit. on pp. 67, 68).
- Lekka, M., D. Gil, K. Pogoda, J. Dulińska-Litewka, R. Jach, J. Gostek, O. Klymenko, S. Prauzner-Behcicki, Z. Stachura, J. Wiltowska-Zuber, K. Okoń, and P. Laidler (2012). “Cancer Cell Detection in Tissue Sections Using AFM.” In: *Archives of Biochemistry and Biophysics* 518.2, pp. 151–156. ISSN: 00039861. DOI: 10.1016/j.abb.2011.12.013 (cit. on p. 82).
- Leloup, D. (2018). “Je n’imaginai pas que Python connaîtrait un tel succès.” In: *Le Monde.fr. Pixels*. ISSN: 1950-6244 (cit. on p. 206).
- Li, Q., G. Lee, C. Ong, and C. Lim (2008). “AFM Indentation Study of Breast Cancer Cells.” In: *Biochemical and Biophysical Research Commu-*

Bibliography

- nations* 374.4, pp. 609–613. ISSN: 0006291X. DOI: 10.1016/j.bbrc.2008.07.078 (cit. on p. 67).
- Lidstrom, M. E. and M. C. Konopka (2010). “The Role of Physiological Heterogeneity in Microbial Population Behavior.” In: *Nature Chemical Biology* 6.10, pp. 705–712. ISSN: 1552-4450, 1552-4469. DOI: 10.1038/nchembio.436 (cit. on p. 69).
- Louise Meyer, R., X. Zhou, L. Tang, A. Arpanaei, P. Kingshott, and F. Besenbacher (2010). “Immobilisation of Living Bacteria for AFM Imaging under Physiological Conditions.” In: *Ultramicroscopy* 110.11, pp. 1349–1357. ISSN: 03043991. DOI: 10.1016/j.ultramicro.2010.06.010 (cit. on pp. 27, 28, 103).
- Luca, S. and T. Mihaescu (2013). “History of BCG.” In: *MAEDICA – a Journal of Clinical Medicine* 8.1, pp. 53–58 (cit. on p. 59).
- Mahaffy, R. E., C. K. Shih, F. C. MacKintosh, and J. Käs (2000). “Scanning Probe-Based Frequency-Dependent Microrheology of Polymer Gels and Biological Cells.” In: *Physical Review Letters* 85.4, pp. 880–883. ISSN: 0031-9007, 1079-7114. DOI: 10.1103/PhysRevLett.85.880 (cit. on p. 66).
- Markowski, C. A. and E. P. Markowski (1990). “Conditions for the Effectiveness of a Preliminary Test of Variance.” In: *The American Statistician* 44.4, p. 322. ISSN: 00031305. DOI: 10.2307/2684360 (cit. on p. 153).
- Marti, O., B. Drake, and P. K. Hansma (1987). “Atomic Force Microscopy of Liquid-covered Surfaces: Atomic Resolution Images.” In: *Applied Physics Letters* 51.7, pp. 484–486. ISSN: 0003-6951. DOI: 10.1063/1.98374 (cit. on p. 25).
- Martin, Y., C. C. Williams, and H. K. Wickramasinghe (1987). “Atomic Force Microscope–Force Mapping and Profiling on a Sub 100-Å Scale.” In: *Journal of Applied Physics* 61.10, pp. 4723–4729. ISSN: 0021-8979. DOI: 10.1063/1.338807 (cit. on p. 19).
- Matzke, R., K. Jacobson, and M. Radmacher (2001). “Direct, High-Resolution Measurement of Furrow Stiffening during Division of Adherent Cells.” In: *Nature Cell Biology* 3.6, pp. 607–610. ISSN: 1465-7392, 1476-4679. DOI: 10.1038/35078583 (cit. on p. 72).
- Maugis, D. (1992). “Adhesion of Spheres: The JKR-DMT Transition Using a Dugdale Model.” In: *Journal of Colloid and Interface Science* 150.1, pp. 243–269. ISSN: 0021-9797. DOI: 10.1016/0021-9797(92)90285-T (cit. on p. 202).
- Medina, E. and D. H. Pieper (2016). “Tackling Threats and Future Problems of Multidrug-Resistant Bacteria.” In: *How to Overcome the An-*

Bibliography

- Antibiotic Crisis: Facts, Challenges, Technologies and Future Perspectives*. Current topics in microbiology and immunology Volume 398. OCLC: 971216190. Cham: Springer. ISBN: 978-3-319-49282-7 978-3-319-49284-1 (cit. on pp. 62, 63).
- Meincken, M., D. L. Holroyd, and M. Rautenbach (2005). "Atomic Force Microscopy Study of the Effect of Antimicrobial Peptides on the Cell Envelope of Escherichia Coli." In: *Antimicrobial Agents and Chemotherapy* 49.10, pp. 4085–4092. ISSN: 0066-4804, 1098-6596. DOI: 10.1128/AAC.49.10.4085-4092.2005 (cit. on p. 71).
- Menozi, F. D., J. H. Rouse, M. Alavi, M. Laude-Sharp, J. Muller, R. Bischoff, M. J. Brennan, and C. Lochter (1996). "Identification of a Heparin-Binding Hemagglutinin Present in Mycobacteria." In: *Journal of Experimental Medicine* 184.3, pp. 993–1001. ISSN: 0022-1007, 1540-9538. DOI: 10.1084/jem.184.3.993 (cit. on p. 57).
- Minne, S. C., G. Yaralioglu, S. R. Manalis, J. D. Adams, J. Zesch, A. Atalar, and C. F. Quate (1998). "Automated Parallel High-Speed Atomic Force Microscopy." In: *Applied Physics Letters* 72.18, p. 2340. ISSN: 00036951. DOI: 10.1063/1.121353 (cit. on pp. 86, 87).
- Mohan, S. K. (2009). *Gram Stain: Looking Beyond Bacteria to Find Fungi in Gram Stained Smear. a Laboratory Guide for Medical Microbiology*. AuthorHouse. 190 pp. ISBN: 978-1-4389-6028-9 (cit. on p. 54).
- Mohr, K. I. (2016). "History of Antibiotics Research." In: *How to Overcome the Antibiotic Crisis: Facts, Challenges, Technologies and Future Perspectives*. Current topics in microbiology and immunology Volume 398. OCLC: 971216190. Cham: Springer. ISBN: 978-3-319-49282-7 978-3-319-49284-1 (cit. on pp. 59, 61, 62).
- Moler, C. (2004). *The Origins of MATLAB*. URL: <https://www.mathworks.com/company/newsletters/articles/the-origins-of-matlab.html> (visited on 2018) (cit. on p. 123).
- Mortensen, N. P., J. D. Fowlkes, C. J. Sullivan, D. P. Allison, N. B. Larsen, S. Molin, and M. J. Doktycz (2009). "Effects of Colistin on Surface Ultrastructure and Nanomechanics of Pseudomonas Aeruginosa Cells." In: *Langmuir* 25.6, pp. 3728–3733. ISSN: 0743-7463. DOI: 10.1021/la803898g (cit. on p. 71).
- Mou, J., G. Huang, and Z. Shao (1995). "Semi-automatic Atomic Force Microscope for Imaging in Solution." In: *Review of Scientific Instruments* 66.12, pp. 5527–5531. ISSN: 0034-6748, 1089-7623. DOI: 10.1063/1.1146079 (cit. on p. 91).

Bibliography

- Moy, V. T., E.-L. Florin, and H. E. Gaub (1994). “Intermolecular Forces and Energies between Ligands and Receptors.” In: *Science*, pp. 257–259 (cit. on p. 65).
- Nečas, D. and P. Klapetek (2011). “Gwyddion: An Open-Source Software for SPM Data Analysis.” In: *Open Physics* 10.1, pp. 181–188. ISSN: 2391-5471. DOI: 10.2478/s11534-011-0096-2 (cit. on p. 119).
- O’Reilly, L. and C. Daborn (1995). “The Epidemiology of Mycobacterium Bovis Infections in Animals and Man: A Review.” In: *Tubercle and Lung Disease* 76, pp. 1–46. ISSN: 09628479. DOI: 10.1016/0962-8479(95)90591-X (cit. on p. 59).
- Ohnesorge, F. M., J. K. Hörber, W. Häberle, C. P. Czerny, D. P. Smith, and G. Binnig (1997). “AFM Review Study on Pox Viruses and Living Cells.” In: *Biophysical journal* 73.4, pp. 2183–2194 (cit. on p. 25).
- Otsu, N. (1979). “A Threshold Selection Method from Gray-Level Histograms.” In: *IEEE transactions on systems, man, and cybernetics* 9.1, pp. 63–66 (cit. on p. 138).
- Ozkan, A. D., A. E. Topal, F. B. Dikecoglu, M. O. Guler, A. Dana, and A. B. Tekinay (2018). “Probe Microscopy Methods and Applications in Imaging of Biological Materials.” In: *Seminars in Cell & Developmental Biology. Application of Atomic Force Microscopy in cell biology* 73, pp. 153–164. ISSN: 1084-9521. DOI: 10.1016/j.semcdb.2017.08.018 (cit. on pp. 27, 140).
- Park, S., D. Koch, R. Cardenas, J. Käs, and C. K. Shih (2005). “Cell Motility and Local Viscoelasticity of Fibroblasts.” In: *Biophysical Journal* 89.6, pp. 4330–4342. ISSN: 0006-3495. DOI: 10.1529/biophysj.104.053462 (cit. on p. 82).
- Peric, O., M. Hannebelle, J. D. Adams, and G. E. Fantner (2017). “Microfluidic Bacterial Traps for Simultaneous Fluorescence and Atomic Force Microscopy.” In: *Nano Research* 10.11, pp. 3896–3908. ISSN: 1998-0124, 1998-0000. DOI: 10.1007/s12274-017-1604-5 (cit. on pp. 102, 164, 165, 186).
- Picco, L. M., P. G. Dunton, A. Ulcinas, D. J. Engledew, O. Hoshi, T. Ushiki, and M. J. Miles (2008). “High-Speed AFM of Human Chromosomes in Liquid.” In: *Nanotechnology* 19.38, p. 384018. ISSN: 0957-4484. DOI: 10.1088/0957-4484/19/38/384018 (cit. on p. 44).
- Pillet, F., L. Chopinet, C. Formosa, and É. Dague (2014). “Atomic Force Microscopy and Pharmacology: From Microbiology to Cancerology.” In: *Biochimica et Biophysica Acta (BBA) - General Subjects* 1840.3, pp. 1028–

Bibliography

1050. ISSN: 03044165. DOI: 10.1016/j.bbagen.2013.11.019 (cit. on p. 64).
- Pittenger, B., N. Erina, and C. Su (2010). “Quantitative Mechanical Property Mapping at the Nanoscale with PeakForce QNM.” In: *Bruker Application Note* 128, pp. 1–12 (cit. on p. 33).
- Pittenger, B. and A. Slade (2013). “Performing Quantitative Nanomechanical AFM Measurements on Live Cells.” In: *Microscopy Today* 21.06, pp. 12–17. ISSN: 1551-9295, 2150-3583. DOI: 10.1017/S1551929513001077 (cit. on p. 34).
- Plodinec, M., M. Loparic, C. A. Monnier, E. C. Obermann, R. Zanetti-Dallenbach, P. Oertle, J. T. Hyotyla, U. Aebi, M. Bentires-Alj, C.-A. Schoenenberger, and R. Y. Lim (2013). “The Nanomechanical Signature of Breast Cancer.” In: *Nature Nanotechnology* 7.2, pp. 757–765. ISSN: 00063495. DOI: 10.1038/NNANO.2012.167 (cit. on pp. 68, 81, 146).
- Plopper, G. (2014). *Principles of Cell Biology*. Jones & Bartlett Publishers. 588 pp. ISBN: 978-1-284-04762-2 (cit. on p. 48).
- Polesel-Maris, J., L. Aeschmann, A. Meister, R. Ischer, E. Bernard, T. Akiyama, M. Giazon, P. Niedermann, U. Staufer, R. Pugin, N. F. de Rooij, P. Vettiger, and H. Heinzelmann (2007). “Piezoresistive Cantilever Array for Life Sciences Applications.” In: *Journal of Physics: Conference Series* 61, pp. 955–959. ISSN: 1742-6588, 1742-6596. DOI: 10.1088/1742-6596/61/1/189 (cit. on p. 87).
- Pollard, T. D., W. C. Earnshaw, J. Lippincott-Schwartz, and G. Johnson (2016). *Cell Biology E-Book*. Elsevier Health Sciences. 900 pp. ISBN: 978-0-323-40002-2 (cit. on p. 47).
- Popoff, M. (2014). “Étude à l’échelle du nanomètre des propriétés mécaniques et électriques de systèmes biologiques.” Lille, France: Université de Lille 1. 150 pp. (cit. on pp. 120–122).
- Popov, V. L. and J. Gray (2010). *Contact Mechanics and Friction: Physical Principles and Applications*. OCLC: 845639266. Berlin: Springer. 362 pp. ISBN: 978-3-642-10802-0 978-3-642-10803-7 (cit. on pp. 200–202).
- Prabhune, M., G. Belge, A. Dotzauer, J. Bullerdiek, and M. Radmacher (2012). “Comparison of Mechanical Properties of Normal and Malignant Thyroid Cells.” In: *Micron* 43.12, pp. 1267–1272. ISSN: 09684328. DOI: 10.1016/j.micron.2012.03.023 (cit. on p. 67).
- Pürckhauer, K., A. J. Weymouth, K. Pfeffer, L. Kullmann, E. Mulvihill, M. P. Krahn, D. J. Müller, and F. J. Giessibl (2018). “Imaging in Biologically-Relevant Environments with AFM Using Stiff qPlus Sen-

Bibliography

- sors.” In: *Scientific Reports* 8.1, p. 9330. ISSN: 2045-2322. DOI: 10.1038/s41598-018-27608-6 (cit. on p. 87).
- R Core Team (2018). *R: A Language and Environment for Statistical Computing*. Vienna, Austria: R Foundation for Statistical Computing (cit. on p. 122).
- Radmacher, M., R. W. Tillamnn, M. Fritz, and H. E. Gaub (1992). “From Molecules to Cells: Imaging Soft Samples with the Atomic Force Microscope.” In: *Science* 257.5078, pp. 1900–1905 (cit. on p. 25).
- Rajendra Kumar, R. T., S. U. Hassan, O. Sardan Sukas, V. Eichhorn, F. Krohs, S. Fatikow, and P. Boggild (2009). “Nanobits: Customizable Scanning Probe Tips.” In: *Nanotechnology* 20.39, p. 395703. ISSN: 0957-4484, 1361-6528. DOI: 10.1088/0957-4484/20/39/395703 (cit. on p. 93).
- Razatos, A., Y.-L. Ong, M. M. Sharma, and G. Georgiou (1998). “Molecular Determinants of Bacterial Adhesion Monitored by Atomic Force Microscopy.” In: *Proceedings of the National Academy of Sciences* 95.19, pp. 11059–11064. ISSN: 0027-8424, 1091-6490. DOI: 10.1073/pnas.95.19.11059 (cit. on p. 27).
- Rebelo, L. M., J. S. de Sousa, J. Mendes Filho, and M. Radmacher (2013). “Comparison of the Viscoelastic Properties of Cells from Different Kidney Cancer Phenotypes Measured with Atomic Force Microscopy.” In: *Nanotechnology* 24.5, p. 055102. ISSN: 0957-4484, 1361-6528. DOI: 10.1088/0957-4484/24/5/055102 (cit. on p. 67).
- Rigato, A., A. Miyagi, S. Scheuring, and F. Rico (2017). “High-Frequency Microrheology Reveals Cytoskeleton Dynamics in Living Cells.” In: *Nature Physics*. ISSN: 1745-2473, 1745-2481. DOI: 10.1038/nphys4104 (cit. on p. 85).
- Rigato, A., F. Rico, F. Eghiaian, M. Piel, and S. Scheuring (2015). “Atomic Force Microscopy Mechanical Mapping of Micropatterned Cells Shows Adhesion Geometry-Dependent Mechanical Response on Local and Global Scales.” In: *ACS Nano* 9.6, pp. 5846–5856. ISSN: 1936-0851, 1936-086X. DOI: 10.1021/acsnano.5b00430 (cit. on pp. 163, 186).
- Roduit, C., B. Saha, L. Alonso-Sarduy, A. Volterra, G. Dietler, and S. Kasas (2012). “OpenFovea: Open-Source AFM Data Processing Software.” In: *Nature methods* 9.8, pp. 774–775 (cit. on p. 120).
- Roduit, C., S. Sekatski, G. Dietler, S. Catsicas, F. Lafont, and S. Kasas (2009). “Stiffness Tomography by Atomic Force Microscopy.” In: *Biophysical Journal* 97.2, pp. 674–677. ISSN: 00063495. DOI: 10.1016/j.bpj.2009.05.010 (cit. on p. 203).

Bibliography

- Rojas, E. R., G. Billings, P. D. Odermatt, G. K. Auer, L. Zhu, A. Miguel, F. Chang, D. B. Weibel, J. A. Theriot, and K. C. Huang (2018). “The Outer Membrane Is an Essential Load-Bearing Element in Gram-Negative Bacteria.” In: *Nature* 559.7715, pp. 617–621. ISSN: 0028-0836, 1476-4687. DOI: 10.1038/s41586-018-0344-3 (cit. on p. 56).
- Rother, J., H. Noding, I. Mey, and A. Janshoff (2014). “Atomic Force Microscopy-Based Microrheology Reveals Significant Differences in the Viscoelastic Response between Malign and Benign Cell Lines.” In: *Open Biology* 4.5, pp. 140046–140046. ISSN: 2046-2441. DOI: 10.1098/rsob.140046 (cit. on p. 67).
- Rotsch, C. and M. Radmacher (1997). “Mapping Local Electrostatic Forces with the Atomic Force Microscope.” In: *Langmuir* 13.10, pp. 2825–2832. ISSN: 0743-7463. DOI: 10.1021/la960874s (cit. on p. 23).
- (2000). “Drug-Induced Changes of Cytoskeletal Structure and Mechanics in Fibroblasts: An Atomic Force Microscopy Study.” In: *Biophysical Journal* 78.1, pp. 520–535 (cit. on p. 72).
- Roy, A., M. Eisenhut, R. J. Harris, L. C. Rodrigues, S. Sridhar, S. Habermann, L. Snell, P. Mangtani, I. Adetifa, A. Lalvani, and I. Abubakar (2014). “Effect of BCG Vaccination against Mycobacterium Tuberculosis Infection in Children: Systematic Review and Meta-Analysis.” In: *The BMJ* 349 (aug04 5), g4643–g4643. ISSN: 1756-1833. DOI: 10.1136/bmj.g4643 (cit. on p. 60).
- Ruggiero, M. A., D. P. Gordon, T. M. Orrell, N. Bailly, T. Bourgoin, R. C. Brusca, T. Cavalier-Smith, M. D. Guiry, and P. M. Kirk (2015). “A Higher Level Classification of All Living Organisms.” In: *PloS one* 10.4, e0119248 (cit. on p. 46).
- Sadeghian, H., T. Bijmagte, R. Herfst, G. Kramer, L. Kramer, and B. Dekker (2017). “Automated Cantilever Exchange and Optical Alignment for High-Throughput Parallel Atomic Force Microscopy.” In: *IEEE/ASME Transactions on Mechatronics* 22.6, pp. 2654–2661. ISSN: 1083-4435, 1941-014X. DOI: 10.1109/TMECH.2017.2766573 (cit. on p. 93).
- Sadeghian, H., R. Herfst, B. Dekker, J. Winters, T. Bijmagte, and R. Rijnbeek (2015). “High-Throughput Atomic Force Microscopes Operating in Parallel.” In: *Review of Scientific Instruments* 88.3, p. 033703. ISSN: 0034-6748, 1089-7623. DOI: 10.1063/1.4978285 (cit. on p. 89).
- Sánchez, H. and C. Wyman (2015). “SFMetrics: An Analysis Tool for Scanning Force Microscopy Images of Biomolecules.” In: *BMC Bioinformatics* 16.1. ISSN: 1471-2105. DOI: 10.1186/s12859-015-0457-8. pmid: 25627825 (cit. on p. 120).

Bibliography

- Sastri, V. R. (2013). *Plastics in Medical Devices: Properties, Requirements, and Applications*. William Andrew. 324 pp. ISBN: 978-0-323-26563-8 (cit. on p. 111).
- Scheuring, S. (2005). “Chromatic Adaptation of Photosynthetic Membranes.” In: *Science* 309.5733, pp. 484–487. ISSN: 0036-8075, 1095-9203. DOI: 10.1126/science.11110879 (cit. on p. 66).
- Schierbaum, N., J. Rheinlaender, and T. E. Schäffer (2017). “Viscoelastic Properties of Normal and Cancerous Human Breast Cells Are Affected Differently by Contact to Adjacent Cells.” In: *Acta Biomaterialia*. ISSN: 17427061. DOI: 10.1016/j.actbio.2017.04.006 (cit. on p. 68).
- Schillers, H., I. Medalsy, S. Hu, A. L. Slade, and J. E. Shaw (2016). “Peak-Force Tapping Resolves Individual Microvilli on Living Cells: Imaging of Soft and Flexible Microvilli on Living Cells.” In: *Journal of Molecular Recognition* 29.2, pp. 95–101. ISSN: 09523499. DOI: 10.1002/jmr.2510 (cit. on pp. 25, 31–33, 35, 65).
- Schillers, H., C. Rianna, J. Schäpe, T. Luque, H. Doschke, M. Wälte, J. J. Uriarte, N. Campillo, G. P. A. Michanetzis, J. Bobrowska, A. Dumitru, E. T. Herruzo, S. Bovio, P. Parot, M. Galluzzi, A. Podestà, L. Puricelli, S. Scheuring, Y. Missirlis, R. Garcia, M. Odorico, J.-M. Teulon, F. Lafont, M. Lekka, F. Rico, A. Rigato, J.-L. Pellequer, H. Oberleithner, D. Navajas, and M. Radmacher (2017). “Standardized Nanomechanical Atomic Force Microscopy Procedure (SNAP) for Measuring Soft and Biological Samples.” In: *Scientific Reports* 7.1. ISSN: 2045-2322. DOI: 10.1038/s41598-017-05383-0 (cit. on pp. 76, 79, 80, 128, 142).
- Schneider, C. A., W. S. Rasband, and K. W. Eliceiri (2012). *NIH Image to ImageJ: 25 Years of Image Analysis*. URL: <http://www-nature-com/articles/nmeth.2089> (visited on 2018) (cit. on p. 120).
- Scintilla and SciTE* (2018). URL: <https://www.scintilla.org/> (visited on 2018) (cit. on p. 115).
- Scully, J. L. (2004). “What Is a Disease?” In: *EMBO Reports* 5.7, pp. 650–653. ISSN: 1469-221X. DOI: 10.1038/sj.embor.7400195. pmid: 15229637 (cit. on p. 60).
- Seltmann, G. and O. Holst (2002). *The Bacterial Cell Wall*. Springer Science & Business Media. 296 pp. ISBN: 978-3-540-42608-0 (cit. on pp. 53–56).
- Senden, T. and W. Ducker (1994). “Experimental Determination of Spring Constants in Atomic Force Microscopy.” In: *Langmuir* 10.4, pp. 1003–1004. ISSN: 0743-7463. DOI: 10.1021/1a00016a600 (cit. on p. 77).

Bibliography

- Shao, Z., J. X. Mou, and G. Huang (1998). “Automatic Atomic Force Microscope with Piezotube Scanner.” U.S. pat. 5834644 A. The University Of Virginia Patent Foundation. U.S. Classification 73/105, 310/365, 850/33, 977/870; International Classification G01Q60/00, G01B21/30, G01B11/30; Cooperative Classification Y10S977/87, B82Y35/00, G01Q10/04, G01Q60/38, G01Q20/02; European Classification B82Y35/00, G01Q10/04, G01Q20/02, G01Q60/38 (cit. on p. 91).
- Shi, Y., H. Inoue, J. C. Wu, and S. Yamanaka (2017). “Induced Pluripotent Stem Cell Technology: A Decade of Progress.” In: *Nature Reviews Drug Discovery* 16.2, pp. 115–130. ISSN: 1474-1776, 1474-1784. DOI: 10.1038/nrd.2016.245 (cit. on p. 65).
- Shibata, M., H. Watanabe, T. Uchihashi, T. Ando, and R. Yasuda (2017). “High-Speed Atomic Force Microscopy Imaging of Live Mammalian Cells.” In: *Biophysics and Physicobiology* 14.0, pp. 127–135. ISSN: 2189-4779. DOI: 10.2142/biophysico.14.0_127 (cit. on p. 44).
- Slusser, J. (2017). *ScintillaNET: A Windows Forms Control, Wrapper, and Bindings for the Scintilla Text Editor* (cit. on p. 115).
- SMI (2015). *Identification of Yersinia Species*. 3. Public Health England, p. 22 (cit. on p. 57).
- Sneddon, I. N. (1965). “The Relation between Load and Penetration in the Axisymmetric Boussinesq Problem for a Punch of Arbitrary Profile.” In: *International journal of engineering science* 3.1, pp. 47–57 (cit. on p. 201).
- Sokolov, I., M. E. Dokukin, and N. V. Guz (2013). “Method for Quantitative Measurements of the Elastic Modulus of Biological Cells in AFM Indentation Experiments.” In: *Methods* 60.2, pp. 202–213. ISSN: 10462023. DOI: 10.1016/j.ymeth.2013.03.037 (cit. on p. 82).
- Soon, R. L., R. L. Nation, P. G. Hartley, I. Larson, and J. Li (2009). “Atomic Force Microscopy Investigation of the Morphology and Topography of Colistin-Heteroresistant *Acinetobacter Baumannii* Strains as a Function of Growth Phase and in Response to Colistin Treatment.” In: *Antimicrobial Agents and Chemotherapy* 53.12, pp. 4979–4986. ISSN: 0066-4804, 1098-6596. DOI: 10.1128/AAC.00497-09. pmid: 19786595 (cit. on p. 71).
- Spedden, E., D. L. Kaplan, and C. Staii (2013). “Temperature Response of the Neuronal Cytoskeleton Mapped via Atomic Force and Fluorescence Microscopy.” In: *Physical biology* 10.5, p. 056002 (cit. on p. 72).
- Sri Muthu Mrinalini, R. and G. R. Jayanth (2016). “A System for Replacement and Reuse of Tips in Atomic Force Microscopy.” In: *IEEE/ASME*

Bibliography

- Transactions on Mechatronics* 21.4, pp. 1943–1953. ISSN: 1083-4435, 1941-014X. DOI: 10.1109/TMECH.2016.2544401 (cit. on p. 93).
- Stadler, M. and P. Dersch, eds. (2016). *How to Overcome the Antibiotic Crisis: Facts, Challenges, Technologies and Future Perspectives*. Current topics in microbiology and immunology Volume 398. OCLC: 971216190. Cham: Springer. 496 pp. ISBN: 978-3-319-49282-7 978-3-319-49284-1 (cit. on p. 62).
- Stanier, R. Y. and C. B. van Niel (1962). “The Concept of a Bacterium.” In: *Archiv für Mikrobiologie* 42.1, pp. 17–35 (cit. on p. 46).
- Stolz, M., R. Gottardi, R. Raiteri, S. Miot, I. Martin, R. Imer, U. Staufer, A. Raducanu, M. Düggelin, W. Baschong, A. U. Daniels, N. F. Friederich, A. Aszodi, and U. Aebi (2009). “Early Detection of Aging Cartilage and Osteoarthritis in Mice and Patient Samples Using Atomic Force Microscopy.” In: *Nature Nanotechnology* 4.3, pp. 186–192. ISSN: 1748-3387, 1748-3395. DOI: 10.1038/nnano.2008.410 (cit. on p. 69).
- Stolz, M., R. Raiteri, A. U. Daniels, M. R. VanLandingham, W. Baschong, and U. Aebi (2004). “Dynamic Elastic Modulus of Porcine Articular Cartilage Determined at Two Different Levels of Tissue Organization by Indentation-Type Atomic Force Microscopy.” In: *Biophysical Journal* 86.5, pp. 3269–3283. ISSN: 0006-3495. DOI: 10.1016/S0006-3495(04)74375-1 (cit. on p. 202).
- Struckmeier, J., R. Wahl, M. Leuschner, J. Nunes, H. Janovjak, U. Geisler, G. Hofmann, T. Jähnke, and D. J. Müller (2008). “Fully Automated Single-Molecule Force Spectroscopy for Screening Applications.” In: *Nanotechnology* 19.38, p. 384020. ISSN: 0957-4484, 1361-6528. DOI: 10.1088/0957-4484/19/38/384020 (cit. on p. 96).
- Sunyer, R., X. Trepas, J. J. Fredberg, R. Farré, and D. Navajas (2009). “The Temperature Dependence of Cell Mechanics Measured by Atomic Force Microscopy.” In: *Physical Biology* 6.2, p. 025009. ISSN: 1478-3975. DOI: 10.1088/1478-3975/6/2/025009 (cit. on pp. 72, 171).
- Suvorov, M., J. F. Fisher, and S. Mobashery (2008). “Bacterial Cell Wall Morphology and Biochemistry.” In: *Practical Handbook of Microbiology*. 2nd ed. CRC Press, pp. 159–189. ISBN: 978-1-4200-0933-0 (cit. on pp. 53–55).
- Uchihashi, T. and S. Scheuring (2017). “Applications of High-Speed Atomic Force Microscopy to Real-Time Visualization of Dynamic Biomolecular Processes.” In: *Biochimica et Biophysica Acta (BBA) - General Subjects*. ISSN: 03044165. DOI: 10.1016/j.bbagen.2017.07.010 (cit. on p. 44).

Bibliography

- Van der Mei, H. C., H. J. Busscher, R. Bos, J. de Vries, C. J. Boonaert, and Y. F. Dufrêne (2000). “Direct Probing by Atomic Force Microscopy of the Cell Surface Softness of a Fibrillated and Nonfibrillated Oral Streptococcal Strain.” In: *Biophysical Journal* 78.5, pp. 2668–2674. ISSN: 00063495. DOI: 10.1016/S0006-3495(00)76810-X (cit. on p. 27).
- Van Lommel, A. T. L. (2003). *From Cells to Organs*. Boston, MA: Springer US. ISBN: 978-1-4613-5035-4 978-1-4615-0353-8. DOI: 10.1007/978-1-4615-0353-8 (cit. on pp. 48, 49, 51).
- Venners, B. (2003). *The Making of Python*. In collab. with G. van Rossum (cit. on p. 206).
- Verbelen, C., V. Dupres, F. D. Menozzi, D. Raze, A. R. Baulard, P. Hols, and Y. F. Dufrêne (2006). “Ethambutol-Induced Alterations in Mycobacterium Bovis BCG Imaged by Atomic Force Microscopy.” In: *FEMS Microbiology Letters* 264.2, pp. 192–197. ISSN: 0378-1097 (cit. on pp. 71, 154).
- Vettiger, P., M. Despont, U. Drechsler, U. Dürig, W. Häberle, M. I. Lutwyche, H. E. Rothuizen, R. Stutz, R. Widmer, and G. K. Binnig (2000). “The “Millipede”—More than Thousand Tips for Future AFM Storage.” In: *IBM Journal of Research and Development* 44.3, pp. 323–340 (cit. on p. 86).
- Villarrubia, J. S. (1994). “Morphological Estimation of Tip Geometry for Scanned Probe Microscopy.” In: *Surface science* 321.3, pp. 287–300 (cit. on pp. 39, 177).
- (1997). “Algorithm for Scanned Probe Microscope Image Simulation, Surface Reconstruction, and Tip Estimation.” In: *Journal of Research-National Institute of Standards and Technology* 102, pp. 425–454 (cit. on pp. 177, 179).
- Walsh, C. (2000). “Molecular Mechanisms That Confer Antibacterial Drug Resistance.” In: *Nature* 406.6797, p. 775. ISSN: 00280836 (cit. on p. 63).
- Wang, J., M. Liu, Y. Shen, J. Sun, Z. Shao, and D. Czajkowsky (2018). “Compressive Force Spectroscopy: From Living Cells to Single Proteins.” In: *International Journal of Molecular Sciences* 19.4, p. 960. ISSN: 1422-0067. DOI: 10.3390/ijms19040960 (cit. on p. 70).
- Wang, Z., L. Liu, Y. Wang, N. Xi, Z. Dong, M. Li, and S. Yuan (2012). “A Fully Automated System for Measuring Cellular Mechanical Properties.” In: *Journal of Laboratory Automation* 17.6, pp. 443–448. ISSN: 2211-0682, 1540-2452. DOI: 10.1177/2211068212460236 (cit. on pp. 96, 97).
- Watanabe, I. (1967). “Effects of Temperature on Growth Rate of Cultured Mammalian Cells (L5178Y).” In: *The Journal of Cell Biology* 32.2,

Bibliography

- pp. 309–323. ISSN: 0021-9525, 1540-8140. DOI: 10.1083/jcb.32.2.309 (cit. on p. 171).
- Weder, G., F. Mélanie, R. Ischer, M. Liley, H. Heinzelmann, and M. Despont (2016). “Parallel Atomic Force Microscopy for Rapid Nanomechanical Tissue Diagnostics.” Poster. 22nd Congress of the European Society of Biomechanics (Lyon, France) (cit. on p. 87).
- Welch, B. L. (1947). “The Generalization of ‘Student’s’ Problem When Several Different Population Variances Are Involved.” In: *Biometrika* 34.1-2, pp. 28–35. DOI: 10.1093/biomet/34.1-2.28 (cit. on p. 153).
- WHO (2004). *A Glossary of Terms for Community Health Care and Services for Older Persons*. Vol. 5. World Health Organization. 111 pp. (cit. on pp. 60, 61).
- (2017). *Global Tuberculosis Report*. World Health Organization (cit. on p. 59).
- (2018). *BCG Vaccines: WHO Position Paper*. Weekly epidemiological record 8. World Health Organization, pp. 73–96 (cit. on p. 60).
- Williams, P. M. (1996). “Blind Reconstruction of Scanning Probe Image Data.” In: *Journal of Vacuum Science & Technology B: Microelectronics and Nanometer Structures* 14.2, p. 1557. ISSN: 0734211X. DOI: 10.1116/1.589138 (cit. on pp. 177, 178).
- Woese, C. R., O. Kandler, and M. L. Wheelis (1990). “Towards a Natural System of Organisms: Proposal for the Domains Archaea, Bacteria, and Eucarya.” In: *Proceedings of the National Academy of Sciences* 87.12, pp. 4576–4579 (cit. on p. 46).
- Wu, F., B. G. C. van Schie, J. E. Keymer, and C. Dekker (2015). “Symmetry and Scale Orient Min Protein Patterns in Shaped Bacterial Sculptures.” In: *Nature Nanotechnology* 10.8, pp. 719–726. ISSN: 1748-3387, 1748-3395. DOI: 10.1038/nnano.2015.126 (cit. on p. 162).
- Xu, W., R. Mezencev, B. Kim, L. Wang, J. McDonald, and T. Sulchek (2012). “Cell Stiffness Is a Biomarker of the Metastatic Potential of Ovarian Cancer Cells.” In: *PLOS ONE* 7.10, e46609. ISSN: 1932-6203. DOI: 10.1371/journal.pone.0046609 (cit. on p. 67).
- Yao, X., M. Jericho, D. Pink, and T. Beveridge (1999). “Thickness and Elasticity of Gram-Negative Murein Sacculi Measured by Atomic Force Microscopy.” In: *Journal of Bacteriology* 181, p. 11 (cit. on p. 67).
- Yim, E. K., E. M. Darling, K. Kulangara, F. Guilak, and K. W. Leong (2010). “Nanotopography-Induced Changes in Focal Adhesions, Cytoskeletal Organization, and Mechanical Properties of Human Mesenchymal

Bibliography

- Stem Cells.” In: *Biomaterials* 31.6, pp. 1299–1306. ISSN: 01429612. DOI: 10.1016/j.biomaterials.2009.10.037 (cit. on pp. 67, 162).
- Young, J. M., C. B. Prater, D. A. Grigg, C. R. Meyer, W. H. Hertzog, J. A. Gurley, and V. B. Elings (1998). “Scanning Probe Microscope Having Automatic Probe Exchange and Alignment.” U.S. pat. 5705814 A. Digital Instruments, Inc. U.S. Classification 850/2, 250/307, 977/850, 250/423.00P, 850/6, 850/53, 850/33; International Classification G01Q60/24, G01Q10/02, G01Q20/02, G01Q70/02, G01Q30/06; Cooperative Classification Y10S977/85, G01Q30/06, G01Q70/02; European Classification B82Y35/00, G01Q30/06, G01Q70/02 (cit. on pp. 91, 135).
- Yourek, G., M. A. Hussain, and J. J. Mao (2007). “Cytoskeletal Changes of Mesenchymal Stem Cells During Differentiation:” in: *ASAIO Journal* 53.2, pp. 219–228. ISSN: 1058-2916. DOI: 10.1097/MAT.0b013e31802deb2d (cit. on p. 67).
- Zandiatashbar, A., B. Kim, Y.-k. Yoo, K. Lee, A. Jo, J. S. Lee, S.-J. Cho, and S.-i. Park (2015). “High-Throughput Automatic Defect Review for 300mm Blank Wafers with Atomic Force Microscope.” In: p. 94241X. DOI: 10.1117/12.2086042 (cit. on p. 96).
- Zhang, A. and M. J. Groves (1988). “Size Characterization of Mycobacterium Bovis BCG (Bacillus Calmette Guérin) Vaccine, Tice™ Substrain.” In: *Pharmaceutical Research* 5.9, pp. 607–610. ISSN: 0724-8741, 1573-904X. DOI: 10.1023/A:1015954316139 (cit. on p. 60).
- Zhong, Q., D. Inniss, K. Kjoller, and V. B. Elings (1993). “Fractured Polymer/Silica Fiber Surface Studied by Tapping Mode Atomic Force Microscopy.” In: *Surface science* 290.1-2, pp. L688–L692. DOI: 10.1016/0039-6028(93)90582-5 (cit. on pp. 19, 25).